DELIVERABLE D2.4

REPORT ON NOVEL ACCESS TECHNOLOGIES IN BROADCASTING FREQUENCIES

13TH DECEMBER 2012

Editor: Tero Jokela

University of Turku, Finland

EXECUTIVE SUMMARY

In ENGINES work package two (WP2), individual system architecture components were studied, and the results from these studies have been forwarded to standardization work (DVB-T2 Lite, DVB-NGH). The outcome of WP2 work is collected in five deliverables. Deliverable 2.1 focuses on system architectural work performed by ENGINES partners. Deliverable 2.2 deals with DVB-NGH receiver implementation related issues. Devised advanced component techniques for DVB-NGH are presented in deliverable 2.3. Additionally there is work on overall architectures, including issues not covered by direct standardization that are novel access technologies (deliverable 2.4) and end-to-end system integration (deliverable 2.5).

In this deliverable the work on novel access technologies on broadcasting frequencies is presented. Hybrid satellite-terrestrial networks and cognitive radio are considered. In more detail, the topics considered are:

- *The satellite role in the DVB-NGH hybrid profile architecture and satellite link characterization.*
  This topic starts with an overview on the start-of-art of mobile services over satellite, specifying the current issues and the DVB technologies used for satellite broadcasting. After this, a characterization of the different DVB-NGH satellite scenarios is presented and the main distribution requirements are established. A final study is focused on the satellite link characterization where some examples of DVB-NGH link budgets are presented according to the latest information available from DVB. The link budget examples consider medium and high power satellites and a channelization of 1.7MHz in OFDM mode.

- *The SC-OFDM for the implementation of the satellite transmissions in the DVB-NGH Hybrid Profile*.
  It is shown that the SC-OFDM (Single Carrier OFDM) modulation is intrinsically robust to the Power Amplifier non-linear degradations with the ability to operate with a reduced OBO in comparison to OFDM and a total degradation improved by 1.6 dB. It is thus possible to improve the power efficiency of the PA (Power Amplifier) while improving the coverage. It must be pointed out that this result still holds when considering the PAPR reduction solutions for OFDM such as the Tone Reservation approach used in DVB-T2. This kind of solution actually performs well for large IBOs but not for the small IBOs (a few dBs) commonly used in satellite transmissions. In a third wing, the section shows that the SC-OFDM behaves similarly to OFDM when it comes to compensate for the degradation due to the channel and mobility, either in SISO or MIMO.

- *The Convolutional interleaving scheme selected for the Long TI Feature of DVB-NGH*.
  It is shown that the best performance is achieved by single FEC with a uniform CI profile. The performance of single FEC with the CI uniform-late profile is reduced about 2 dB compared to the CI uniform profile. CI with TI length of 10s achieves gains between 6-8 dBs.

- *The robustness of L1 signaling schemes provisioned in the DVB-NGH standard for the satellite segment*.
  It is shown that the mechanisms devised in the Terrestrial profile to improve L1 signaling robustness satisfy the requirements of the Satellite path.

- *Time and frequency synchronization algorithms in the context of satellite transmissions*
  A set of algorithms designed for improving the performance of time and frequency synchronization over the satellite channel is described. Most of these algorithms rely on the DVB-T2/NGH P1 symbol that also serves to detect DVB-T2/NGH transmission. It is shown that the P1 detection is very robust (for SNR down to -8dB). The overall performances of an SC-OFDM system have been evaluated when applying the proposed algorithms. It is shown that synchronization algorithms are quite robust for SNR values higher than -3dB.

- *Cognitive radio* sensing studies
  An experimental implementation of a sensing device in a mobile computer is presented and results of sensing measurements with the device are shown.

- *Spectrum Occupancy and Hidden Node Margins for Cognitive Radio Applications in the UHF Band*
  Field measurement data that could serve as a reference for the technical discussions around the possible use of White Spaces in the UHF band is provided. Results show that a top occupancy of 32% of the bandwidth is achieved in the roof and that the hidden node margin obtained range from 8 to 38 dB on channel 22 depending on the environment and lead to the conclusion that cognitive communications to be performed in the UHF TV band need the joint use of geolocation databases and spectrum sensing technique to avoid harmful interference to the primary services of the broadcasters.

- *Mobile digital terrestrial television network measurements for studying measurement-based geolocation database update algorithms*
  Field measurements used for studying geolocation database update algorithms are presented.

TABLE OF CONTENTS

LIST OF CONTRIBUTORS

- **CNES**
  Laurence Clarac, Frédéric Lacoste, Benjamin Ros, Christelle Boustie

- **Hispasat**
  Inés Sanz, Jorge Rodriguez, Marcos Iglesias

- **iTEAM, Polytechnic University of Valencia**
  David Gómez-Barquero, Pedro F. Gómez, Jose Llorca, David Gozálvez

- **MERCE**
  Arnaud Bouttier, Cristina Ciochină, Damien Castelain

- **Nokia**
  Pekka Talmola

- **TeamCast**
  Laurent Boher

- **University of the Basque Country (UPV/EHU)**

- **University of Turku**
  Juha Kalliovaara

1 INTRODUCTION

In this deliverable the work on novel access technologies on broadcasting frequencies are is presented. Hybrid satellite-terrestrial networks and cognitive radio are considered. The outcomes of the studies on hybrid access networks are reported to the standardization of DVB-NGH. The document is structurized as follows.

Chapter 2 dealing with hybrid access technologies is divided into three main sections. Section 2.1 provides an overview on satellite broadcasting systems accompanied with link budget considerations. The remaining part of the chapter focuses on the design of the satellite link itself. Section 2.2 provides a brief overview of the Land Mobile Channel Satellite (LMS) models as proposed to DVB-NGH for performing link level performance evaluations. Section 2.3 addresses the definition of the satellite link's physical layer with an emphasis on four key issues:

1 – The performances of the Single Carrier-Orthogonal Frequency Multiplexing (SC-OFDM) modulation and its comparison to OFDM and TDM solutions.

2 – The performances of long time interleaving solutions for the satellite channel.

3 – The definition of robust layer 1 signalling schemes.

4 – The definition and performances of synchronization algorithms with application to SC-OFDM.

Chapter 3 presents the studies performed on cognitive radio. First the cognitive radio concept is briefly described. Further an experimental implementation of a sensing device in a mobile computer is presented in section 3.3 and accompanied with sensing measurement results. In section 3.4 field measurement data that could serve as a reference for the technical discussions around the possible use of White Spaces in the UHF band is provided. Finally, in section 3.5, field measurements used for studying geolocation database update algorithms are presented.

2 HYBRID ACCESS TECHNOLOGIES

2.1 DVB-NGH Satellite Hybrid Profile

2.1.1 State-of-art: Mobile Services via Satellite

2.1.1.1 Current Issues for Mobile Devices Broadcasting

Satellites are ideal for broadcast services since they are able to cover large areas with minimal ground infrastructure deployment. Satellite communications have been widely used for mobile communications by transferring services based on voice and data. However, transmission of new multimedia content presents higher requirements in terms of bandwidth, fault tolerance, access time or delay.

DVB-S (Digital Video Broadcasting - Satellite services [1]) was standardized in 1993 for the provision of video services via satellite. Its second version, DVB-S2 [2], was standardized in 2005 to achieve better performance through the use of new coding and modulation techniques. Both DVB-S and DVB-S2 were designed for transmission to fixed user stations equipped with antennas located in direct line of sight with the satellite at any time. Therefore, physical layer protection mechanisms used in these standards are designed for fixed reception with the aim to correct the errors caused by interferences and thermal noise. Mobile reception is characterized by the presence of both fast and slow signal fluctuations, known as fast fading and shadowing, respectively. These fluctuations produce bursts of errors in the received information which cannot be corrected by the physical layer protection mechanisms of DVB-S and DVB-S2.

In order to increase the protection provided by the physical layer of DVB-S and DVB-S2, and also to enable the transmission of new content in mobility conditions, it is possible to incorporate additional protection techniques in the upper layers. UL-FEC (Upper Layer - Forward Error Correction) can operate transparently over the physical layer to repair error bursts originated in mobility conditions. The main advantage of UL-FEC is that it can be incorporated into existing broadcast systems such as DVB-S and DVB-S2 reusing the already deployed infrastructure with a minimal cost for the operator, as shown in the figure below. UL-FEC also allows great configuration flexibility, enabling the possibility of applying particular protection to each service transmitted.

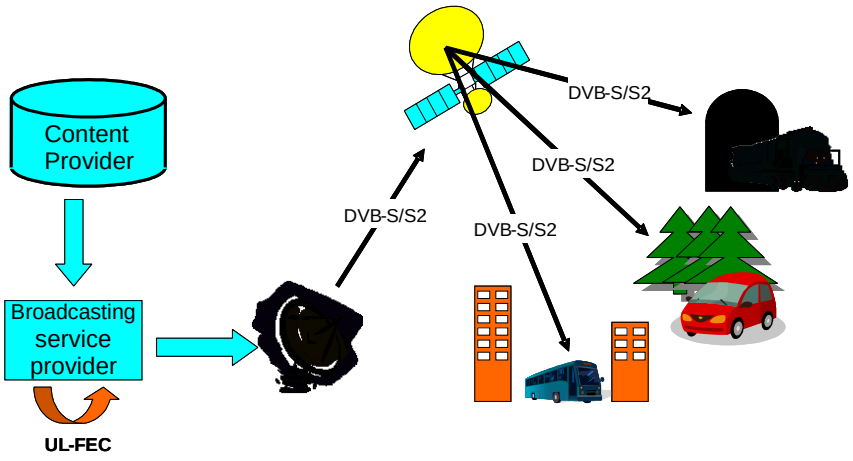

Figure 1: Mobile Satellite Network Architecture.

2.1.1.2 DVB technologies for satellite broadcasting

This section presents a review of the main DVB standards for satellite broadcasting depending on the frequency band to be used.

2.1.1.2.1 L/S Bands

Transmission in L-Band offers significant advantages over higher spectrum bands. Among these advantages, there is less vulnerability to obstructions caused by trees as well as no rain attenuation of the transmitted signal. The operation in L-band also allows the implementation of small antennas where high pointing accuracy to the satellite is not required. However, the available spectrum in this frequency band is only tens of MHz, making difficult the provision of broadband services.

One clear example of service using these bands is DVB-SH [3].

DVB-SH (Digital Video Broadcasting – Satellite Handheld) derives from DVB-H (Digital Video Broadcasting - Handheld) and ETSI SDR (Satellite Digital Radio) to provide broadcasting services to various types of mobile devices.

This system provides a huge coverage through the SC (Satellite Component), which is complemented by a CGC (Complementary Ground Component) that comes from the deployment of a terrestrial network in those areas where the satellite signal is severely degraded and also in urban environments. Thus, all reception

scenarios for mobile devices are supported. Figure 2 below shows the architecture of a typical DVB-SH network.

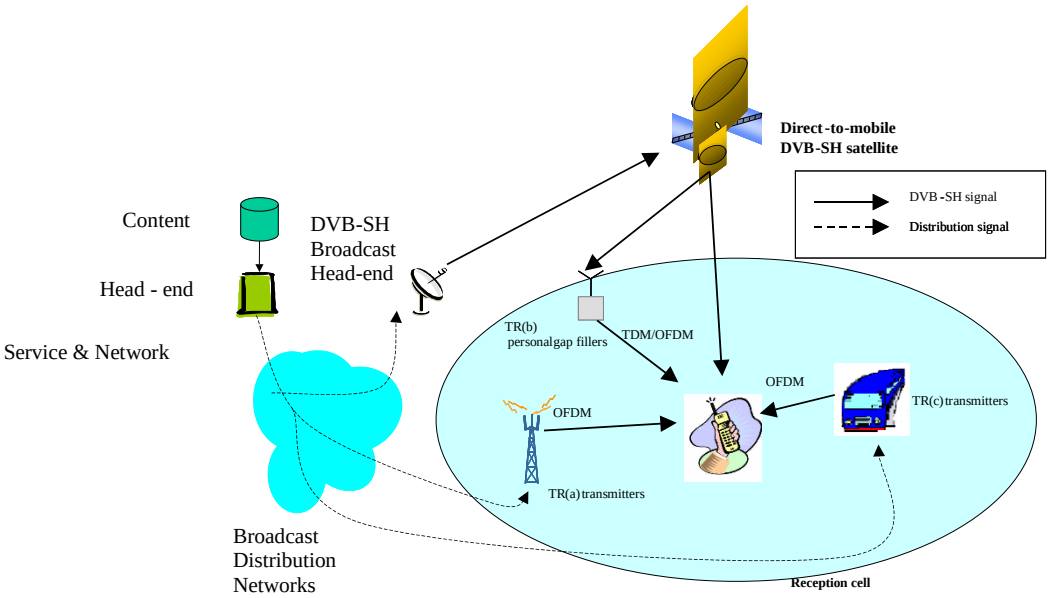

Figure 2: DVB-SH network architecture.

The standard defines two architectures:

- SH-A Architecture, where the satellite and terrestrial components use OFDM modulation (*Orthogonal Frequency Division Multiplexing*).
- SH-B Architecture, where the satellite component uses TDM (*Time Division Multiplex*), while the terrestrial component uses OFDM.

SH-A architecture enables the creation of single frequency networks (SFN) between the SC component and the CGC component, so that both components transmit the same content at the same frequency. The advantage of an SFN is spectral efficiency. However, it also presents a drawback, since it requires the signal transmitted via satellite and the signal transmitted via the terrestrial network to be exactly the same, which implies less variety in the configurations that DVB-SH provides.

Finally, one of the highlighted features incorporated in DVB-SH is the new upper layer correction system UL-FEC (Upper Layer - Forward Error Correction), called MPE-IFEC (intra-burst FEC), which is designed to be used in difficult or large shadow areas of the satellite channel.

2.1.1.2.2 C/Ku/Ka Bands

The transmission of mobile satellite services in Ku-band requires the deployment of antennas equipped with complex pointing and tracking mechanisms due to a higher directivity in this frequency range. This directivity leads to a higher vulnerability of the signal to the presence of obstacles in direct line of sight between the transmitter and the receiver. Nevertheless, today it is possible to develop antennas able to meet all the requirements associated in Ku band transmission. In the future, development of technology related with this type of antennas will allow its incorporation into all types of vehicles. Thus, it will be possible to take advantage of the wide available bandwidth in this frequency band to offer broadband services on the move.

DVB-S and DVB-S2 standards operate in the frequency range of Ku band (10.7-12.75 GHz in the downlink and 14.0-14.5 GHz in the uplink), which is used in satellite broadcasting TV and many VSAT systems.

In America, C-band (3.7-4.2 GHz in the downlink and 5.925-6.425 GHz in the uplink) is also used, and recently Ka band (17.7-21.2 GHz in the downlink and 27.5-31.0 GHz in the uplink) has started to be used in next-generation multi-spot satellites, mainly for bidirectional broadband applications.

Developed by the European Telecommunication Standard Organization, DVB-S [1] is a standard for satellite video broadcasting. It applies only to Ku-band satellites and its main purpose is to provide Direct-To-Home services through geostationary satellites.

DVB-S implements several techniques against noise and interference, as well as an efficient use of the spectrum. It uses a QPSK modulation scheme linked with powerful error correction techniques based on the concatenation of convolutional and Reed-Solomon (RS) algorithms.

DVB-S is optimized to use TDM, although it is compatible with FDM. Furthermore, the system is based on MPEG-2 coding. Depending on link characteristics, it is possible to select the appropriate coding rate (from 18.4 to 48.4 Mbit/s). This flexibility gives a compromise between spectrum efficiency (use of high-speed transmission rates) and power efficiency (low carrier-to-noise ratio).

DVB-S standard was primarily developed for one-way TV and radio broadcasting, since these are the main traditional services. However, data distribution both point-point and point-multipoint networks are also considered.

DVB-S2 (EN 302 307 [2]) is a digital satellite transmission system developed by the DVB Project. It makes use of the latest modulation and coding techniques to achieve performances that approach the theoretical limit for such systems. Satellite transmission was the first area addressed by the DVB Project in 1993, and DVB standards form the basis of most satellite DTV services around the world today, and therefore of most digital TV in general. DVB-S2 will not replace DVB-S in the short or even the medium term, but makes it possible to provide services that could never have been delivered using DVB-S.

DVB-S2 incorporates robust protection error algorithms by using two concatenated encoders (BCH – Bose Chaudhuri Hocquenghem and LDPC - Low Density Parity Check), achieving a near-Shannon limit capacity. Also, the system is more flexible and allows services with variable bit rates, modulation schemes (QPSK, 8PSK, 16APSK & 32APSK) and roll-offs (α=0.35, α=0.25 y α=0.20).

Thanks to the new coding and modulation techniques, DVB-S2 performance gain over DVB-S is around 30% at the same satellite transponder bandwidth and emitted signal power. DVB-S2 is compatible with current DVB-S receivers on the market.

2.1.2 Satellite Role in DVB-NGH architecture

2.1.2.1 Introduction

There are three scenarios considered in DVB-NGH:

1) *Satellite-only scenario*

   For rural areas where terrestrial networks are inexistent or signal reception is poor, satellite guarantees direct reception. Gap-fillers may be used to increase coverage indoor.

2) *Hybrid scenario*

   In this scenario satellite signal is received by a new network element: the Complementary Ground Component (CGC) and retransmitted to the mobile device. This new element has to be designed so that integration with existent mobile networks (2G, 3G) is easy.

3) *Terrestrial-only scenario*

   Satellite coverage is poor and terrestrial infrastructure exists.

Table 1 summarizes the three scenarios considered, detailing the coverage area and a possible application.

Table 1: DVB-NGH satellite scenarios.

	Business to consumer (Direct Service provision)	**Business to business to consumer (Indirect service provision)**
Satellite-Only	Rural or suburban area with no terrestrial infrastructure.	Airborne, Ships
Hybrid	Global coverage	Railway, commercial centres. Urban communities
Terrestrial-Only	Suburban and urban areas with terrestrial infrastructure. Underground.	

2.1.2.2 Satellite-Only Scenario

Satellite is the best technology to cover rural or suburban areas where there are no terrestrial infrastructures. Service provision to airborne or ships are some of the most relevant examples of business to business consumers. The content distribution in this scenario uses S-band. Here we present the main characteristics.

S-band distribution

S band is defined by an IEEE standard for radio waves with frequencies ranging from 2 to 4 GHz, crossing the conventional boundary between UHF and SHF at 3GHz. S band coverage is typically smaller with respect to other frequency bands such as Ku. One possible solution is to use multi-spot configurations that would also allow greater frequency reuse. Obviously this solution increases satellite complexity and, therefore its associated cost.

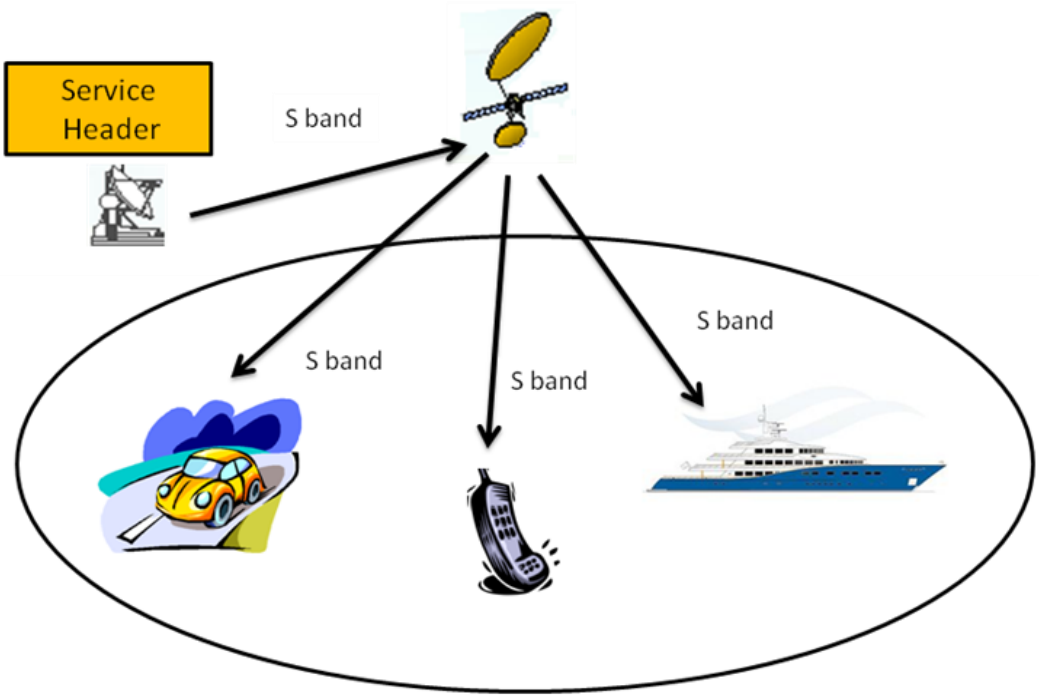

Figure 3: Satellite only architecture.

The main advantage of this system is that it requires a single signal to feed the end consumer terminals. The main disadvantage of this strategy is that S-band has not been widely used in satellite communications, so receivers cost is higher than the equivalent in Ku-band.

2.1.2.3 Hybrid scenario

In a normal communication operation mode, the user device is normally in line of sight with satellite. However, there are many occasions in which the receiver may lose sight of the satellite and so a signal quality degradation can be perceived; even signal reception can be totally lost. To overcome this situation, the hybrid architecture introduces a Complementary Ground Component (CGC). CGC is a network of re-transmitters that act as repeaters of the signal received from the satellite. These repeaters are also known as Gap-fillers, since they "fill" the areas where satellite signal is not received.

Gap-fillers are normally designed for frequency re-use, so that the downlink frequency and the re-transmission frequency are the same. These types of networks are called SFN (Single Frequency Network).

The application of this kind of retransmission requires the receiver to be able to apply echo-compensation techniques.

Figure 4 below shows the hybrid network architecture.

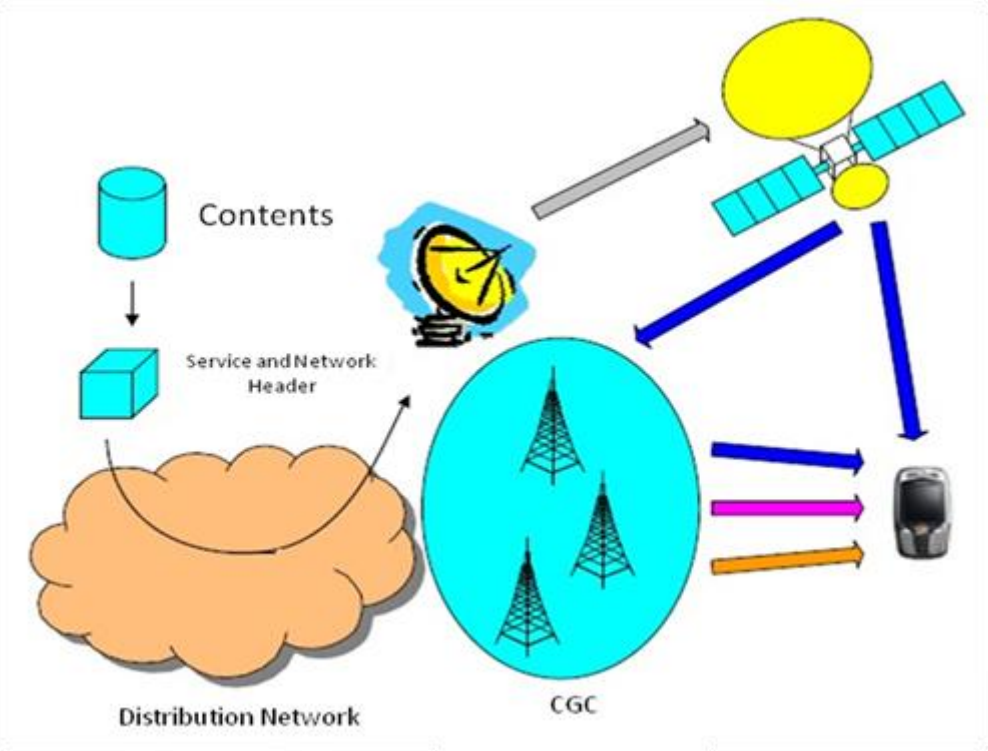

Figure 4: DVB-NGH network architecture.

As shown in the previous figure, CGC receives the content transmitted by the satellite and retransmits it within its coverage areas, which are the areas where satellite reception is difficult. The different elements which compose the CGC network topology are:

- **Content Generation**: Generates the contents that will be transmitted to the DVB-NGH terminals.
- **Network and Service Frontend**: It is in charge of content adaptation and encapsulation so that the transmitted signal can be interpreted by the receivers.
- **Network Distribution**: Sends the information to the transmission centres, which may be ground stations which transmit contents to the satellite, or gap-fillers.
- **Satellite/Gap-fillers**: Transmit the amplified signal received to the user terminals. In most cases, distribution to gap-fillers will be done using the downlink satellite signals aimed to user terminals.
- **DVB-NGH receivers**: receive information, de-encapsulate the signal and represent the content on the display.

2.1.2.3.1 Signal Distribution to CGC

As previously mentioned, CGC is responsible for complementing the satellite signal in areas where coverage is weak or nonexistent. In these cases, terrestrial repeaters (gap-fillers) are needed to forward the information to the end terminal. Depending on the strategy to reach this terminal, there are several possibilities:

- Use a satellite transmission in S-band.

- Use a satellite transmission at another frequency band (typically Ku).
- Getting the information through terrestrial transmitters.

Next we will go into details for the first two possibilities. The third one is widely discussed in other ENGINES deliverables, since there are significant variations in signal delay and echo canceller design is complex.

S-band distribution

In this scenario, S-band is used for transmitting the information to shadowed areas. It presents the following characteristics:

SFN (Single Frequency Network)

Satellite and terrestrial repeaters use the same frequency band. Terminals can be simplified so that receivers with echo cancellation technology can receive information from the satellite or terrestrial broadcaster depending on the one that arrives with higher quality.

Bandwidth Re-use

Additionally to what has been said about SFN, a direct conclusion is that frequency reuse is possible for this scenario. The same frequency can be used to transmit the information to the terminals and to re-transmitters. Thus, the information source can be the same satellite in both cases and it would not require additional bandwidth rent to transmit the content, with the consequent cost saving.

Limited Coverage

S band coverage is typically smaller with respect to other frequency bands such as Ku. One possible solution is to use multi-spot configurations that would also allow greater frequency reuse. Obviously this solution increases satellite complexity and, therefore its associated cost.

The main advantage of this system is that it requires a single signal to feed both repeaters and end terminals. Processing in gap-fillers is simplified basically consists in signal acquisition and amplification. The main disadvantage of this strategy is that S-band has not been widely used in satellite communications, so receivers cost is higher than the equivalent in Ku-band.

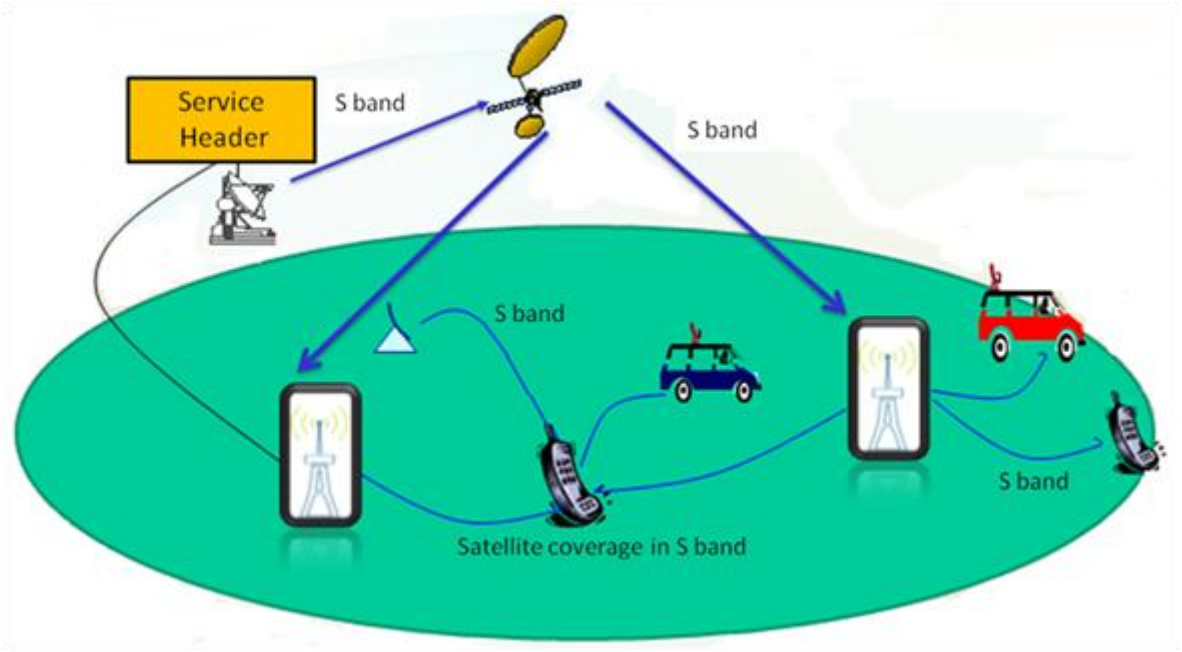

Figure 5: S-band Architecture Contribution to the CGC.

Ku band Distribution

Ku band is primarily used for satellite communications, most notably for fixed and broadcast services. The use of Ku band for the distribution of content to terrestrial repeaters presents the following characteristics:

Wide Coverage

Ku-band coverage is much larger than for S-band. This way it is possible to increase the number of potentially covered terrestrial repeaters and therefore increment the total number of costumers.

High Available Bandwidth

Currently, existing regulations regarding Ku frequency band for satellite communications reserve 750 MHz for this type of services. In S-band the allocated bandwidth is only 30MHz.

Consolidated Ground Segment

Ku band has been widely used in satellite communications so that its associated equipment (including ground segment) is much more developed than the S-band equivalent and so equipment costs in Ku band are also lower.

In this scenario, satellite transmits content in Ku band (14.0-14.5 GHz) to repeaters and S band is used to transmit towards the user terminals. A frequency conversion is needed in gap-fillers in order to reduce complexity in DVB-NGH terminals. Figure 6 below shows the scenario architecture.

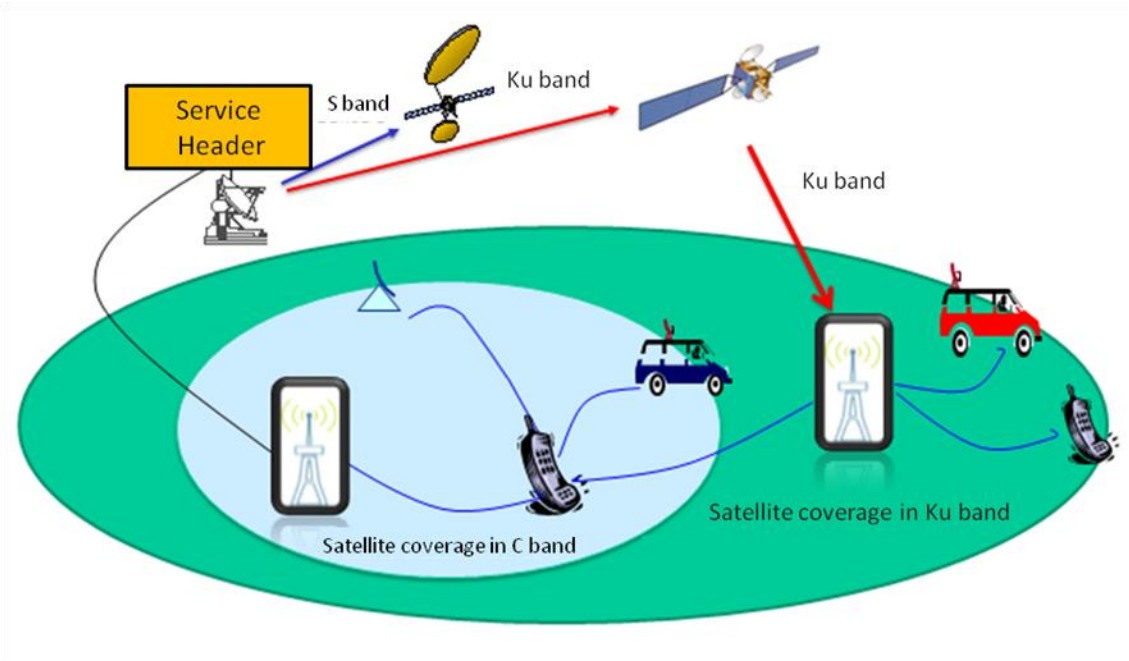

Figure 6: CGC Architecture Contribution in Ku-band.

The main advantage of this transmission mode is its associated technology, fully extended and cheap, the great satellite capacity and coverage. The main disadvantage is that, because there is no frequency reuse, satellite resource expenses will be greater. Additionally, since frequency conversion is required in gap-fillers, these are more complex. Processing complexity is higher than for the direct reception case, and so end user terminals will have to be able to cancel echoes with significant delays.

This strategy has been analyzed in detail and results are provided in the final section of this document.

2.1.2.4 Network Distribution Requirements

The content distribution network must meet the following characteristics:

High Availability

Most of the content sent through the network will be multimedia, so high availability must be ensured. This characteristic has to be met both for the final receivers and for the re-transmitters of the CGC. Availability depends on the propagation characteristics of the signals involved, being rain attenuation one of the most important parameters to consider. Rain attenuation causes a decrease in signal level and can be as strong as to damage completely the link. Analyzing the frequencies commonly used in satellite communications with respect to rain attenuation, Ku band more sensitive to this effect than S band. The higher the frequency the more influence of rain attenuation.

Links are designed according to statistical parameters of rainfall and additional margins are considered to ensure the required availability. This way, the higher the margins considered the higher the channel availability. A typical design objective for television signal distribution over satellite is an availability of 99.7% a.y. (average year).

Quality of Service

In the same way as availability, high quality of service must be ensured in the link between the station which sends data to the satellite and the re-transmission elements which receive this data.

Availability and quality of service are strongly related: quality of service depends directly on the quality of the received signals. In digital communications, the parameter that determines this quality of service is usually BER (Bit Error Ratio), which refers the number of incorrect bits received with respect to the number of transmitted bits. BER depends on the ratio between the energy of the received bits and the noise energy (E_b/N_0).

For example, for a DVB-S transmission with FEC = 3/4, E_b/N_0 = 5.5 dB, the ensured BER is smaller than 2×10^{-4}. This is a typical design objective.

Ground Segment Performance

To ensure quality and availability of the transmitted signal, the ground stations (both transmitters and receivers) must have the necessary equipment. Repeater stations are of vital importance since they must receive the signal, trans-modulate it and re-send it to the remote terminals with no signal degradation.

Good ground segment performance allows the system to be more robust against external interferences (such as other satellites) and internal interferences (from other carriers received from the same satellite). Performance requirements depend on satellite characteristics and equipment of the stations involved in the communications, as well as on the frequency band used.

In Ku band, for small stations a typical requirement is a radiation pattern whose envelope is lower than $29-25\times\log(\theta)$ at ±1.5º, and a transmission isolation of 28 dB. These are desired characteristics; however, the link can always be designed to compensate possible problems in stations.

2.1.3 DVB-NGH Satellite Link

This section will examine the main satellite link parameters in the DVB-NGH architecture.

2.1.3.1 Link Budgets Calculations

First we present the methodology to be followed in order to calculate a satellite link budget. In a satellite link there are two components: the uplink or upstream and the downlink or downstream. The uplink C/N is defined as:

$$\left[\frac{C}{N}\right]_U = \frac{1}{kB} EIRP_{GW} \frac{1}{L_U}\left[\frac{G}{T}\right]_{SAT}, \quad (2.1)$$

where:

k: Boltzman constant,

B: Noise BW,

$EIRP_{GW}$*: Gateway EIRP (transmission earth station),*

L_U*:Uplink losses,*

$[G/T]_{SAT}$ *: Satellite Antenna figure of merit (Gain to system noise temperature).*

Furthermore:

$$EIRP_{GW} = \frac{P_{GWTX} G_{GW}}{L_T L_{FTX}}, \tag{2.2}$$

where P_{GWTX} is the total power transmitted by the earth station, G_{GW} is the antenna transmission gain, L_T are pointing error losses and L_{FTX} are the attenuation losses between transmitter and antenna.

$L_U = L_{FS} L_A$, where L_{FS} are free space losses and L_A, losses related to atmospheric attenuation in the uplink.

$$L_{FS} = \left(\frac{4\pi R}{\lambda} \right)^2. \tag{2.3}$$

R is the distance between the transmitting earth station and satellite.

For the uplink we define the following parameters:

$$\left[\frac{C}{N} \right]_D = \frac{1}{kB} EIRP_{SAT} \frac{1}{L_D} \left[\frac{G}{T} \right]_{ES}, \tag{2.4}$$

where:

$EIRP_{SAT}$: Satellite EIRP,

L_D: Downlink losses,

$[G/T]_{ES}$: Earth station figure of merit (Gain to system noise temperature).

Furthermore:

$$EIRP_{SAT} = \frac{P_{SAT} G_{SAT}}{L_T L_{FTX}}, \tag{2.5}$$

where P_{SAT} is the satellite transmitted power, G_{SAT} is the satellite antenna gain, L_T are pointing error losses, L_{FTX} are the attenuation losses between transmitter and antenna.

$L_D = L_{FS} L_A$ where L_{FS} are free space losses and L_A, losses related to atmospheric attenuation in the downlink.

In addition to the above mentioned formulas, it is necessary to take into account the contribution of interferences. In general, interference is considered an additional source of noise, so that:

$$\left[\frac{C}{N+I} \right]^{-1} = \left[\frac{C}{N} \right]^{-1} + \left[\frac{C}{I} \right]^{-1}, \tag{2.6}$$

where I is the total interference (various sources): Intermodulation (IM), co-channel interference (CC) and adjacent channel interference (ACI).

$$I = I_{IM} + I_{CC} + I_{ACI}. \tag{2.7}$$

The link budget for transparent satellites is therefore calculated as:

$$\left[\frac{C}{N+I}\right]^{-1} = \left[\frac{C}{N+I}\right]_{uplink}^{-1} + \left[\frac{C}{N+I}\right]_{downlink}^{-1}. \quad (2.8)$$

To have a positive margin in the link, the signal-to noise and interference should be greater than the signal to noise ratio given by the modulation-coding configuration:

$$\left[\frac{C}{N+I}\right] \geq \left[\frac{C}{N}\right]_{\text{REQUIRED MODCOD}}. \quad (2.9)$$

Link margin is defined as:

$$M = \left[\frac{C}{N+I}\right](dB) - \left[\frac{C}{N}\right]_{\text{REQUIRED MODCOD}}(dB). \quad (2.10)$$

Considering the attenuation in the downlink, signal strength degrades and the attenuation factor α appears. If the source of degradation comes from intermodulation or interference between beams of the same frequency, attenuation affects both the carrier and interference. That is:

$$\left[\frac{C.\alpha}{I.\alpha}\right] = \left[\frac{C}{I}\right] \text{ if } I = I_{IM} + I_{CC}. \quad (2.11)$$

Therefore, the total C / (N + I) is:

$$\left[\frac{C}{N+I}\right]_{Fadedownlink}^{-1} = \left[\frac{C\alpha}{N}\right]^{-1} + \left[\frac{C}{I}\right]^{-1}. \quad (2.12)$$

From this relationship, link margin is calculated as follows:

$$M_{fade} = -\alpha(dB) = \left[\frac{C}{N}\right](dB) + 10\log\left[\left[\frac{C}{N}\right]_{\text{REQUIRED MODCOD}}^{-1} - \left[\frac{C}{I}\right]^{-1}\right]. \quad (2.13)$$

2.1.3.2 DVB-NGH Link Budget Considerations

Work related to the satellite link technical requirements in DVB-NGH is still going on and certain parameters have to be defined or agreed. At this regard the following link budget study is based on the last draft of the ETSI EN 303 105 DVB-NGH document dated on September 2012 and the information which is still applicable in the DVB-SH implementation guideline as many aspects regarding the satellite component are still the same.

2.1.3.2.1 Rx Terminal definition

The Rx terminal definition is in line with the one described for DVB-SH. There are three main categories:

- Category 1 : Car-mounted terminals (also called "vehicular").
- Category 2 : Portable TV devices with 2 sub-categories.
  - 2a : Large screen (≥ 10'') portable devices, battery or mains powered.
  - 2b : Pocketable (handheld) TV devices, mainly battery powered.
- Category 3 : Handheld terminal with embedded cellular telecom modem (or "convergence" terminal).

2.1.3.2.2 Rx Terminal G/T considerations

This section presents the G/T hypothesis for each of the terminals under consideration.

Hypothesis:

- Vehicular receiver (category 1) : NF=2dB (LNA 0.8 dB, filter 2.5 dB, tuner 3 dB)
- Handheld receiver (category 2b and 3) : NF=4.5 dB (filter 1.5 dB, tuner 3 dB)

Table 2: Receiver typical G/T versus terminal category.

Usage	**Handheld**	**Handheld**	**Portable**	**Vehicular**
Classification	category 3	category 2b	category 2a	category 1
Antenna polarization	L or C	L or C	L or C	C
Tuner	DVB-NGH	DVB-NGH	DVB-NGH	DVB-NGH
Antenna gain (dBi) or (dBic)	-3	0	2	4
Total Gain (dB)	-3	0	2	4
Antenna Temperature (K)	290	290	200	150
Active antenna	No	No	Yes	Yes
Noise Figure (dB) max	4.5	4.5	3	2
Total Noise temperature (°K)	817	817	489	320
G/T (dB/K)	**-32.1**	**-29.1**	**-24.9**	**-21.0**

Polarization losses are defined in the respective satellite and terrestrial link budgets. Table 2 gives typical figures of basic receivers (without diversity consideration) related to the terminal categories. Active antenna corresponds to an antenna with an attached LNA.

2.1.3.2.3 Minimum C/N requirements

This section presents the minimum C/N requirements for the transmission in AWGN channel. The next two tables presents the theoretical performance for OFDM and TDM configurations.

Table 3: Theoretical C/N (dB) in AWGN channel for OFDM @ BER = 10-5.

Code rate	QPSK	16QAM
1/5	-3.6	0.7
2/9	-3.1	1.3
1/4	-2.5	1.9
2/7	-1.8	2.8
1/3	-0.9	3.7
2/5	0.1	5.0
1/2	1.4	6.8
2/3	3.5	9.7

Table 4: Theoretical C/N (dB) in AWGN channel for TDM @ BER = 10-5.

Code rate	QPSK	8PSK	16APSK
1/5	-3.9	-1.3	0.4
2/9	-3.4	-0.7	1.0
1/4	-2.8	-0.1	1.6
2/7	-2.1	0.7	2.5
1/3	-1.2	1.6	3.4
2/5	-0.2	2.7	4.7
1/2	1.1	4.4	6.5
2/3	3.2	6.9	9.4

For AWGN, the following implementation losses to the C/N values are considered.

Table 5: Implementation losses in AWGN.

Modulation	Implementation loss (dB)
TDM- QPSK	0.5
TDM- 8PSK	1.0
TDM- 16APSK	1.5
OFDM- QPSK	1.1
OFDM- 16QAM	1.5

2.1.3.2.4 Allowed parameter settings for the DVB-NGH hybrid profile

The next table presents the parameters allowed for the hybrid profile in DVB-NGH.

Table 6: Allowed parameter settings for the hybrid profile in DVB-NGH.

Parameters		**Hybrid waveform**	
Modulation		OFDM	SC-OFDM
Bandwidth (MHz)	1.7	☑	☑
	2.5	☑	☑
	5	☑	☑
Constellation	QPSK	☑	☑
	16-QAM	☑	☑
FTT Size	0.5k		☑
	1k	☑	☑
	2k	☑	☑
Guard Interval	1/32	☑	☑
	1/16	☑	☑
	1/8	☑	
	1/4	☑	
Preamble	P1 + aP1	☑	☑
Pilot Pattern	Continuous pilot symbols	☑	
	PP1	☑	
	PP2	☑	
	PP3	☑	
	PP4	☑	
	PP5	☑	
	PP9		☑
FEC code rate	1/5 (=3/15)	☑	☑
	4/15	☑	☑
	1/3 (=5/15)	☑	☑
	2/5 (=6/15)	☑	☑
	7/15	☑	☑
	8/15	☑	☑
	3/5 (=9/15)	☑	☑
	2/3 (=10/15)	☑	☑
	11/15	☑	☑
	3/4	☑	☑

2.1.3.3 DVB-NGH Link budgets

This section presents several satellite link budget analysis for the DVB-NGH service in OFDM mode. The study considers a channalization of 1.7MHz, the use of different MODCODS and two satellite EIRP effective beam levels as to characterize both low and medium power satellites.

2.1.3.3.1 Low power satellite link budgets

The next table shows the main considerations for the link budget analysis using a low power satellite system. These satellites are characterized by an EIRP effective beam level of 63dBW over the region of interest.

Table 7: DVB-NGH link budget analysis for 1.7MHz channel and 63dBW EIRP.

LINK BUDGET DVB-NGH 1,7MHz Channel OFDM-QPSK 63dBW Satellite EIRP Effective beam				
Modulation	OFDM - QPSK	OFDM - QPSK	OFDM - QPSK	OFDM - QPSK
Example Code Rates	1/5 1/3 2/3	1/5 1/3 2/3	1/5 1/3 2/3	1/5 1/3 2/3
OFDM noise bandwidth (MHz)	1,52	1,52	1,52	1,52
UPLINK				
C/(N+I) uplink (dB)	19,5	19,5	19,5	19,5
DOWNLINK				
Rx Terminal ID	Handheld Cat. 3	Portable Cat. 2b	Portable Cat. 2a	Vehicular Cat. 1
Downlink Frequency (GHz)	2,0	2,0	2,0	2,0
Satellite EIRP @ location (dBW)	63,0	63,0	63,0	63,0
Athmospheric atenuation (dB)	0,5	0,5	0,5	0,5
Polarisation losses (dB)	3,0	3,0	3,0	0,0
Free space loss (dB)	190,7	190,7	190,7	190,7
G/T E/T Rx. (dB/K)	**-32,1**	**-29,1**	**-24,9**	**-21,0**
C/N downlink (dB)	-1,8	1,2	5,4	12,3
C/I downlink total (dB)	14,0	14,0	14,0	14,0
C/(N+I) downlink (dB)	-1,9	1,0	4,8	10,1
GLOBAL RESULTS				
C/(N+I) Total (dB)	-1,9	0,9	4,7	9,6

2.1.3.3.1.1 OFDM-QPSK

Three example MODCODs are considered: OFDM-QPSK 1/5, 1/3 and 2/3.

Table 8: DVB-NGH link budget closure for OFDM-QPSK 1/5 at physical layer and 63dBW EIRP.

GLOBAL RESULTS OFDM-QPSK 1/5 1,7 MHz Channel 63dBW Satellite EIRP Effective beam				
Useful bit rate at physical layer (Mbps)	0,46	0,46	0,46	0,46
Modulation	OFDM - QPSK	OFDM - QPSK	OFDM - QPSK	OFDM - QPSK
Code Rate	1/5	1/5	1/5	1/5
C/(N+I) Total (dB)	-1,9	0,9	4,7	9,6
Required C/N at physical layer at BER 10^-5 (dB)	-3,6	-3,6	-3,6	-3,6
Implementation loss in AWGN (dB)	1,1	1,1	1,1	1,1
LOS Margin at Physical Layer wrt AWGN (dB)	0,6	3,4	7,2	12,1

Table 9: DVB-NGH link budget closure for OFDM-QPSK 1/3 at physical layer and 63dBW EIRP.

GLOBAL RESULTS OFDM-QPSK 1/3 1,7 MHz Channel 63dBW Satellite EIRP Effective beam				
Useful bit rate at physical layer (Mbps)	0,77	0,77	0,77	0,77
Modulation	OFDM - QPSK	OFDM - QPSK	OFDM - QPSK	OFDM - QPSK
Code Rate	1/3	1/3	1/3	1/3
C/(N+I) Total (dB)	-1,9	0,9	4,7	9,6
Required C/N at physical layer at BER 10^-5 (dB)	-0,9	-0,9	-0,9	-0,9
Implementation loss in AWGN (dB)	1,1	1,1	1,1	1,1
LOS Margin at Physical Layer wrt AWGN (dB)	-2,1	0,7	4,5	9,4

Table 10: DVB-NGH link budget closure for OFDM-QPSK 2/3 at physical layer and 63dBW EIRP.

GLOBAL RESULTS OFDM-QPSK 2/3 1,7 MHz Channel 63dBW Satellite EIRP Effective beam				
Useful bit rate at physical layer (Mbps)	1,53	1,53	1,53	1,53
Modulation	OFDM - QPSK	OFDM - QPSK	OFDM - QPSK	OFDM - QPSK
Code Rate	2/3	2/3	2/3	2/3
C/(N+I) Total (dB)	-1,9	0,9	4,7	9,6
Required C/N at physical layer at BER 10^-5 (dB)	3,5	3,5	3,5	3,5
Implementation loss in AWGN (dB)	1,1	1,1	1,1	1,1
LOS Margin at Physical Layer wrt AWGN (dB)	-6,5	-3,7	0,1	5,0

2.1.3.3.1.2 OFDM-16QAM

Three example MODCODs are considered: OFDM-16QAM 1/5, 1/3 and 2/3.

Table 11: DVB-NGH link budget closure for OFDM-16QAM 1/5 at physical layer and 63dBW EIRP.

GLOBAL RESULTS OFDM-16QAM 1/5 1,7 MHz Channel 63dBW Satellite EIRP Effective beam				
Useful bit rate at physical layer (Mbps)	2,66	2,66	2,66	2,66
Modulation	OFDM - 16QAM	OFDM - 16QAM	OFDM - 16QAM	OFDM - 16QAM
Code Rate	1/5	1/5	1/5	1/5
C/(N+I) Total (dB)	-1,9	0,9	4,7	9,6
Required C/N at physical layer at BER 10^-5 (dB)	0,7	0,7	0,7	0,7
Implementation loss in AWGN (dB)	1,5	1,5	1,5	1,5
LOS Margin at Physical Layer wrt AWGN (dB)	-4,1	-1,3	2,5	7,4

Table 12: DVB-NGH link budget closure for OFDM-16QAM 1/3 at physical layer and 63dBW EIRP.

GLOBAL RESULTS OFDM-16QAM 1/3 1,7 MHz Channel 63dBW Satellite EIRP Effective beam				
Useful bit rate at physical layer (Mbps)	4,43	4,43	4,43	4,43
Modulation	OFDM - 16QAM	OFDM - 16QAM	OFDM - 16QAM	OFDM - 16QAM
Code Rate	1/3	1/3	1/3	1/3
C/(N+I) Total (dB)	-1,9	0,9	4,7	9,6
Required C/N at physical layer at BER 10^-5 (dB)	3,7	3,7	3,7	3,7
Implementation loss in AWGN (dB)	1,5	1,5	1,5	1,5
LOS Margin at Physical Layer wrt AWGN (dB)	-7,1	-4,3	-0,5	4,4

Table 13: DVB-NGH link budget closure for OFDM-16QAM 2/3 at physical layer and 63dBW EIRP.

GLOBAL RESULTS OFDM-16QAM 2/3 1,7 MHz Channel 63dBW Satellite EIRP Effective beam				
Useful bit rate at physical layer (Mbps)	8,87	8,87	8,87	8,87
Modulation	OFDM - 16QAM	OFDM - 16QAM	OFDM - 16QAM	OFDM - 16QAM
Code Rate	2/3	2/3	2/3	2/3
C/(N+I) Total (dB)	-1,9	0,9	4,7	9,6
Required C/N at physical layer at BER 10^-5 (dB)	9,7	9,7	9,7	9,7
Implementation loss in AWGN (dB)	1,5	1,5	1,5	1,5
LOS Margin at Physical Layer wrt AWGN (dB)	-13,1	-10,3	-6,5	-1,6

2.1.3.3.2 Medium power satellite link budgets

The next table shows the main considerations for the link budget analysis using a medium power satellite system. This satellites are characterized by an EIRP effective beam level of 68dBW over the region of interest.

Table 14: DVB-NGH link budget analysis for 1.7MHz channel and 68dBW EIRP.

LINK BUDGET DVB-NGH 1,7MHz Channel OFDM-QPSK 68dBW Satellite EIRP Effective beam				
Modulation	OFDM - QPSK	OFDM - QPSK	OFDM - QPSK	OFDM - QPSK
Example Code Rates	1/5 1/3 2/3	1/5 1/3 2/3	1/5 1/3 2/3	1/5 1/3 2/3
OFDM noise bandwidth (MHz)	1,52	1,52	1,52	1,52
UPLINK				
C/(N+I) uplink (dB)	19,5	19,5	19,5	19,5
DOWNLINK				
Rx Terminal ID	Handheld Cat. 3	Portable Cat. 2b	Portable Cat. 2a	Vehicular Cat. 1
Downlink Frequency (GHz)	2,0	2,0	2,0	2,0
Satellite EIRP @ location (dBW)	68,0	68,0	68,0	68,0
Athmospheric atenuation (dB)	0,5	0,5	0,5	0,5
Polarisation losses (dB)	3,0	3,0	3,0	0,0
Free space loss (dB)	190,7	190,7	190,7	190,7
G/T E/T Rx. (dB/K)	**-32,1**	**-29,1**	**-24,9**	**-21,0**
C/N downlink (dB)	3,2	6,2	10,4	17,3
C/I downlink total (dB)	14,0	14,0	14,0	14,0
C/(N+I) downlink (dB)	2,9	5,5	8,8	12,3
GLOBAL RESULTS				
C/(N+I) Total (dB)	2,8	5,4	8,5	11,6

2.1.3.3.2.1 OFDM-QPSK

Three example MODCODs are considered: OFDM-QPSK 1/5, 1/3 and 2/3.

Table 15: DVB-NGH link budget closure for OFDM-QPSK 1/5 at physical layer and 68dBW EIRP.

GLOBAL RESULTS OFDM-QPSK 1/5 1,7 MHz Channel 63dBW Satellite EIRP Effective beam				
Useful bit rate at physical layer (Mbps)	0,46	0,46	0,46	0,46
Modulation	OFDM - QPSK	OFDM - QPSK	OFDM - QPSK	OFDM - QPSK
Code Rate	1/5	1/5	1/5	1/5
C/(N+I) Total (dB)	2,8	5,4	8,5	11,6
Required C/N at physical layer at BER 10^-5 (dB)	-3,6	-3,6	-3,6	-3,6
Implementation loss in AWGN (dB)	1,1	1,1	1,1	1,1
LOS Margin at Physical Layer wrt AWGN (dB)	5,3	7,9	11,0	14,1

Table 16: DVB-NGH link budget closure for OFDM-QPSK 1/3 at physical layer and 68dBW EIRP.

GLOBAL RESULTS OFDM-QPSK 1/3 1,7 MHz Channel 63dBW Satellite EIRP Effective beam				
Useful bit rate at physical layer (Mbps)	0,77	0,77	0,77	0,77
Modulation	OFDM - QPSK	OFDM - QPSK	OFDM - QPSK	OFDM - QPSK
Code Rate	1/3	1/3	1/3	1/3
C/(N+I) Total (dB)	2,8	5,4	8,5	11,6
Required C/N at physical layer at BER 10^-5 (dB)	-0,9	-0,9	-0,9	-0,9
Implementation loss in AWGN (dB)	1,1	1,1	1,1	1,1
LOS Margin at Physical Layer wrt AWGN (dB)	2,6	5,2	8,3	11,4

Table 17: DVB-NGH link budget closure for OFDM-QPSK 2/3 at physical layer and 68dBW EIRP.

GLOBAL RESULTS OFDM-QPSK 2/3 1,7 MHz Channel 63dBW Satellite EIRP Effective beam				
Useful bit rate at physical layer (Mbps)	1,53	1,53	1,53	1,53
Modulation	OFDM - QPSK	OFDM - QPSK	OFDM - QPSK	OFDM - QPSK
Code Rate	2/3	2/3	2/3	2/3
C/(N+I) Total (dB)	2,8	5,4	8,5	11,6
Required C/N at physical layer at BER 10^-5 (dB)	3,5	3,5	3,5	3,5
Implementation loss in AWGN (dB)	1,1	1,1	1,1	1,1
LOS Margin at Physical Layer wrt AWGN (dB)	-1,8	0,8	3,9	7,0

2.1.3.3.2.2 OFDM-16QAM

Three example MODCODs are considered: OFDM-16QAM 1/5, 1/3 and 2/3.

Table 18: DVB-NGH link budget closure for OFDM-16QAM 1/5 at physical layer and 68dBW EIRP.

GLOBAL RESULTS OFDM-16QAM 1/5 1,7 MHz Channel 63dBW Satellite EIRP Effective beam				
Useful bit rate at physical layer (Mbps)	2,66	2,66	2,66	2,66
Modulation	OFDM - 16QAM	OFDM - 16QAM	OFDM - 16QAM	OFDM - 16QAM
Code Rate	1/5	1/5	1/5	1/5
C/(N+I) Total (dB)	2,8	5,4	8,5	11,6
Required C/N at physical layer at BER 10^-5 (dB)	0,7	0,7	0,7	0,7
Implementation loss in AWGN (dB)	1,5	1,5	1,5	1,5
LOS Margin at Physical Layer wrt AWGN (dB)	0,6	3,2	6,3	9,4

Table 19: DVB-NGH link budget closure for OFDM-16QAM 1/3 at physical layer and 68dBW EIRP.

GLOBAL RESULTS OFDM-16QAM 1/3 1,7 MHz Channel 63dBW Satellite EIRP Effective beam				
Useful bit rate at physical layer (Mbps)	4,43	4,43	4,43	4,43
Modulation	OFDM - 16QAM	OFDM - 16QAM	OFDM - 16QAM	OFDM - 16QAM
Code Rate	1/3	1/3	1/3	1/3
C/(N+I) Total (dB)	2,8	5,4	8,5	11,6
Required C/N at physical layer at BER 10^-5 (dB)	3,7	3,7	3,7	3,7
Implementation loss in AWGN (dB)	1,5	1,5	1,5	1,5
LOS Margin at Physical Layer wrt AWGN (dB)	-2,4	0,2	3,3	6,4

Table 20: DVB-NGH link budget closure for OFDM-16QAM 2/3 at physical layer and 68dBW EIRP.

GLOBAL RESULTS OFDM-16QAM 2/3 1,7 MHz Channel 63dBW Satellite EIRP Effective beam				
Useful bit rate at physical layer (Mbps)	8,87	8,87	8,87	8,87
Modulation	OFDM - 16QAM	OFDM - 16QAM	OFDM - 16QAM	OFDM - 16QAM
Code Rate	2/3	2/3	2/3	2/3
C/(N+I) Total (dB)	2,8	5,4	8,5	11,6
Required C/N at physical layer at BER 10^-5 (dB)	9,7	9,7	9,7	9,7
Implementation loss in AWGN (dB)	1,5	1,5	1,5	1,5
LOS Margin at Physical Layer wrt AWGN (dB)	-8,4	-5,8	-2,7	0,4

2.2 Satellite radio channels

2.2.1 Description of SISO LMS propagation channel provided for DVB-NGH standardization

2.2.1.1 CNES LMS_PROPA DLL

Inherited from previous works carried out within the framework of TM-SSP group, a software implementating the so-called "3-state Markov chain" model has been proposed to DVB-NGH standardisation working group. This narrowband generative empirical model was developed during the 90's based on S-band measurements using an aircraft to emulate a satellite and a vehicular receive antenna. The experimental dataset and the model are described in details in [44] and [45].

The input parameters of this generative model are:

- Initial state vector: [W]
- Transition matrix: [P]
- Correlation distance of the shadowing: d_{corr}
- Lognormal parameters (for each state): α and ψ
- Diffuse component power (for each state): MP
- Frame length (minimum state length): L_{frame}
- State Transition length: L_{trans}
- Doppler shift of the satellite direct path (normalized to maximum Doppler): $f_{d,direct}$ (default value = 0.7)

For a GEO satellite at S-band in various environments, the CNES software uses the input parameters values shown on Table 21 (inferred from [44] and [45]).

Despite they have been extensively used in the last two decades, these input parameters datasets probably contain small biases due to inaccurate Line-Of-Sight level calibration of experimental datasets. This default of the current model can be put in evidence when comparing data synthesised for a 40° elevation angle and for other elevation angles (corresponding input parameters also available in [44] and [45]) for a given environment. Figure 7 illustrates this default for suburban environment: the figure on the left side shows the cumulative distribution of fading synthesised with the model used by TM-SSP and proposed to the DVB-NGH group. Depending on the target coverage, some inconsistencies can appear when comparing different elevation angles. For a given environment and a given elevation angle (40° being the one of interest for DVB-NGH), it can be solved simply by assessing on a subjective basis a single offset to apply to α, ψ and MP parameters. The improvement due to such a calibration can be shown on the right side of Figure 7. In this particular case, a 0.8 dB offset should be subtracted to the 40° input parameters to improve the model physical soundness.

Nevertheless, such a calibration is quite subjective. Moreover, S-band input parameters appearing in [44] and [45] are generally based on short distances (a few hundreds of meters) datasets depending on the considered environment. Consequently, for high coverage system (typically higher than 90%), other sources of inaccuracy can impact the 3-state model. Therefore, the calibration default presented here is maybe not so much critical.

Table 21: Satellite channel model input parameters (top: Direct component and multipath parameters for the 3-state Markov model, bottom: other input parameters).

Environment	State 1: LOS			State 2: Shadowing			State 3: Deep shadow		
	α (dB)	ψ (dB)	MP (dB)	α (dB)	ψ (dB)	MP (dB)	α (dB)	ψ (dB)	MP (dB)
Open	0.1	0.37	-22.0	-1.0	0.5	-22.0	-2.25	0.13	-21.2
Suburban	-1.0	0.5	-13.0	-3.7	0.98	-12.2	-15.0	5.9	-13.0
Intermediate Tree-Shadow	-0.4	1.5	-13.2	-8.2	3.9	-12.7	-17.0	3.14	-10.0
Heavy Tree-Shadow	-	-	-	-10.1	2.25	-10.0	-19.0	4.0	-10.0

Environment	[P]			[W]	d_{corr} (m)	L_{frame} (m)	L_{trans} (m)
Open	0.9530	0.0431	0.0039	0.5	2.5	8.9	12.4
	0.0515	0.9347	0.0138	0.375		7.5	
	0.0334	0.0238	0.9428	0.125		4.0[1]	
Suburban	0.8177	0.1715	0.0108	0.4545	1.7	5.2	2.2
	0.1544	0.7997	0.0459	0.4545		3.7	
	0.1400	0.1433	0.7167	0.091		3.0[1]	
Intermediate Tree-Shadow	0.7193	0.1865	0.0942	0.3929	1.5	6.3	2.6
	0.1848	0.7269	0.0883	0.3571		6.3	
	0.1771	0.0971	0.7258	0.25		4.5	
Heavy Tree-Shadow	0.7792	0.0452	0.1756	0	1.7	-	3.5
	0	0.9259	0.0741	0.5		4.8	
	0	0.0741	0.9259	0.5		4.5	

[1] These values have been extrapolated since they are not explicitly given in [44] or [45].

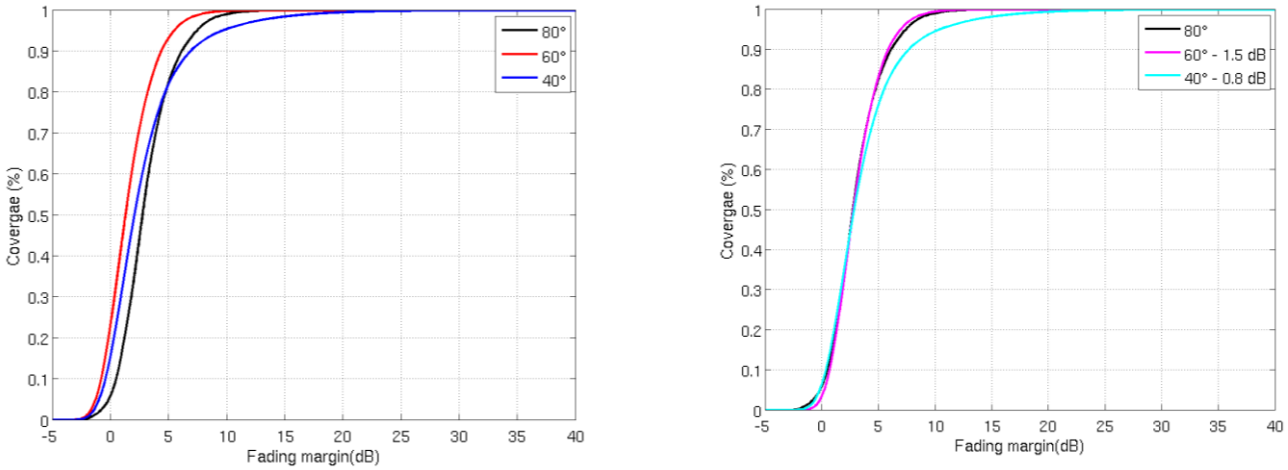

Figure 7: Cumulative distribution of fading margin relative to LOS for suburban environment left: initial input datasets, right: subjective calibration of input datasets.

The CNES LMS_PROPA DLL implements the model version directly inferred from [44] and [45] (no calibration). The DLL implementation was selected to enable users to include it into a more complete simulation chain since it generates LMS propagation channel series sample after sample. At the opposite, the ESA MIMO_LMS software presented hereafter generates a file corresponding to a given simulated distance. Then this file must be read by the air interface simulation chain.

In the CNES LMS_PROPA DLL, small scale fading is synthesized using the Zheng-Xiao model described in [50]. It corresponds to a classical Doppler spectrum assumption that can be questioned in the LMS context. However, very few alternatives have been published and can be considered as consolidated. At least for tree shadowed environments, CNES past activities have shown that such a typical terrestrial assumption is quite realistic even for a GEO satellite link at S-band.

2.2.1.2 ESA MIMO_LMS executable

This second generative empirical model has been proposed to DVB-NGH group by ESA to address specifically LMS MIMO software simulations [47]. Nevertheless, this MIMO model relies on a SISO model corresponding to a recent evolution of the 3-state Markov chain model developed from the same S-band experimental datasets: the enhanced 2-state approach (detailed in [46]). This new approach actually gave birth to two models: one based on a Markov chain approach (like the previous 3-state model) and one based on a semi-Markov chain approach. The latter seems to be slightly more realistic than the first one, but both 2-state models bring improvement when compared with the 3-state Markov chain approach. In the reference document [48] provided by ESA with the MIMO_LMS software, it is mentioned that the embedded SISO model is a 3-state model, but it refers to [49] where it is clearly written that the SISO model is the enhanced 2-state Markov chain model.

Consequently, in the framework of DVB-NGH activities, the MIMO_LMS software could be used to address not only MIMO simulations but also SISO LMS simulations as an alternative to the 3-state model used during the last two decades. Nevertheless, a significant step forward would be the possibility to perform LMS channel simulations using the enhanced 2-state semi-Markov approach that is (probably) not included yet in MIMO_LMS.

Being based on the same experimental datasets as the 3-state model, this new model fully parameterized in [46] should suffer from quite the same inaccuracies due to short distances of measurement routes.

2.2.2 Link with other models detailed for MIMO

These two models (corresponding to LMS_PROPA and MIMO_LMS softwares) are mentioned and compared with other available models in the document ”TR 3.1 - MIMO CHANNEL MODELS”. Other available models are in particular:

- A physical-statistical generative model suitable for user-defined tree shadowed environement simulations
- Another enhanced 2-state Marko/semi-Markov model developed from CNES experimental datasets.

2.3 Air interface technologies

2.3.1 SC-OFDM waveform

2.3.1.1 Introduction

Satellite systems are due to cope with specific propagation conditions but also stringent technological constraints related to the satellite carrier itself. On top of those lies the power amplifier (PA) that must bring the signal to be transmitted at a level compatible with the receiver sensibility over large areas. In order to guarantee the durability of the satellite, it is critical to keep low the power consumption of the system, and thus to optimize the amplifier power efficiency, i.e. to drive the amplifier close to saturation. Single carrier (SC) modulations also described as time division multiplexing (TDM) modulations have long been the reference scheme for satellite transmissions, e.g. such as in the DVB-S2 system developed in 2003 [29], for their suitability to achieve low power fluctuations compatible with good power efficiency. However, the orthogonal frequency division multiplexing (OFDM) modulation is taking over single carrier schemes thanks to a better flexibility and a comparatively lower complexity when it comes to compensate for high channel degradations. OFDM is now used in many systems such as 3GPP/LTE cellular networks, IEEE 802.11 WiFi solutions, IEEE 802.16 WiMax systems, etc. Dealing with broadcast, the DVB-SH (Satellite to Handhelds) standard developed in 2007 [35] specifies 2 modes of operation, one OFDM mode allowing the deployment of single frequency networks (SFN) on both the terrestrial and satellite links and a second mode with TDM on the satellite link and OFDM on the terrestrial link for multiple frequency networks (MFN).

Despite its obvious advantages, the OFDM modulation is not perfectly well suited for satellite transmissions. Indeed, the more sub-carriers are added together the more the signal behaves like a Gaussian noise with large power fluctuations. The power amplifier shall either be operated in a linear mode far from saturation and thus with a poor power efficiency or in a clipping mode at the cost of significant performance degradations due to saturation. This weakness of OFDM is well known and several means have been studied to reduce its power fluctuations such as the tone reservation (TR) or active constellation extension (ACE) techniques specified in the DVB-T2 standard [19]. However, as it will be shown in the sequel, the gain of these techniques appears to be marginal in the context of satellite transmissions. More recently, the 3GPP selected the single carrier-frequency division multiple access (SC-FDMA) technique for the uplink of LTE networks [21] in the purpose of reducing the power consumption of handled devices. The SC-FDMA scheme is actually a derivation of the orthogonal frequency division multiple access (OFDMA) where each user is allocated with a given sub-set of contiguous OFDM sub-carriers. But unlike in OFDMA, the symbols to be transmitted are precoded in the frequency domain by means of a discrete Fourier transform (DFT) prior OFDM modulation. It is thus possible to benefit from the good PAPR properties of the original symbols to save power in the amplification stage.

It is on the basis of these obvious similarities with the satellite context that the SC-FDMA was proposed as a candidate waveform for the DVB-NGH hybrid profile. A broadcast signal is inherently transmitted towards all receivers. The SC-OFDM terminology was selected to identify the specific case where the whole bandwidth is allocated to all users. As shown in this chapter, the SC-OFDM modulation is clearly suitable

for satellite transmissions. It was adopted in the DVB-NGH standard thanks to its ability to preserve a lot of commonalities with pure OFDM while benefiting from the low power fluctuations of single carrier (SC) signals.

The purpose of this chapter is to introduce the principle of the SC-OFDM modulation and to characterize its properties and performance in the particular case of the DVB-NGH hybrid profile. The rest of the chapter is structured as follows. Section 2.3.1.2 briefly compares the merits of the different waveforms used for satellite transmissions. Section 2.3.1.3 summarizes the specifications of the SC-OFDM modes in the DVB-NGH standard. The last section is dedicated to the analysis of the performances of the SC-OFDM modulation.

2.3.1.2 Combining the TDM and OFDM strengths

TDM modulations combine low power fluctuations with reasonable receiver complexity using frequency domain equalization (FDE). But SC-FDE schemes do not allow inserting pilot within data in the frequency domain, and present some loss in spectral efficiency due to the roll-off implementation. Moreover, it is generally needed to double the sampling frequency at the receiver for practical implementation of the demodulation. The OFDM can actually be interpreted as a derivation of the SC-FDE approach where it becomes possible to allocate data in both the time and frequency domains and where the roll-off can be set to zero. However, this improved flexibility comes at the expense of a reduced peak to average power ratio (PAPR, see Section 2.3.1.4.2). The SC-OFDM modulation actually combines the advantages of the two worlds, the low power fluctuations of the SC modulation and the flexibility and high spectral efficiency of the OFDM waveform. As shown on Figure 8, this is obtained by generating the frequency domain samples of the OFDM modulation by means of a discrete Fourier transform (DFT) applied onto preferably constant amplitude samples. It is thus possible to recover the low PAPR properties of the original symbols in the time domain after OFDM modulation. In the case of the SC-FDE technique, the translation in the frequency domain at the receiver is used to perform the equalization. Similarly for the SC-OFDM, the translation in the frequency domain at the transmitter can be used to perform the sub-carrier mapping of user data and reference pilot just like in the OFDM modulation. Moreover, null sub-carriers can (must) be inserted at the edges of the frequency multiplex in order to perform a zero roll-off oversampling.

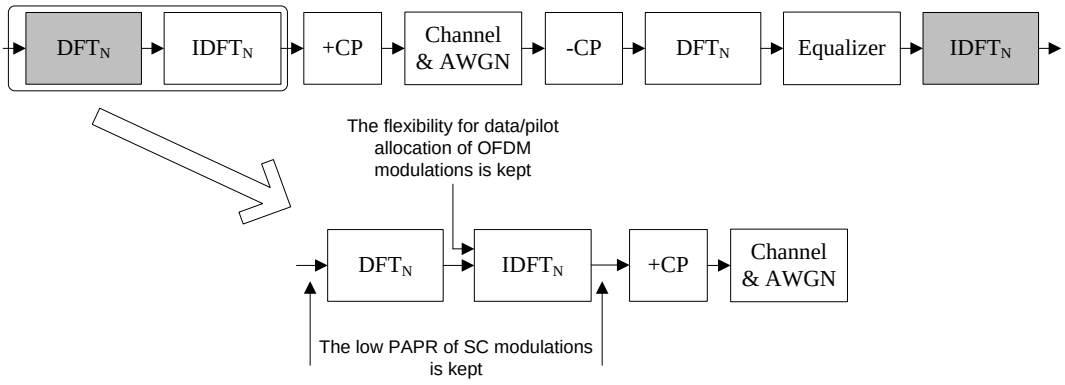

Figure 8: From OFDM to SC-OFDM.

Figure 9 illustrates the relationships between the SC-OFDM, OFDM and SC-FDE techniques. As shown on this figure, the first DFT at the transmitter can be actually be computed over M samples where $M \leq N$. The result of the M-point DFT is then mapped in the central part of the OFDM multiplex padding the unallocated sub-carriers with zeros. The resulting signal is simply the zero roll-off oversampled version of the original M-sample signal, thus leading to the preservation of the original low PAPR. As explained in the introductory

section, the name SC-OFDM was derived from the SC-FDMA terminology used in the 3GPP/LTE system where this technique is used in combination to frequency division multiple access in uplink. In the present case, all users can demodulate the signal that is transmitted over the whole bandwidth. Other approaches are possible: it is possible for instance to alternatively insert *m*-1 null sub-carrier between each sample obtained at the output of the *M*-point DFT. In this case, the resulting signal is periodic as *m* replica of the original signal, thus keeping its low PAPR property. Other alternatives have been devised to define multiple access schemes in cellular networks (IFDMA, MC-CDMA, SS-MC-MA, etc). The computation of the first DFT can also be interpreted as a spreading on the symbols to be transmitted. For that reason, SC-OFDM is also known as the DFT-spread OFDM modulation.

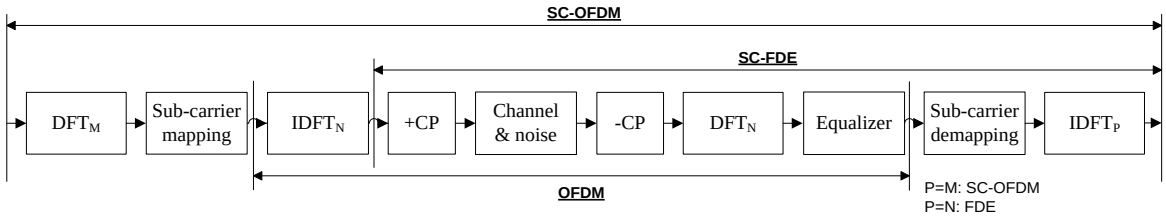

Figure 9: Relationships between the OFDM, SC-FDE and SC-OFDM modulations.

The SC-OFDM modulation can be implemented either in the time-domain (IFDMA) or in the frequency-domain (DFT-spread OFDM). The frequency domain implementation is generally preferred, especially at the receiver. The frequency domain implementation of the SC-OFDM transmitter is described in Figure 10. It mainly consists in adding a spreading stage, i.e. a DFT of size *M*, to the OFDM transmitter. As already expressed, the SC-OFDM signal can be interpreted as an interpolated version of the signal prior to spreading, the interpolation ratio being equal to *N/M*. The interpolation filter being performed by DFT/IDFT is about as sharp as possible. Therefore, the SC-OFDM signal is roughly equivalent to a TDM signal with a zero roll-off.

Figure 10: SC-OFDM transmitter.

Figure 11 depicts the general architecture of the SC-OFDM receiver in the frequency domain. It clearly appears that the SC-OFDM receiver shows a lot of commonalities with the OFDM receiver. There is only one new function, the de-spreading DFT, and the other modules are only slightly modified with a reasonable increase of complexity. As an illustration, Table 22 compares a possible implementation of the different key functionalities in a multi-carrier receiver for both the OFDM and SC-OFDM modulations. It can be noticed that the functions are very similar except for the occurrence of a summation on the individual OFDM terms when dealing with SC-OFDM. This similarity has actually been one of the rationales for the adoption of the SC-OFDM modulation along with pure OFDM for the satellite segment of the DVB-NGH standard.

Table 22: Complexity of SC-OFDM versus OFDM.

	SC-OFDM	OFDM
Demodulation	$r_k'' = DFT\{r_k'\}$	
Equalization (MMSE)	$\hat{s}_k = \frac{H_k^*}{\lvert H_k \rvert^2 + \sigma^2} r_k''$	
De-spreading	$\hat{x}_n' = DFT\{\hat{s}_k\}$	$\hat{x}_n' = \hat{s}_n$
Normalization	$\hat{x}_n = \hat{x}_n' / \tilde{\alpha}\,,\ \tilde{\alpha} = \frac{1}{M}\sum_{k=0}^{M-1} \frac{\lvert H_k \rvert^2}{\lvert H_k \rvert^2 + \sigma^2}$	$\hat{x}_n = \hat{x}_n' / \tilde{\alpha}_n\,,\ \tilde{\alpha}_n = \frac{\lvert H_n \rvert^2}{\lvert H_n \rvert^2 + \sigma^2}$
LLR weighting	$\Gamma_n^j = \frac{4\sum_{k=0}^{M-1} \lvert H_k \rvert^2}{\sigma^2} LLR_n^j$	$\Gamma_n^j = \frac{4\lvert H_k \rvert^2}{\sigma^2} LLR_n^j$

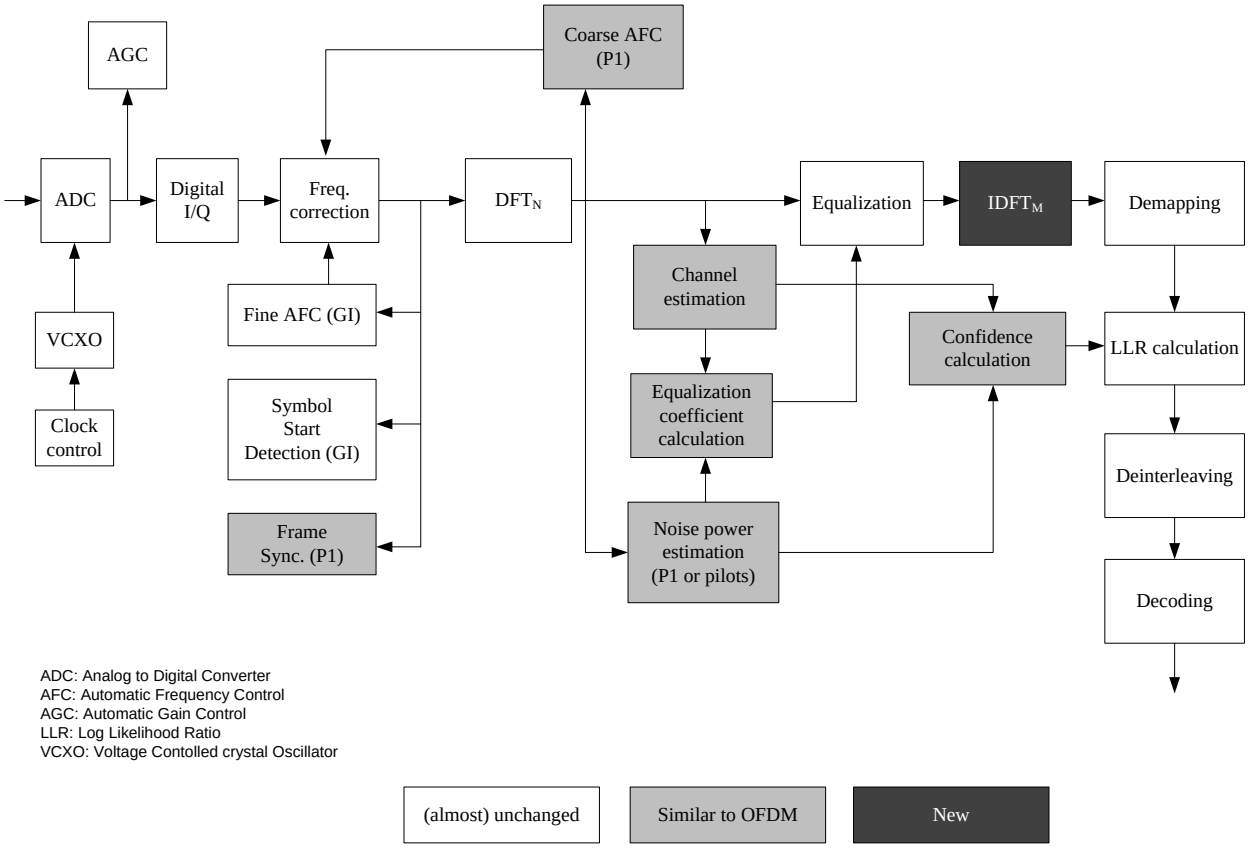

Figure 11: SC-OFDM receiver.

2.3.1.3 SC-OFDM modulation in DVB-NGH

2.3.1.3.1 System Parameters

The DVB-NGH standard specifies a mandatory sheer terrestrial profile (also called core or base profile) and an optional terrestrial/satellite hybrid profile. The hybrid profile is composed of a main component coming from the terrestrial network and an additional component coming from a satellite. The SC-OFDM modulation has been selected with OFDM as the two reference waveforms for the hybrid profile. Besides defining the transmitted waveforms, the hybrid profile also defines the mechanisms to receive two waveforms simultaneously and combine their outputs into a single stream. The hybrid waveform can be transparent to the receiver, when an identical signal is transmitted by the terrestrial and satellite transmitters (SFN mode), or two different waveforms (MFN mode) can be used. The following hybrid modes are identified:

- **SFN in OFDM**: In this case the OFDM satellite parameter set is applicable to both the terrestrial and satellite components.
- **MFN in OFDM**: In this case the terrestrial component is built according to the Core Profile while the satellite component is set according to the OFDM hybrid profile.
- **SFN in SC-OFDM**: This mode concerns only the case of terrestrial gap fillers that amplify the signal from the satellite (in the same frequency). The SC-OFDM satellite component setting is applicable to both the terrestrial and satellite components.
- **MFN in SC-OFDM on the satellite component and OFDM on the terrestrial component**: The terrestrial component is set according to the core profile while the satellite component is set according to the SC-OFDM mode of the hybrid profile.

The satellite component of the hybrid profile is defined for two bandwidths, 2.5 and 5 MHz for a transmission in the L and S-bands. Table 23 describes the main system parameters defined for the SC-OFDM satellite mode.

Table 23: Main system parameters for SC-OFDM transmissions in DVB-NGH.

Bandwidth	2.5 MHz	5 MHz
Sampling Freq.	20/7 MHz	40/7 MHz
FFT Size (*N*)	512, 1024	512, 1024 and 2048
Guard Interval	1/16 and 1/32 (w.r.t. to *N*)	
Constellation	QPSK and 16QAM	

2.3.1.3.2 Pilot Pattern

One strong advantage of OFDM is the possibility to use pilots scattered in the time and frequency domains, a key feature when it comes to estimate the channel at high speeds, i.e. for large Doppler values. As an illustration, Figure 12 depicts the PP1 pilot scheme of the DVB-T2 standard. Note that DVB-T2 specifies 8 different pilot patterns, where PP1 already used in DVB-T offers a good compromise between Doppler and long echoes robustness (see Table 24).

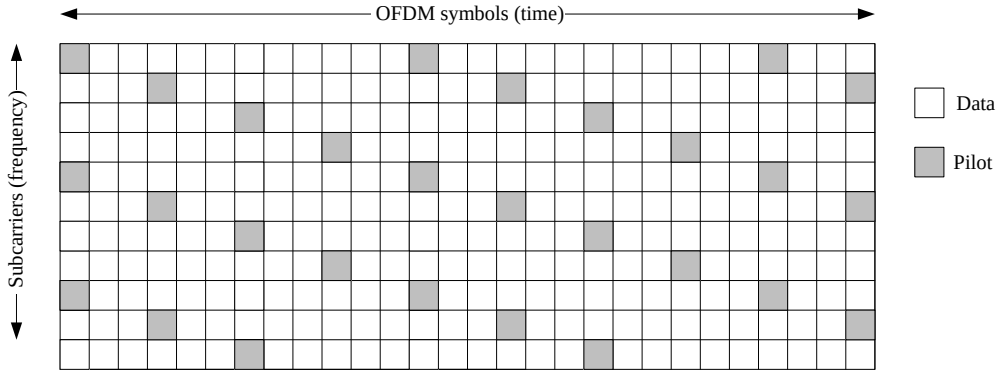

Figure 12: DVB-T2 PP1 pilot pattern.

The main issue is that a pilot pattern such as the one on Figure 12 cannot be multiplexed with SC-OFDM data without completely degrading the PAPR structure of the transmitted signal. In such a case, the complementary cumulative distribution function (CCDF) of the transmitted signal amplitude is actually similar to the one of an OFDM signal. To solve this issue, the 3GPP/LTE body selected for the uplink a pilot pattern similar to the one depicted on Figure 13 (see 3GPP/LTE TS 36.211 [21]).

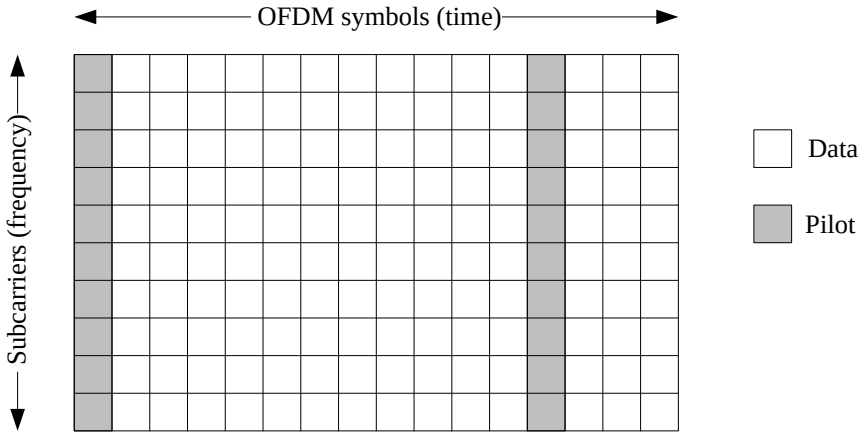

Figure 13: LTE-like pilot structure for SC-OFDM.

According to the 3GPP/LTE approach, a complete SC-OFDM symbol (i.e. all the subcarriers), referenced as a pilot symbol, is constituted solely by pilots and is dedicated to channel estimation and synchronization purposes. Such a symbol is regularly inserted in the frame (twice in each 1ms sub-frame made of 14 SC-OFDM symbols). In this case, a classical way of performing channel estimation is represented on Figure 14. The channel is estimated at the pilot positions (cells in the DVB terminology), then the noise level is reduced by means of a frequency domain smoothing such as a Wiener filter, and finally the channel is estimated at all positions by performing a time interpolation between two pilot symbols. The 3GPP/LTE scheme shows its limits when it comes to implement time interpolation. In order to maximize the user data throughput, one must limit the number of pilot symbols inserted among data cells. For example, in DVB-T2, the pilot insertion rate per sub-carrier depicted in Figure 12 is 1/12. If one wants to keep the same throughput as in the LTE approach, it implies that a full pilot symbol shall be inserted every 12 OFDM symbols. This limits the capability of the system to follow the channel variations of the signal for example due to velocity. According to the Nyquist theorem, if the OFDM rate is $1/T$, a bound on the maximum acceptable Doppler frequency is equal to:

$$f_{\max} = \frac{1}{2D_Y T} = \frac{1}{24T} \tag{14}$$

where D_Y (= 12) is the number of symbols forming one scattered pilot sequence. The bound is actually even lower when considering practical algorithms to perform time interpolation with a reasonable complexity. It must be understood that this bound is due to the pilot structure itself (Figure 13), and not to the related estimation method. With the DVB-T2 scattered pilots showed in Figure 12, the bound falls down to $(8T)^{-1}$. The other OFDM pilot patterns specified in the DVB-T2 standard are compared in Table 24.

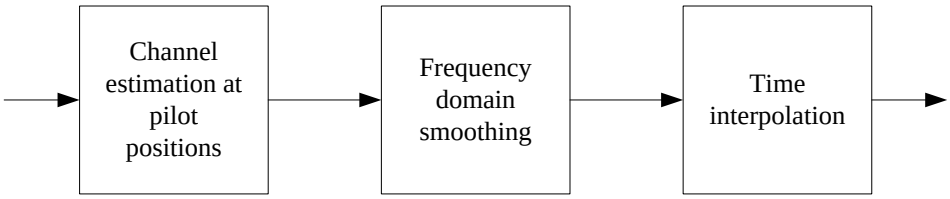

Figure 14: Typical channel estimation for multi-carrier modulations (OFDM and SC-OFDM).

The SC-OFDM mode of the NGH hybrid profile specifies a new pilot pattern (defined as PP9) which divides by two the bound of Eq. (14) while preserving the low PAPR structure of SC-OFDM. Typically, Zadoff-Chu (ZC) sequences [22] are used as pilot patterns, due to their low PAPR and their good orthogonality and correlation properties. ZC sequences are constant amplitude zero autocorrelation (CAZAC) sequences, both in the time and frequency domains. Roughly, the generation of the pilot and data structure can be summarized in three steps:

- In the last SC-OFDM symbol of each NGH data section made of 6 symbols (see Figure 16), half of the subcarriers are allocated to DFT-spread data, while the other half of subcarriers convey pilots (see Figure 15). Data and pilots multiplexed in the frequency domain.
- For the pilot subcarriers, a constant amplitude sequence such that its DFT counterpart (in the time domain) has also fixed amplitudes is used. If L denotes the ZC sequence length ($L = M/2$), then the complex value at each position k of each p-root ZC sequence with integer shift l is (the size L of the ZC sequence is even here):

$$x_k = e^{-2j\frac{\pi}{L}\left(p\frac{k^2}{2}+lk\right)}. \tag{15}$$

  As only one sequence is needed for broadcasting, the index p is set to one ($p = 1$) and the shift l to zero ($l = 0$).
- This Zadoff-Chu pilot sequence is modified by adding a half period shift:

$$x_k = e^{-2j\frac{\pi}{L}\left(\frac{k^2}{2}+0.5k\right)}. \tag{16}$$

Constant amplitude should be understood as evaluated on a non-oversampled ZC sequence. After oversampling (OFDM modulation and of digital to analog conversion), the ZC sequence is not constant amplitude, but has very low envelope fluctuations, lower than the fluctuations of a typical TDM QPSK sequence.

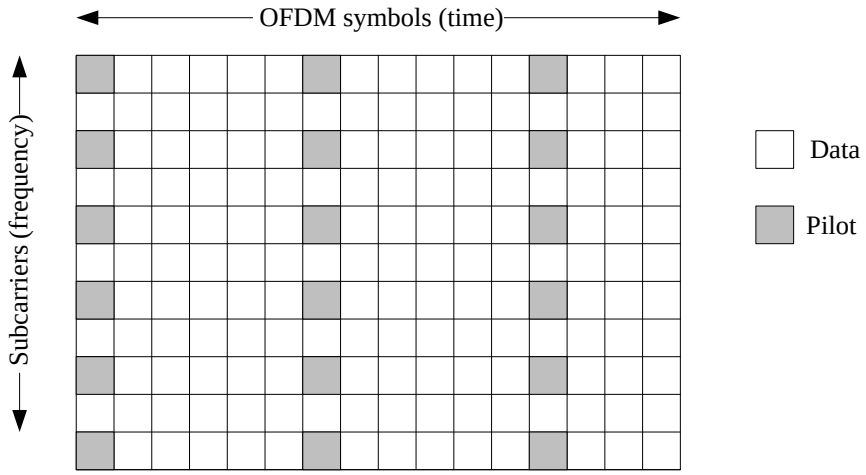

Figure 15: NGH pilot structure for SC-OFDM.

The introduction of the fractional time shift is justified as follows: the global signal, in frequency or time dimensions, corresponds to the sum of two signals, data and pilots. As the interpolation is a linear process, the global interpolated signal corresponds also to the sum of two signals: the interpolated data signals and the interpolated pilot signals. For the data in the time domain, if no interpolation is performed and if a x-PSK constellation is used, a constant amplitude is obtained every sample period, and the maximum peaks after interpolation are placed just in-between these time instants. The same phenomenon occurs with the classical Zadoff-Chu sequence. Therefore, in this case, we add two signals, the peaks of which are placed at the same positions. By time shifting the Zadoff-Chu sequence of half a sampling period, the peaks of each signal are now interleaved. This implies that the peaks of the global signal, sum of both, are reduced.

If a non constant constellation is used, e.g. 16QAM, the amplitude is no longer constant every sample period. However, the peaks will still be placed at the same positions, i.e. just in-between these time instants, and the peaks of the global signal will still be reduced by modifying the original ZC pilot sequence.

Table 24 lists the different pilot patterns: PP1 to PP7 for OFDM waveform, PP9 for the SC-OFDM waveform. When comparing the SC-OFDM pattern PP9 to the terrestrial one, It can be noticed that large Dy values decrease the Doppler performance. However, it can be noted that:

- The lower D_X values improve the smoothing filter performance and then decreases the noise on the channel estimates.
- The DFT size is generally lower for the satellite component, which will improve Doppler performance.
- As the satellite channel is single path, the use of an Automatic Frequency Control (AFC) improves Doppler performance.

Table 24: Parameters defining the scattered pilot patterns.

Pilot pattern	Separation of pilot bearing carriers (D_X)	Number of symbols forming one scattered pilot sequence (D_Y)
PP1	3	4
PP2	6	2
PP3	6	4
PP4	12	2
PP5	12	4
PP6	24	2
PP7	24	4
PP9	2	6

In accordance with this new pilot scheme, the DVB-NGH specifies a specific frame structure for the hybrid profile (see Figure 16). At the top level, the frame structure is made of super-frames, which are divided into NGH-frames that contain data sections made of 6 consecutive SC-OFDM symbols. As shown on Figure 16, the last symbol of each data section is a PP9 pilot pattern as described above. Note that this structure is typical of the SC-OFDM satellite link. The frame structure for the core profile remains similar to the DVB-T2 structure.

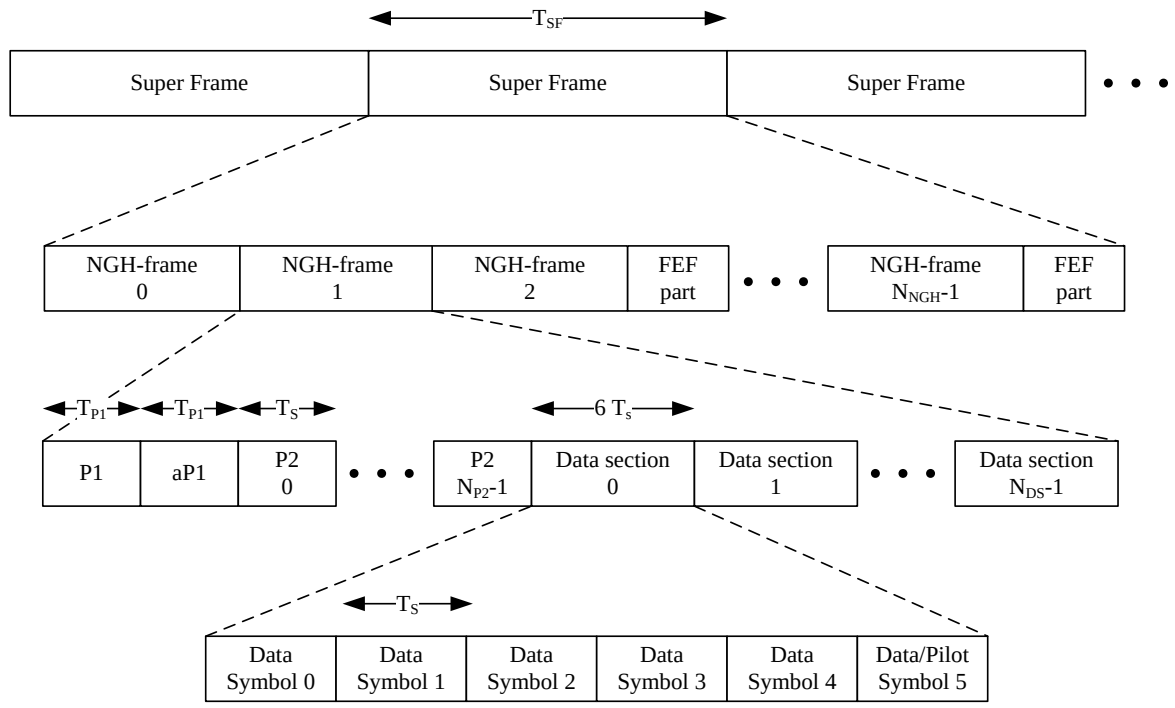

Figure 16: The DVB-NGH frame structure of the hybrid terrestrial-satellite profile.

2.3.1.3.3 MIMO

With an increasing pressure on both the frequencies (analog switch off and digital dividend/digital switch over) and the bandwidth requirements, it is critical to take the most of the available spectrum. Just like most of the recent wireless systems, the DVB-NGH system relies on multi-antenna schemes to either improve the robustness (spatial diversity) or to increase the capacity (spatial multiplexing) of the broadcasting transmissions. The DVB-NGH standard specifies two spatial diversity schemes, a modified Alamouti code and an enhanced SFN solution (the so-called called rate 1 schemes). These two schemes are actually part of the core profile along with SISO for sheer terrestrial transmissions. Spatial multiplexing schemes called rate 2 schemes in DVB-NGH are specified in an optional MIMO profile dedicated to the core profile. In addition, the DVB-NGH specifies a 2×2 enhanced spatial multiplexing (eSM) precoding with an optional phase hopping (PH). In parallel of these schemes dedicated to sheer terrestrial transmissions, the DVB-NGH standard also includes the so-called hybrid MIMO profile that has been devised specifically to facilitate the use of MIMO on the terrestrial and/or satellite elements within a hybrid transmission scenario. This profile encompasses two branches described hereunder.

2.3.1.3.3.1 Hybrid MIMO MFN

The hybrid MIMO MFN scenario describes the case where the satellite and terrestrial parts of the transmission are on different carrier frequencies and do not necessarily share any common frame or symbol timing at the physical layer. At least one of the transmission elements (i.e. terrestrial or satellite) must be made using multiple antennas; otherwise the use case lies within the hybrid profile, not the hybrid MIMO profile. Dealing with the single MFN mode implying SC-OFDM (terrestrial component set according to the core profile and a satellite component in SC-OFDM mode), three MIMO configurations can be considered:

- The terrestrial component operates in MIMO according to any scheme from the MIMO profile while the SC-OFDM transmission occurs in SISO.
- The terrestrial component operates in SISO according to the base profile while the SC-OFDM transmission occurs in MIMO using a basic Spatial Multiplexing (SM) scheme neither precoding nor phase hopping).
- Both links operate in MIMO, where the terrestrial component operates in MIMO according to any scheme from the MIMO profile while the satellite link operates in SM mode.

The MIMO SM of the hybrid MIMO profile processing consists in transmitting cell pairs (f_{2i}, f_{2i+1}) on the same SC-OFDM symbol and carrier from Tx-1 and Tx-2 respectively:

$$\begin{pmatrix} g_{2i} \\ g_{2i+1} \end{pmatrix} = \begin{pmatrix} f_{2i} \\ f_{2i+1} \end{pmatrix}, \; i = 0,1,\ldots, N_{cells}/2-1, \tag{17}$$

where i is the index of the cell pair within the FEC block and N_{cells} is the number of cells per FEC block. The insertion of pilots is modified in order to allow for the channel estimation on each transmitter-receiver path. The frequency domain implementation of SC-OFDM makes the SM decoding very simple.

2.3.1.3.3.2 Hybrid MIMO SFN

The hybrid MIMO SFN describes the case where the satellite and terrestrial parts of the transmission use the same carrier frequency and radiate synchronized signals intended to create an effective SFN. SC-OFDM is not an option for the hybrid MIMO SFN profile where a synchronized effective SFN transmission can only exist in OFDM mode (terrestrial emitters other than gap fillers only implement OFDM).

2.3.1.4 Performance evaluation

The knowledge gathered so far on the SC-OFDM technique has been obtained in the context of broadband cellular networks (SC-FDMA for LTE/UL). It was thus required to check the suitability of the SC-OFDM modulation for satellite broadcasting. In that purpose, the performances of the SC-OFDM modulation have been thoroughly evaluated by means of computer simulations. This section provides key performance related to the use of SC-OFDM in a satellite transmission context.

2.3.1.4.1 Power amplifier characterization

As previously mentioned, the SC-OFDM was designed to benefit from reduced power fluctuations in comparison to OFDM while keeping the same flexibility. Variation in the amplitude is actually an issue when dealing with power amplification (PA). Basically, a PA amplifies the amplitude of the incoming signal so as to bring its power level to a value compatible with the transmission requirements (coverage, receiver sensibility). A perfect PA provides a linear gain whatever the level of the incoming signal. Practically, a PA can only amplify signal up to a maximum value called the saturation amplitude $v_{\mathrm{IN(OUT),Sat}}$. A still ideal but more realistic model is the ideal clipper: all peaks above a certain saturation level are clipped, and all the others remain unchanged (Figure 17, black solid line curve). It is common to characterize the PA by its AM/AM characteristic, giving the output amplitude $|v_{\mathrm{OUT}}|$ as a function of the input amplitude $|v_{\mathrm{IN}}|$. In the case of the ideal clipper, the AM/AM response is defined as:

$$\frac{v_{\mathrm{OUT}}}{v_{\mathrm{OUT,Sat}}} = \begin{cases} \dfrac{v_{\mathrm{IN}}}{v_{\mathrm{IN,Sat}}}, & |v_{\mathrm{IN}}| \le v_{\mathrm{IN,Sat}} \\ 1, \text{ otherwise} \end{cases} \tag{18}$$

And the gain of the PA in the linear region is given by $G_1 = v_{\mathrm{OUT,Sat}} / v_{\mathrm{IN,Sat}}$. In practice, PA are not perfectly linear but show a power response like the ones depicted on Figure 17 obtained with the well know Rapp model [16]. The impact of the fluctuations in the signal amplitude appears clearly on Figure 17. If the amplitude of the incoming signal falls in the saturation region, then the output signal will be clipped leading to degradations both in-band with the introduction of noise but also out-of-band with unwanted emissions immediately outside the assigned channel bandwidth (shoulders).

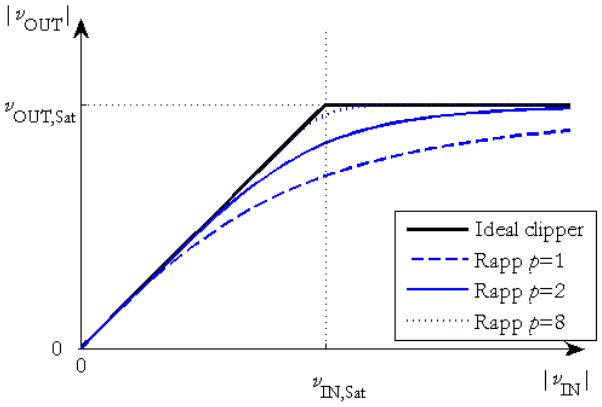

Figure 17: Typical AM/AM PA characteristics.

In order to avoid any degradation on the transmitted signal, it is required to operate the PA solely in its linear region. Typically, the RMS level of the incoming signal is set well below the saturation value so as to leave enough room for higher amplitudes to be amplified without being saturated. The signal is said backed-

off from the saturation point. It is common to define the input back-off (IBO) and output back-off (OBO) with respect to the saturation values as respectively:

$$\text{IBO}\big|_{dB} = -10\log_{10}\frac{P_{\text{IN,Avg}}}{P_{\text{IN,Sat}}}, \tag{19}$$

$$\text{OBO}\big|_{dB} = -10\log_{10}\frac{P_{\text{OUT,Avg}}}{P_{\text{OUT,Sat}}}, \tag{20}$$

where $P_{\text{IN(OUT),Sat}} = \left|v_{\text{IN(OUT),Sat}}\right|^2$ represents the input (output) saturation power and:

$$P_{\text{IN(OUT),Avg}} = \lim_{T\to\infty}\frac{1}{T}\int_0^T \left|v_{\text{IN(OUT)}}(t)\right|^2 dt, \tag{21}$$

is the mean power of a signal $v(t)$ at the PA's input (output).

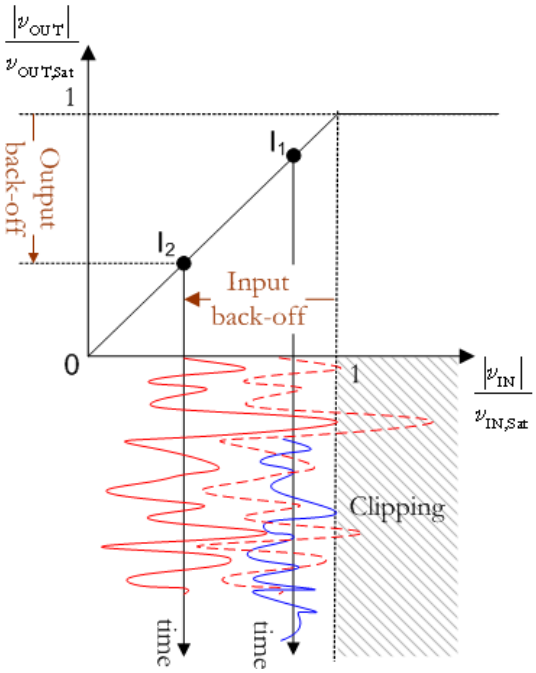

Figure 18: Backing-off signals with different dynamic ranges.

As shown on Figure 18 (red curves), depending on the operating point (I_1 or I_2), the same signal may suffer or not from clipping effects. In order to avoid significant degradations, an OFDM signal requires an IBO of 10-15 dBs while a SC signal can afford an IBO of a few dBs. Using signal with large power fluctuations has two main impacts: it requires high-end PAs with a large linear region and leads to a poor power efficiency. The power efficiency of a PA is measured as the ratio of the radiated output power with respect to the power consumed to operate the PA.

The power efficiency can be defined as follows:

$$\xi = \frac{P_{OUT,Avg}}{P_{OUT,Avg} + P_{DC}} \tag{22}$$

where P_{DC} is the power consumed by the PA on top of the radiated power (e.g. polarization current). It is clear from this definition, that the efficiency of the PA is higher when the average output power is close to the saturation point. For a given transmission, reducing the IBO without saturation enables increasing the power efficiency (blue curve) or relying on a PA with reduced constraints in terms of linearity. This is the kind of advantage that led to the selection of the SC-OFDM modulation for the uplink transmission in the 3GPP/LTE cellular system. Several techniques have been devised to reduce the PAPR of the OFDM modulation. One of them, namely the Tone-Reservation (TR) approach [10] was selected in the DVB-T2 standard [19]. For consistency, the performance of SC-OFDM has been measured against both pure OFDM and OFDM-TR for a number of relevant parameters.

2.3.1.4.2 Peak to average power ratio (PAPR)

Classically, the power fluctuations are measured using the complementary cumulative distribution function (CCDF) of the PAPR, defined as [7]:

$$\text{CCDF(PAPR)} = \Pr\left\{\text{PAPR} > \gamma^2\right\}. \tag{23}$$

The parameter γ^2 is a threshold, expressed in dB, and the CCDF value indicates the probability that the PAPR surpasses this threshold. Should we consider a signal (normalized to unitary mean power, for simplicity) passing through an ideal clipper PA, γ^2 has a direct physical interpretation: it can be assimilated to the input back-off. Indeed, for a signal working at γ^2 dB of IBO to go into saturation and suffer clipping, it would be necessary that its PAPR be higher than γ^2. The probability in (23) is also called clipping probability. Figure 19 displays the result of the evaluation of the CCDF of the PAPR with the following parameters: QPSK, *M*=512 (modulation), *N*=420 (spreading), oversampling factor equal to 4.

Figure 19 clearly shows the advantage of the SC-OFDM modulation over the OFDM with a gain of 2.8 dB in terms of admissible IBO for a clipping probability of 10^{-3}. It can also be noticed that the tone reservation technique is not really well suited for satellite networks where the link budget and the transmitter power amplifier efficiency issues lead to very small back-offs. For the same clipping probability, the advantage of the SC-OFDM still holds against the ODFM with tone reservation but with a lower gain of 1.2 dB.

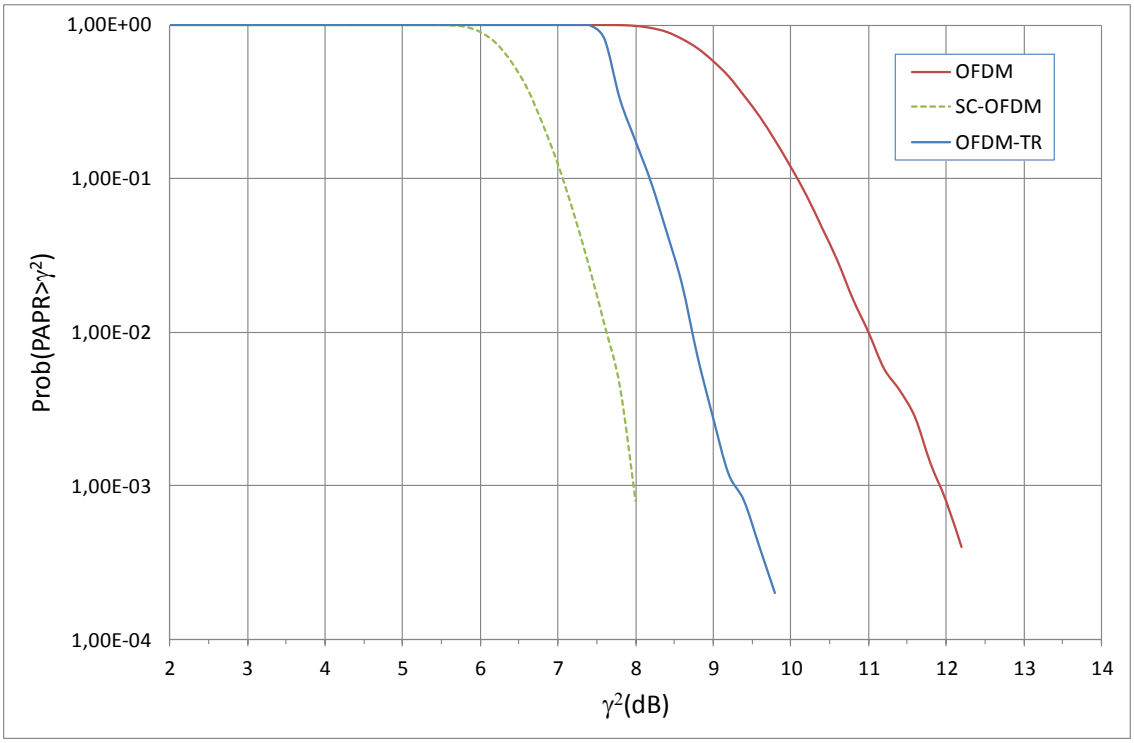

Figure 19: CCDF of PAPR for SC-OFDM, OFDM and OFDM-TR.

2.3.1.4.3 Instantaneous normalized power (INP)

While the CCDF of PAPR is a very popular notion, it has one important drawback. A certain clipping probability ensures that at least one peak per block has an important amplitude and is susceptible to suffer clipping or severe distortion, but gives no information on how many samples in that block are distorted [7]. Yet, in practical scenarios it is of great interest to know how many samples have a certain level and are thus susceptible to be distorted, as all of these samples cause degradation [26]. Indeed, severely clipping one single peak in a large block has a negligible effect on the MER or spectrum shape, while distortion (even mild) of a large number of samples might have unacceptable consequences. From this point of view, it is important to consider a more refined analysis taking into account all the signal samples. This can be done by means of considering the distribution of the instantaneous normalized power (INP) [7]:

$$\mathrm{CCDF(INP)} = \Pr\left\{ \frac{\overbrace{|v[n]|^2}^{\mathrm{INP}(\mathbf{v})}}{\frac{1}{N_s}\sum_{k=0}^{N_s-1}|v[k]|^2} > \gamma^2 \right\}, \tag{24}$$

where N_S is the number of samples considered to evaluate the INP. Note that the INP is defined in the discrete time domain. One must pay attention that the behavior of a signal in the continuous and discrete time domains may not be the same. Continuous and discrete performances will be equivalent only when oversampling the discrete signal at a sufficient level. The CCDF of INP indicates the probability that the INP at a sample level exceeds a certain threshold γ^2. If we look at the range of important values of γ^2 for the CCDF of PAPR, the probability that one sample in a block exceeds such a level is very weak, and should a sample exceed this level it is highly likely to be the only one in that block: The CCDF of INP and the CCDF of PAPR tend asymptotically to the same value. But in the range of lower values of γ^2, the CCDF of INP has a better resolution and shows effects that CCDF of PAPR tends to mask.

Figure 20 displays the result of the evaluation of the CCDF of the INP with the same parameters as in the previous section for the OFDM and SC-OFDM modulations. The figure also gives the CCDF of the INP for the TDM waveform with different roll-offs and the PAPR reduction technique for OFDM specified in DVB-T2, the so-called tone reservation algorithm (TR). These curves confirm the good PAPR properties of the SC-OFDM that outperforms both the OFDM and OFDM-TR modulation even at low IBOs. TDM waveforms exhibit better performance than SC-OFDM but only for roll-offs above 0%, i.e. not for the same spectral occupancy. It occurs that the (SC-)OFDM modulation with rectangular window is spectrally equivalent to TDM with a roll-off of 0%. An evolution of the SC-OFDM (Extended and Weighted SC-OFDM) modulation was devised to allow for controlling the frequency bandwidth with a roll-off factor just like for TDM. Without going into details on its actual principle, Figure 20 shows that the extended SC-OFDM behaves like TDM for the same value of roll-off except for very large power values. But, if the application of zero roll-off is readily achieved for SC-OFDM, it implies severe filtering issues for TDM waveforms. With an increasing pressure on the spectrum, it was decided to keep the SC-OFDM in its original form, i.e. with a roll-off of 0% (smallest bandwidth). *The main result of this study is that the SC-OFDM modulation is strictly similar to TDM modulations in terms of PAPR for the same spectral occupancy*.

The Tone Reservation algorithm brings an improvement to OFDM for INP probability less than $4 \cdot 10^{-3}$, corresponding to a signal power greater than 7 dB. For a terrestrial system and linear amplifiers, this brings an improvement if large input back-offs are considered, i.e. very low out-of-band emission. If operating a PA with large IBO is not a big issue for terrestrial transmission, it is not at all the case for satellite transmissions where limiting the power consumption is critical. Satellite PAs are often driven with IBOs of a few dBs thus leading to a high saturation of the signal. This is compensated by the use of robust modulation and coding schemes. From Figure 20, it is clear that for a satellite system and a foreseen IBO of about 1 dB, TR does not bring any advantage.

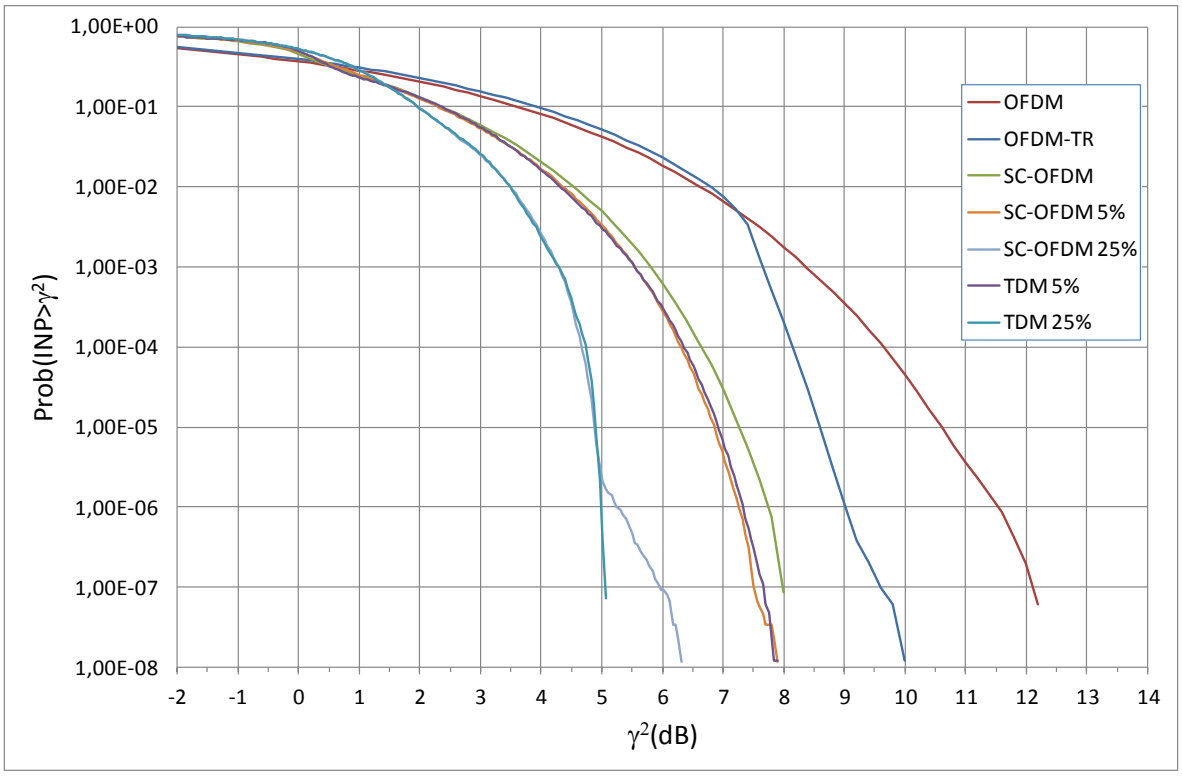

Figure 20: CCDF of INP for SC-OFDM, OFDM and OFDM-TR.

2.3.1.4.4 Satellite Pilot Pattern (PP9)

As explained in Section 2.3.1.3.3, the DVB-NGH standard specifies a pilot pattern specifically dedicated to the SC-OFDM transmission mode. Figure 21 plots the CCDF of INP of the hybrid data and pilot SC-OFDM symbols. Simulation parameters considered a FFT size of 0.5k (N = 512, M=432) and QPSK signal mapping. An oversampling factor of 4 was considered. Results in Figure 21 confirm the overall low envelope fluctuations of the hybrid data and SC-OFDM pilot symbol. At a clipping probability per sample of $2 \cdot 10^{-2}$ SC-OFDM outperforms OFDM by 2 dB and the hybrid symbol has close performance to SC-OFDM, with a slight degradation of 0.4 dB. Since the hybrid symbol appears in a frame once every 6 SC-OFDM symbols, this slight degradation has overall no impact on the performance. At higher clipping probabilities the performance difference between SC-OFDM and OFDM is even higher, and the hybrid symbol has lower envelope variations than the SC-OFDM data symbol. To illustrate the performance of the PP9 pilot scheme, Figure 22 compares the performance of SC-OFDM in an AWGN channel with perfect and real channel estimation. Real channel estimation is carried out according to the scheme introduced in Figure 14 with Wiener filtering. The real channel estimation introduces a loss of 1.2dB, i.e. typical of what is measured in the case of pure OFDM.

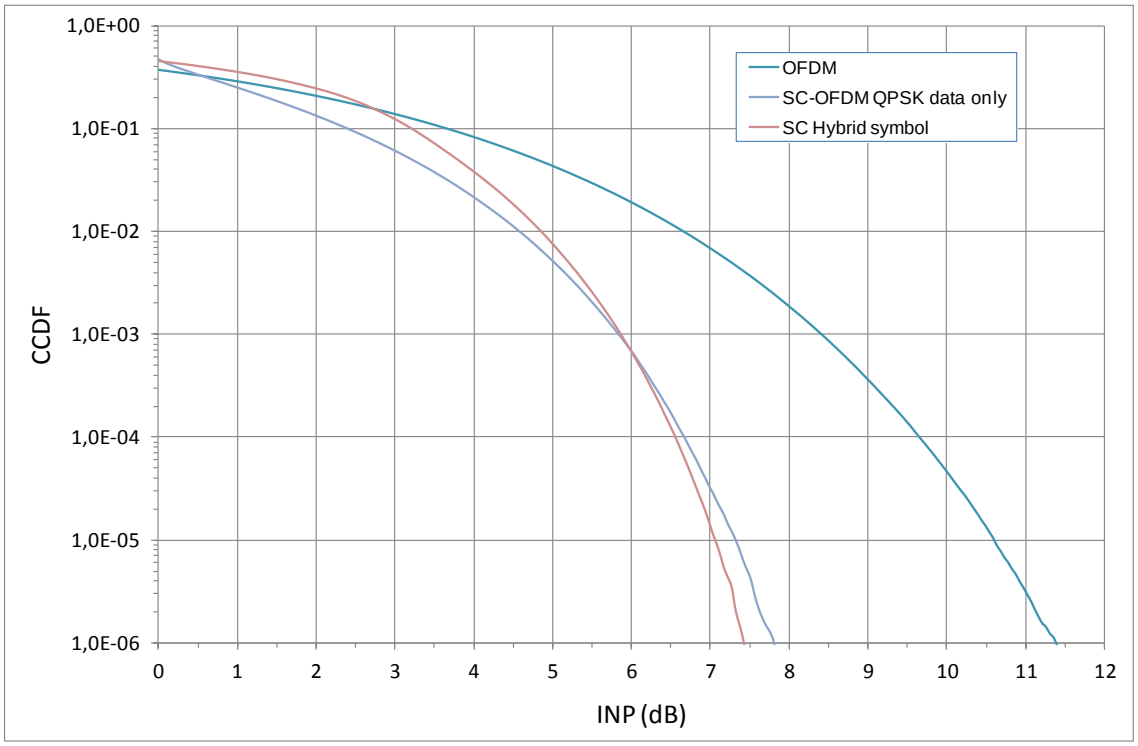

Figure 21: CCDF of INP of OFDM, SC-OFDM and SC-OFDM hybrid pilot.

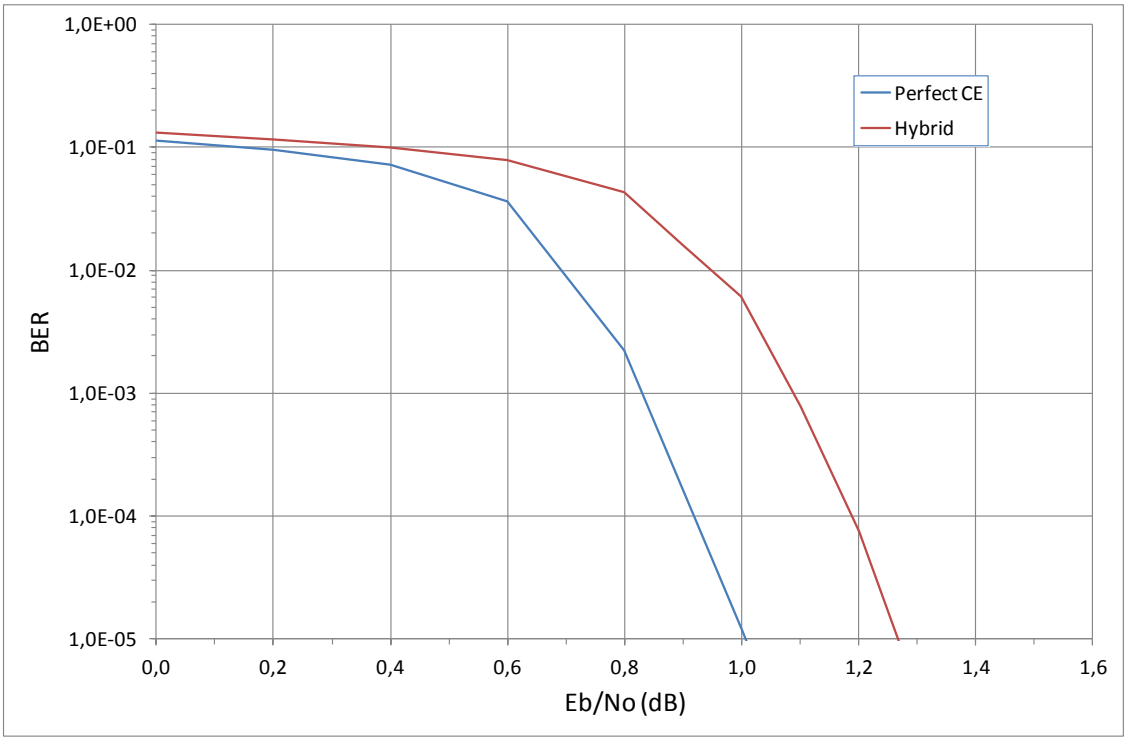

Figure 22: Performance of the PP9 pilot scheme with real channel estimation (CE). QPSK 4/9, LDPC 16k, N = 512, GI = 1/32, AWGN.

2.3.1.4.5 Modulation error ratio (MER)

The CCDF of the PAPR and INP provides a direct insight on the power fluctuations of the signal. As mentioned above, satellites often operate with very low IBOs. The PAPR reduction brought by the SC-OFDM modulation with respect to OFDM is thus not sufficient to transmit without saturation. It is thus of great interest to quantify and compare the impact of the saturation on those modulations. The saturation of the incoming signal by the PA introduces within the signal bandwidth interference that can be assimilated to an additional noise. The impact of the PA non-linearity on the modulation itself (independently from channel coding) is commonly evaluated using the modulation error ratio (MER). The MER basically measures the level of noise introduced by the degradation onto the demodulated constellation samples. The MER is defined in dBs as follows:

$$MER = 10\log_{10}\frac{P_{signal}}{P_{error}}, \tag{25}$$

where P_{error} is the RMS power of the error vector, and P_{signal} is the RMS power of ideal transmitted signal. Note that the MER is closely related to the error vector magnitude (EVM) [27]. The MER was measured for two power amplifiers, an ideal clipper and the linearized TWTA amplifier as used in DVB-S2 [29]. Figure 23 and Figure 24 display the result of the evaluation of the MER respectively for the ideal clipping and linearized TWTA PAs with the following parameters: QPSK, M= 512 (modulation), N=420 (spreading), oversampling factor equal to 4.

The MER evaluation confirms that the SC-OFDM is significantly more robust than the OFDM to saturation with a gain of ~3 dBs. The MER evaluation also shows that the TR method does not bring a significant improvement in a satellite environment, i.e. with a linearized amplifier not so linear, whatever the IBO. Even with an ideal amplifier and for small IBO (less than 5 dB), TR does not bring any improvement over OFDM and remains less robust than SC-OFDM.

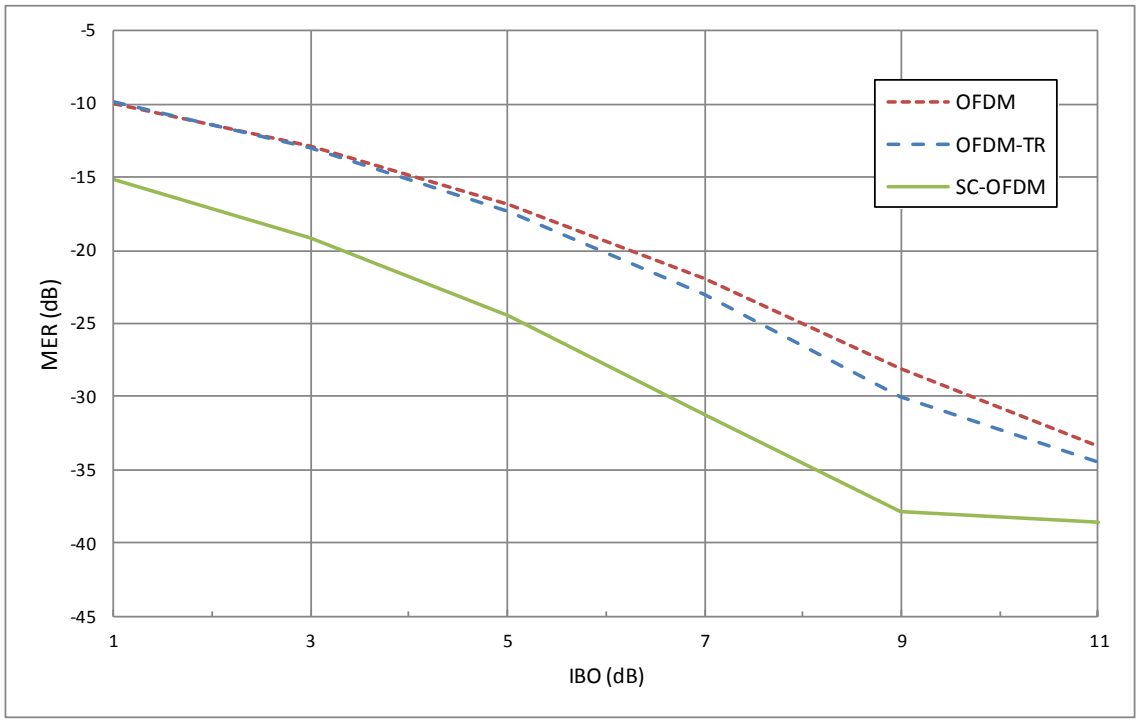

Figure 23: MER for SC-OFDM, OFDM and OFDM-TR – linearized TWTA PA.

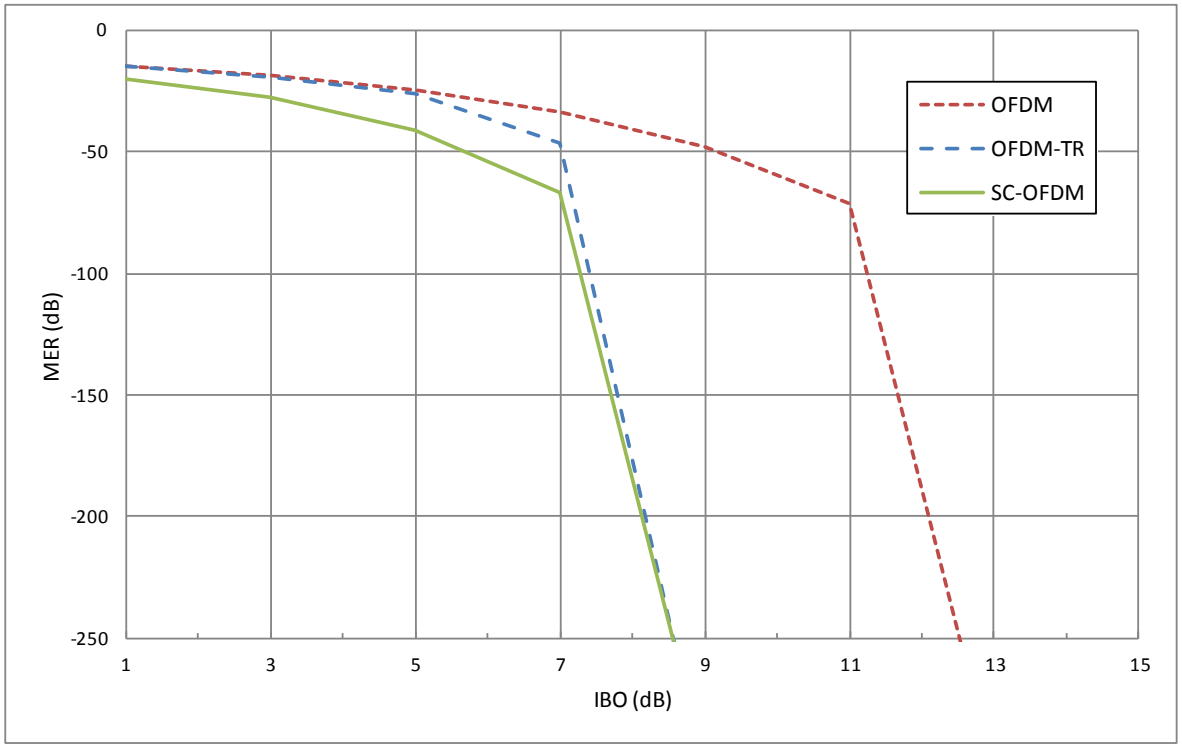

Figure 24: MER for SC-OFDM, OFDM and OFDM-TR – Ideal clipping PA.

2.3.1.4.6 Bit error rate (BER) and total degradation (TD)

When dealing with coded modulations, it is common to evaluate performance in terms of bit error rate (BER) with respect to the signal-to-noise ratio (SNR). In the present case, the objective is to evaluate the losses due to the PA non-linear effects in comparison with the ideal case (linear PA without saturation). As previously explained, a PA should ideally be operated close to its saturation point. Assuming a perfect amplifier, the application of an IBO means that the SNR shall be IBO dBs larger to reach the reference level of performance. In practice, it is obviously not possible to increase the SNR - the application of a given IBO actually results in a reduction of the transmitted power and thus of the coverage. Moreover, the AM/AM response of real power amplifiers is not perfectly linear especially close to the saturation region and the actual loss in SNR is given by the OBO associated to the IBO. The OBO thus represents the first cause of in-band degradations when dealing with non-linear PAs. The second cause of degradation is the in-band noise introduced by the saturation applied onto the incoming signal. It is common to evaluate this degradation as the loss in SNR for a given reference value of target BER between the non-linear amplifier and an ideal linear amplifier for a given output back-off OBO [7]:

$$\mathrm{TD} = \mathrm{OBO} + [\mathrm{SNR}_{PA} - SNR_{linear}]_{BER_{ref}} = OBO + \Delta SNR \,. \tag{26}$$

When the back-off is high, there is virtually no in-band distortion and thus no distortion-related BER loss (ΔSNR<<OBO). When working at low OBO, in-band distortions increase, ΔSNR loss is important and becomes the predominant term in the total degradation. There is an optimal working point I_{opt}, which ensures a compromise between OBO and ΔSNR and yields a minimum total degradation.

Figure 25 and Figure 26 respectively depicts the BER performance of the OFDM and SC-OFDM modulations assuming an AWGN channel and the linearized TWTA amplifier model. The simulation parameters are given in Table 25 below.

Table 25: Parameters for BER and TD simulations

Modulation	OFDM	SC-OFDM
Constellation	QPSK	QPSK
Channel coding	LDPC 16k, 4/9	LDPC 16k, 4/9
FFT size	2048	512
Guard Interval	1/32	1/32

The BER is given for a set of IBOs as a function of a reference E_b/N_0 i.e. the one that will be measured with a linear PA with the same gain operated at the saturation point of the actual PA or equivalently with no amplifier considering that the PA model is normalized in power with a unitary gain for IBO=0. This representation enables to directly measure the combined effect of the OBO and interference noise. The total degradation is simply given by the shift between the ideal reference curve and the measured curve. The Total Degradation for a BER value of 10^{-5} has been extracted from those evaluations as shown on Figure 27. In order to distinguish the impact of the OBO against the one of the saturation noise, Figure 27 also depicts the OBO as a function of the IBO.

It appears from these curves that the optimum IBO for the OFDM is 2 dB leading to a TD of 2.95 dB while the optimum IBO for the SC-OFDM is 1 dB leading to a TD of 1.35 dB. This shows that the SC-OFDM enables operating closer to the saturation point than the OFDM, thus improving the power efficiency of the amplifier for a reduced consumption or an increased coverage. In addition, this comes with a TD smaller of 1.6 dB in favor of SC-OFDM, which means the ability to increase the coverage for a given level of performance.

The results have been given so far under the assumption of a QPSK modulation alphabet. Figure 28 compares the total degradation measured in the case of the QPSK and 16QAM. Due to its higher PAPR, 16QAM requires an IBO greater than 1 dB with a TD of 2.1 dB, logically but not significantly greater than what can be obtained in QPSK.

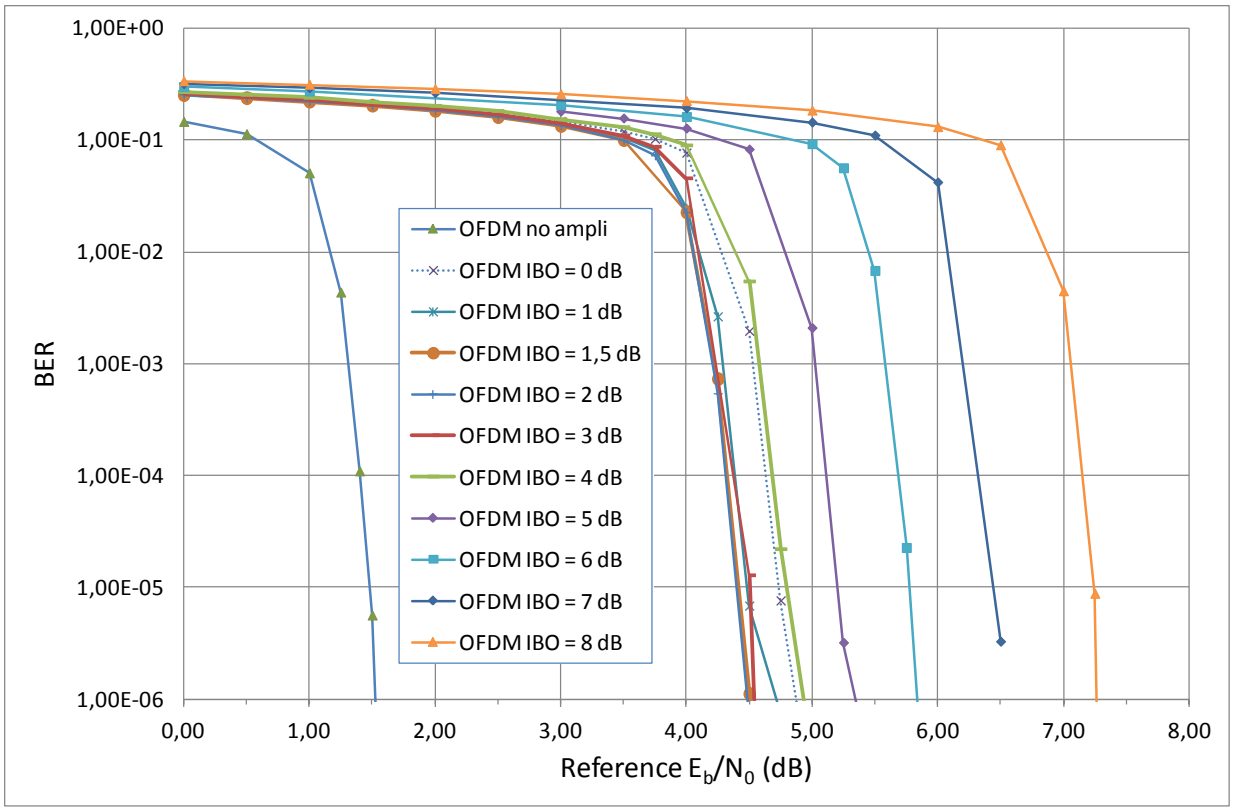

Figure 25: BER performance – OFDM.

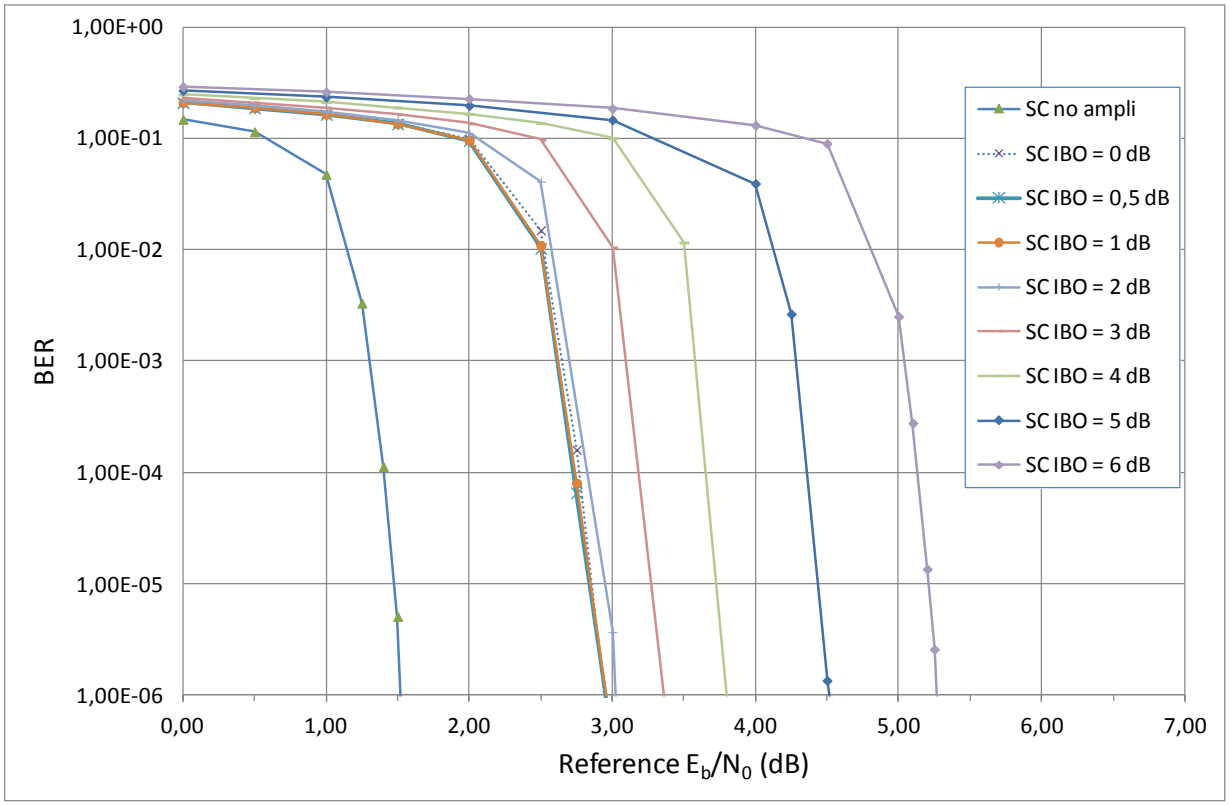

Figure 26: BER performance – SC-OFDM.

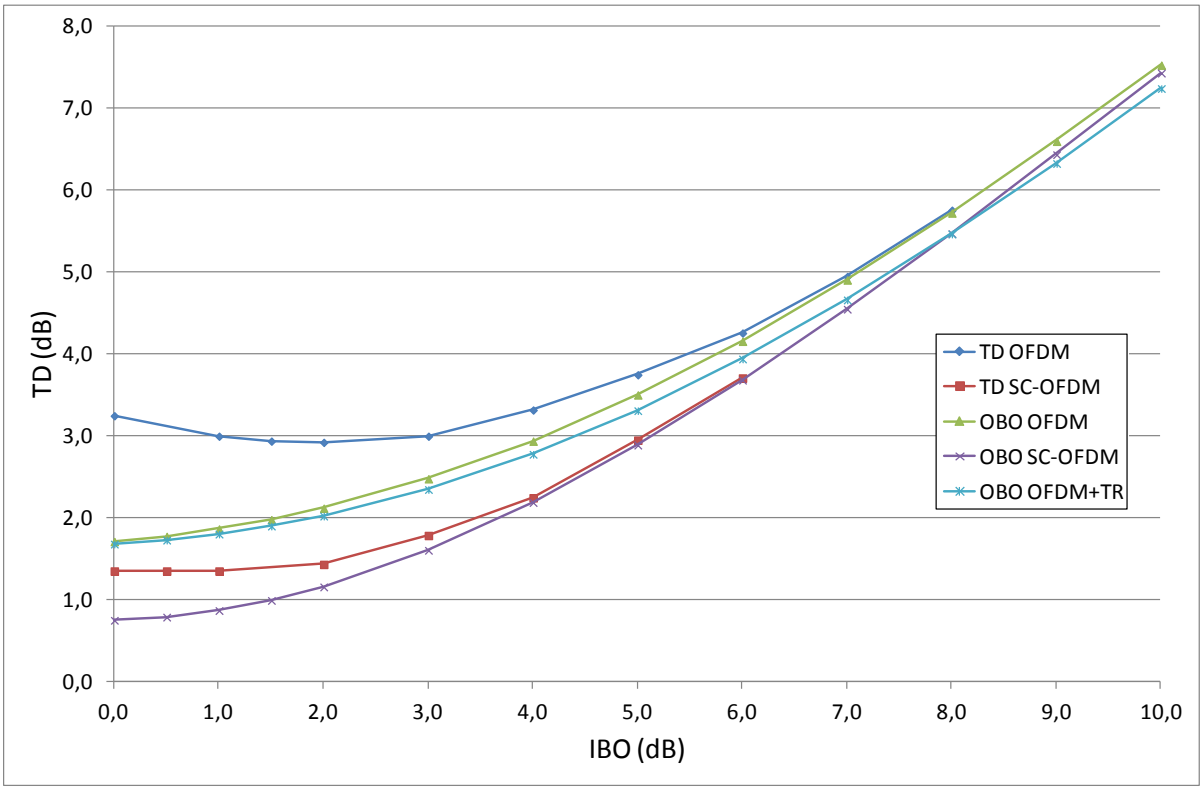

Figure 27: Total degradation and OBO performance.

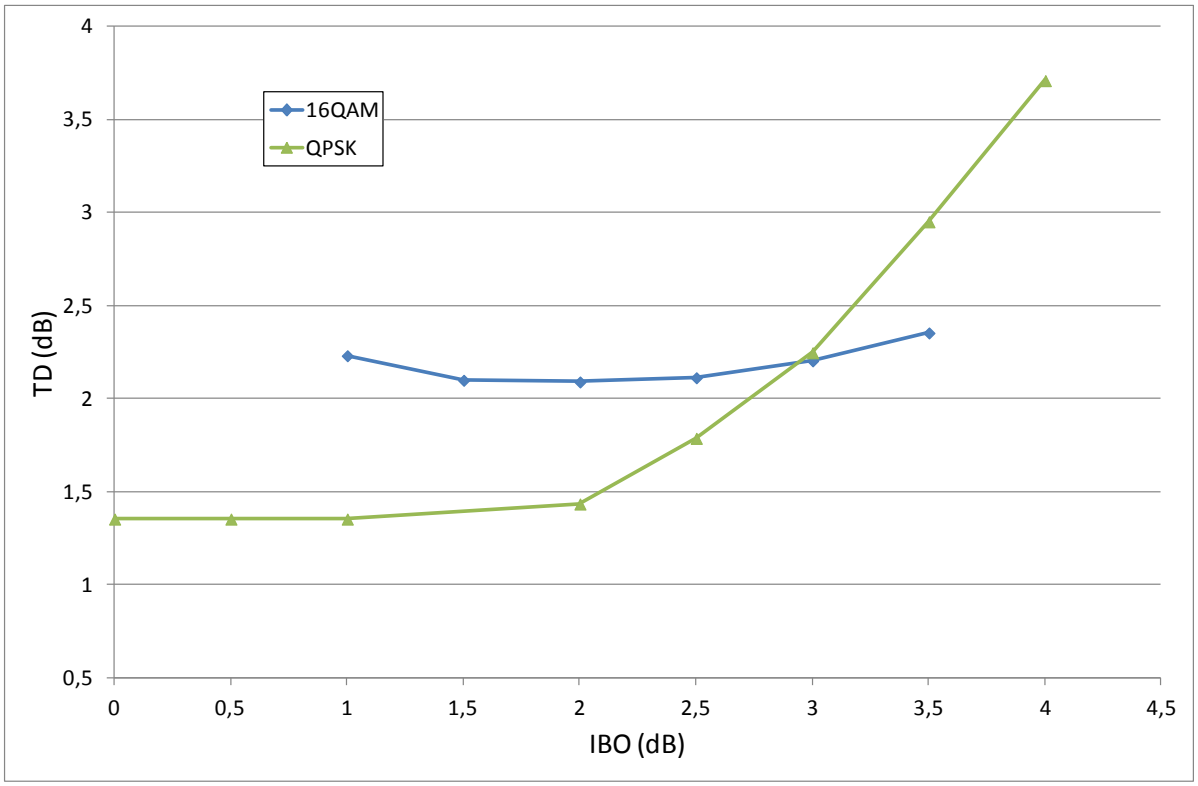

Figure 28: Total degradation and OBO performance - Linearized TWTA PA, AWGN channel – 4/9, LDPC 16k, NFFT = 512, M = 432, GI = 1/32.

2.3.1.4.7 Doppler performances

As mentioned in the DVB commercial requirements, DVB-NGH networks are expected to support moving terminals for speeds up to 350 km/h. The requirement applies to the satellite segment and thus to the SC-OFDM modulation. The SC-OFDM has been evaluated by simulation using the Land Mobile Satellite (LMS) model from CNES as described in [30] for an elevation angle of 40° (Rice fading with K=5). The simulation parameters are given in Table 26.

The pilot pattern inserted for channel estimation is the PP9 scheme, the only one supported for SC-OFDM satellite transmissions. Figure 29 depicts the result of the BER evaluation for 3 different speeds: 100, 500 and 1000 km/h. Figure 29 confirms the robustness of the SC-OFDM modulation to Doppler degradations with a degradation of ~2 dB for a speed of 100 km/h and 3.5 dB for 1000 km/h. Those results are provided without taking into account the gain of 30% typically obtained when considering an elevation angle of 40° for the satellite. SC-OFDM actually behaves closely to OFDM with respect to Doppler in the satellite channel that does not show a lot of frequency selectivity. The support of high speeds here is due to use of a 512 sub-carriers multiplex and the occurrence of the specular component that enables to perform an efficient AFC.

Table 26: Parameters for Doppler simulations.

Parameter	Value
Carrier Frequency	2.2 GHz
Bandwidth	5 MHz
FFT size	512
Guard Interval	1/32
Constellation	QPSK
Channel coding	LDPC R = 4/9
Time interleaving	100 ms

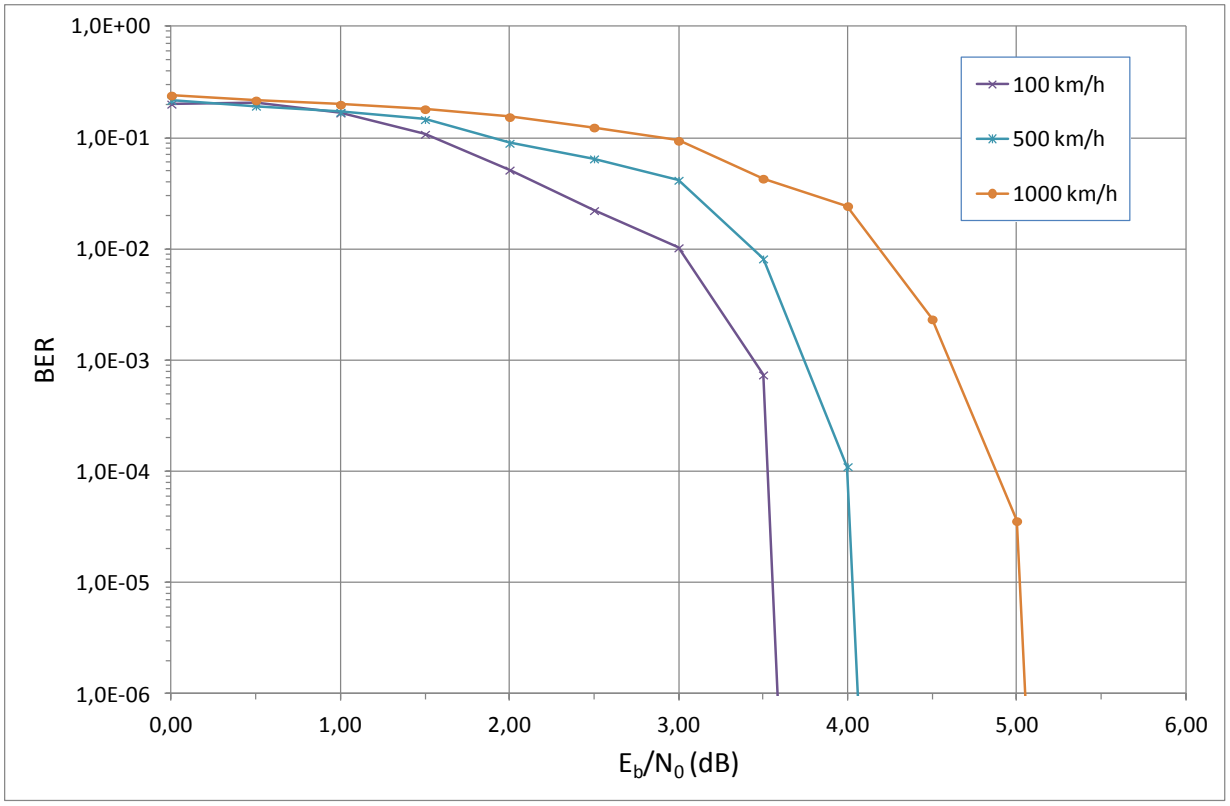

Figure 29: Doppler performance of the SC-OFDM modulation.

2.3.1.4.8 MIMO performances

As mentioned in Section 2.3.1.3.3, a 2×2 spatial multiplexing scheme can be used to perform a MIMO SC-OFDM transmission from the satellite in the hybrid MFN context. The common assumption for Rate 2 MIMO in DVB-NGH is the enhanced SM (eSM) scheme where a rotation precoding matrix is applied onto the reference SDM scheme. This scheme was not selected for SC-OFDM transmissions as it breaks the PAPR properties of the modulation. This is shown on Figure 30 that depicts the MER of the transmitted SC-OFDM signal after passing through the linearized TWTA PA model. The simulations have been performed for a 5 MHz bandwidth, a FFT size of 512 points, in QPSK and two angles for the eSM scheme, 22° and 45°.

The MER curves show that for the IBO of interest (1 dB), an eSM with an angle of 22° (resp. 45°) brings a MER degradation of about 1.1 dB (resp. 1.6 dB).

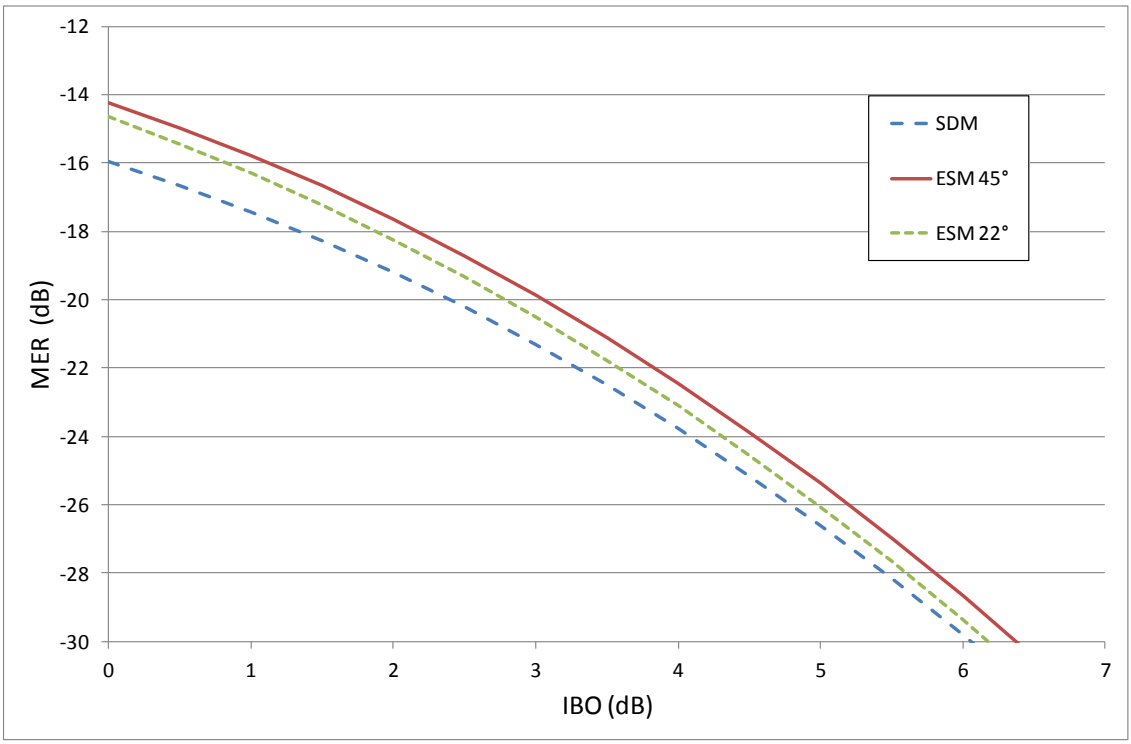

Figure 30: MER for eSM and SDM schemes.

The actual performance of the SM scheme on the SC-OFDM has been evaluated by simulation with a modified version of the BBC channel model [32]. The BBC model is a simple hybrid 4×2 SFN model. It has been modified to obtain a 2×2 sheer satellite model with the following parameters:

- Counter-rotating circular polarization.
- Single-tap Ricean variable $K = 5$.
- Satellite cross-polar discrimination: $\alpha = 2$.

Figure 31 depicts the BER performance assuming a speed of 60 km/h, perfect channel estimation and a simple MMSE MIMO decoding. The SM scheme brings a degradation of only ~0.5 dB with respect to the ideal two SISO parallel transmissions. In comparison to a 16QAM SIMO transmission, the SM scheme provides about 1.9 dB of improvement for the same spectral efficiency. Those results are actually close to the ones obtained in OFDM, when no power amplifier is used.

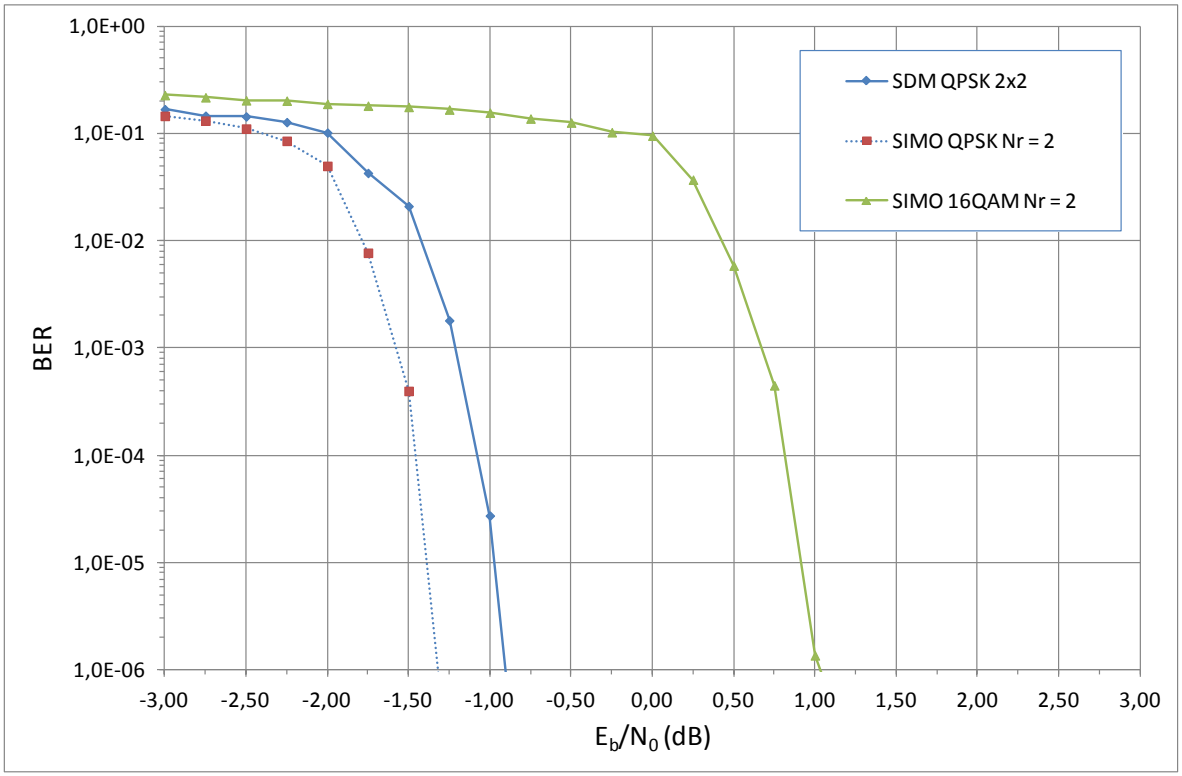

Figure 31: BER performance for the SM scheme in SC-OFDM.

Table 27: Parameters for MIMO SM simulations.

Parameter	Value
Carrier Frequency	2.2 GHz
Bandwidth	5 MHz
FFT size	512
Guard Interval	1/32
Constellation	QPSK
Channel coding	LDPC R = 4/9
Time interleaving	1 s

2.3.1.5Conclusion

This chapter was dedicated to the new waveform selected to implement the transmissions on the satellite link of the DVB-NGH standard, namely the single carrier-orthogonal frequency division multiplexing (SC-OFDM) modulation. This introduction to the SC-OFDM waveform was conducted according to three perspectives. The SC-OFDM is first compared to the two other modulations commonly used for satellite transmissions, the TDM and OFDM waveforms. It is shown that the SC-OFDM modulation enables keeping the low power fluctuations of TDM signals while benefiting from the flexibility and high spectral efficiency of the OFDM modulation. The chapter then focuses on the intrinsic robustness of the SC-OFDM modulation to the Power Amplifier non-linear degradations with the ability to operate with a reduced OBO in comparison to OFDM and a total degradation improved by 1.5 dB. It is thus possible to improve the power

efficiency of the PA while improving the coverage. It must be pointed out that this result still holds when considering the PAPR reduction solutions such as the Tone Reservation approach used in DVB-T2. This kind of solution actually performs well for large IBOs but not for the small IBOs (a few dBs) commonly used in satellite transmissions. In a third wing, the chapter shows that the SC-OFDM behaves similarly to OFDM when it comes to compensate for the degradation due to the channel and mobility, either in SISO or MIMO. These results clearly demonstrate the interest of the SC-OFDM modulation in the context of satellite transmissions.

2.3.2 Comparison between OFDM, SC-OFDM, EW-SC-OFDM and TDM

2.3.2.1 Non linearity consideration

On a satellite payload, weight, power consumption, and power dissipation are the main limitations. It involves that power amplifier design may be critical for the system efficiency. Let's remind that a power amplifier is able to deliver a maximum power P_{sat} when signal is a Continuous Wave (CW). As shown on Figure 32, because of the non linearity, the output signal includes a part of pure signal, C', and a part of intermodulated products Im.

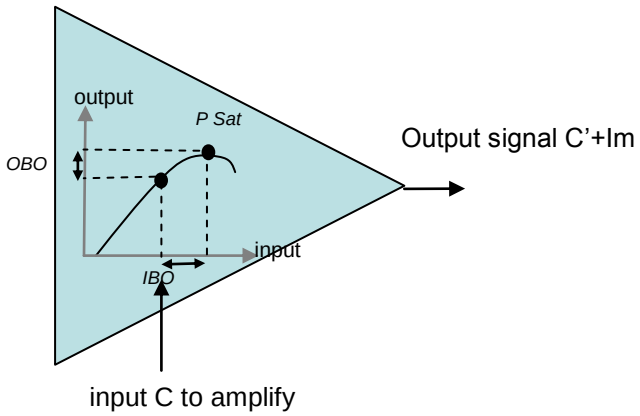

Figure 32: General characterization of a power amplifier.

In Figure 32, we have:

- OBO is defined as the amplifier output back off. It is the power difference between CW saturating power P_{sat} and modulated carrier power $C'+I_m$. Regarding link budget consideration, OBO is a direct loss.
- Im is characterized by C/Im ratio, meaning output signal quality indicator. Im yields to degradations in the transmission, mainly because it is considered as an additional noise, and also because it reduces the useful output power. One shall note that C/Im is increasing when |OBO| is increasing.

Therefore a common trade-off is to optimize OBO level versus C/Im ratio. This trade-off may rely on the waveform, the non linearity characteristic of the amplifier, and also on the payload architecture. Let's precise that there are two classes of payload architectures, depending mainly of the level of flexibility needed (See Figure 32):

- Channelized architecture
  Each signal is amplified by only one amplifier. This configuration offers low flexibility but may offer the best trade-off between OBO and C/Im because of only one signal per amplifier. Note that the trade-off will be mostly waveform dependant.

- Distributed architecture
  Several signals are amplified by a set of amplifiers. This configuration provides a good flexibility while obliging back off the amplifiers, so that the C/Im/OBO trade off will be less waveform dependant.

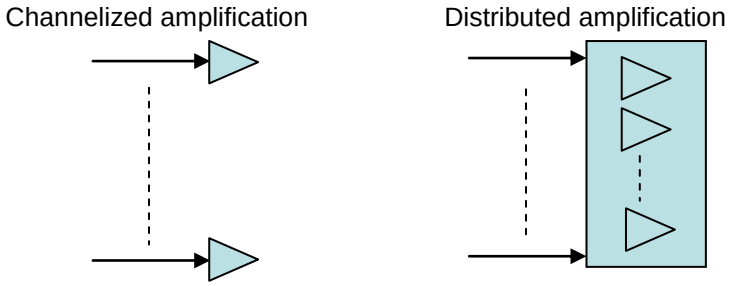

Figure 33: Channelized and distributed amplification.

2.3.2.2 Waveform comparison criteria

Backing on the different metrics descriptions, total losses can be expressed by :

$$\text{Total losses} = |\text{OBO}| + \text{Intermod losses}$$

Figure 34 below introduces a way to compare different waveforms with same comparison basis, C/Im.

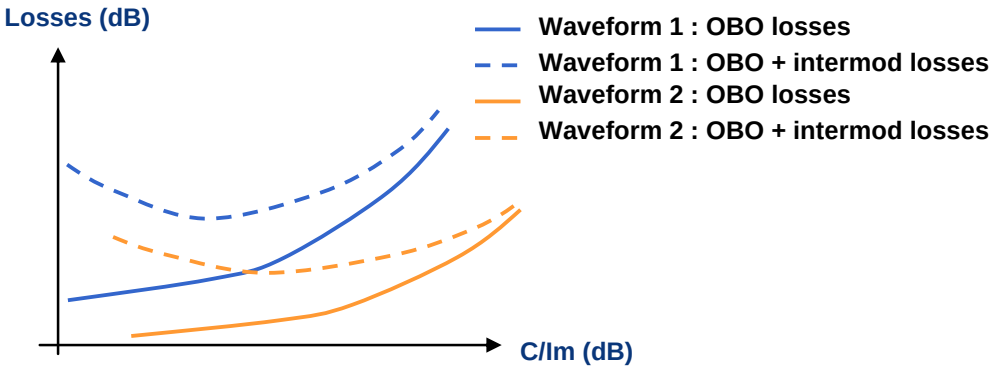

Figure 34: Channelized and distributed amplification.

Note that C/Im is, for satellite link, a relevent metric. Indeed, other C dependant interferences sources are involved in the transmission (example antenna beam crossing), meaning that losses caused by each source of interference may not be dB added. Besides, ”losses” is keeping an relevent metric considering only intermodulation products and OBO losses.

2.3.2.3 Simulation Process

The aim of this sub section is to depict the simulation process used to compute metrics defined above, for each waveform, that is to say:

- OBO
- Intermodulation losses
- C/Im

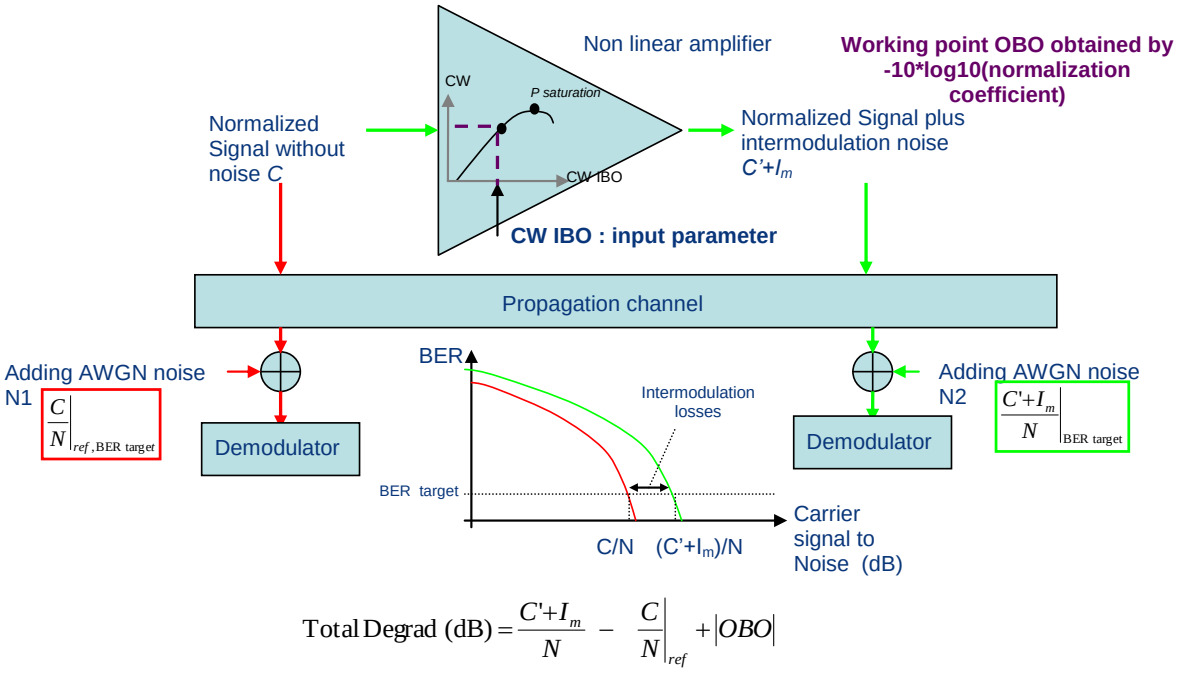

Figure 35: Simulation process.

Step 1: Define a BER target.

Usual BER target is 10^{-7} with LDPC+BCH encoding. In order to reduce simulation time, BER 10^{-5} has been adopted, but without BCH encoding.

Step 2: For each waveform, perform reference curves -i.e without non linearity- to get the required C/N at BER target.

Step 3: For each waveform,

For a set of IBO values,

Perform simulations with non linearity, and search the (C'+Im)/N ratio to reach BER target. Note that as a rule of thumb in simulation process:

- signal is normalized before throwing propagation and noise addition blocks
- saturation power of the amplifier is normalized

Therefore:

- Normalization coefficient of the signal at the amplifier output equals to |OBO|
- (C'+Im)/N – (C/N) at BER target is giving Intermodulation losses

Step 4: For Each waveform,

For the same set of IBO values in Step 3,

Derive equivalent C/Im value from intermodulation losses {(C'+Im)/N – (C/N)}, and required C/N

$$\left(\frac{C+I_m}{N}\right)=\frac{\left(\frac{C}{I_m}\right)^{-1}+1}{\left(\frac{C}{N}\right)^{-1}} \quad \Rightarrow \quad \left(\frac{C}{I_m}\right)=\frac{1}{\left(\frac{C+I_m}{N}\right)\cdot\left(\frac{C}{N}\right)^{-1}-1}$$

Note that this equivalent C/Im expression involves that Im behaves as white noise. It is not exactly true, but for system considerations, it is the equivalent C/Im which is needed to be able to add Im with white noise and other interferences.

2.3.2.4 Compared Waveforms quick summary

The SC-OFDM waveform is described in details in Section 2.3.1. For details on EW-SC-OFDM, refer to the DVB-NGH contribution TM-NGH500 [43]. Thus, this section only recalls the main features of the compared waveforms.

2.3.2.4.1 TDM (Time Division Multiplexing)

In TDM, complex modulated symbols are oversampled and filtered by a Square root cosine (SRRC) filter. Typical example of TDM is the DVB-S2 standard.

TDM is known for its low enveloppe fluctuations and its simplicity, that explains that it is widely used in satellite telecommunication systems. Besides, the waveform is not well suited for multipath environment.

Spectral occupancy is Rs*(1+roll_off), with Rs symbol rate (bauds), and roll off depending on the SRRC filter.

2.3.2.4.2 OFDM (Orthogonal Frequency Division Multiplexing)

In OFDM, serialised modulated complex symbols are parallelized and then passed in a IFFT device to generate blocks called OFDM symbols. Part of OFDM blocks are cyclically duplicated to create a guard interval.

OFDM fluctuation enveloppe is very high because it is behaving as white noise. Otherwise, thanks to the guard interval, it allows good performances in multipath environment with a relative low complexity.

Spectral occupancy is Rs, but efficiency is decreased by the ratio 1/(1+GI), with Rs symbol rate (bauds), and GI guard interval ratio.

2.3.2.4.3 SC-OFDM (Single Carrier Orthogonal Frequency Division multiplexing)

For a technical description of the SC-OFDM modulation, report to Section 2.3.1.

Compared to OFDM, SC-OFDM is decreasing enveloppe fluctuation while keeping main features of OFDM, as robustness against multipath environment.

Spectral occupancy : Rs.

2.3.2.4.4 EW-SC-OFDM (Extended and Weighted Single Carrier Orthogonal Frequency Division multiplexing)

EW-SC-OFDM will be described in the next TF4 deliverable. Refer to the DVB-NGH contribution [43] for a detailled description.

Compared to SC-OFDM, EW-SC-OFDM is introducing in the frequency plan additional carriers making spectrum looking like to the TDM one. Then, enveloppe fluctuation is reduced at the expense of the spectral occupancy.

Spectral occupancy : Rs*(1+roll off), with Rs symbol rate (bauds), and roll off additional carriers ratio.

2.3.2.5 Simulation settings

Simutions are performed with a generic coded OFDM simulation chain, from which some functionnalities have been adapted to be compliant with SC-OFDM and EW-SC-OFDM waveforms. Remind that LDPC encoding is not coupled with BCH coder because of 10^{-5} BER target.

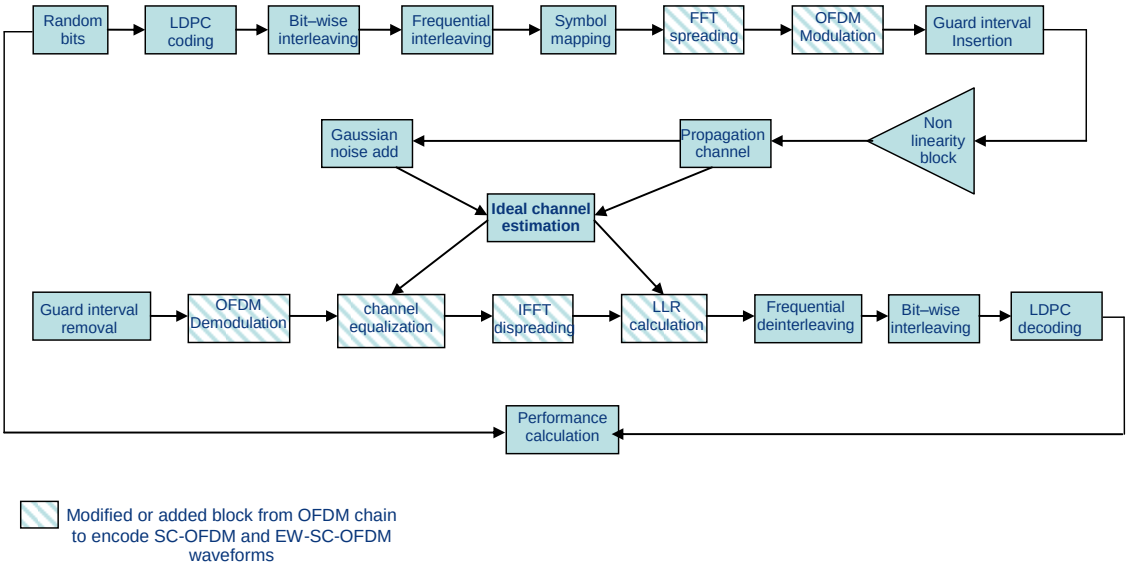

Figure 36: Simulation chain.

One of the limitation of the study is that the simulation chain is working with ideal channel estimation.

Other hypothesis are given hereafter :

- QPSK 1/3 modcod with AWGN channel
- Target BER 10^{-5}
- reference C/N of -1.2 dB (obtained for all waveforms)
- TDM and EW-SC-OFDM waveforms are set with 15% roll off
- Using of fixed point 6 bits LDPC decoding
- Optimization of LLR weighting done for each waveform
- Considered Payload is Channelized amplification
- Amplifier is an S band non linearized TWTA

- AM/AM and AM/PM characteristics are taken from DVB-SH IGv1 (See Figure 37)

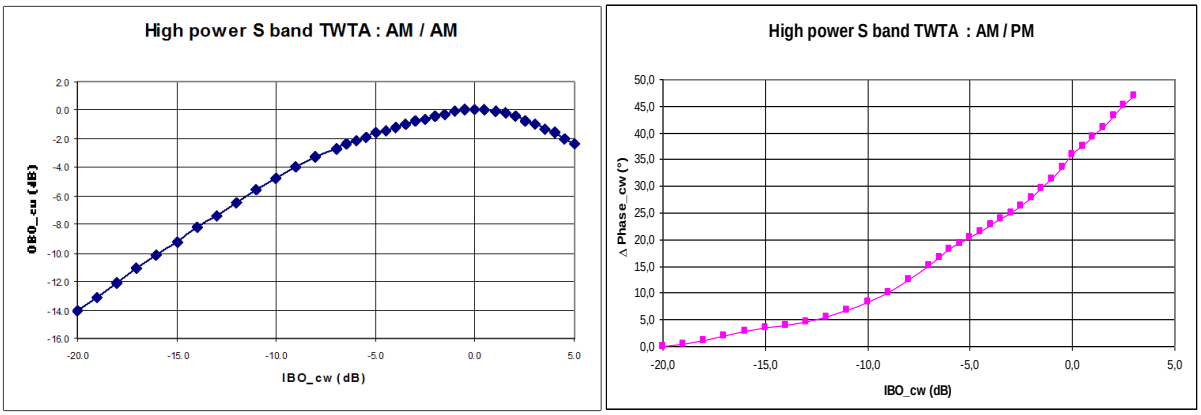

Figure 37: AM/AM and AM/PM characteristics of the TWTA PA.

It can be pointed out that these non linearity curves are especially severe, and will favour difference performance between the different waveforms.

2.3.2.6 Results

Simulation results synthesis is given hereafter. Used representation is justified Section 2.3.2.2.

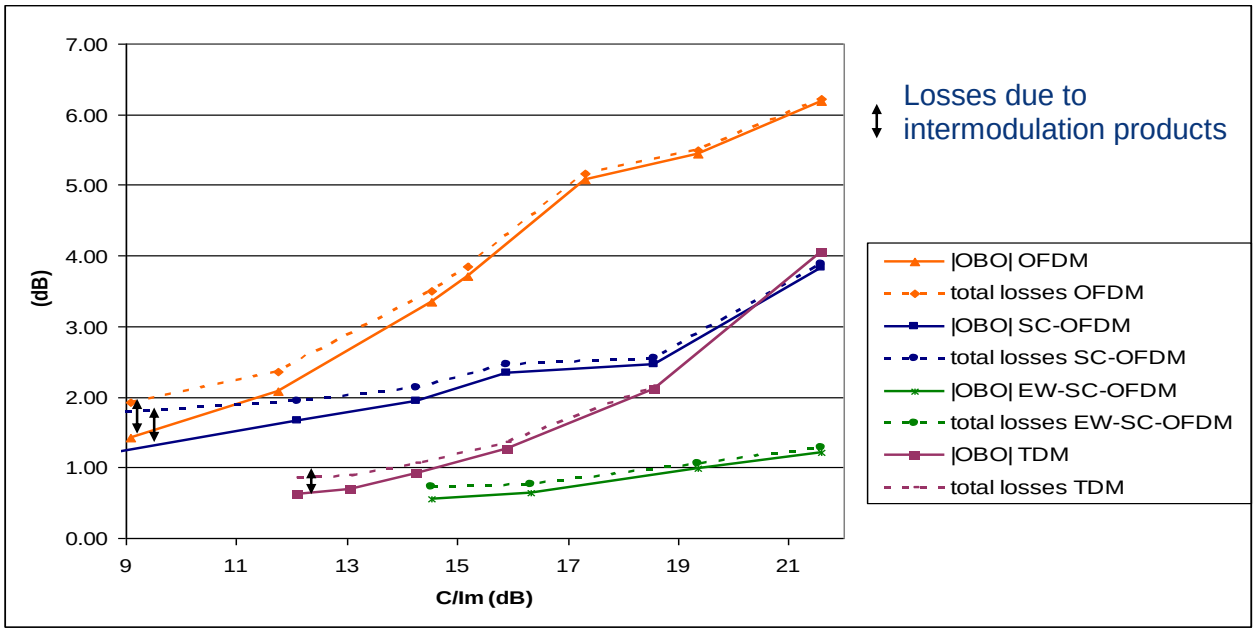

Figure 38: Performance results.

For a channelized amplification, with non linearized TWTA, results show important gap performances between waveforms (that is favored by hypothesis):

- At Low C/Im, total losses difference is not very important
- At higher C/Im, (EW)-SC-OFDM and TDM appear interesting
- (EW)-SC-OFDM always outperforms TDM

2.3.2.7 Conclusions

SC-OFDM and EW-SC-OFDM present a performance enhancement for satellite link compared with OFDM. These new modulations can take advantage of OFDM properties in mobile environment, while reusing OFDM receiver architecture with limited modifications. Finally, it can be pointed out that EW-SC-OFDM outperforms TDM satellite baseline waveform.

Besides, gaps between different waveforms are C/Im dependant: low C/Im shows limited difference between waveforms, so that it may be the preferred working point with low required SNR modulation and for inter-beam interference. Otherwise, EW-SC-OFDM advantage is growing with C/Im.

Lastly, OFDM remains a pertinent waveform solution for non linear satellite transmission, which is reinforced for payload distributed amplification.

2.3.3 Time Interleaving in the satellite context

2.3.3.1 Long Time Interleaving

2.3.3.1.1 Introduction and Background

Mobile satellite reception is characterized by long and deep fades in the received signal [33] (Figure 39). Fades are occasioned when terminals pass through shadowed areas where the signal from the satellite is blocked by trees or buildings. This signal blocking causes error bursts in which all the information received is erroneous. Because of this, in a satellite reception environment, interleaver mechanisms aimed to spread the errors along a large portion of time are of most importance. An interleaver rearranges the information to be transmitted so that portions of information that are close to each other end up being transmitted separated in time.

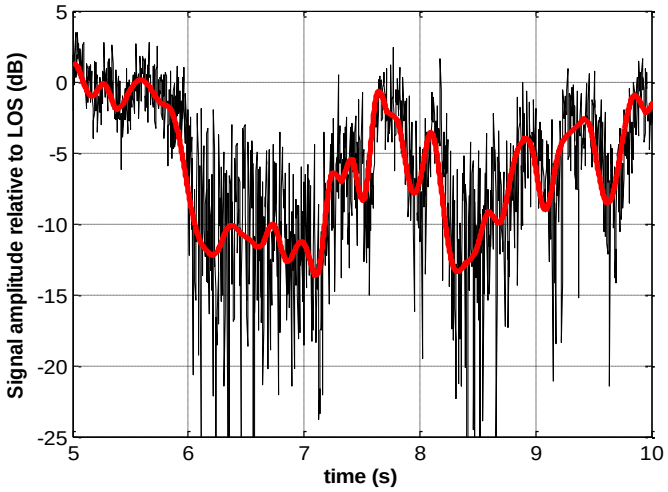

Figure 39: LMS Suburban Channel: Elevation angle= 40°, f_{RF}=2.2 GHz, velocity=60 km/h.

The signal fading duration depends on the reception environment and the user velocity. The blockage derived from trees causes shorter fading durations than the blockage caused by large obstacles such as buildings. On the other hand, if the user is moving at high velocities, he will go faster through shadowed areas and the fades will be shorter than if he is moving at low velocities. The interleaving time needed to guarantee a correct reception of the information is directly related to the length of the erroneous bursts and therefore is also related to the length of the fades. Durations of about 10 seconds have been estimated to be long enough to mitigate the shadowing effects caused by trees, as long as the velocity is not inferior to 10 km/h. The same duration is also long enough to mitigate the shadowing effects caused by large obstacles such as buildings, as long as the velocity is not inferior to 60 km/h [34]. In case reception is taking place at inferior velocities, as in the typical pedestrian velocity of 3 km/h, is advisable to assure service continuity by means of a larger deployment of the terrestrial component instead of increasing the interleaving duration. As the interleaving duration increases, also does the protection against long fades. However, long interleaving durations require more memory available in the terminal and bring along an increase in the delay of the information, which increments the zapping time and might degrade the user experience.

The portion of time between the moment when one user switches to one service and the moment when the information of this service is being displayed is referred to as zapping time. In the case of streaming services, when the user switches from one stream to another, the terminal must wait until the arrival of all the interleaved information before it can display any content. As a consequence, the user will have to stand in front of a black display without any feedback during the time required to switch between services. File delivery services are not affected by zapping time; the user has to wait until the file has been completely downloaded. File delivery services are usually background services because of the fact that the user is not aware of the service until it has been completed. However, streaming services are consumed by the user during its transmission, and it is important that the user has a fast feedback of the service. Because of this, long zapping times can seriously degrade the quality perceived by the user.

2.3.3.1.2 State-of-the-Art – DVB-SH

2.3.3.1.2.1 DVB-SH Overview

DVB-SH (Digital Video Broadcast – Satellite to Handheld), published in 2007 [35], is the European standard for the provision of video, audio and data services to handheld terminals such as mobile phones and portable receivers. The key feature of DVB-SH is that it is a hybrid satellite/terrestrial system that allows the use of a satellite to achieve wide area coverage. Satellite is probably the ideal medium for distributing a TV signal to large audiences covering large areas because the cost of network infrastructure is fixed and independent to the number of users. Whenever a line of sight between terminal and satellite does not exist, for example urban or indoor scenarios, terrestrial repeaters are employed to provide the missing coverage, but also can be used to transmit additional content particularized to each region. This capability increases the offer that is available to the users. DVB-SH hybrid architecture (see Figure 40) is able to combine the advantages of both philosophies supposing a highly efficient method for the provision of mass multimedia mobile services.

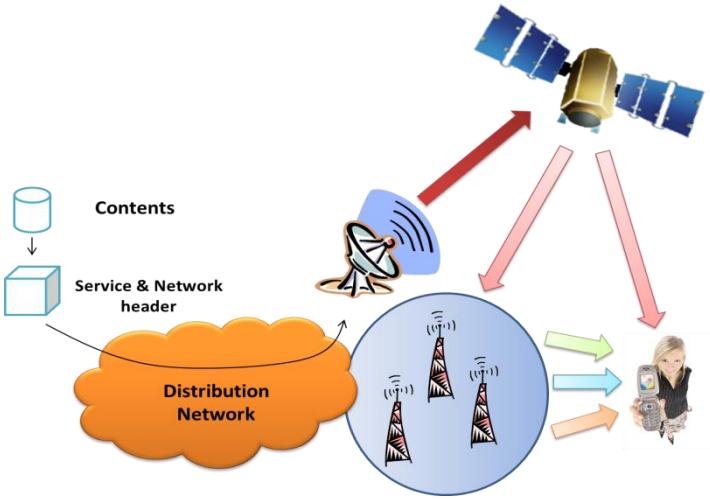

Figure 40: DVB-SH hybrid architecture.

DVB-SH employs an OFDM (Orthogonal Frequency Division Multiplexing) waveform in the complementary terrestrial network and an OFDM or a TDM (Time Division Multiplexing) waveform in satellite transmissions. OFDM waveform allows the deployment of Single Frequency Networks (SFN) in which receivers can combine the signals incoming from all the transmitters, satellite included, as long as the delay between signals does not overcome the guard interval of the OFDM signal. DVB-SH also allows for the TDM waveform in the satellite component, which is capable of supporting higher satellite transmission power. This is due to the fact that multicarrier signals as OFDM are characterized by a high peak power, forcing the on-board high power amplifiers to work far from the saturation point (for which the transmitted power is maximized) in order to avoid nonlinear distortions. TDM waveform allows the on-board transmitters to work closer to the saturation point, which represents a power advantage with respect to OFDM that involves an increase in the coverage provided by the satellite component.

The DVB-SH system has been designed for frequencies below 3 GHz, typically in the S-band around 2.2 GHz adjacent to the 3G terrestrial frequencies. The S-Band is very demanding in terms of signal coverage. Its short wavelength requires a quite dense terrestrial repeater network in towns and cities. Naturally the cost of this network can be reduced if the signal-to-noise ratio (SNR) required for stable reception is low. For that, DVB-SH includes features such as turbo coding for forward error correction (FEC) that enhance the signal robustness and a highly flexible channel interleaver that provides time diversity from about one hundred milliseconds up to 30 seconds [34] that helps to counteract the effects of signal fading on the transmission channel. DVB-SH incorporates on one hand, a physical layer interleaver of long duration, and on the other hand, a link layer multi burst protection mechanism. Both approaches are aimed to cope with the long errors bursts caused by shadowing.

The physical layer of DVB-SH incorporates new protection mechanisms with respect to its predecessor DVB-H (Digital Video Broadcast – Handheld) [36] such as a long duration interleaver and a turbocoder that replaces the convolutional coder found in DVB-H. The interleaver is introduced in order to mitigate the effects of the shadowing present in satellite reception. On the other hand, the turbocoder increases the robustness of the transmission thanks to its proven effectiveness in mobile environments.

Similarly to DVB-H, DVB-SH is based on the transmission of MPEG2 transport streams (TS) carrying information bursts compatible with the time slicing technique of DVB-H. An MPEG2 TS consists of MPEG2 packets of 188 bytes that are transmitted one after another. A CRC-16 is added to each one of these packets, so the receiver can know if any of these packets is erroneous. An MPEG2 TS can follow two different paths before its radio transmission according to the waveform is going to be transmitted. The two possible waveforms, OFDM and TDM, share common subsystems that process the information no matter

what the waveform is. These subsystems are the turbocoder and the physical layer interleaver. The turbocoder incorporated in DVB-SH is the one standardized by the 3GPP2 and also employed by 3G systems. However, the turbocoder implementation in DVB-SH features new code rates in order to increase the flexibility in the level of protection.

2.3.3.1.2.2 Convolutional Interleaver (CI)

The channel interleaver incorporated in DVB-SH is situated right after the turbocoder output and is made of two cascade interleavers, a bit interleaver and a time interleaver. The bit interleaver is in charge of rearranging the bits inside each block word that comes from the turbocoder. After this, a rate adaptation process punctures the block words so they can be multiples of 126 bits, which is the size of one interleaving unit (IU). Following the rate adaptation process, the time interleaver takes as input the sequence of IUs of 126 bits cells and spread them over many distinct time instants by means of a convolutional interleaver. In the receiver, these IUs are again collected, reordered and forwarded to the turbo decoder. There are two different physical layer interleaving durations defined in DVB-SH: one of about 200 ms that can work with a number of IUs up to 6528, and other one of about 10 s that can work with a number of IUs up to 417792. This possibility brings out two different terminal classes: a class 1 terminal, with short physical layer interleaving (200 ms), and a class 2 terminal with long physical layer interleaving (10 s). In order to store and process the interleaved information, class 1 terminals need at least 4 Mb of memory resources whereas class 2 terminals need at least 256 Mb [34].

2.3.3.1.2.3 MPE-iFEC

The implementation of long interleaving depths at the physical layer involves an increase in the memory requirements, which has an important impact in the hardware complexity and cost of user terminals. On the other hand, the implementation of interleaving at upper layers requires between 10 and 30 times less memory. Moreover, upper layer FEC mechanisms can use the general purpose memory of the user terminals for interleaving purposes. Because of this, it is possible to implement long interleaving depths at upper layers without the need of additional hardware.

DVB-SH introduces a new inter burst protection technique at the link layer called MPE-iFEC (Multi Protocol Encapsulation – Inter burst Forward Error Correction) MPE-iFEC is a *multi-burst* sliding mechanism that performs an interleaving able to repair fading typical of mobile satellite reception. However, another scheme based in Raptor codes is referred in the standard as optional. The RS sliding mechanism can benefit from the reuse of a well-known code such as the RS (255,191), whereas the Raptor based mechanism can benefit from a full software implementation of a fountain code, but are under the protection of the intellectual property. In a multi-burst codification, several bursts are coded together to generate the parity information. Later, this parity is spread over time. This *multi-burst* coding, in contrast to *intra-burst* coding, can recover burst completely lost.

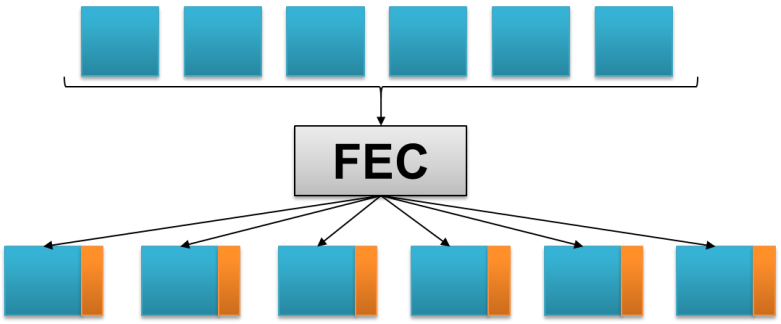

Figure 41: MPE-iFEC Encoding process.

2.3.3.1.2.4 Convolutional interleaving for the Long TI Feature of DVB-NGH

DVB-NGH has adopted for the sheer terrestrial profile (i.e., terminals without external TDI memory), a convolutional interleaver for inter-frame time interleaving, keeping the block interleaving only for intra-frame interleaving. This way, longer TI durations can be achieved for a given memory. In the BICM module at the transmitter side, the CI is introduced before the BI. This allows combining the BI and CI into one single interleaver, such that each interleaver does not need dedicated memory.

Since the CI is adopted for the sheer terrestrial profile, and it is used in DVB-SH, it was considered as the reference point for the hybrid terrestrial-satellite profile of DVB-NGH. The CI can provide fast zapping with long time interleaving using a uniform-late profile or a uniform-early profile. The uniform-late profile has the advantage that full protection is progressively and smoothly achieved with time, and that the end-to-end latency is constant. The robustness after zapping is given by the amount of parity data transmitted in the late/early part. The size of the early/late part represents a trade-off between overall performance in mobile channels and performance after zapping. In DVB-SH, it is recommended to employ a code rate 4/5 [34] such that users in good reception conditions (e.g., in line-of-sight with the satellite), can benefit of fast zapping. In DVB-SH, the uniform-late profile of the CI provides good zapping performance at the expense of reducing the overall performance in the LMS channel with respect to the uniform profile (between 2 to 4 dB [34]). However, the use of CI with a single FEC is cumbersome in DVB-NGH because, unlike turbo-codes, LDPCs exhibit very poor performance with heavy puncturing (erasures).

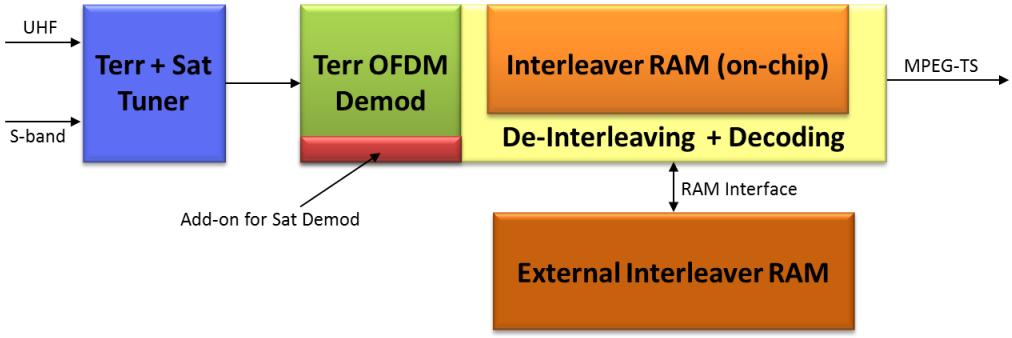

Figure 42: Functional overview of a NGH hybrid terminal.

Hybrid terminals have two TDI memories. On-chip and external RAM. On-chip is same memory as sheer terrestrial terminals. This memory is used only for intra-frame interleaving. DVB-NGH has the same on-chip memory size than DVB-T2 (i.e., $2^{19} + 2^{15}$cells). On the other hand, external RAM is dedicated for long TI providing. The size of external TDI memory has been set by the standard to 2^{22} cells.

2.3.3.1.2.5 Simulation Results

This section deals with the performance of convolutional interleaving with single FEC for the following channels: the AWGN (Additive White Gaussian Noise), the TU6 (Typical Urban 6-path) mobile, and the SU LMS sub-urban (SU) [33]. Table 28 shows the simulation parameters used for the simulations.

Table 28: Simulation parameters for time interleaving performance evaluation.

Bandwidth	8 MHz (AWGN/ TU6) 5 MHz (LMS)	f_{RF}	600 MHz (TU6) 2.2 GHz (LMS)
FFT Size	8K (AWGN/TU6) 2K (LMS)	**FEC Codeword**	16200
Antenna Conf.	SISO	**Velocity**	60 km/h
Guard Interval	1/4	**Overall Code Rate**	1/3
Frame Duration	200 ms	**Sub-slicing**	Maximum
Cycle Time	1 s.	**Time interleaving**	10 s.
Constellation	QPSK	**Simulation time**	1 hour
Rotated	Disabled	**Service Rate***	250 kbits/s
Ch. Estimation	Ideal	**QoS Criterion**	ESR5(20) 90%

*Assumptions: 6 bytes BB frame header, 168 bits BCH

2.3.3.1.2.6 Fast zapping results

As previously mentioned, the TI can be configured to provide fast zapping using Uniform-Late (UL) profiles. The UL profile ensures that a big part of the encoded code word is available already with the first frame. In case of good reception conditions this part is already sufficient for successful decoding. In the worst case, when all of the transmitted redundancy is required to receive the data the zapping time may be up to the full TI length. The UL profile is recommended, if a short zapping time is important. However using UL profile involves a performance penalization in comparison to using uniform profile.

Figure 43 compares performance of single FEC with a code rate 1/3 with two sizes of the late part (40% and 50%) in AWGN channel. The early decoding performance of single FEC depends on the size of the late part, which determines the effective code rate after zapping.

Single FEC suffers performance degradation because, unlike turbo-codes, LDPCs exhibit very poor performance with heavy puncturing (erasures). It should be noted that this puncturing in DVB-NGH is at cell level, and it cannot be optimized like the one performed for layer 1 signaling in DVB-T2 [34]. When the late part of the CI profile is 50%, there is an effective puncturing after zapping of 50% of the codeword (effective code rate after zapping is 2/3). In this case, the degradation at frame error rate 10^{-3} is around 0.5 dB. The performance degradation increases for lower sizes of the late part, because the puncturing is higher. If the late part is 40%, there is an effective puncturing after zapping of 60% of the codeword (effective code rate after zapping is 5/6). In this case, the degradation at frame error rate 10^{-3} is around 4 dB.

Figure 44 shows the performance over time of single FEC with CI in the TU6 channel model at 10 Hz Doppler with two CI profiles configuration: Uniform and Uniform-Late 50% in comparison with Single FEC 2/3 without time interleaving. In the figure, it can be observed that single FEC with a uniform CI profile is not capable of providing fast zapping. We can also see that the performance degradation of single FEC after zapping is significantly larger in fading channels than in AWGN. If in Figure 43 the degradation for a 50% uniform-late CI was just 0.5 dB, in Figure 44 the degradation is 4 dB.

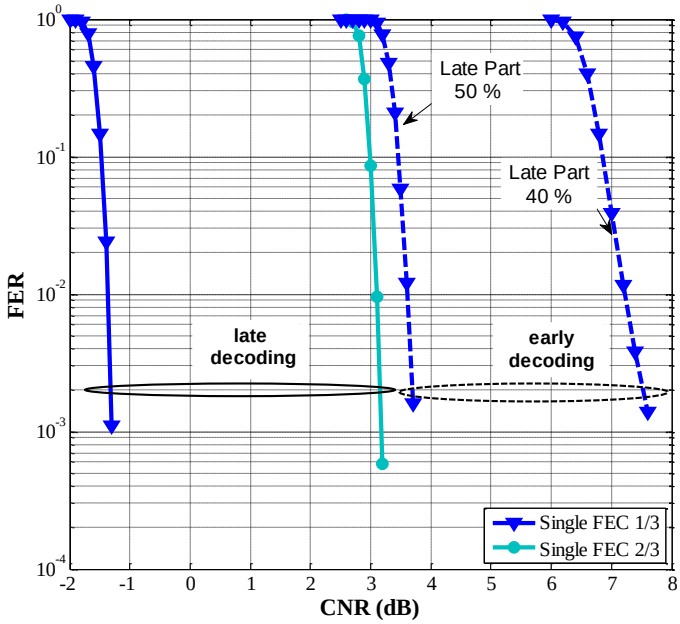

Figure 43: Performance comparison in AWGN channel of different CI profiles configuration.

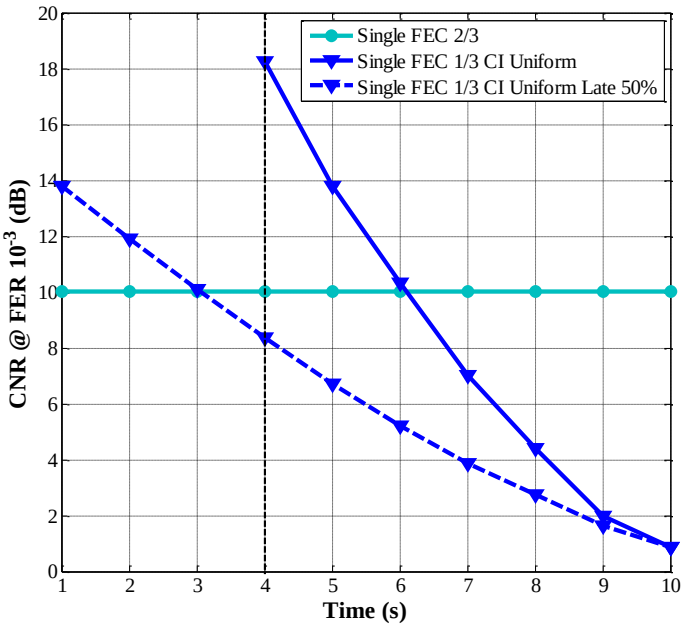

Figure 44: Performance comparison between CI Uniform and CI Uniform Late 50% for an overall code rate CR 1/3 in the TU6 channel at 10 Hz Doppler. Modulation is QPSK.

2.3.3.1.2.7 Time interleaving length

The maximum TI length depends on the data rate of the PLP, the amount of TDI memory available in the receivers, the FEC code rate, the constellation order and the TI profile selected. For a fixed TI length, the memory required by a CI is always less than half of the memory required by a BI. This involves that for a certain TDI memory - set by the standard – the maximum TI length provided by a BI could be increased or even doubled using a CI.

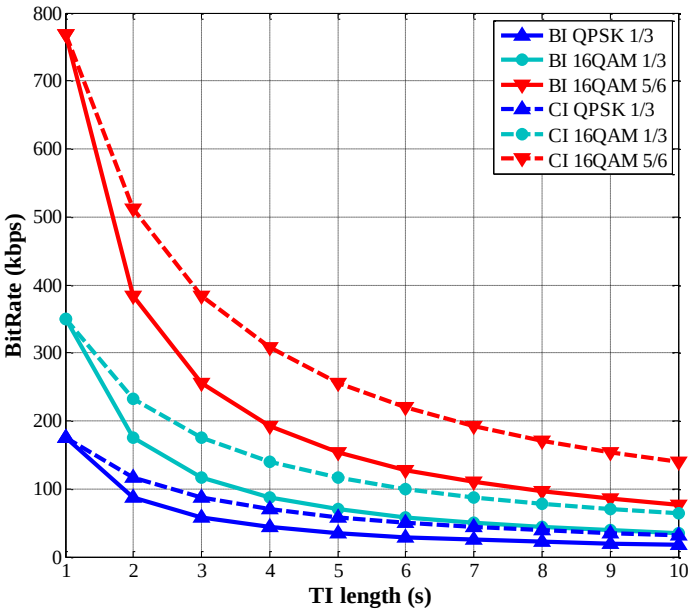

Figure 45: Maximum PLP data rate supported in NGH (CI) in comparison with T2-Lite (BI) with respect to the interleaving duration for different constellations and code rates. TDI memory is fixed to 218 cells.

2.3.3.1.2.8 Long Time Interleaving Results

Land Mobile Satellite (LMS) channel is characterized by long signal outages (e.g., due to the blockage of the line of sight with the satellite caused by tunnels, buildings, trees, etc.), which can only be compensated with a long time interleaving duration. Figure 46 shows simulation results in the LMS Sub-Urban (SU) channel of the late decoding performance for single FEC with two different configurations of the CI for providing inter-frame interleaving: uniform and uniform-late with 50% late part (TI length of 10 s.) in comparison with using only intra-frame interleaving (TI length of 200ms). The ESR5(20) quality of service (QoS) criteria represents the percentage of intervals of twenty seconds which contain at most one second with errors. The best performance is achieved by single FEC with a uniform CI profile, as expected. The performance of single FEC with the CI uniform-late profile is reduced about 2 dB compared to the CI uniform profile. CI with TI length of 10 s. achieves gains between 6-8 dBs.

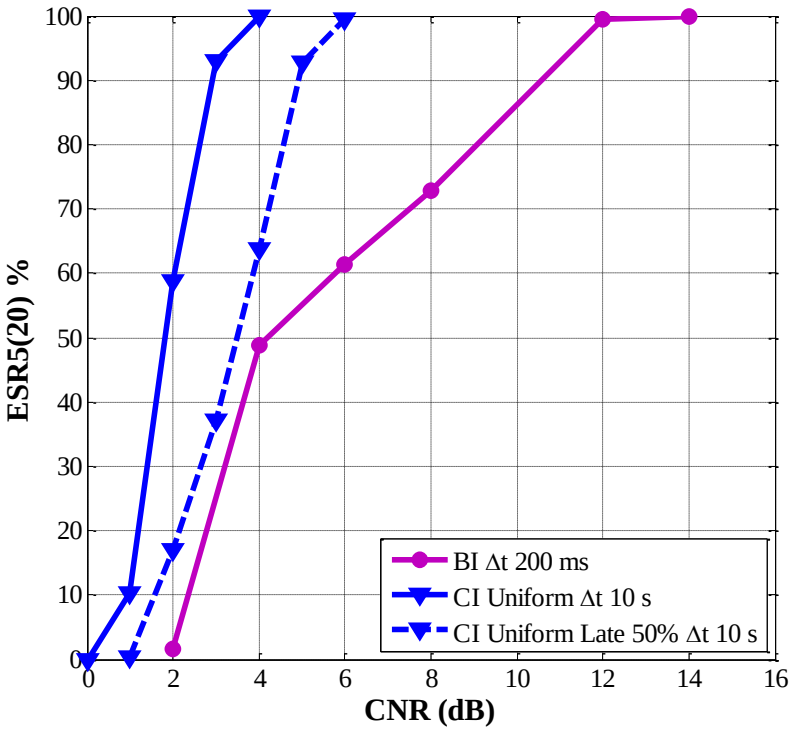

Figure 46: Performance comparison in LMS channel of the different CI profiles (Uniform and Uniform-Late 50%) for providing long time interleaving (10s.) and BI providing only intra-frame interleaving (200ms.). Overall code rate is 1/3.

2.3.3.2 Performance analysis of time interleaving

For a satellite part, a long interleaver is needed to cope with the fluctuation of the shadowing effect seen by the mobile receivers while the code-rate is tightly tuned to the optimization of the satellite link budget and the compromise with data throughput. Two solutions have been introduced in DVB-SH: one solely on the physical layer with the class 2 physical time interleaver, and the other one on the link layer with the class 1 physical time interleaver. The class 2 interleaver must be implemented at the physical layer. This solution obtains the best performance in terms of decoding capability but it has zapping and service access times higher than those expected with NGH standards. The class 2 interleaver is a good compromise between robustness and zapping time. The interleaver added with MPE-IFEC on top of class 1 physical interleaver is less performing but it allows lower zapping and service access time. The class 1 interleaver is a good compromise between zapping time and implementation easiness. The use of a return channel may improve the performance of this solution as well in a compromise to be done with the additional use of the forward link it will trigger.

2.3.3.2.1 Physical interleaver description

On the physical layer, four families of time interleavers have been analyzed in DVB-SH standard: the short uniform, the long uniform, the long uniform late and the long early late.

- The short uniform: the SH frame is not divided, it is sent in one time.
- The long uniform: the SH frame is divided as much as possible and sent during a long time.
- The long uniform late: the SH frame is divided in 2, the first half is sent and the other one is re-divided in small piece and sent during the rest of the time.

- The long early rate is only divided in two parts and sent in a long time.

Figure 48 below illustrates their typical behavior on a satellite transmission channel.

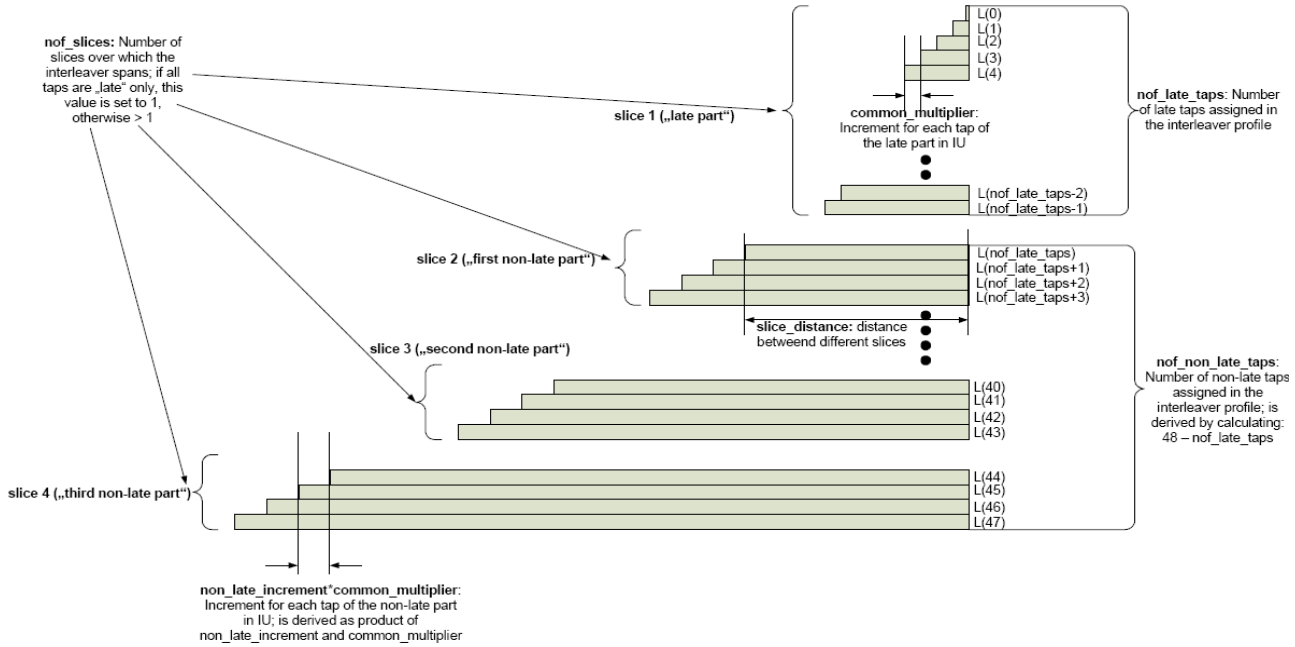

Figure 47: All the parameters for the time interleaver (from DVB-SH standard).

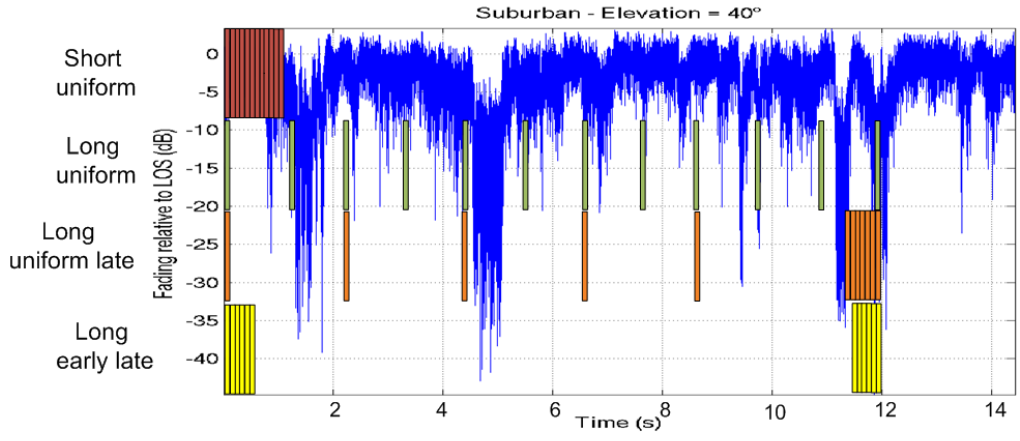

Figure 48: The 4 different families of time interleaver.

The short uniform is the best one for the zapping time. In fact, the receivers will capture faster a big amount of information than for the other temporal interleavers. The long uniform is the best against the shadowing effect. The long uniform late is the best compromise for a good zapping time and against long shadowing.

2.3.3.2.1.1 Link layer interleaver description

On the link layer, the MPE-IFEC (Multi Protocol Encapsulation- Inter Burst FEC) framework was defined to implement both erasure coding and interleaving on the link layer and is used to improve the reception when the protection level of the physical layer is not sufficient. This mechanism is described in the DVB-SH

implementation guidelines [34], in Section 6.2. The principle is to use several coding windows (called ADT: Application Data Table) filled with several parts of different data bursts to build redundancy packets which are sent along with the data.

For MPE-IFEC, a datagram burst is made of one or several consecutives datagrams of the network layer (for example IP packets). The number of datagram in a burst can vary on burst by burst basis. Indeed, the principle is that the datagram burst has to contain the data corresponding to a constant duration of the video and the video can have a variable data rate. The MPE-IFEC burst is build by the addition of the redundancy created by the MPE-IFEC mechanism and the datagram burst. When MPE-IFEC is not used, the datagram burst is directly transmitted to the physical layer and the data of a link layer burst are sent during a physical layer burst.

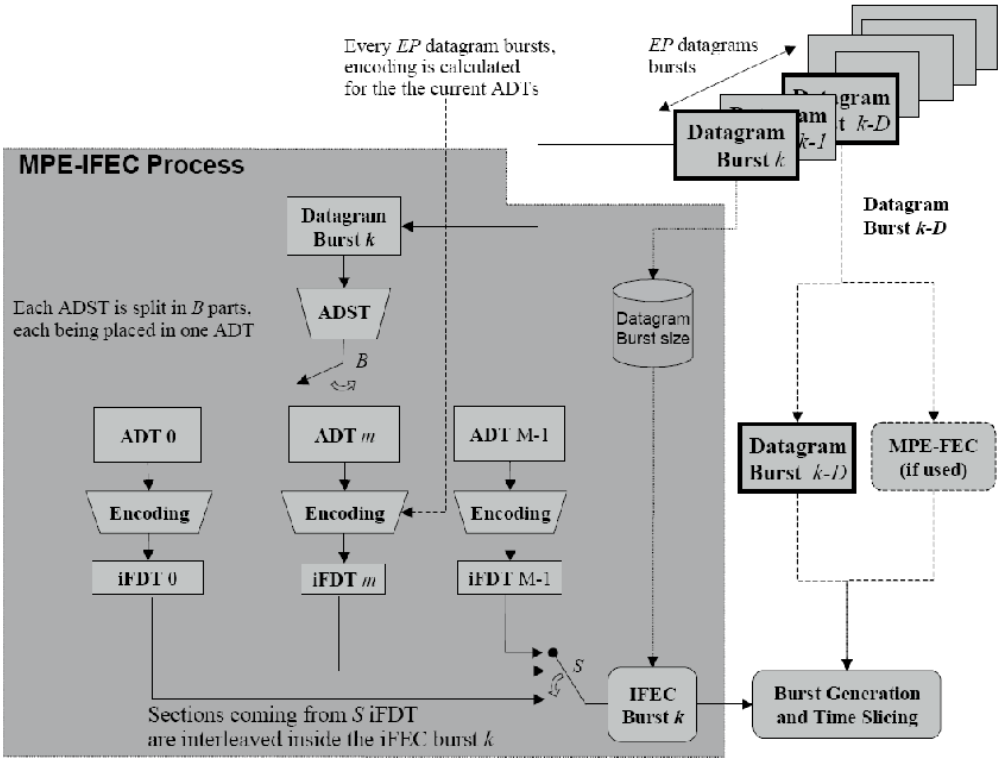

Figure 49: Overview of the MPE-IFEC process.

The different parameters of the MPE-IFEC mechanisms are:

- *B* is the number of ADT to spread the data burst
- *M* is the number of ADT in the system
- *S* is the number of iFDT used to build a redundancy burst (a redundancy burst is build by the collection of the redundancy packet sent in a complete MPE-IFEC burst)
- *D* is the delay introduced on the data packet transmission
- *EP* is the encoding period

The MPE-IFEC mechanism will perform the following operations for each burst reception:

- The burst is spread over the *B* active ADT packet by packet,

- The encoding operation is performed when the ADT is completed,
- The redundancy packet are stored in the iFDT table corresponding to the active ADT,
- The redundancy burst is build using the redundancy packets from the previous *S* iFDT packet by packet,
- The MPE-IFEC is then composed by the data burst and the redundancy burst and the ADT are shifted.

Finally the decoding process is made as soon as possible (early decoding); it is needed to receive a sufficient number of redundancy packets to compensate the data packets losses.

2.3.3.2.2 ESR5 criteria

Definition is taken for DVB-SH implementation guidelines [34], in Annex A. It is important to distinguish the ESR5 criterion from the ESR5(20) ratio. Literal and mathematic definitions are given hereafter.

- ESR5(20) is the ratio of time windows for which ESR5 is fulfilled, over the total number of time windows.
- ESR5 criterion is fulfilled when in a time interval of 20 seconds there is at most one second in error.

The exact formulation of the ERS5(20) ratio is:

$$ESR5(20) = 1 - \frac{\sum_{w=1}^{Nw} ceil\left\{\frac{\max[0; n\_of\_erroneous\_seconds(w) - 1]}{20}\right\}}{N_w},$$

where we assumed an individual observation window size of 20 seconds.

- *Nw* represents the number of observation windows,
- *n_of_erroneous_seconds*(*w*) is the number of erroneous seconds in the window *w*,
- The ceil function round the specified number up, and return the smallest number that is greater than or equal to the specified number.

The previous formula needs to be adapted to the type of measurements possible within the receiver:

- It is very important that ESR5(20) statistics are obtained over a long enough measurement time in particular at low mobile speed,
- The *Nw* 20 s windows used for the measurement may be disjoint or overlapped.

- When a burst is sent every second, ESR5(20) will be computed with 20s delay window:

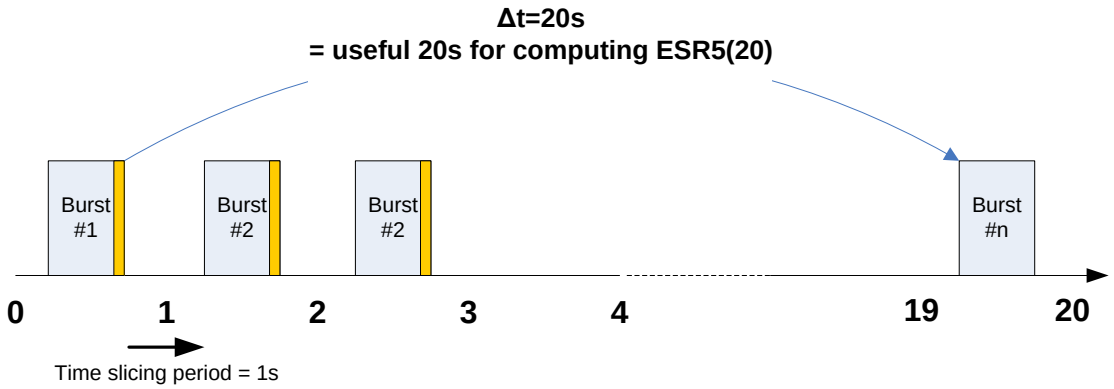

Figure 50: Computation of ESR5(20) for a 1s time slicing.

- When a burst is sent every 2 seconds, ESR5(20) will be computed with real time 40s delay window (but useful 20s window):

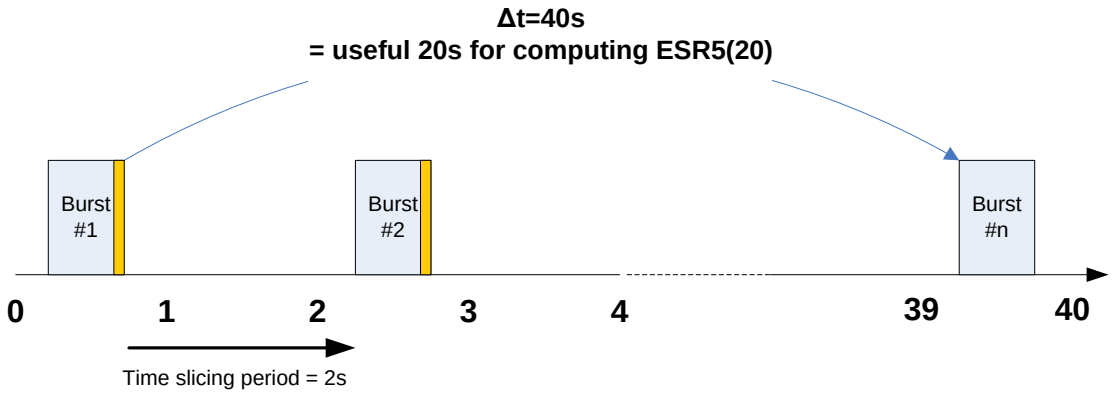

Figure 51: Computation of ESR5(20) for a 2s time slicing.

2.3.3.2.3 Which interleaver is the most suitable for Satellite transmission

Three main criteria can be considered to choose the most suitable interleaver for satellite transmission:

- performances,
- zapping time,
- Memory requirements on the receiver side.

In this paragraph, we present the results of the comparison of the first criteria "Performances". Simulations have been done in the DVB-SH framework in order to compare the performance of the different solutions. Simulations are done with short uniform (identified as S), long uniform (identified as U) and uniform late (identified as UL).

The characteristics of the physical layer are: OFDM, Mode of 2K, Guard Interval of ¼ and Bandwidth of 5 MHz. The modulation used is QPSK and Coding rate of 1/3. The channel model is Land Mobile Satellite (LMS) channel at a speed of 50km/h. Different Interleaver lengths are simulated:

- - For the long Uniform: 11 s, (40, 0, 12 4, 2)
- - For the Uniform Late: 10 s, (10, 24, 9, 5, 12)

- - For the Short Uniform: 211 ms, (5, 48, 1, 0, 0)
- - For another Short Uniform: 86 ms, (2, 48, 1, 0, 0)

The different interleaving schemes are compared according to the ESR5 criterion.

2.3.3.2.3.1 Uniform and Uniform Late vs. Short interleavers in ITS LMS channel

The environment is Intermediate Tree Shadowing and the speed is of 50 km/h.

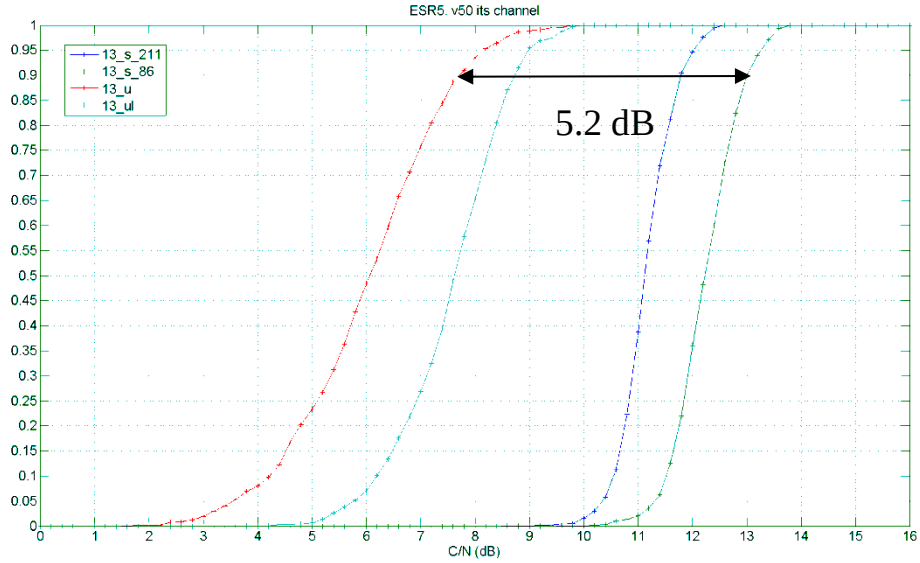

Figure 52: Physical interleaver performance in ITS environment.

These simulations results enable to verify the gain brought by the use of long interleaving: Long Uniform interleaver (U) outperforms Short interleaver (s_211ms) as about 4 dB and the difference can reach 5.2 dB between the Long Uniform interleaver (U) of 11s and the Short interleaver of 86ms. Moreover, the Long Uniform interleaver (U) outperforms the Uniform Late interleaver (UL), but will have less zapping time performance.

2.3.3.2.3.2 Uniform and Uniform Late vs. Short interleavers in SUBURBAN LMS channel

The environment is Suburban and the speed is of 50 km/h. The satellite reception in suburban environment is easier than in the LMS-ITS environment.

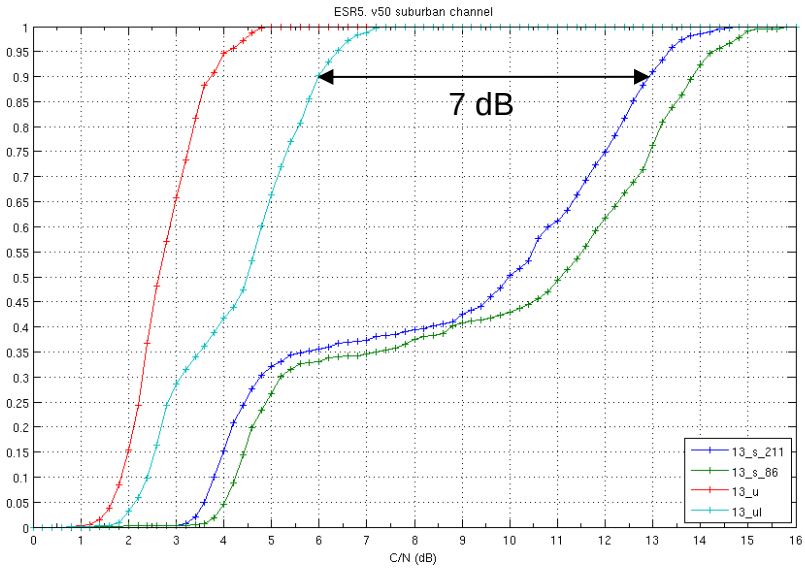

Figure 53: Physical interleaver performance in suburban environment.

Uniform Late interleaver (UL) outperforms Short interleaver (s_211ms) as about 7 dB. The landing of the curves for short interleavers is due to the LMS channel in Suburban environment.

2.3.3.2.3.3 Short interleaving combined with upper Layer FEC in ITS environment

For link layer interleaver, the simulations are run using MPE-IFEC with the following characteristics:

- ⇨ *EP*= 1: Encoding process occurs at every burst,
- ⇨ *B*=5: Encoding parallelization; the burst is split into *B* parts distributed over *B* parallel encoding matrices,
- ⇨ *S*=5: Depth of the FEC spreading factor,
- ⇨ *B*+*S*=10: give the number of bursts required to have complete information for the decoding of one given burst.
- ⇨ Code Rate is 2/3

In the simulations, one burst of the considered data stream is received every second.

The environment is the Intermediate Tree Shadowing for a speed of 50 km/h.

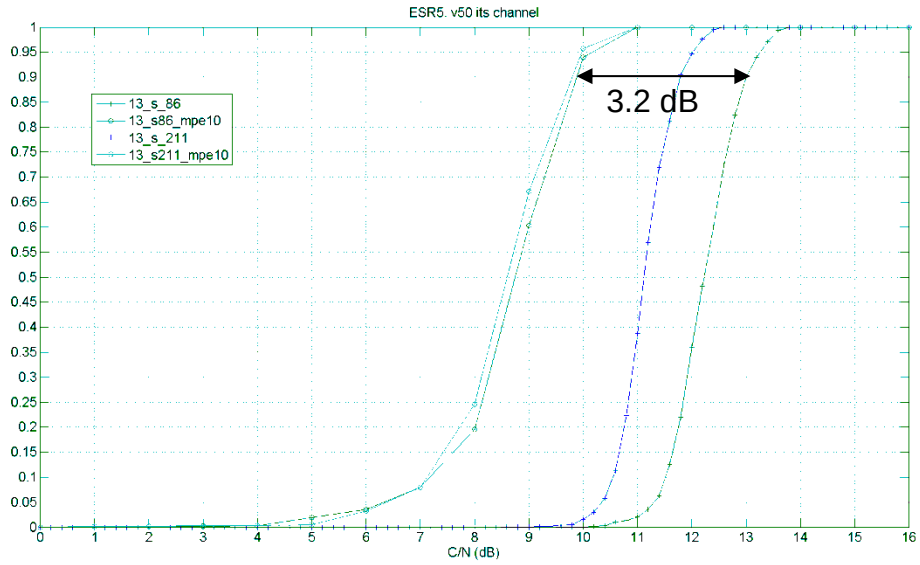

Figure 54: MPE-iFEC added to short physical interleaver.

The impact between the length of 86 ms or 211 ms of the short interleaver combined with the upper Layer FEC is reduced.

The upper layer FEC improves the performance of about 3.2dB of the short interleaver at the expense of spectrum efficiency.

2.3.3.2.3.4 Upper Layer FEC vs. Long time interleaver in ITS environment

The environment is Intermediate Tree Shadowing and the speed is of 50 km/h.

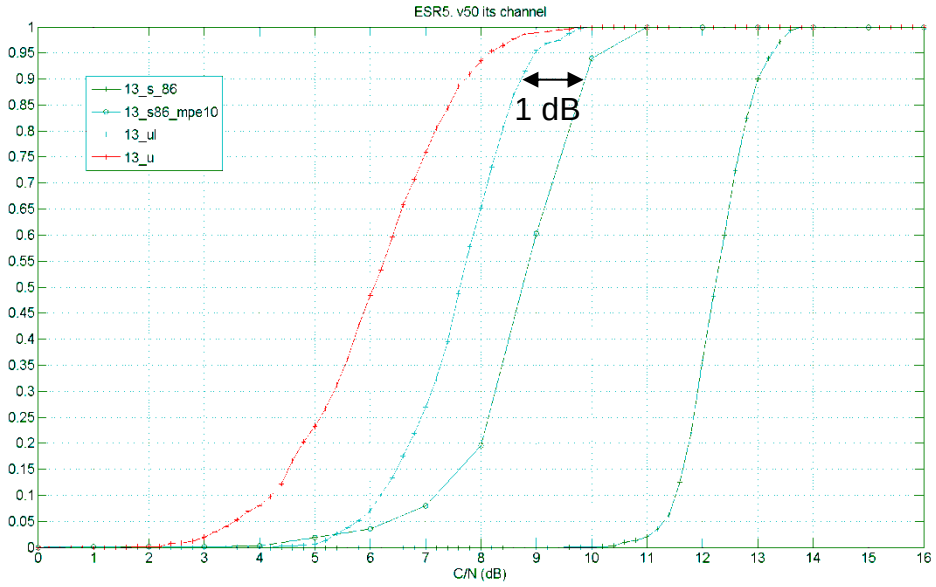

Figure 55: Performance comparison between physical and link layer interleavers.

In LMS-ITS channel, Upper layer FEC performance is close to Uniform Late time interleaver performance at the expense of spectrum efficiency. *B*+*S* can also be increased to improved MPE-IFEC performance.

2.3.3.2.3.5 Upper Layer FEC with higher B+S value in ITS environment

For link layer interleaver, the simulations are run using MPE-IFEC with the following characteristics:

- *EP*= 1: Encoding process occurs at every burst,
- *B*=5: Encoding parallelization ; the burst is split into B parts distributed over B parallel encoding matrices,
- *S*=5: Depth of the FEC spreading factor,
- *B*+*S*=20: give the number of bursts required to have complete information for the decoding of one given burst.
- Code Rate is 2/3 for "13_s211_mpe20" and 1/2 for "12_s211_mpe20".

In the simulations, one burst of the considered data stream is received every second.

The environment is Intermediate Tree Shadowing and the speed is of 50 km/h.

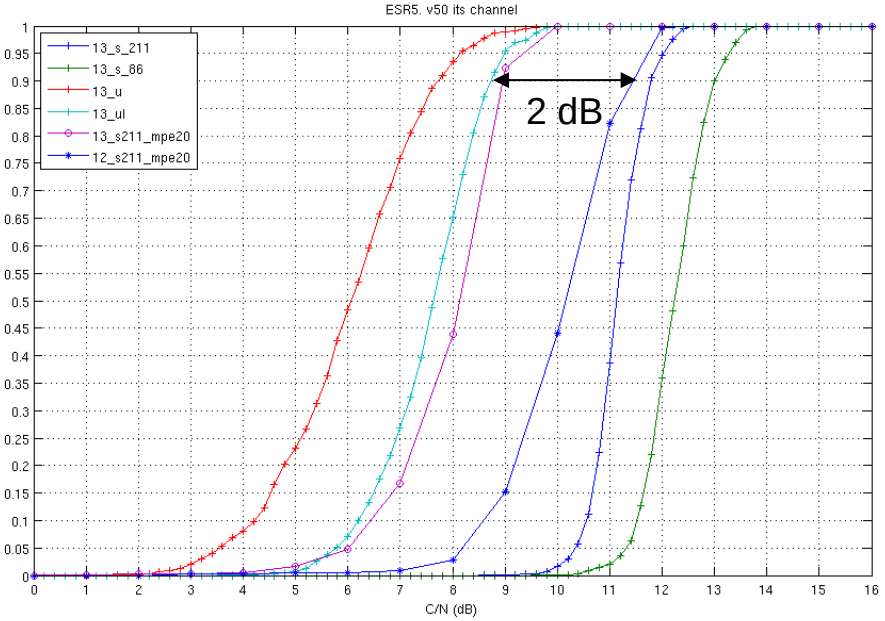

Figure 56: Performance comparison between physical and link layer (with higher value of B+S) interleavers.

Uniform Late interleaver ("13_ul") outperforms MPE-IFEC ("12_s211_mpe20" curve) by only 2 dB with the same spectrum efficiency (overall code rate of 1/3).

The two solutions achieve the same performance at the cost of spectrum efficiency. Overall code rate is 2/9 for solution with FEC solution ("13_s211_mpe20" curve) and 1/3 for solution without FEC ("13_ul" curve).

2.3.3.2.3.6 Analysis of the DVB-SH solutions

The simulations performed on the DVB-SH waveform, shows the interest of long interleaving by showing the important gain brought by this technology, and also its superiority in terms of performance in comparison to link layer solution MPE-IFEC.

Nevertheless, other criteria have to be taken into account for the selection, i.e. the zapping time performance of each solution and the constraints in term of complexity and memory.

2.3.3.2.4 Strategies for time interleaving and interleaving solutions retained in DVB-NGH standard

In the DVB-NGH standard, the work has been focused on the physical layer solutions. The satellite profile includes the time interleaver options retained for the terrestrial profile, i.e. the concept of a combination of block and convolutional interleaver for inter frame interleaving. Block interleaver only can be used for intra frame interleaving. The working assumption is that the interleaver unit size is in this case equals to the FEC Frame divided by the number of the interleaved frame. Moreover, the need for long time interleaving is required in certain scenarios for the satellite; Convolution Interleaving with a Uniform Late profile is available for those contexts.

2.3.4 L1 Signaling in the satellite context

2.3.4.1 L1 Signaling for the Hybrid Profile

2.3.4.1.1 Introduction

The sheer terrestrial profile in DVB-NGH has adopted three new mechanisms in order to enhance the robustness of the layer 1 (L1) signaling: 4K LDPC codes (mini-codes), Additional Parity (AP), and Incremental Redundancy (IR). These mechanisms are used in conjunction with the L1 repetition scheme from DVB-T2, being the use of In Band signaling optional in DVB-NGH.

The hybrid satellite-terrestrial profile of DVB-NGH is more robust than the sheer terrestrial profile, because it includes a more robust code rate for the data (i.e., 1/5 instead of 1/3), and the long-time interleaving feature.

The goal of this section is to investigate the feasibility of the new techniques for L1 signaling robustness for the hybrid profile. A summary of L1 signaling robustness in the sheer terrestrial is provided first. Then, the simulation performances and results are given.

2.3.4.1.2 Summary of L1 Robustness in the Sheer Terrestrial NGH Profile

The physical layer signaling of DVB-T2 was designed such that it can always be made more robust than the data path. The transmission and detection of the preamble P1 symbol is very robust, and it can be correctly received even at negative signal-to-noise ratios (SNR) under mobility conditions. The transmission of the rest of the physical layer signaling in the P2 symbol(s) can be configured sufficiently robust in rather static reception conditions. However, in mobile reception conditions the robustness of the L1 signaling, in particular the L1-post field, may not be high enough due to the lack of time diversity.

DVB-NGH has enhanced the physical layer signaling of DVB-T2 in three different aspects:

- Improved transmission robustness.
- Reduced signaling overhead.
- Higher signaling capacity.

The improvement in the signaling robustness is especially relevant, because DVB-NGH adopts for the data path code rates more robust than in DVB-T2 (i.e., 1/3 for the sheer terrestrial profile, and 1/5 for the hybrid satellite-terrestrial profile). DVB-NGH adopts for L1 signaling new mini LDPC codes of size 4320 bits (4K) with a code rate 1/2. Although 4K LDPC codes have a worse performance than the 16K LDPC codes of size 16200 bits used in DVB-T2 for L1 signaling, the reduced size of the 4K LDPC codes is more suitable for the L1 signaling because it reduces the amount of shortening and puncturing. In DVB-T2, LPDC codewords with L1 are shortened (i.e., padded with zeros to fulfill the LDPC information codeword) and punctured (i.e., not all the generated parity bits are transmitted), which decreases the LDPC decoding performance.

The adopted 4K LDPC codes have the same parity check matrix structure than the 16K LDPC codes used for data protection. This allows for efficient implementations at the transmitter and receiver side efficiently sharing the same logic. On the other hand, two mechanisms have been adopted in DVB-NGH to improve the robustness of the L1 signaling known as Incremental Redundancy (IR) and Additional Parity (AP). These two mechanisms are used as a complement of L1 repetition. The additional parity mechanism transmits punctured bits in the following frame. In case there is need for more parity bits, the incremental redundancy mechanism extends the original 4K LDPC code into an 8K LDPC code of 8640 bits. The overall code rate is thus reduced from 1/2 down to 1/4. L1 repetition can be used to further improve the robustness of the L1 signaling as a complement of AP and IR.

The robustness improvement of the L1 signaling in DVB-NGH can be translated into a reduction of the signaling overhead for the same coverage. But DVB-NGH has restructured the L1 signaling structure of DVB-T2 in order to further reduce the signaling overhead. Instead of signaling the configuration of each PLP (MODCOD, TI, modulation, code rate, and time interleaving configuration), PLPs are associated in groups with the same settings, reducing the required L1 signaling information. Furthermore, it is possible to split in several frames signaling parameters which are in practice static, and which are transmitted in DVB-T2 in every frame.

DVB-NGH has also increased the signaling capacity. A new signaling L1 PLP has been defined for the L1-post information. The signaling L1 PLP is transmitted at the beginning of the frame and can be transmitted outside the P2 symbols in data OFDM symbols.

2.3.4.1.3 The physical layer signaling in the Hybrid NGH Profile

The satellite component of DVB-NGH is optional. The satellite profile of DVB-NGH has been designed with the goal of keeping the maximal commonality with the terrestrial component to ease its implementation at the receiver side.

For the hybrid profile of DVB-NGH, an additional preamble P1 (aP1) symbol has been introduced in order to increase the signaling capacity of the P1 symbol. The P1 symbol signals the presence of the aP1 symbol. The aP1 symbol is only transmitted for hybrid terrestrial-satellite DVB-NGH networks, such that it is not transmitted if it is not needed.

In the Hybrid profile study, the main objective of the study was to check if there was any issue to solve concerning the robustness of L1 signaling in the Satellite path and to suggest the extra tools needed to be added. The studies showed that the available L1 signaling robustness tools in the Terrestrial profile were sufficient to meet the requirements in the Satellite path, but with some configuration of Additional Parity (AP2) L1-dyn repetition is needed. In addition, with AP3 configuration the robustness of L1 signaling is enough to get better performance than data. As a conclusion, the tools assumed for the Terrestrial profile (4k, AP/IR and Fabrice decoding) in conjunction with L1-dyn repetition are enough sufficient to meet the requirements in the Satellite path.

2.3.4.1.4 Performance of L1 Robustness in the Hybrid NGH Profile

The following results were presented by Samsung at the DVB-Forum [37] and [38]. Samsung assessed the performance shown in these results with the tools adopted for the Terrestrial profile in the LMS channel.

In the Terrestrial profile, 4k PF72 codes were adopted for the NGH baseline after an exhaustive performance assessment with AP/IR over TU 6 channel [39], where the L1 signaling coding with AP was demonstrated to provide better performance than data performance (16k; 1/3, 100ms TI) and, therefore, solved the robustness issue of L1 signaling.

In the Hybrid profile study, the main objective of the study was to check if there was any issue to solve concerning the robustness of L1 signaling in the Satellite path and to suggest the extra tools needed to be added.

Samsung evidenced that the tools assumed for the Terrestrial profile (4k, AP/IR and Fabrice decoding) were not enough. The L1 signaling in the Hybrid profile with the Terrestrial tools lacked of robustness if

compared to data (CR1/5, QPSK). In order to overcome this lack of robustness, Samsung suggested using the L1-dyn repetition strategy from DVB-T2 with some combinations of Additional Parity (AP2) and without L1-dynamic repetition AP3.

Finally, Samsung's report showed that the available L1 signaling robustness tools in the Terrestrial profile were sufficient to meet the requirements in the Satellite path. Therefore, no extra tools were found necessary to be added.

Next results were presented in [38] by Samsung. The following tables summarize the simulation conditions used:

Parameter	Value
LMS Channel Model	Perez-Fontan3 state statistical model
Center Frequency	2.2 GHz
Elevation	40 degree
Receiver Speed	60 km/h
Receiver Environment	SU (Sub-Urban)

	Parameter	Value
OFDM	FFT Size	2048
	BW	8MHz
	GI	¼
	PP	PP1
	FEF + T2 frame	300ms
Data (for reference point)	MODCOD	QPSK, CR =1/5, 1/3
	Time Interleaver	100ms, Type 1 PLP
	QEF FER	10^{-5}
	Decoding	50 iterations, LLR : MAX_LOG

	Parameter			Value
L1 Signaling	Number of PLPs, N			1, 4, 8,16, 32
	L1 Post (Config+Dyn)	QEF FER		10^{-4}
		Length	Joint Encoding	136 + 89N + 79 + 48N + 32 (CRC)
	MODCOD	Constellation		BPSK
		Coding	4K	CR=1/2 with IR (BCH parity= 60, t=5)
		Decoding		50 iterations, LLR: MAX_LOG
				w/or w/o Fabrice'sproposal if possible w/o repetition

Code rate achieved with Additional Parity:

				AP0		AP1		AP2		AP3	
PLP	**FEC Block**	**Ksig bits**	**BCH bits**	**Par. bits**	**L1 Post Eff_ Rate**	**Par. bits**	**L1 Post Eff_ Rate**	**Par. bits**	**L1 Post Eff_ Rate**	**Par. bits**	**L1 Post Eff_ Rate**
1	1	384	60	894	0.287	1206	0.232	1518	0.2	1830	0.17
4	1	795	60	1427	0.287	1926	0.232	2425	0.21	2925	0.18
8	1	1343	60	2139	0.287	2887	0.232	3636	0.27	4384	0.19
16	2	1220	60	1979	0.287	2671	0.232	3364	0.26	4056	0.19
32	3	1544	60	2410	0.287	3253	0.232	4097	0.27	4940	0.2

Eight PLPs have been taken into account as an example of the L1 signaling in the Satellite path. As it can be seen on Figure 57 and Figure 58, there is a lack of robustness compared to the most robust data method (CR1/5, QPSK). It is observed that Fabrice Decoder gives a gain of 2-3.0dB.

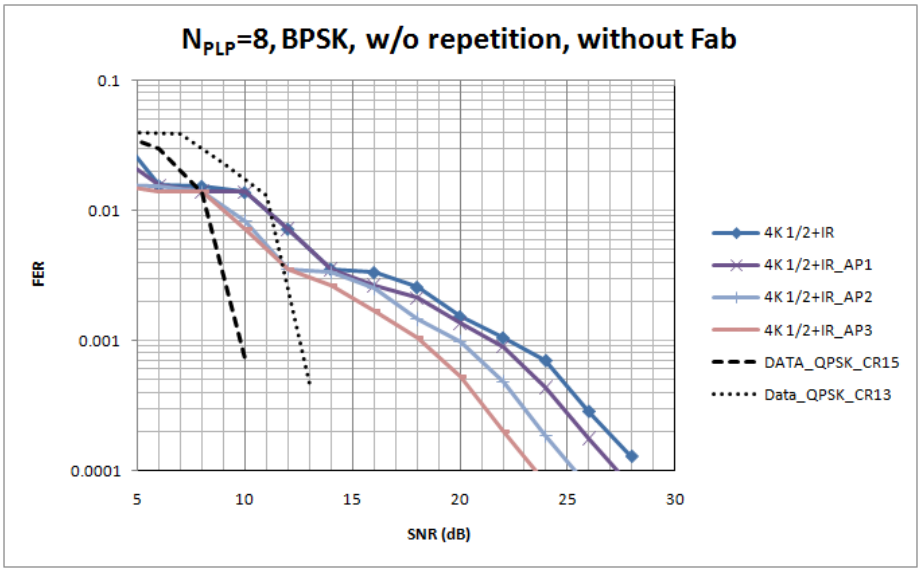

Figure 57: L1 signaling Performance over LMS Channel (NPLP = 8, without Rep and Fabrice Decoding).

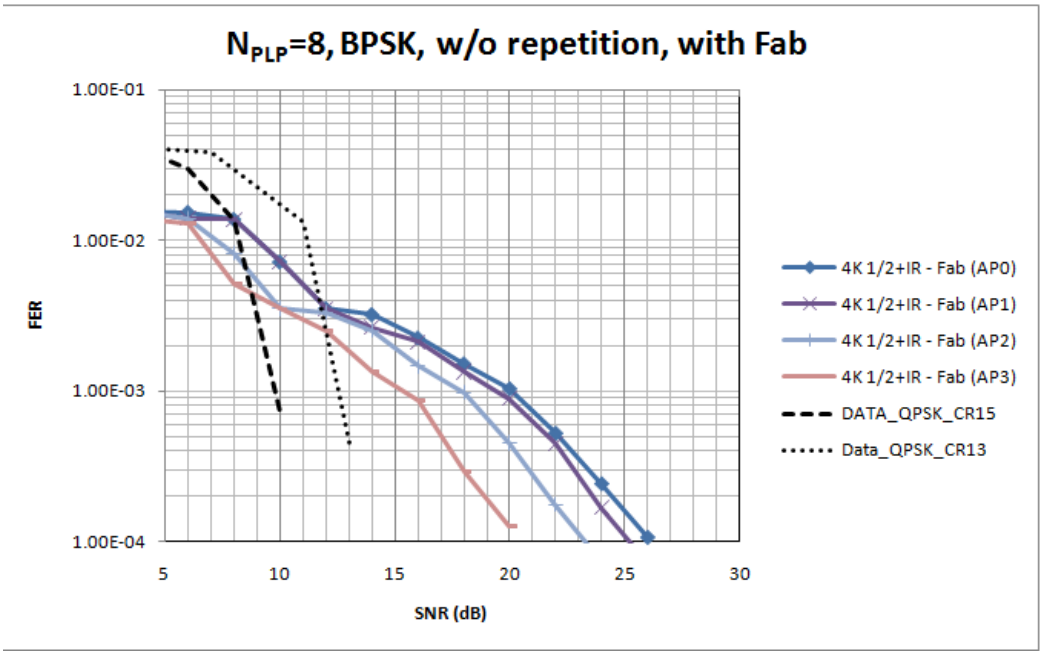

Figure 58: L1 signaling Performance over LMS Channel (NPLP = 8, without Rep and with Fabrice Decoding).

Figure 57 shows the L1 signaling performance with 8 PLPs without using Fabrice decoding. The most robust mode AP3 has a gain of 2.0dB. Figure 58 shows the L1 signaling performance in case of using Fabrice decoding. AP1 has a gain of 3.0dB. The results considered the FER metric (vs. SNR) and show that FER performance of L1 signaling with AP does not meet the requirement to ensure better performance than data in the Satellite path.

The following results were presented in [37] by Samsung, where they suggested using the L1-dyn repetition from DVB-T2 to overcome this lack of robustness. Using of ESR5 metric instead of FER as the former was more relevant to assess the robustness in the Satellite path. The simulation conditions used throughout these results were the same used at [38].

L1 Signaling Performance over LMS (@ ESR5(20) = 90%)			
	Repetition, Additional Parity Gain	**Robustness Compared to Data (R1/5, TI=200ms**	
AP0	L1-dyn gains of 2.7~3.2 dB	**w/o Rep:**	Not sufficient
	-	**w/ Rep**	Not sufficient
AP1	L1-dyn gains of 2.7~3.2 dB	**w/o Rep:**	Not sufficient
	AP1 gain compared to AP0 is 0.7~**2.1 dB**	**w/ Rep**	Not sufficient
AP2	L1-dyn gains of 2.7~3.2 dB	**w/o Rep:**	Not sufficient
	AP2 gain compared to AP0 is 1.5~**4.2 dB**	**w/ Rep**	**Sufficient**
AP3	L1-dyn gains of 2.7~3.2 dB	**w/o Rep:**	**Sufficient**
	AP3 gain compared to AP0 is 2.5~**4.7 dB**	**w/ Rep**	**Sufficient**

The following figures show the L1 signaling outperformance using ESR5(20) metric over LMS channel for the Satellite path. These figures are those which its combination of L1-dyn rep and AP are enough to get better performance than data.

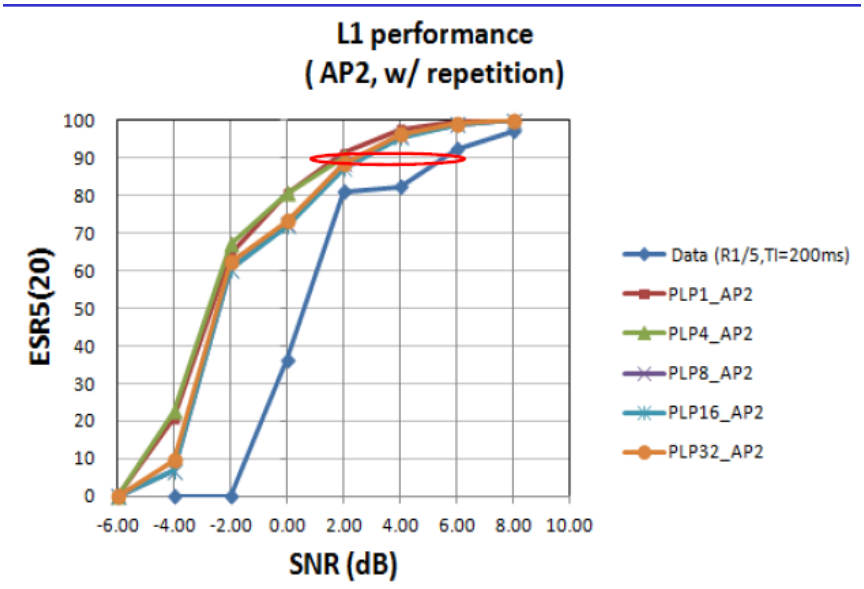

Figure 59: L1 signaling Performance over LMS Channel (AP2 with Rep and with Fabrice Decoding).

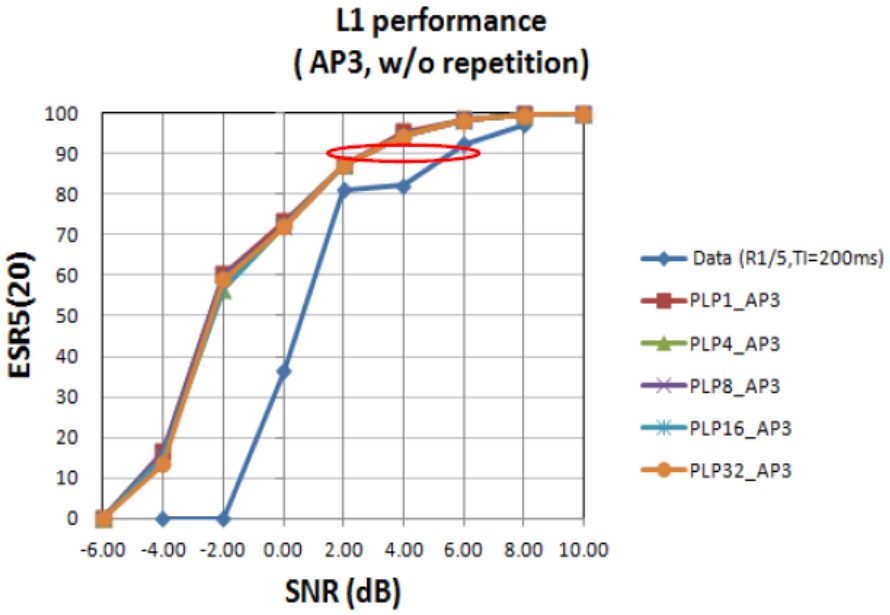

Figure 60: L1 signaling Performance over LMS Channel (AP3 without Rep and with Fabrice Decoding).

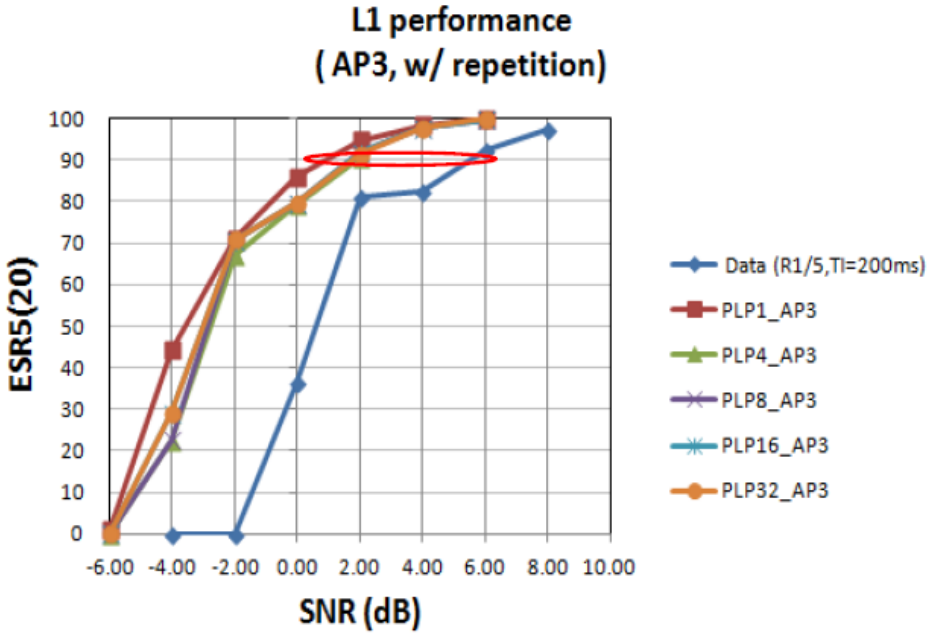

Figure 61: L1 signaling Performance over LMS Channel (AP3 with Rep and with Fabrice Decoding).

2.3.4.1.5 Conclusion

This section shows that the mechanisms devised in the Terrestrial profile to improve for L1 signaling robustness are sufficient to meet the requirements of the Satellite path, but with some configurations of

Additional Parity (AP2) L1-dyn repetition is needed. In addition, with AP3 configuration, the robustness of L1 signaling is enough to get better performance than data. As a conclusion, the mechanisms assumed for the Terrestrial profile (4k, AP/IR and Fabrice decoding) in conjunction with L1-dyn repetition meet the requirements of the Satellite path.

2.3.4.2 Robust Layer 1 Signaling schemes

2.3.4.2.1 Introduction

Focusing study on L1-post field:
From 2010 to end of year 2011, the NGH standardization process has shown that L1-post signaling detection was a critical problem especially for mobile channels. Indeed, detection of L1-post enables localizing PLPs into the NGH frame; that is to say if the L1 post field is not correctly decoded, all PLP data will be lost. Reader shall note that information included in L1-pre fields, while being mandatory for correct reception of PLPs, may not usually change, except in case of network reassignment. Besides, the location of PLPs, included in L1 post field, may change (for a worst case) each frame. This is the reason why this section focuses only on L1 post detection field.

Positioning work into standardization process:
During the standardization process, some contributors of the NGH standard have proposed different solutions to deal with L1 post detection problems. CNES has particularly focalized on the evolution of the dealings, because discussions about the need to improve L1 might not have taken into account the specificity of the Land Mobile Satellite (LMS) channel. One Samsung contribution (NGH 755) has particularly caught the attention, offering both better robustness of the single decoding process and adjustable time diversity. By the time refinements and dealings with the NGH standardization group have lead to a slightly less robust solution (NGH 1319), while being close to the first contribution.

Because robustness of the highly punctured LDPC code was strongly decreased, especially in case of few PLP, it has been decided to work during summer 2011 on a solution closed to NGH 755 contribution. Main difference was about the amount of additional parity which would become a fix part, preventing from LDPC code capacity-nil correction. This solution aimed not to become the definitive solution, but to demonstrate that there were some configurations allowing L1 post detection in a satellite mobile environment. Thus, the conducted analysis consisted on running simulations to verify if additional parity solution was robust enough in the context of the LMS channel environment.

2.3.4.2.2 Study description: Additional Parity like

This section details the studied L1 post encoding improvement solution.

2.3.4.2.2.1 L1 field

In DVB-T2, L1 signalization field is located in the P2 symbols of T2 frame.

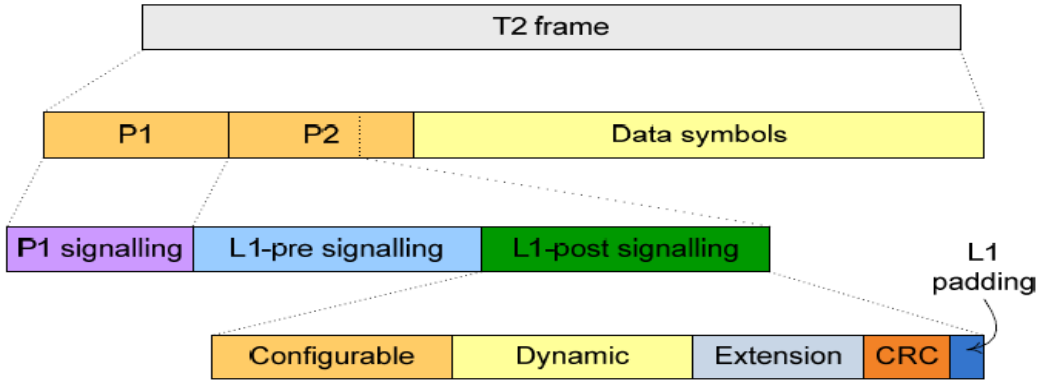

Figure 62: DVB-T2 L1-post signaling framing.

From an OFDM waveform point of view, L1 post cells are mapped as seen in the below figure.

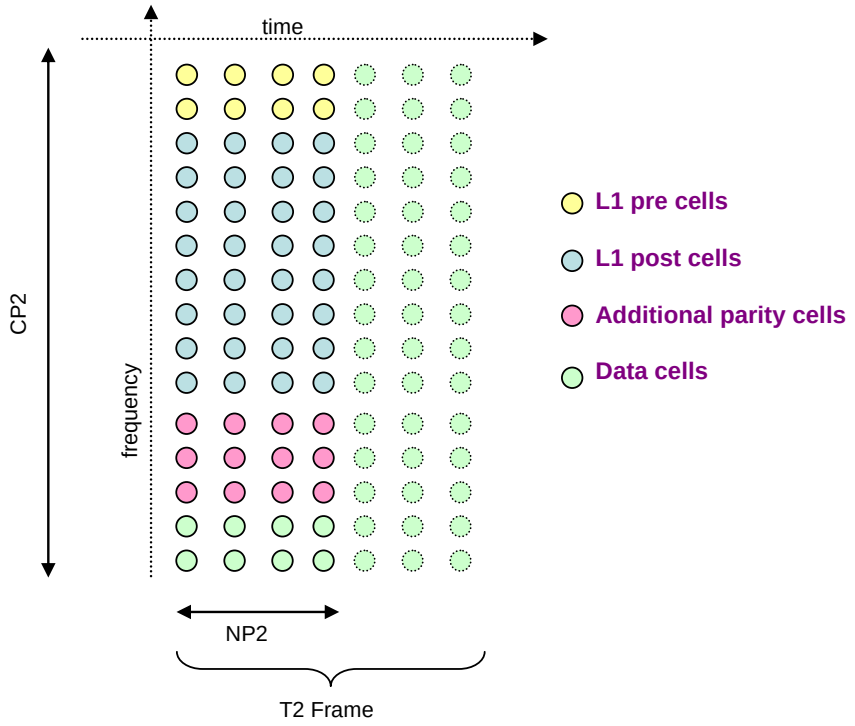

Figure 63: L1 cells disposition in the OFDM stream. Additional parity cells are an additional feature of NGH standard.

Size of L1 field is PLP number dependant. Here is briefly reminded the L1 size computation in DVB-T2.

- L1 pre number of bits : 168 + 32 (CRC) = 200 bits
- L1 post : 213 + 137×Num_PLP bits
  - L1 post config : 102 + 89×Num_PLP bits
  - L1 post dynamic : 79 + 48×NumPLP bits
  - 32 CRC bits

To implement additional parity scheme, new fields have to be defined in order to localize and quantize new additional parity bits. Besides, new fields are taken from Samsung NGH 755 contribution. Taking into account these new fields, L1 post size calculation with new robustness solution becomes:

- Having a look only on new fields :
  - (L1_AP_Start + L1_NUM_AP_blocks) + (L1_AP_lenght + L1_AP_Frame_pointer+ L1_AP_RSV) ×NumPLP
  - 20 + 12 × NumPLP
- Total L1 post size calculation
  - 233 + 149 × Num_PLP bits

Table 29: L1 post size in DVB-T2 and NGH standard.

PLP number	DVB-T2	NGH with AP
1	350	382
2	487	531
10	1583	1723
16	2405	2617
32	4597	5001

The table above, which summarizes the L1 field size, let us understand that for a same coding rate, fulfillment of the DVB-T2 LDPC would be totally non equal, depending on the number of PLPs.

2.3.4.2.2.2 L1 encoding solution with additional parity

L1 basic encoding process is strictly taken from DVB-T2 specifications. At the date of this chapter drafting, LDPC 4K codes have been approved. Nevertheless, the study has been done considering 16K codes to assess the effect of the fulfillment of the code and additional parity (4K codes were not definitely approved when the study began).

Steps of the L1 post encoding:

(1) BCH block code is zero padded in complement to L1 post to fulfill BCH input.

(2) Zero padded data + BCH parity bits are encoded with LDPC.

(3) LDPC parity is punctured according to the size of L1 post.

(4) In DVB-T2, only L1 post, BCH_FEC and remaining LDPC parity bits are sent.

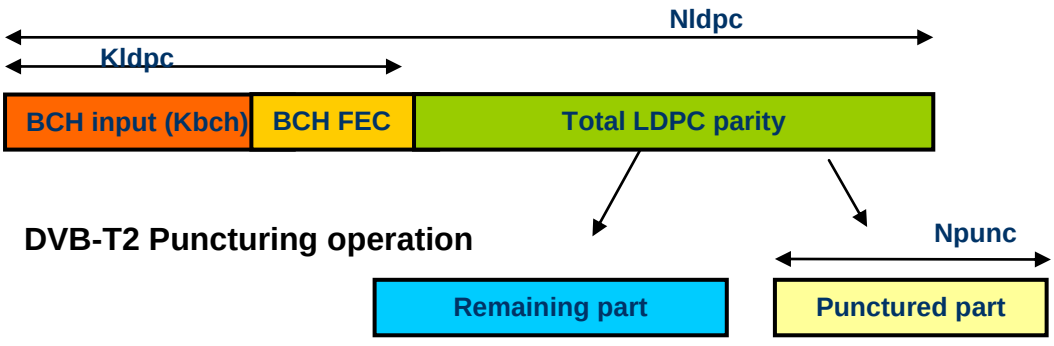

Figure 64: Puncturing of the LDPC.

From step (4), additional parity is then applied. Total LDPC parity is sorted in a circular buffer starting with punctured bits, and then Additional Parity vector is built by parsing circular buffer. By this, robustness is first reached by taking better performance of the LDPC code before sending parity bits sent yet.

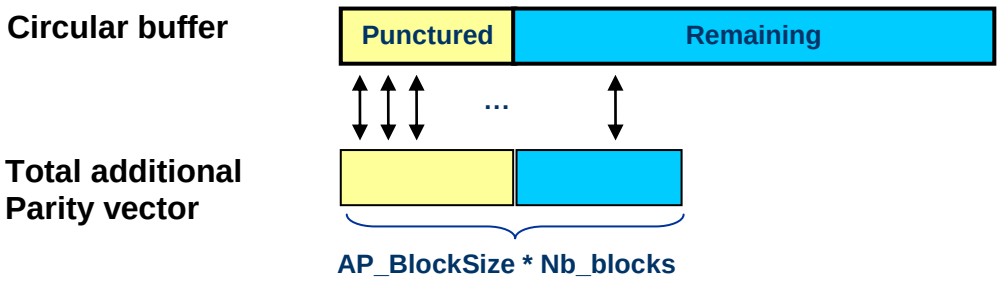

Figure 65: Additional parity vector building.

Total size of Additional parity vector is arbitrary called AP_BlockSize×Nb_blocks, names being directly linked to the additional parity mapping scheme (as seen later in the section).

Independently from the number of PLPs, keeping additional parity size as a fixed value was chosen. This solution may provide:

- Very low Coding Rates with few PLP when there is a need to make more robust the LDPC code,
- Higher Coding Rates when there is just a time diversity need.

Additional parity size is then fixed to the total LDPC parity size (N_{LDPC} - K_{LDPC}). Equivalent Coding Rate is computed as:

$$CR = \frac{L1post(Nb\_PLP)}{L1\_post(Nb\_PLP) + BCH\_parity + LDPC\_remaining\_bits(Nb\_PLP) + Total\_AP\_bits}$$

- L1post: size of the field to encode (including CRC)
- BCH parity: 168 bits
- LDPC remaining bits: LDPC parity bits which are sent
- Total AP bits: total amount of Additional parity bits, equal in our case to total parity size (before puncturing) ~ 9000 bits

To bring time diversity, it may be suitable to spread the total Additional Parity in several blocks, as depicted below. The new fields defined by NGH standard for signaling additional Parity are consequently explained: Additional parity blocks have to be localized.

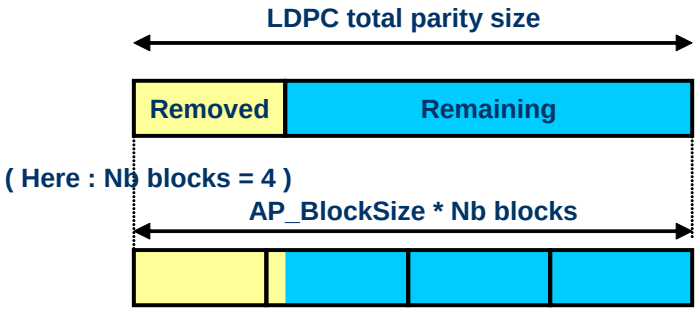

Figure 66: Total additional parity bits splitting.

For each frame, additional Parity blocks linked to this frame are mapped in previous frames as the following figure; example is given for additional Number of blocks equals to 2, and additional parity frame interval equals to 3.

Lastly, native L1 post is transmitted synchronously with Additional Parity blocks relative to other frames. Reader shall note Additional Parity blocks corresponding to different frames are transmitted in the same P2 field.

Once bits encoded, they are grouped and mapped into QPSK symbols into the OFDM cells, according to the DVB-T2 specifications. Note that L1 pre + L1post +Additional parity cells should be less than [CP2] ×[NP2] (T2 specification parameters).

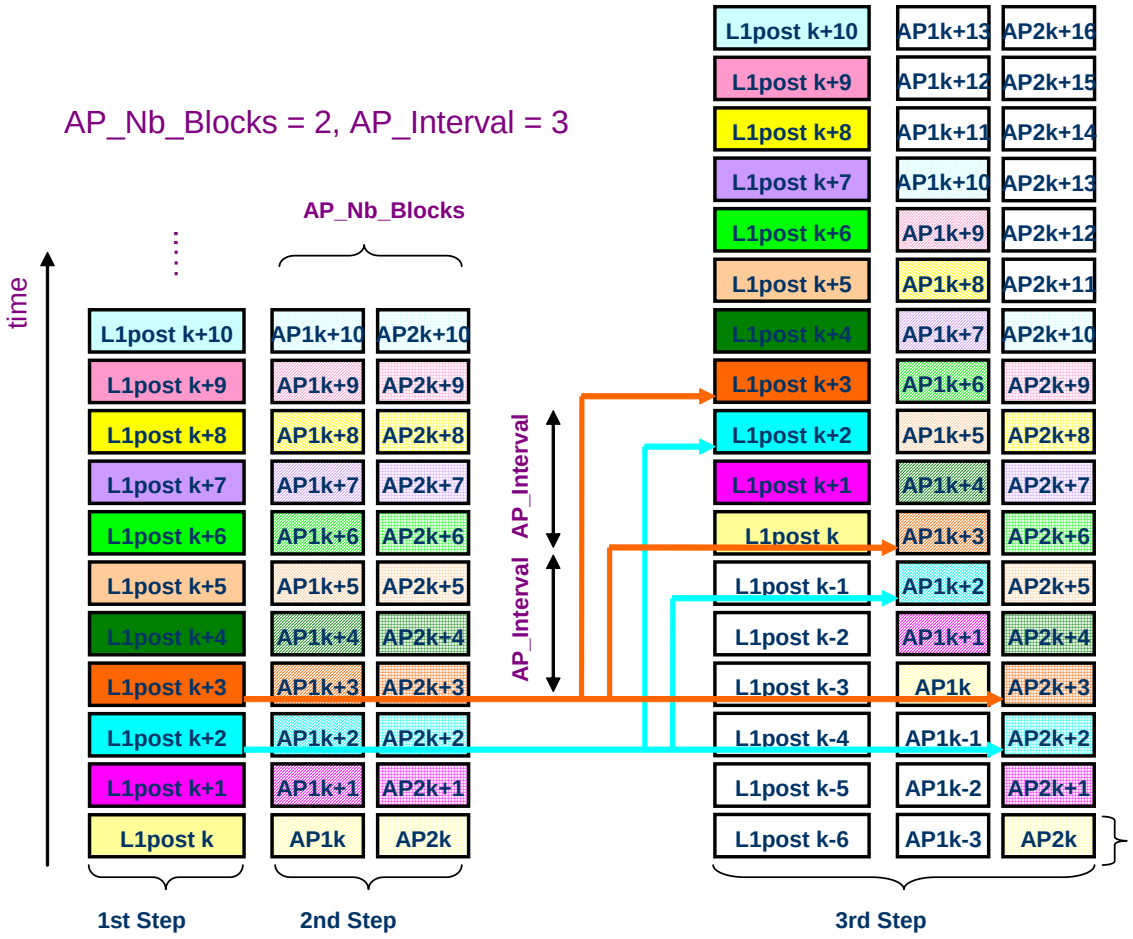

- 1st Step : L1 post native encoding is buffered
- 2nd Step : Additional Parity blocks are computed and buffered
- 3rd Step : AP blocks are transmitted in advance, every AP_interval frames

Figure 67: Example of realization.

2.3.4.2.3 Simulations results

2.3.4.2.3.1 Software device

L1 encoding simulations have been carried out using a C-ANSI simulator, compliant with DVB-T2 specifications. According to the previous section, Additional Parity algorithm (encoding and spreading) is implemented.

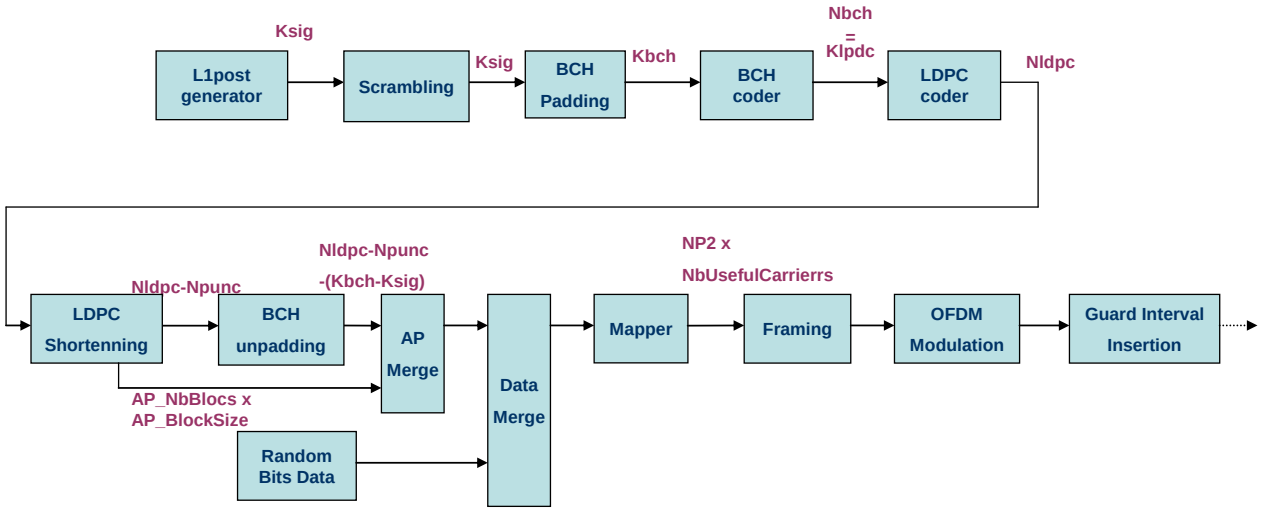

Figure 68: L1 encoding + AP transmitter architecture.

2.3.4.2.3.2 Validation

Validation of the software was done according to Nokia/Samsung simulations [40] when the LDPC code is very low punctured. Other curves (1 or 5 PLP) are not plotted, but they converge at higher C/N.

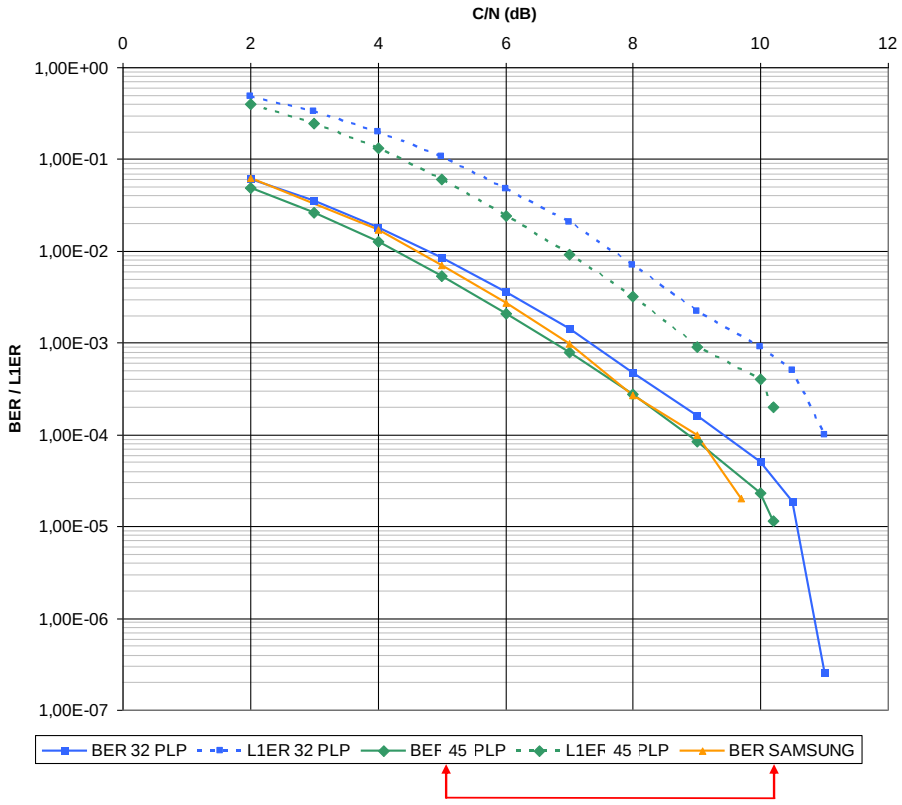

Figure 69: Validation curve of the chain.

Simulations have been run in TU6 channel, with 80 Hz Doppler, on a QPSK ½ modulation under 8 MHz bandwidth. About OFDM parameters, ¼ guard interval ratio was chosen associated with 8k FFT mode. Frame periodicity was set to 0.25s. Additional parity block was bypassed.

2.3.4.2.3.3 Simulations Hypothesis

Hypotheses are given hereafter.

Channel	LMS ITS Channel with 40° elevation, 60 Km/h
ModCod	QPSK ½, LDPC 16K
Bandwidth, OFDM	BW = 5 MHz, FFT 2k, Guard Interval 1/8
NGH Frame period	250 ms
Aditional parity	5, 10, 20 Frame interval

About the NGH framing, reader shall note that there is only NGH frame in the stream, because only satellite link is considered in this study.

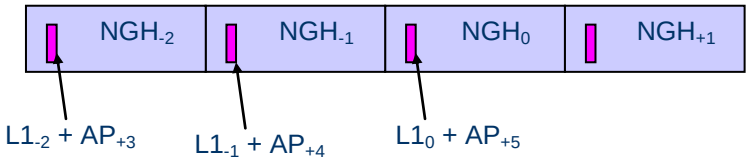

Figure 70: Framing for the study: only NGH frames.

On the below table, summary of Additional Parity parameters are given. Note that different parameters on Nb_AP_cells_per_block and Nb_blocks, keep the same amount of additional parity, as explained in the previous section.

NbPLP	Nb AP cells per block	Nb blocks	Frame Interval	Interleaving length	Overhead on LDPC parity	Effective Coding Rate
16	2248	2	20	10 s	243.29%	0.169
16	1128	4	10	10 s	244.16%	0.169
16	1128	4	5	5 s	244.16%	0.169
22	1128	4	10	10 s	189.26%	0.201
22	1128	4	5	5 s	189.26%	0.201

The choice of these parameters would make it possible to deal with:

- The effect of the parity blocks spreading granularity.
- The interleaving duration.
- The Coding Rate.

Chosen configurations may appear oversized, but the aim of the study was to demonstrate that additional parity with spreading is a robust solution, despite small parameters changes.

2.3.4.2.3.4 Results

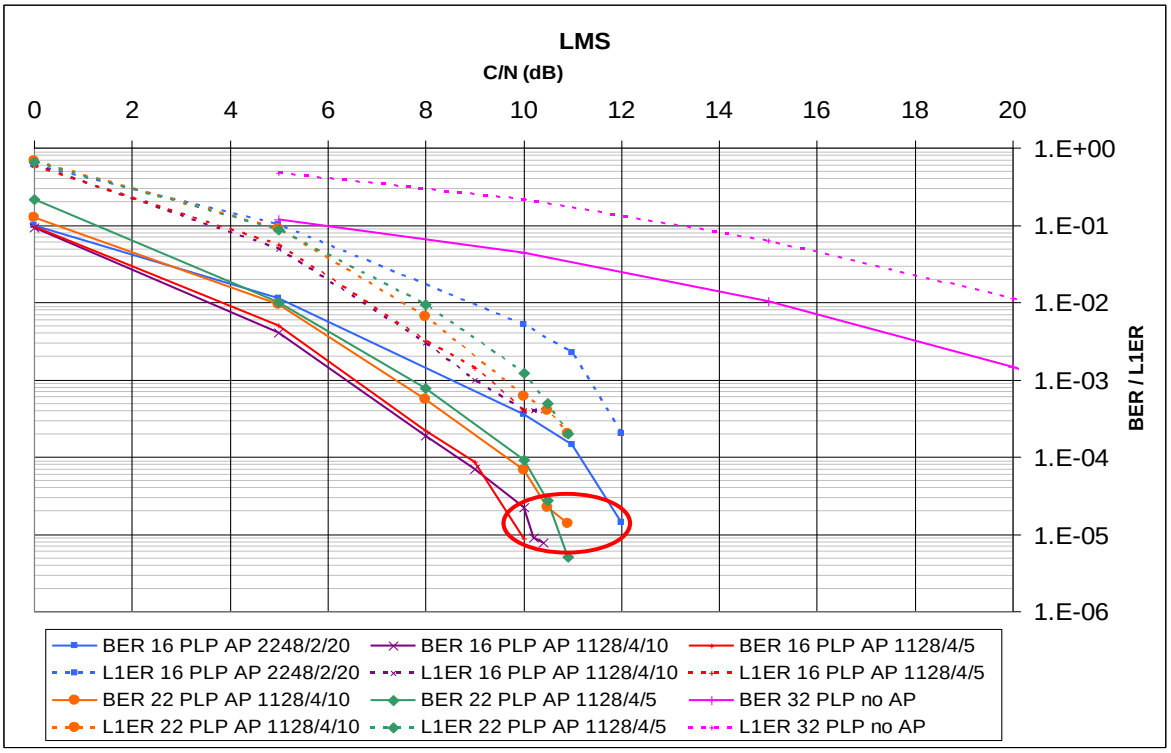

Figure 71: Additional parity BER/L1ER results.

Results show that BER=10^{-5} is reached between 10 and 12 dB of SNR, depending on the configuration. L1 Error Rate 10^{-4} is expected at least around 11 dB of SNR.

Although wide additional parity brings very good results compared to L1 detection Error Rate without additional parity, it can be pointed out that spreading the same additional parity amount over the same interleaving duration is giving better results when 4 AP blocks are used instead of 2.

Besides, given a 60 km/h speed parameter, 5s interleaving seems to be sufficient to counteract channel effects, because results are closed to 10s interleaving. Lastly, it can be seen that applying using Coding rate 0.17 instead of 0.2 brings around 0.7 dB gain.

In a satellite environment, ESR5 criteria may take more sense than usual Modulation Error Ratio (MER). This is why results are also presented with this metric. Results in Figure 71 above show that order between different curves is the same as BER curves. Besides, the C/N area where the criteria is 90% fulfilled (agreed reference point in satellite community and especially in DVB-SH standard) is around 7 to 9 dB.

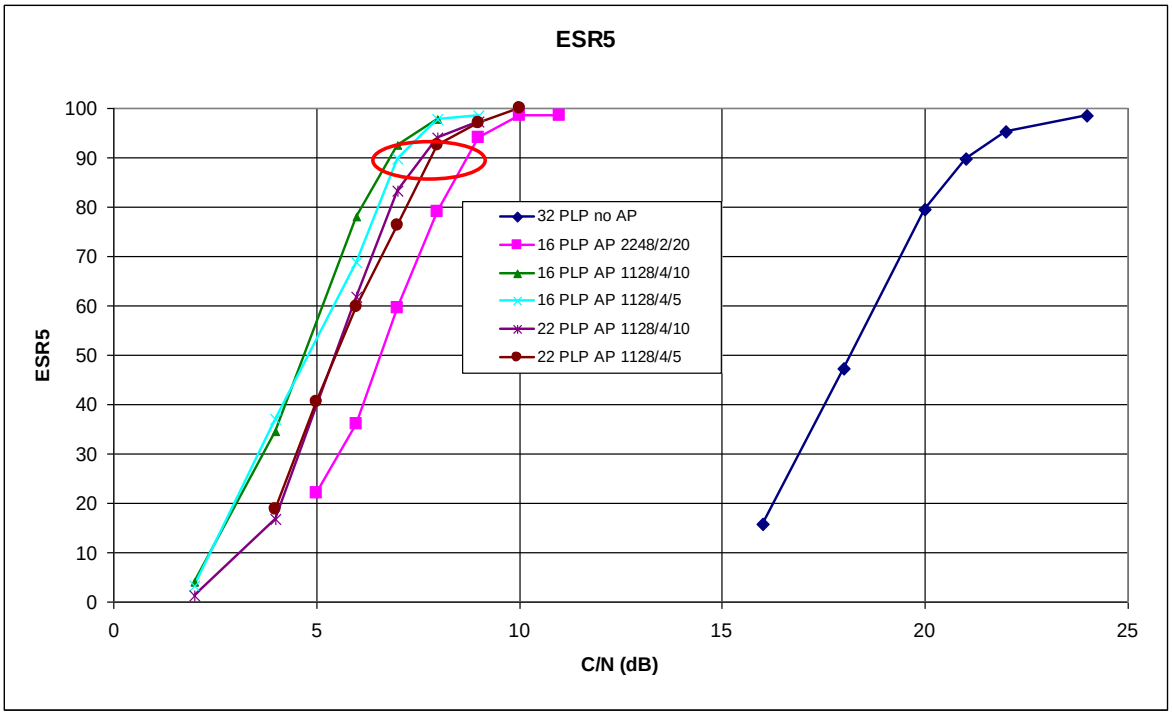

Legend : number of PLP ; AP_1block_cell_size /AP_Nb_Blocks/AP_interval

Figure 72: Additional parity ESR5 results.

2.3.4.2.4 Comparison with NGH adopted solution

In September 2011, Samsung presented simulation results based on the Additional Parity definitive definition (see TR1.1). Main differences between the CNES solution and additional parity are:

- The using of BPSK modulation, instead of the QPSK modulation (3 dB gain on E_S/N_0).
- The use of 4K LDPC instead of 16K LDPC.
- The definition of 3 effective coding rates, taking into account the Additional parity: ~1/3, ~1/5, ~1/6, instead of constant amount of parity bits.
- Additional parity is put in the previous NGH frame, instead of spread additional parity blocks in several previous frames.

About simulations setting differences, note that:

- Samsung have used a LMS-SU (Sub-Urban) satellite channel, which is a bit more favorable than LMS-ITS (Intermediate Tree Shadowing) channel.
- Terrestrial NGH framing was used (NGH----DVB-T2----NGH) with 600ms gap duration between 2 NGH frames: DVB-T2 frame was 400 ms duration whereas DVB-NGH frame included into Future Extension Frame has only 200ms duration.
- Coding rate was ~1/6 (with BPSK).

Compared to CNES simulations (LMS-ITS, QPSK with effective coding rate ~1/5, LDPC 4K), ESR5 criteria reaches 90% fulfillment at 3 or 4 dB, that is showing clearly better results, but not really comparable

(modulation, channel, coding rate, code size). In fact, no matter about this, because Samsung has made the proof that their proposal was enough robust for a suburban reception.

Nevertheless, weakness of the proposal is that there is no possibility (only using Additional parity device) to split additional parity in several previous frames, especially for satellite link with only 250 ms between two NGH frames (compared to 600 ms used in the Samsung simulations).

2.3.4.2.5 Conclusion and warnings

Thanks to Samsung, Additional Parity, powerful mean of robustness for L1 signaling, has been introduced in NGH standardization process. In this study it has been demonstrated that this technology was getting more efficient when associated with spreading. Nevertheless, despite of hard receiving conditions in satellite mobile environment, it has been seen that reduced spreading could be introduced providing more robust modulation (BPSK), very low coding rate (~1/6) and reduced size code (LDPC 4K), as it is approved now in the NGH standard.

Adopted decision is well suited for the scenario with a 600ms spreading duration between satellite frames (scenario with satellite frames put in two long DVB-T2 frames and used in SAMSUNG simulations).

Nevertheless, for satellite transmission, only satellite NGH frames are emitted (Stand-alone mode) with 250ms spreading duration that might be a weak point. Fortunately, NGH standard implements another mechanism, Incremental redundancy (not studied here) enabling using another previous frame to carry other bit redundancy.

2.3.5 Synchronization in the satellite context – Application to the SC-OFDM waveform

This chapter deals with synchronization in the satellite context with application to the SC-OFDM waveform adopted along with pure OFDM for the satellite link of the NGH Hybrid Profile. Just like in DVB-T2, data is transmitted as frames starting with the so-called P1 symbol [19], [20]. This symbol is meant to serve for the synchronization of the receiver. After a short remainder about the SC-OFDM modulation already described in Section 2.3.1, this section briefly introduces the most common synchronization algorithms as described in the literature. A comprehensive set of new algorithms is then described in details with their respective performances. The impact of these algorithms on SC-OFDM transmissions is finally evaluated in terms of bit error rate (BER) for different propagation channels.

2.3.5.1 SC-OFDM waveform

The waveform considered in this section is the SC-OFDM modulation retained as a solution along with pure OFDM for the satellite link in MFN configurations. The NGH standard specifies a set of system parameters covering the different needs for SAT transmission. We focus here on a specific configuration:

- Carrier frequency = 2.2 GHz
- Bandwidth = 5 MHz
- FFT size = 512 sub-carriers
- Modulation = QPSK
- LDPC/BCH code rate of 1/3 or 1/2
- Pilot pattern = PP9 (See Figure 73)

According to the specification for the size of the de-interleaving buffer, the time interleaving can vary between 0.2 second up to several seconds.

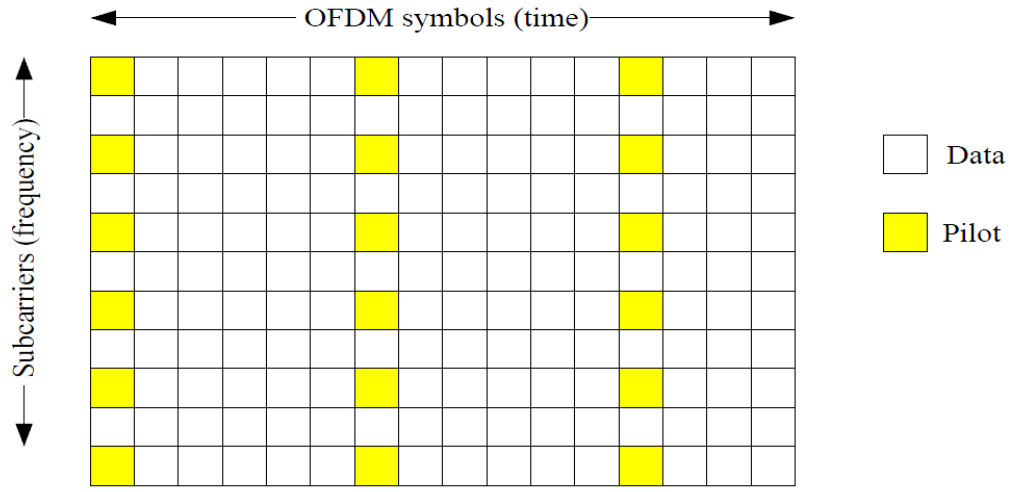

Figure 73: PP9 pilot pattern for SC-OFDM transmission.

Transmission occurs according to the frame format for SC-OFDM as described in the NGH standard. It is supposed here that the frame is made of one P1 symbol, one P2 symbol (where L1 signaling is carried within a PP9 hybrid symbol) and 61 blocks of six SC-OFDM symbols terminated by a PP9 reference symbol (thus leading to a total of 367 SC-OFDM symbols).

2.3.5.2 State of the art

DVB-T2 introduced a special frame structure for synchronization and signal acquisition. The P1 symbol is located before each data frame and its first purpose is to allow for the fast recognition of the T2 signals (or signal present in the FEFs). The P1 contains signaling data providing the transmission type and basic transmission parameters needed by the receiver to be able to process the remaining part of the data frame. The P1 symbol is also meant to allow for the robust acquisition of the time and frequency synchronizations. The remaining part of the present section focuses on the mechanisms used for P1 detection and time/frequency synchronization. A number of algorithms are presented along with performance simulation results for various propagation channels.

2.3.5.2.1 P1 symbol

The P1 symbol is a 1K OFDM symbol with two guard intervals (C and B) that are frequency shifted in order to enable the receiver to distinguish this preamble from conventional multi-carrier symbols with a standard cyclic prefix [19]. The general structure of the P1 symbol is depicted on Figure 74 and Figure 75.

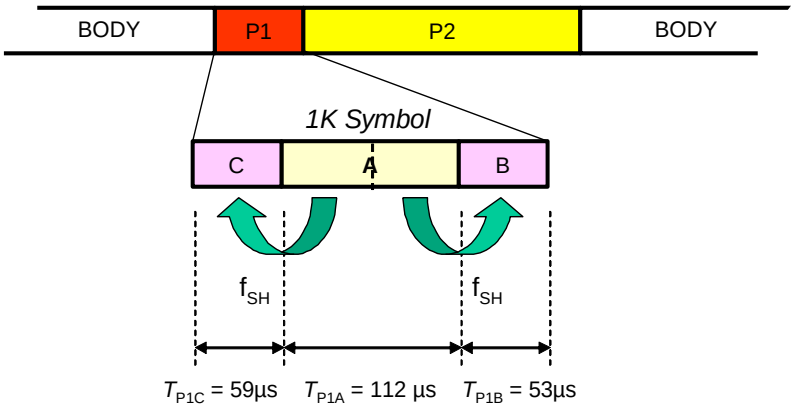

Figure 74: P1 symbol structure in the time domain.

All the useful carriers of the 1K symbol are not used. About a half of them are set to zero in order to facilitate the detection of the P1 symbol even with a large frequency offset (up to 500 kHz). The 384 active carriers are used to code 7 bits of information leading to 128 different P1 symbols.

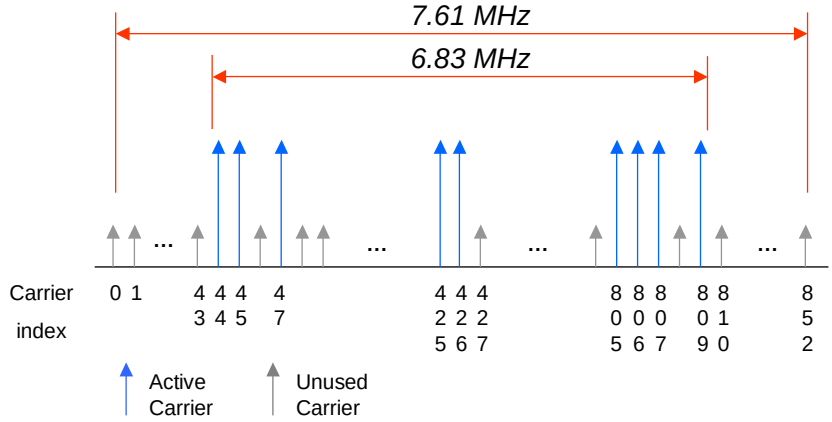

Figure 75: P1 symbol structure in the frequency domain (only the A part).

The DVB-T2 implementation guidelines [20] suggest a technique for time and frequency synchronization, exploiting the correlation among the main part of the received P1 symbol and the two guard intervals. This approach allows for a robust acquisition of the time and frequency synchronization. For better performance, a refined synchronization may be needed. Figure 76 below presents an example of simple synchronization mechanism only based on the correlation of P1 symbol.

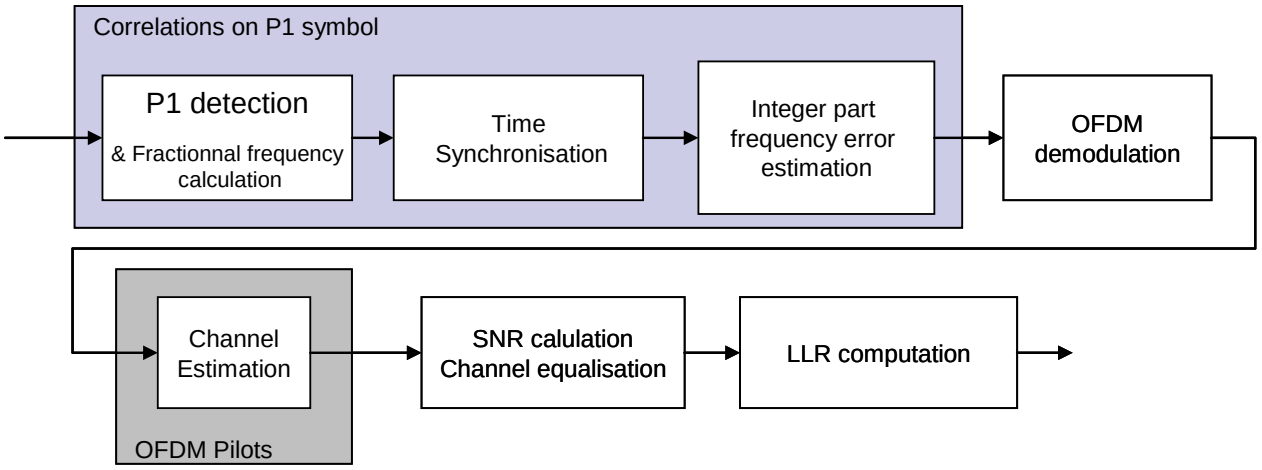

Figure 76: Typical architecture of a DVB-T2/NGH receiver.

The receiver starts by performing the detection of the P1 symbol. The detection algorithm provides an estimation of the fractional part of the frequency error and a coarse estimation of the start of the P1 symbol (plus or minus a few samples at high SNR and plus or minus hundreds of samples at very low SNR). It is then possible to evaluate the integer part of the frequency error using the knowledge by the receiver of the specific positions of the modulated and null subcarriers in the P1 symbol. Following the frequency synchronization, the time synchronization is performed and aims at finding the exact position of the first sample in the received P1 symbol (it is performed by correlation). After completion of these algorithms, the signal is synchronized in time but a residual frequency error may still be present and degrade the channel estimation mechanism. Indeed in order to have good channel estimation, an average in time is performed and the residual frequency error may cause the phase of the signal to vary too much during the time averaging.

In order to guaranty a reasonable low residual frequency error, an additional algorithm is used to obtain a fine frequency synchronization using the pilot of the hybrid symbols. This algorithm requires that the initial frequency error does not make the phase rotate more than 2π between two hybrid symbols. In order to enhance the performance on propagation channel of type LMS ITS, it is possible to add an estimation of the frequency error after the time synchronization and before the fine frequency synchronization.

2.3.5.2.2 P1 detection

As described in DVB-T2 guidelines, the detection of P1 can be performed using the algorithm described on Figure 77 by calculating the correlation over the central symbol A with its 2 guard intervals B and C.

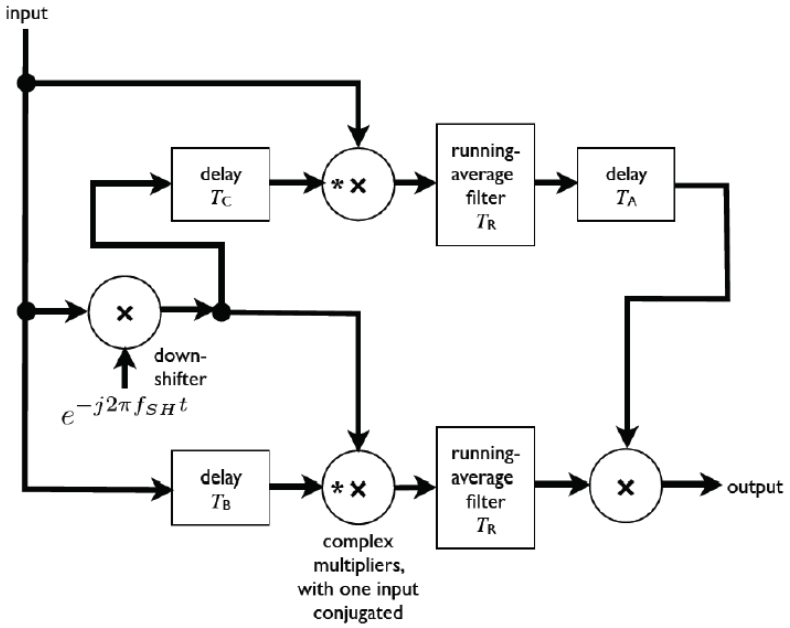

Figure 77: Block diagram of a P1 detection algorithm.

As shown on Figure 78, the correlation between A and B gives a complex pulse whose magnitude is a trapezoid of base (T_A+T_B) and top (T_A-T_B).

The correlation between A and C gives also a trapezoid of base (T_A+T_C) and top (T_A-T_C).

The two trapezoids are then multiplied together and a coarse estimation of the P1 symbol position is given by the center of the resulting trapezoid while the fractional part of the frequency offset is given by its argument.

The detection of a valid detection trapezoid can be obtained by defining an adequate threshold.

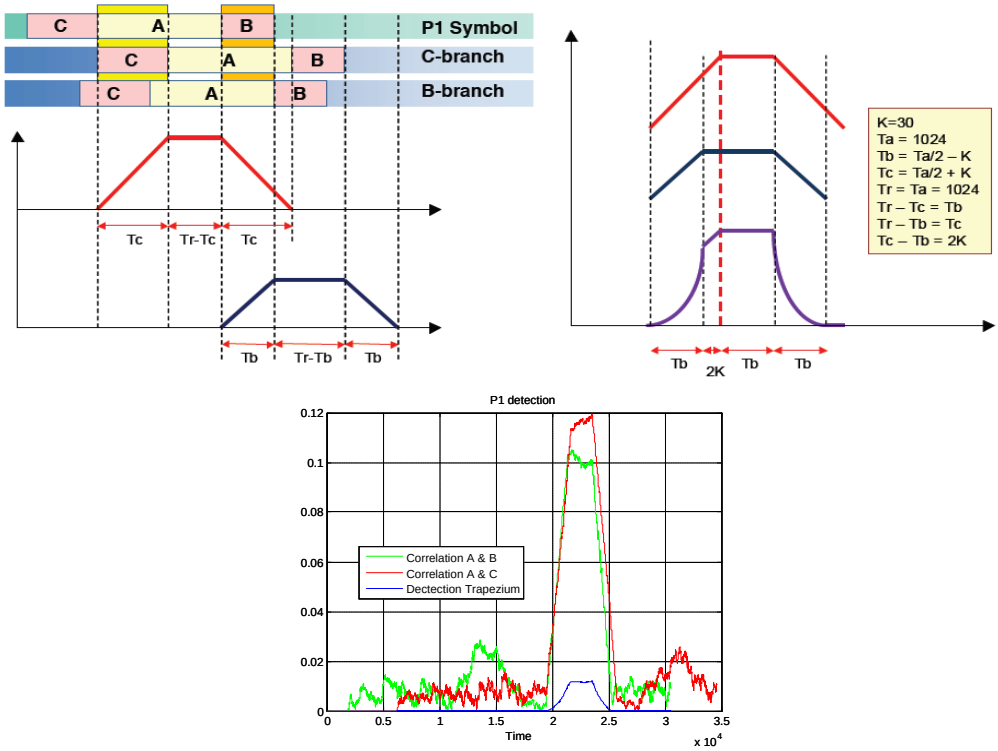

Figure 78: Principle of the correlation algorithm for P1 detection.

2.3.5.2.3 Fine time synchronization

At the output of the correlation, a coarse estimation of the start of P1 is obtained. The fine synchronization consists in estimating the sample corresponding to the start of the P1 symbol.

It is assumed that the receiver stores in memory the "X128" symbol corresponding to the "average" of the 128 possible P1 configurations.

Considering an oversampling factor (OVF) of 4, the X128 symbol is composed of 8192 samples. The fine synchronization is performed by correlating the input stream with the X128 symbol. The P1 symbol being composed of 8192 samples, the correlation for one position is rather time/resource consuming but also robust towards noise.

Unfortunately, any frequency error decreases the strength of the correlation peak that can vanish if the frequency error is greater or equal to the subcarriers interval. Alternatives to be more robust to frequency errors are:

- Perform the correlation with the module of X128 and the received signal. This solution is insensitive to frequency error but less robust to noise.
- Perform the frequency synchronization prior to the time synchronization.

2.3.5.2.4 Estimation of the integer part of the frequency error

The correlation performed during P1 detection provides an estimate of the fractional frequency error. The integer part is then to be determined. The P1 symbol that is composed of 384 active sub-carriers over 1024 is aimed at enabling this synchronization. The integer part is obtained by performing the correlation between:

- The FFT of P1 symbol without the guard intervals (that is to say the "A" part of P1 that is a 4096 points FFT considering an oversampling factor of 4).
- A reference vector of 1024 "zeros" except at the position of the active sub-carriers.

Just like for time synchronization:

- If a complex correlation is performed (that is to say the active subcarriers of the reference vector have the value +1 or -1), good time synchronization is needed to obtain a clear correlation peak.
- If the correlation is made using the modules (that is to say the active subcarriers of the reference vector have the value +1), the correlation is robust towards time synchronization errors but more sensitive to noise.

2.3.5.2.5 First estimation of the residual frequency error

The fractional frequency error is first estimated during P1 detection. In certain cases, this estimation is not precise enough to estimate the residual frequency error between the hybrid symbols because of a low SNR.

If the SNR increases over a NGH frame, e.g. in the case of the LMS ITS channel, the LLR provided by the decoder may be high (because the SNR is high) but with an erroneous sign (because of the residual frequency error that has not been corrected). This could lead to errors in reception despite the fact that the average SNR on the transmission is high enough to be error free.

In order to solve this issue, an additional fine frequency estimator can be implemented after the time synchronization stage and before the frequency error estimation on the pilot symbols. This estimator needs to know which P1 symbol among the 128 possible values has been received. The 8192 sample of the received P1 are correlated with the P1 symbol stored in memory of the receiver. The P1 samples without noise can be written as:

$$P1 = [|P1_1| e^{j(Arg(P1_1)+2\pi df\,1+\phi_0)} \quad ... \quad |P1_{8192}| e^{j(Arg(P1_{8192})+2\pi df\,8192+\phi_0)}]. \tag{27}$$

After multiplying by its conjugate defined as:

$$P1^* = [|P1_1| e^{-j(Arg(P1_1))} \quad ... \quad |P1_{8192}| e^{-j(Arg(P1_{8192}))}], \tag{28}$$

we obtain:

$$|P1|^2 = [|P1_1|^2 e^{j(2\pi df\,1+\phi_0)} \quad ... \quad |P1_{8192}|^2 e^{j(2\pi df\,8192+\phi_0)}]. \tag{29}$$

The first 4096 correlation products are then correlated with the last 4096 correlation products, and a 4096 sample vector is obtained:

$$[|P1_1|^2 |P1_{4097}|^2 e^{-j(2\pi df\,4096)} \quad ... \quad |P1_{4096}|^2 |P1_{8192}|^2 e^{-j(2\pi df\,4096)}], \tag{30}$$

The frequency error df is obtained as the argument of the sum of this 4096 correlation product.

2.3.5.2.6 Estimate of the residual frequency error

After the P1 synchronization, time and frequency synchronization is obtained, however a residual frequency error remains. After synchronization, the channel estimation is performed using the PP9 pilot symbols as follows:

- The channel is evaluated for each pilot,
- The channel is filtered and an interpolation is performed to obtain an estimate of the hybrid symbols over all the subcarriers,
- For each subcarrier, the channel is averaged in time over *N* hybrid symbols,
- For each subcarrier, a linear interpolation is made of the channel between two hybrid symbols.

In complex notation, the frequency is equivalent to the rotation velocity of the phase. If the frequency error is greater than *1/2N*, the phase turns more than π radians over *N* hybrid symbols, and consequently the channel estimation is biased at step 3 when the channel estimate is averaged over *N* hybrid symbols. It is needed to add an estimator capable of reducing the residual frequency error.

Recall that the PP9 pilot symbols are spread every *K*=6 SC-OFDM symbols. The residual frequency error is less that the inverse of the period of the hybrids symbols. It is assumed that between two hybrid symbols the phase of the signal does not rotate more than π/2 (See Figure 73). The difference of the signal is equivalent to the rotation velocity of the phase. The frequency δk is then estimated by differentiating the phase divided by the time between the pilots *P* of two consecutive hybrid symbols:

$$\delta k \approx \frac{1}{2\pi} \frac{1}{KN_{FFT}\left(1+1/GI\right)} Arg\left(E\left\{P_k^* P_{k+1}\right\}\right), \tag{31}$$

where $E\left\{P_k^* P_{k+1}\right\}$ is the correlation between N_P pilots of the hybrid symbols *k* and *k*+1:

$$E\left\{P_k^* P_{k+1}\right\} = \frac{1}{N_P}\sum_{i=1}^{N_P} P_{k,i}^* P_{k+1,i}, \tag{32}$$

In order to have an accurate estimation, it is needed that between 2 hybrid symbols, the signal phase rotation is lower than π/2, i.e.:

$$\left|df - \hat{df}\right| < \frac{1}{2} \frac{1}{T_{symb} K\left(1+1/GI\right)}, \tag{33}$$

with T_{symb} SC-OFDM symbol time in the guard interval.

2.3.5.3 Improvement of the P1 detection

This section describes algorithms that aim at improving the performance of SC-OFDM synchronization.

2.3.5.3.1 Filtering prior to P1 detection

In the case of a dynamic Rice channel, the SNR can drop dramatically and reach values below -10dB. In order to increase the chance of a correct P1 detection in this case, the samples are filtered prior to the correlation. The filter is used for data demodulation; it only aims at removing the noise out of the useful band. Considering that the 384 active subcarriers of P1 start at index 44 and end at index 809, the bandwidth of the filter is, assuming an oversampling factor of 4 by symbol:

$$B = \frac{809 - 44}{1024 * 4} \approx 0{,}187\,, \tag{34}$$

Thus leading to a gain of $10 * \log_{10} 0.187^{-1} \approx 7dB$ on P1detection.

2.3.5.3.2 Detection threshold computation

This section describes a possible threshold calculation for the P1 detection algorithm described in Section 2.3.5.2.2. The proposed solution is based on the following algorithm.

Considering that:

X_1 and X_2 are two independent Gaussian variables, with null mean and standard deviation σ_X and variance σ_X^2, the following rules apply:

1. The product $X_1 X_2$ follows a "normal product law" with standard deviation σ_X^2
2. The sum of N variables $Y_1 + Y_2 ... + Y_N$, having an arbitrary distribution, but centered and independent with standard deviation σ_X is a normal law of standard deviation $\sqrt{N}\sigma_X$, and variance $N\sigma_X^2$
3. The Euclidian norm $\frac{\sqrt{X_1{}^2 + X_2{}^2}}{\sigma_X^2}$ is a Chi distribution with two degree of freedom
4. If there is a value K and a probability p so that:

$$\Pr\left\{\frac{\sqrt{X_1{}^2 + X_2{}^2}}{\sigma_X^2} > K\right\} = p\,, \tag{35}$$

Then:

$$\Pr\left\{\sqrt{X_1{}^2 + X_2{}^2} > K\sigma_X^2\right\} = p\,. \tag{36}$$

The general architecture of the P1 detection algorithm is recalled on Figure 79. Let's assume that P1 is not present and the input signal X is only a white noise with zero mean and variance of σ_X^2.

On Figure 79, U and V are both the result of the product of two independent variables normally distributed with zero mean. They consequently have a normal product distribution of zero mean and variance σ_X^4.

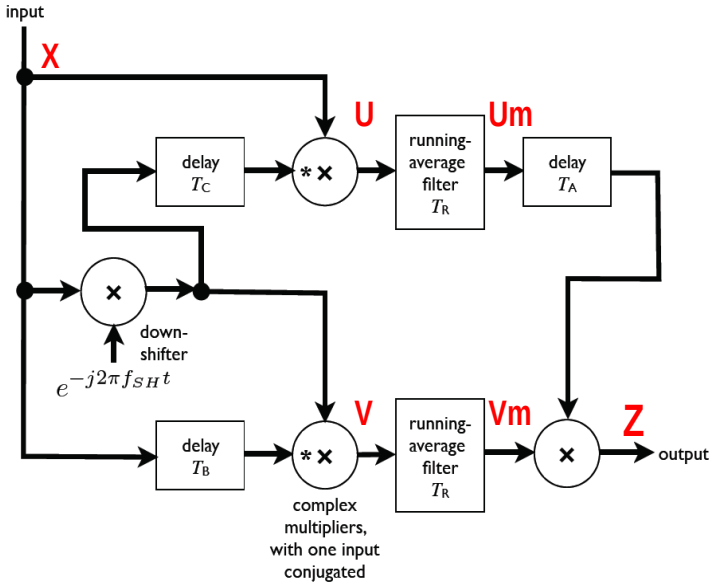

Figure 79: Block diagram of a P1 detection algorithm.

$U_m = \frac{1}{T_R}\sum_{i=1}^{T_R} U_i$ and $V_m = \frac{1}{T_R}\sum_{i=1}^{T_R} V_i$ are the sum of T_R independent variables U_i divided by T_R. According to the axiom 2 in the above theorem, U_m and V_m can be modeled as centered Gaussian variables of standard deviation $\sigma_{U\,m} = \frac{1}{T_R}\sqrt{T_R}\sigma_U$, and variance $\sigma^2_{U_m} = \frac{1}{T_R}\sigma^2{}_U = \frac{\sigma_X^4}{T_R}$.

If the input signal *X* is noise of variance σ^2, correlated with a period *t*:

$$E\left\{X_i X^*{}_{i-j}\right\} = 0 \text{ if } j \geq t$$

$$E\left\{X_i X^*{}_{i-j}\right\} \neq 0 \text{ if } j < t$$

U and *V* are the result of the product of two independent variables X_1 and X_2, that have the same distribution, and each auto-correlated with the same period t, so *U* and *V* are also auto-correlaled with a period *t*:

$$E\left\{U_i U^*_{i-j}\right\} = E\left\{X_1(i)X_2(i)X_1^*(i-j)X_2^*(i-j)\right\} = E\left\{X_1(i)X_1^*(i-j)\right\} \times E\left\{X_2(i)X_2^*(i-j)\right\}, \quad (37)$$

So $E\left\{U_i U^*{}_{i-j}\right\} = 0$ if $E\left\{X_i X^*{}_{i-j}\right\} = 0$, wich is equivalent to $j \geq t$.

U_m is the result of the sum of T_R variables, that can be divided in T_R/t sub-groups of independent variables:

$$U_m = \frac{1}{T_R}\sum_{i=1}^{T_R} U_i = \frac{1}{T_R}\sum_{i=1}^{T_R/t}\left(\sum_{j=1}^{t} U_{i*t+j}\right). \quad (38)$$

The sum of *t* correlated variables is modeled as $\sum_{j=1}^{t} U_{i*t+j}$ by the sum of the same variable:

$$\sum_{j=1}^{t} U_{i*t+j} = tU_{i*t+1}. \tag{39}$$

The standard deviation of this sum is $t\sigma_U$.

Considering the axiom 2, U_m has a normal distribution of standard deviation: $\sigma_{U\,m} = \frac{1}{T_R}\sqrt{\frac{T_R}{t}}t\sigma_U = \sqrt{\frac{t}{T_R}}\sigma_U$ and of variance $\sigma^2_{U_m} = \frac{t}{T_R}\sigma^2{}_U = \frac{t\sigma_X^4}{T_R}$.

The conclusion is:

If *X* is a white noise, then $\sigma^2_{U_m} = \frac{\sigma_X^4}{T_R}$.

If *X* if a noise filtered by a filter of bandwidth B = 1/t, or a signal of band =1/t then $\sigma^2_{U_m} = \frac{t\sigma_X^4}{T_R} = \frac{\sigma_X^4}{BT_R}$.

If *X* is the simulated DVB-NGH signal, then the band B is equal to the useful band of the signal divided by the observation band, that is to say:

$$B = \frac{N_u}{OVS \times N_{FFT}} = \frac{426}{4 \times 512}. \tag{40}$$

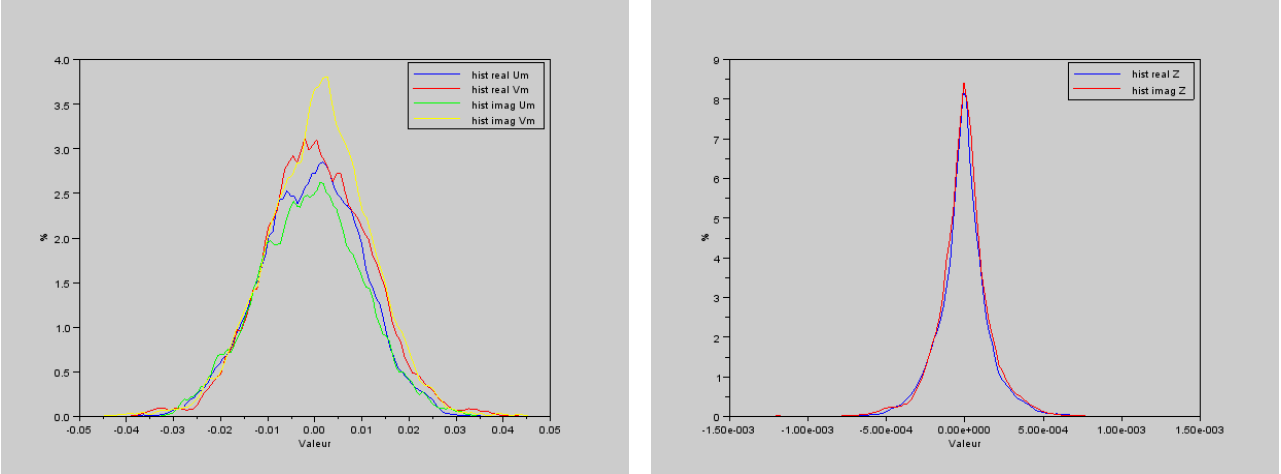

Figure 80: For white noise in input, distribution of the output of the average filters (left) and distribution of the output of the detection algorithm.

2.3.5.3.2.1 *Variable threshold depending of SNR*

U_m and V_m are two variables with a Gaussian distribution. The variance of U_m and V_m is dependant of the power and the band of the input signal; it can easily be computed. Considering the axioms (3) and (4), it is possible to compute the threshold using $\|U_m\|^2$ and $\|V_m\|^2$:

There is a probability *p* that $\|U_m\|^2 > K(p)\sigma^2_{\mathrm{Re}\{U_m\}}$ where:

1. $K(p)$ the inverse chi-square function calculated with the probability *p*.
2. The variance of the real or imaginary part of U_m : $\sigma^2_{\mathrm{Re}\{U_m\}} = \sigma^2_{\mathrm{Im}\{U_m\}} = \frac{\sigma^2_{U_m}}{2}$

The output *Z* of the detection algorithm is the product of two normally distributed variables V_m and U_m with zero mean and finite variance. Considering the axiom (1), the variable *Z* is a distribution of normal product law. In order to compute a threshold based on $\|Z\|^2$ it is needed to know:

- The variance of $\|Z\|^2$
- The inverse function of the cumulated distribution

As $\|Z\|^2 = \|U_m\|^2 \|V_m\|^2$, the threshold on $\|Z\|^2$ is approximated like the product of the threshold on $\|U_m\|^2$ and $\|V_m\|^2$.

It is assumed that *X*, the input signal of the P1 detection algorithm, is composed of a white noise with power P_n and a useful signal with power P_s and bandwidth B_s.

If the SNR is high, this threshold shall be high to avoid false alarm and to obtain a precise estimate of the fractional frequency error.

If the SNR is low, the threshold shall be chosen in order to maximize the chance of detecting P1.

In order to find a good compromise between the two recommendations, the proposed threshold is a combination of two values:

$$S_Z = S_Z^{noise} + S_Z^{signal} = K_n^2 \left(\frac{P_n^2}{T_R} \right) + K_S^2 \left(\frac{P_S^2}{T_R B_S} \right)^2, \quad (41)$$

with $K_n = 5$ and $K_s = 55$ for example.

If a filter of bandwidth $B_F \leq B_s$ is added before the P1 detection, then the noise is not white anymore and the threshold becomes:

$$S_Z = S_Z^{noise} + S_Z^{signal} = K_n^2 \left(\frac{P_n^2}{T_R B_F} \right)^2 + K_S^2 \left(\frac{P_S^2}{T_R B_F} \right)^2, \quad (42)$$

where P_n and P_S are respectively the power of noise and signal after filtering.

Then, it is obtained that:

- At low SNR, a threshold with a value corresponding to the Khi-2 inverse value equals to about K_n
- At high SNR a threshold with a value corresponding to the Khi-2 inverse value equals to about K_s

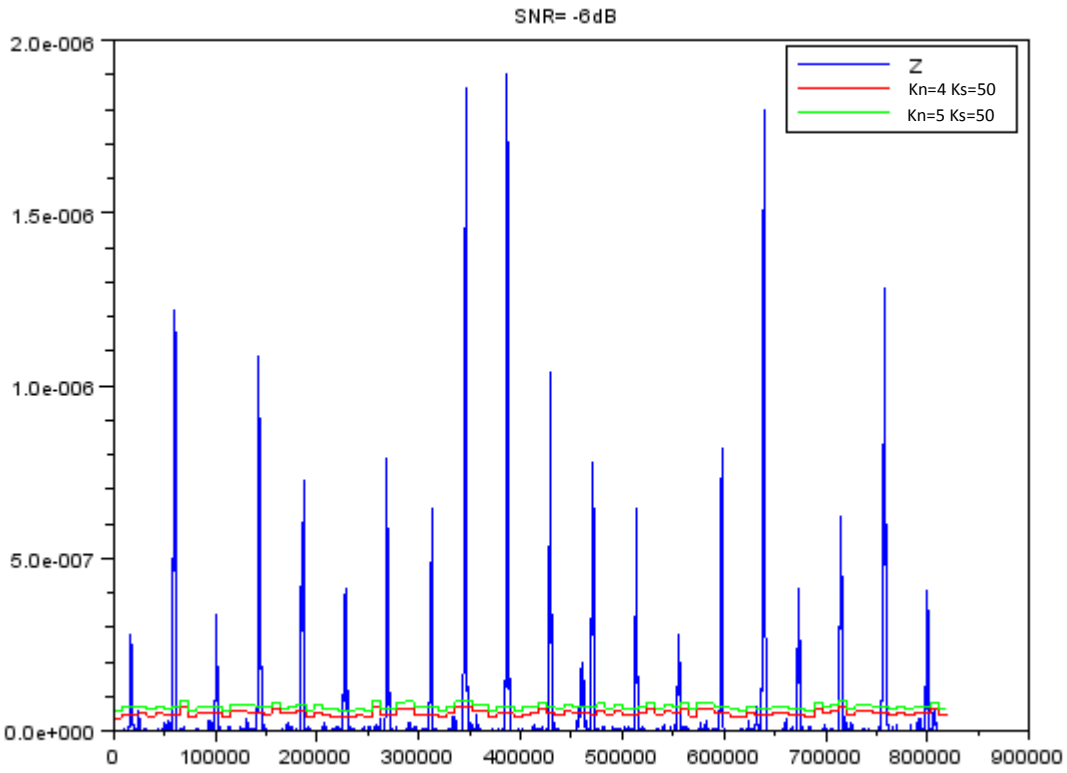

Figure 81: Output of the P1 detection (Z in blue), and two values of threshold.

2.3.5.3.2.2 Fixed threshold

If the signal is filtered before the P1 detection with mean power *P*, then the variance of U_m and V_m is given by:

$$\sigma_{U_m}^2 = \frac{P^2}{B_F T_R}, \tag{43}$$

The output *Z* of the detection algorithm is the product of U_m and V_m and consequently has a normal product distribution with zero mean and variance $\sigma_{U_m}^4$.

The distribution of $\|Z\|^2$ is unknown but it can be approximated by running simulations.

It can be noticed that if U_m and V_m have a unitary variance and that there is a probability *p* so that $\|Z\|^2$ is greater than *K*.

Consequently, if U_m and V_m have a variance $\sigma_{U_m}^2$, $\|Z\|^2$ has a probability p to be greater than $K\sigma_{U_m}^4$.

It is then possible to define a threshold in function of $\sigma_{U_m}^2$, that is to say in function of the mean power of the input signal, by choosing an appropriate value for K. The following table gives the probabilities to be greater than the measured threshold $K\sigma_{U_m}^4$.

Table 30: Probabilities of exceeding the threshold.

K	$\Pr(\|Z\|^2 > K\sigma_{U_m}^2)$
5	0.0326786
10	0.0059646
15	0.0015966
20	0.0005128
25	0.0001874
30	0.0000754
35	0.0000316
40	0.0000129
45	0.0000064
50	0.0000028
55	0.0000011

It is then possible to simply determine the threshold by measuring the power P of the signal at the input of the P1 detection algorithm:

$$S_Z = K\left(\frac{P^2}{B_F T_R}\right)^2 . \quad (44)$$

2.3.5.3.3 Performances

The performance of the algorithm described in the previous section has been evaluated under the following assumptions:

- 512 subcarriers with 426 modulated subcarriers
- Gaussian noise with SNR computed for an OFDM signal
- Oversampling factor of 4

The input signal is filtered prior to P1 detection. The threshold is computed with a perfect knowledge of the SNR and Kn = 5 and Ks = 50. A P1 is declared as detected when at least 420 consecutive points of $\|Z\|^2$ are above the threshold.

2.3.5.3.3.1 Detection performance

The performance of the P1 detection algorithm has been evaluated over 2000 P1 symbols for each SNR. Results are given in Table 31.

Conclusion:

- At SNR = -8dB the non-detection rate is 30%
- The false alarm probability is about 1/1000

Table 31: P1 detection performance.

SNR	Detection error ratio	Number of false alarms
-8	0,2955	26
-5	0,003	6
-2	0	0
1	0	1
4	0	0
7	0	1
10	0	0
13	0	0
16	0	2

2.3.5.3.3.2 Coarse time synchronization precision

For each detected P1, the error in coarse time estimation is computed. A large error can be considered as a false alarm, in particular if the error is greater than the search window of the following time/frequency synchronization algorithms. Table 32 below gives for various SNR, the ratio of P1 that have not been detected and the percentage of coarse estimation that are greater than 100, 1000, 1200 or 2000 samples.

Table 32: Coarse time synchronization performance.

SNR	% ND	% > 100	% > 1000	% > 1200	% > 2000
-8	20%	70%	13%	6%	4%
-6.5	0%	85%	9%	5%	3%
-5	0%	67%	2%	1%	1%
-3	0%	46%	0%	0%	0%

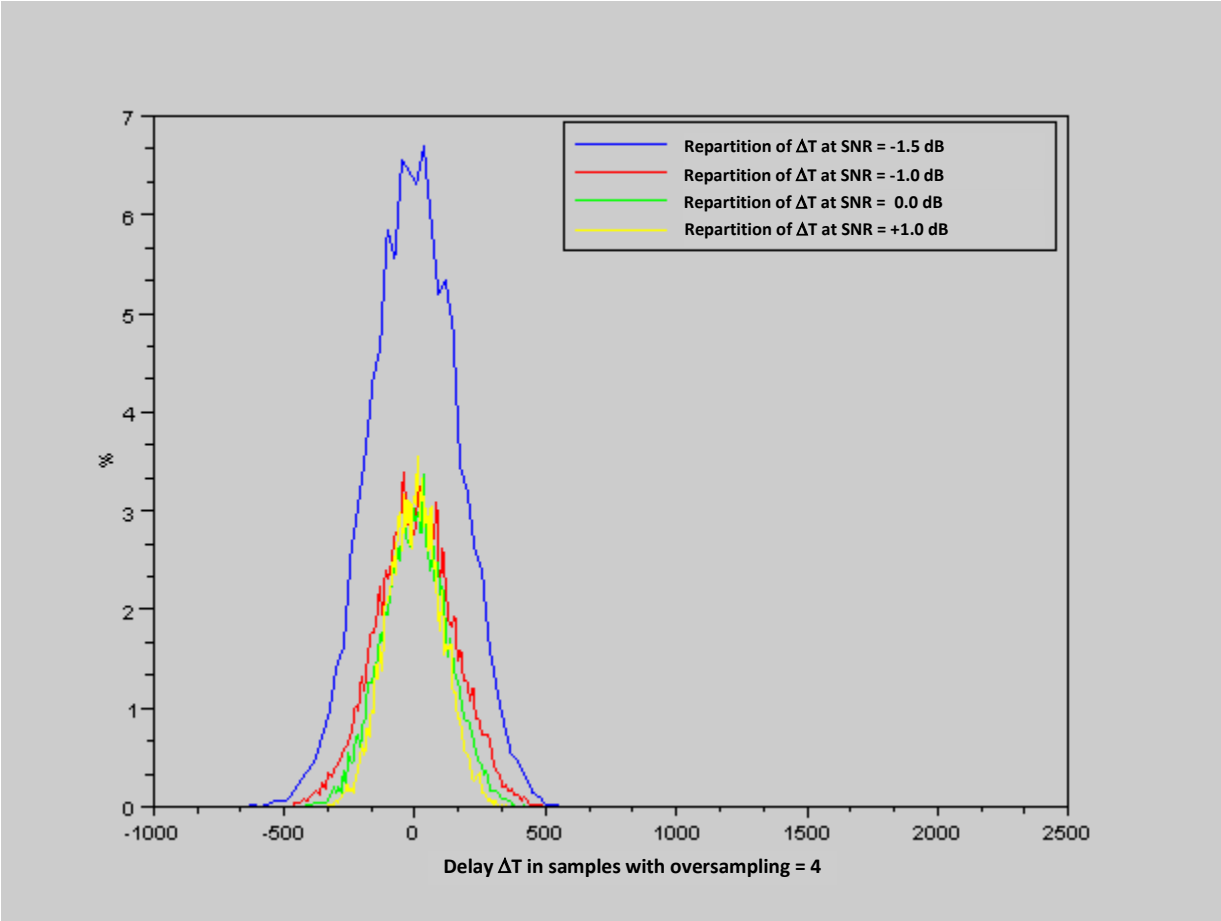

Figure 82: Error distribution of the coarse time estimation of the start of P1 (without filtering).

2.3.5.3.3.3 Frequency fractional error estimation precision

In parallel to the coarse time estimation, the receiver also performs the detection of the fractional part of the frequency offset. After the integer part is computed, the residual frequency error can easily be estimated using the SC-OFDM hybrid symbols if the phase between two hybrid symbols rotates less than π radians. The maximal error of the P1 detection algorithm shall not be greater than half of the inverse of time between two hybrid symbols:

$$df_{\max} = \frac{SC-OFDM_{carriersapcing}}{2T_{Hybrid}\left(1+\frac{1}{GI}\right)}, \qquad (45)$$

where:

- $SC-OFDM_{carriersapcing}$ is the spacing between the subcarriers of the SC-OFDM symbols,
- T_{Hybrid} is the period of the hybrid symbols, expressed in number of SC-OFDM symbols,
- GI^{-1} is the fraction of SC-OFDM symbol copied as guard interval (GI =4, 8 ,16 or 32).

Table 33 below gives the percentage of the estimated fractional frequency error greater than $df_{\max}$ with:

- SC_OFDM symbols with N_FFT = 512, GI =8
- T_{Hybrid}=6.

Table 33: Error rate of the fractional frequency error estimate.

GI	SNR = -8dB	SNR = -6.5dB	SNR = -5dB	SNR = -2dB
1/4	7,0%	4,55%	0,3%	0,0%
1/8	4,0%	1,84%	0,2%	0,0%
1/16	3,3%	1,26%	0,2%	0,0%
1/32	3,0%	0,87%	0,2%	0,0%

2.3.5.4 Estimation of the integer part of the frequency offset

2.3.5.4.1 Description of the algorithms

This section presents two methods for estimating the integer part of the frequency offset. After P1 detection, only a coarse estimation of the timing offset τ_0 of the start of P1 symbol is known and the maximum tolerable error on τ_0 is the fine synchronization search space. The non-regular spreading of the active carriers of P1 symbol is used to estimate the integer part of the frequency (See Figure 83).

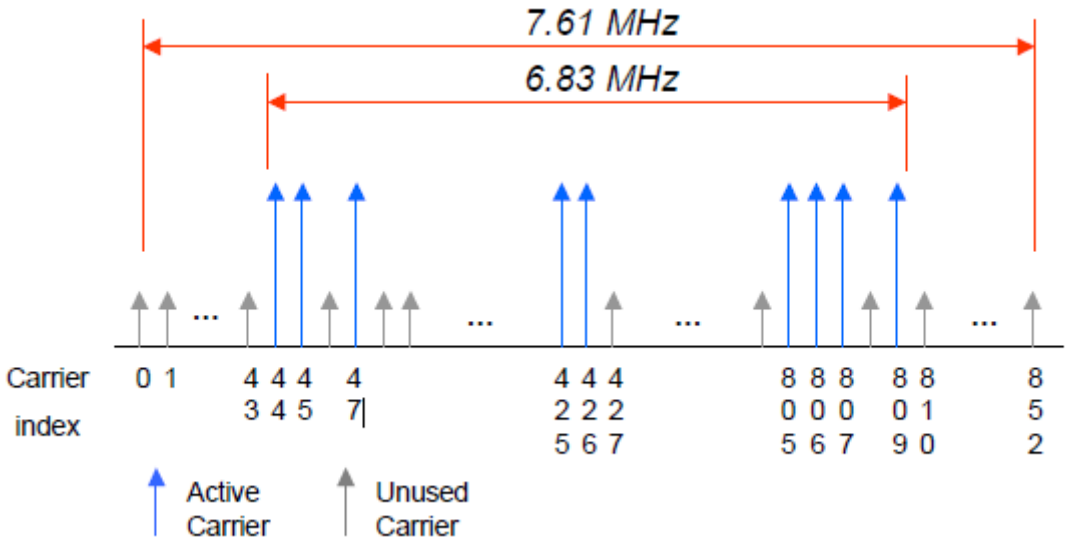

Figure 83: Spectrum mask of the P1 symbol.

The two proposed methods are:

- Method 1 : module correction
  - The FFT is performed on the A part of the P1 symbol which is coarsely synchronized: 1024×oversampling factor (OVF) samples over the time interval: $\tau_0 + T_C$ to $\tau_0 + T_C+T_A$-1
  - A correlation is performed between this FFT and a reference vector with zeros except where active carriers are present where the is a 1
  - The frequency error is obtained by the index of the correlation peak.

- Method 2 : complex correlation
  - The first sample is taken at τ_0 -FINE_SYNCHRO_SEARCH_SPACE+T_C, the FFT is performed on 1024×OVF samples from the start.
  - The correlation is performed between this FFT and a reference vector composed of zeros except where the X128 symbol has non zero values that are +1 or -1 (carriers are BPSK modulated).
  - It is needed to be synchronized in time with less that OVF samples of error in order to have a correlation peak. So the computation is performed by shifting from 1 to OVF samples in the data flow and doing several FFT and correlations.
  - It stops at sample τ_0 +FINE_SYNCHRO_SEARCH_SPACE+T_C.
  - The frequency error is given by the index of the maximum of the correlation peak.
  - If a maximum is found, then the start of P1 symbol is known with a precision of +/-OVF/2.

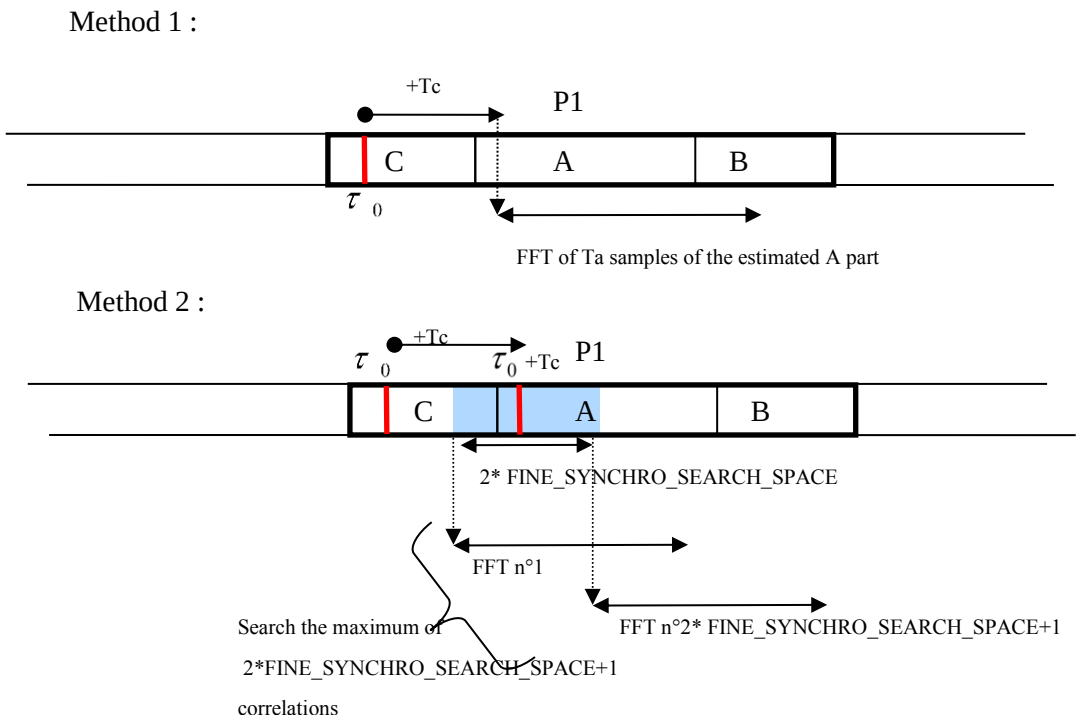

Figure 84 : Illustration of the 2 methods for the integer frequency offset estimation (IFS).

Method 2 is more robust to noise, but is also more complex. However, the total complexity IFS + FTS of the 2 methods is equivalent, because with Method 2 the precision of time synchronization after FTS reduces the number of correlation to perform for the FTS.

Table 34 presents the complexity ratio between the two methods:

- "search step" is the number of samples of the shift to perform FFT+correlation if method 2 is used.
- FFT size can be reduced to 2048 instead of 4×1024 =4096 (if one sample over 2 is used).
- The number of FFT with method 2 is calculated with Erreur_max_CTS = 1200 samples.

- "NB corr X128" is the number of correlation with the symbol X128 necessary to perform the fine time synchronization.
- "Nop M1" is the number of operation of method 1 + the fine frequency synchronization performed with 2×Error_max_CTS correlations with the X128 symbol.
- It can be noticed that the complexity are of the same order with the two methods.

Table 34: Comparison of complexity between Method 1 and Method 2.

Search step	size FFT	Number of FFT	NB Corr X128	Nop M1	Nop M2	Ratio Nop M2/M1
1	2048	2400	0	19660800	37524527,2	1,9
2	2048	1200	3	19660800	18786839,6	1,0
3	2048	800	4	19660800	12540943,7	0,6
4	2048	600	5	19660800	9422091,81	0,5
1	4096	2400	0	19660800	81814968,5	4,2
2	4096	1200	3	19660800	40932060,3	2,1
3	4096	800	4	19660800	27304424,2	1,4
4	4096	600	5	19660800	20494702,1	1,0

2.3.5.4.2 Performance evaluation

This section illustrates the performance of the 2 aforementioned methods for estimating the integer part of the carrier frequency offset. Figure 85 gives the percentage of success of the integer frequency error estimation for Method 1 with respect to the precision of the initial coarse time synchronization for various SNR. Figure 86 gives the same kind of result for Method 2.

It appears from those results that Method 2 is more robust to noise. However considering the SNR used for the systems simulations (around 0 dB) Method 1 will also provide good results.

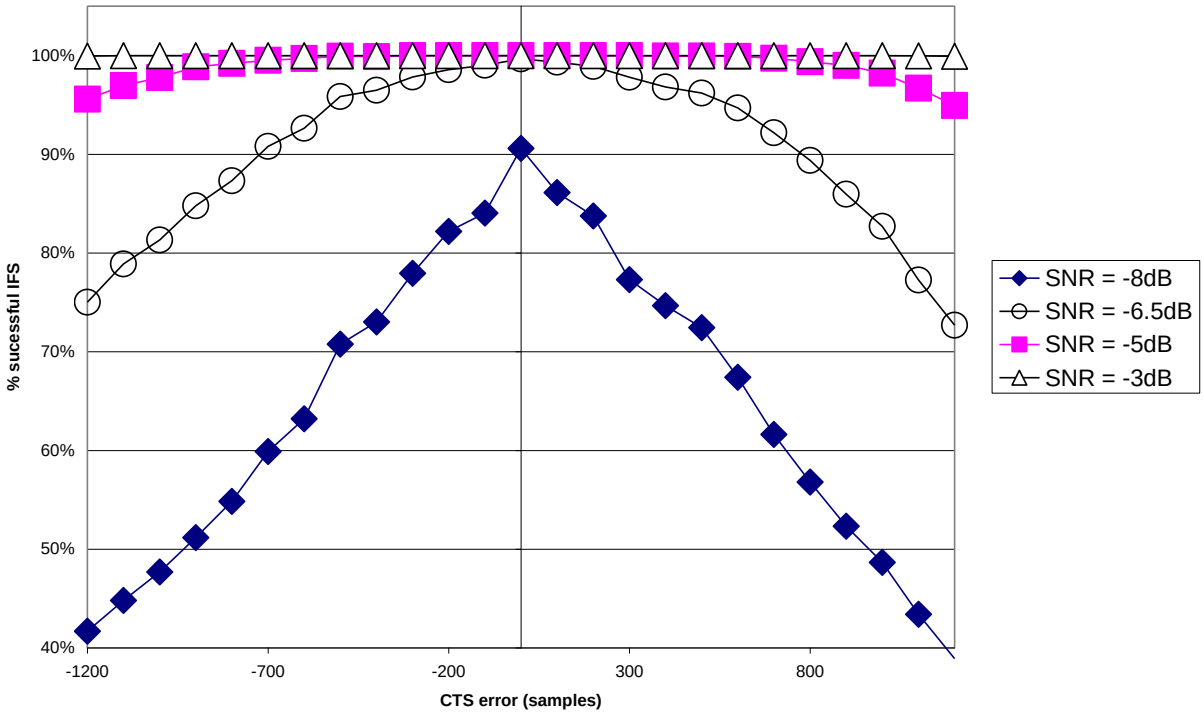

Figure 85: IFS detection performance - Method 1.

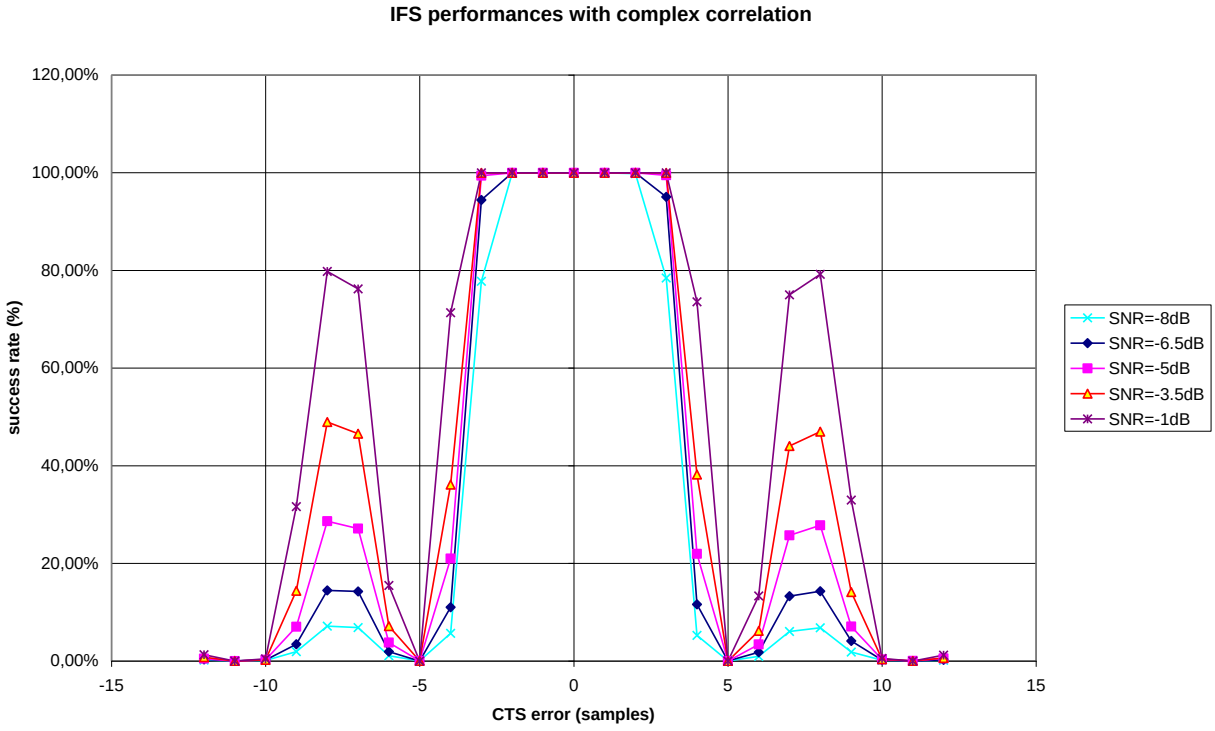

Figure 86: IFS detection performance - Method 2.

2.3.5.5 Time synchronization

2.3.5.5.1 Algorithm description

The time synchronization is performed after the integer frequency error estimation. The inputs are:

- A coarse estimation τ_0 of the start of the P1 symbol obtained after P1 detection,
- The estimate of the frequency error.

The observed SNR being as low as -8dB (minimal SNR for detection) the correlation γ with the X128 symbol shall be performed in complex in order to be robust to noise in AWGN channel:

- The signal is corrected with the estimated frequency.
- The maximum is searched of the complex correlation products $\|\gamma_N\|^2$ between the samples x_k of the X128 and the samples y_{k-N} of the input signal:

$$\|\gamma_N\|^2 = \left\| \sum_{k=1}^{M} x_k y_{k-N}^{*} \right\|^2 . \quad (46)$$

  Note that $\|\gamma_N\|^2$ is a complex correlation and not a module correlation ($\gamma_N = \sum_{k=1}^{M} \|x_k\|^2 \|y_{k-N}\|^2$).

- In order to compute the correlation product $\|\gamma_N\|^2$ with the X128 symbol, 8192 complex products are needed, X128 being composed of 8192 samples: this operation is computationally consuming.
- The parameter FINE_SYNCHRO_SEARCH_SPACE corresponds to the worst time error on τ_0, the calculation of $\|\gamma_N\|^2$ is made for *N* going from τ_0 - FINE_SYNCHRO_SEARCH_SPACE to τ_0 + FINE_SYNCHRO_SEARCH_SPACE, that is 2×FINE_SYNCHRO _SEARCH_SPACE+1 correlations $\|\gamma_N\|^2$.
- Each correlation product $\|\gamma_N\|^2$ is calculated over 8192 points, the needed memory is:
  2×FINE_SYNCHRO_SEARCH_SPACE+1 +8192.
- FINE_SYNCHRO_SEARCH_SPACE is set to 1200 samples if the integer part of the frequency error was estimated using Method 1 and 3 samples if the integer part of the frequency error was estimated with Method 2.

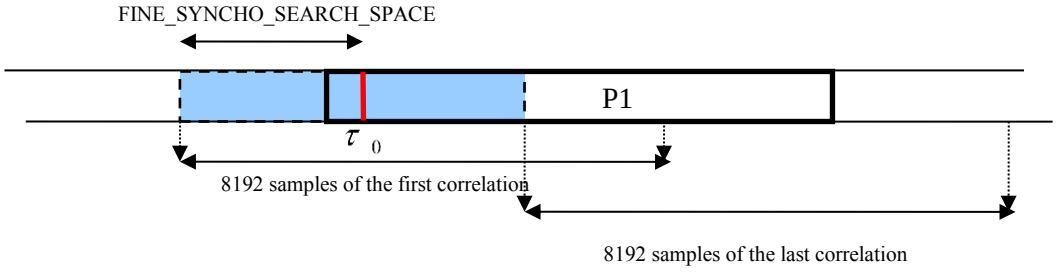

Figure 87: Illustration of the fine time synchronization implementation (FTS).

2.3.5.5.2 Performances evaluation

Without any frequency error, the correlation between the P1 symbol with unitary power and the X128 is defined as:

$$\gamma = \frac{1}{8192}\sum_{k=1}^{8192} x_k X128_{k-N}^{*}, \tag{47}$$

where:

- x_k is a complex white Gaussian noise $n = n_I + jn_Q$ with variance $\sigma_n^2 = \sigma_{\mathrm{Re}(n)}^2 + \sigma_{\mathrm{Im}(n)}^2 = 2\sigma_{\mathrm{Re}(n)}^2$,
- The determinist X128 symbol is assumed with power 1.

Eq. (47) is the result of the sum of 8192 independent variables $x_k X128_{k-N}^{*}$ of variance σ_n^2. As a consequence, γ is a random complex variable with a variance given by:

$$\sigma_\gamma^2 = \left(\frac{1}{8192}\right)^2 8192\sigma_n^2 = \frac{\sigma_n^2}{8192}, \tag{48}$$

As the sum of two zero-mean squared independent Gaussian variables γ_I and γ_Q, $\|\gamma\|^2 = \gamma_I^2 + \gamma_Q^2$ follows a Khi square law with two degrees of freedom. γ_I and γ_Q have variance equal to:

$$\sigma_{\mathrm{Re}\{\gamma\}}^2 = \sigma_{\mathrm{Re}\{\gamma\}}^2 = \frac{\sigma_n^2}{2}\frac{1}{8192}. \tag{49}$$

Consequently, it is possible to compute the value of σ_n^2 in order to have $\|\gamma\|^2 = 0.33$ with probability *p*:

$$\sigma_n^2 = \frac{0.33\times 8192\times 2}{Khideuxinverse(p)}, \tag{50}$$

under the assumption of a SC-OFDM transmission data with N_FFT = 512 and Nu = 426, a unitary mean power (because 0.33 is the value if the power of P1 is 1), and an oversampling factor of 4. It is finally possible to derive the SNR from the noise power as:

$$SNR = 10\log_{10}\left(\frac{4\times\frac{512}{426}}{P_{noise}}\right), \tag{51}$$

Table 35 provides the SNR value required to obtain different target probabilities.

Table 35: Probability of bad fine time synchronization vs. SNR and intermediate metrics.

Pr(Corr>0,33)	KHI2INV(p)	Pnoise	SNR
1,E-01	4,61	1 174,05	-24
1,E-02	9,21	587,03	-21
1,E-03	13,82	391,35	-19
1,E-04	18,42	293,51	-18
1,E-05	23,03	234,81	-17
1,E-06	27,63	195,68	-16

From Table 35, it can be noticed that the fine time synchronization is very robust, mainly due to the high number (8192) of mean computations performed to obtain a correlation product.

In conclusion, the fine time synchronization can only fail if:

- The coarse time estimation τ_0 computed during P1 detection is greater than FINE_SYNCHRO_SEARCH_SPACE
- The frequency error estimation is in the order of magnitude of 50% of a subcarrier.

Figure 88 below shows the values of $\|\gamma\|^2$ obtained for various P1, various random chooses, and various frequency errors (estimated in % of a SC-OFDM subcarrier with N_FFT = 512, that is half of the error in % of a P1 subcarrier) and SNR = 0dB.

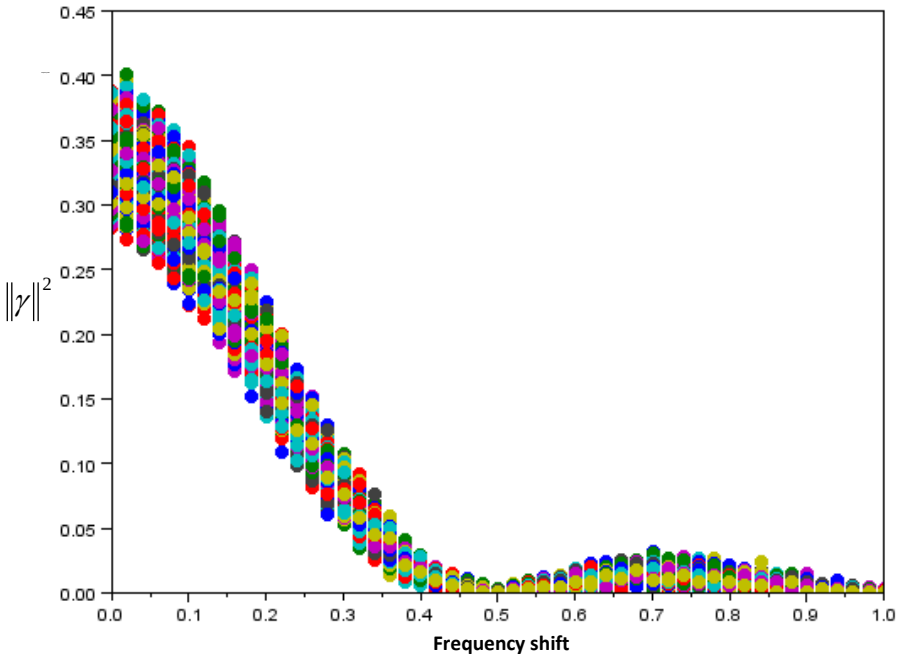

Figure 88: Values of various correlations between P1 and X128 symbol.

2.3.5.5.3 False alarm computation

Let's consider the following correlation:

$$\gamma = \frac{1}{8192}\sum_{k=1}^{8192} x_k X128_{k-N}^{*}, \tag{52}$$

with:

- $x_k = s_k + n_k$
- s_k, an SC-OFDM signal with a power σ_s^2 and a bandwidth $b = \frac{426}{4\times 512}$ (426 useful carriers over 512, observed with 4 samples by symbol)
- n_k white Gaussian complex noise with variance σ_n^2

It can be shown that the variance of the correlation γ is given by:

$$\sigma_\gamma^2 = \frac{1}{8192}\frac{\sigma_n^2}{2} + \frac{1}{8192}\frac{\sigma_s^2}{2b}. \quad (53)$$

The squared module $\|\gamma\|^2$ follows a Khi square law with two degrees of freedom. The false alarm threshold with a probability *p* is obtained as:

$$Threshold = \sigma_\gamma^2 Khi2^{-1}(p), \quad (54)$$

If after fine time synchronization, the maximum of $\|\gamma\|^2$ is below the threshold, it is assumed that the correlation was not performed on a P1 symbol and consequently the frame is not validated.

It is also possible to compute a threshold based on the correlation value between a P1 of power σ_s^2 shifted in frequency and the X128 symbol:

- If *df*=0 then $\|\gamma\|^2 = 0.33\sigma_s^2$
- If *df*>0.3% of a SC-OFDM subcarrier then $\|\gamma\|^2 < 0.1\sigma_s^2$
- It is needed to have $df < \frac{1}{2}\frac{1}{T_{Hybrid}\left(1+1/GI\right)} = 0.074$ if T_{Hybrid} = 6 and GI = 8 so it is possible to use a threshold of $0.1\times\sigma_s^2$ in order to validate a P1 frame.

The power values σ_n^2 and σ_s^2 are estimated using:

- The estimated SNR given by the P1 detection block
- The total power at the input of the algorithm $\sigma_n^2 + \sigma_s^2$
- The formula $SNR = 10\log_{10}\left(\frac{1}{b}\frac{\sigma_s^2}{\sigma_n^2}\right)$ with *b* the useful band of the signal *s*.

2.3.5.6 Fine frequency synchronization over pilot symbols

2.3.5.6.1 Description of the algorithm

The residual frequency error *df* is estimated as follows:

$$\widehat{df_k} = \frac{1}{T_{Hybrid}} Arg\left\{E\left\{P_k^* P_{k+1}\right\}\right\} = \frac{1}{T_{Hybrid}} Arg\left\{\frac{1}{N_P}\sum_{i=1}^{N_P} P_{k,i}^* P_{k+1,i}\right\}, \quad (55)$$

where:

- *i* is the index of the subcarrier and *k* the index of the hybrid symbol,

- T_{Hybrid} is the time between two hybrid symbols (expressed in seconds in order to have $\widehat{df}$ in Hz, or expressed in number of symbols if $\widehat{df}$ is to be expressed relatively to the subcarrier space),
- $Arg\{Z\} = \tan^{-1}\{\mathrm{Im}\{Z\} / \mathrm{Re}\{Z\}\}$.

Considering that the SNR varies during the frame and that it is not possible to determine if an estimate of $\widehat{df}_k$ is correct, $\widehat{df}_k$ is estimated for each pair of hybrid symbols and $\widehat{df}_k$ is used to correct data symbols between symbols k and k+1. It is possible to accumulate the correlation products between the pilot subcarriers over more than 2 hybrid symbols:

$$\widehat{df}_a = \frac{1}{T_{Hybrid}} Arg\left\{E\left\{P_k^{*} P_{k+1}\right\}\right\} = \frac{1}{T_{Hybrid}} Arg\left\{\frac{1}{K}\frac{1}{N_P}\sum_{k=a}^{K+a-1}\sum_{i=1}^{N_P} P_{k,i}^{*} P_{k+1,i}\right\}, \quad (56)$$

with K lying between 1 and the total number of possible sums, that is to say the total number of hybrid symbols in the frame minus 1.

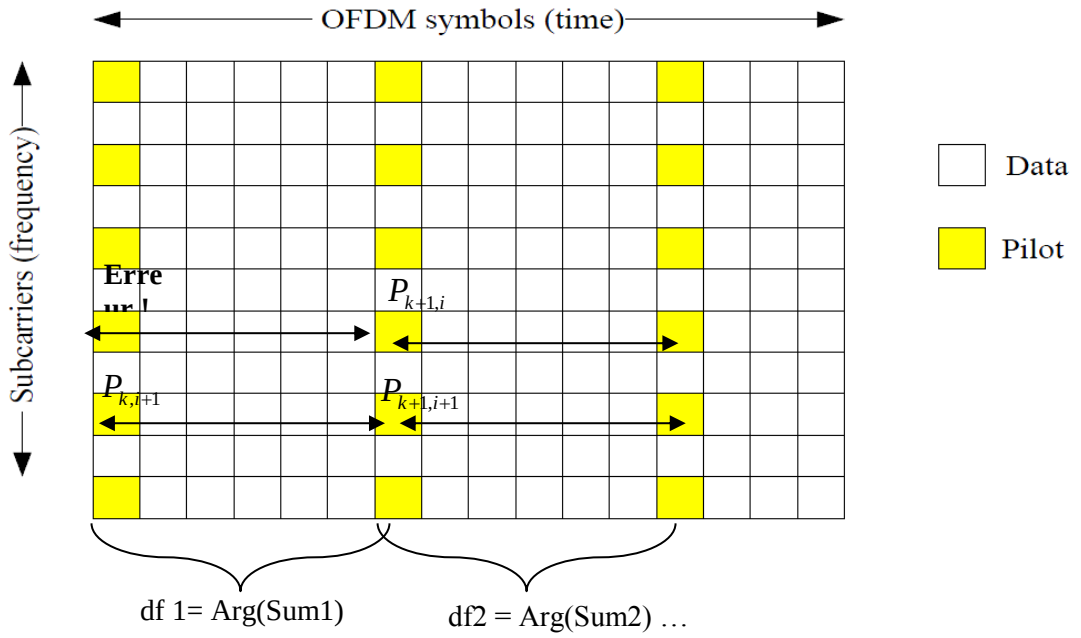

Figure 89: Illustration of fine frequency estimation.

2.3.5.6.2 Performances evaluation

Let's consider the fine time estimate defined as:

$$\widehat{df}_k = \frac{1}{2\pi T_{Hybrid}} Arg\left\{\frac{1}{N_P}\sum_{i=1}^{N_P} P_{k,i}^{*} P_{k+1,i}\right\}. \quad (57)$$

The received signal $P_{k,i}$ is given by:

$$P_{k,i} = H_{k,i} X_{k,i} + N_{k,i}, \quad (58)$$

where $X_{k,i}$ is the pilot, $H_{k,i}$ the channel coefficient and $N_{k,i}$ the noise with power σ_n^2.

In (57), the sum $\sum_{i=1}^{N_P} P_{k,i}{}^{*} P_{k+1,i}$ follows a normal law with variance $N_p\left(\sigma_n^4 + 2\sigma_n^2\right)$. Thus we have:

$$\begin{aligned} E\left\{\left(H_{k,i}X_{k,i}+N_{k,i}\right)\left(H_{k+1,i}X_{k+1,i}+N_{k+1,i}\right)^{*}\right\} &= E\left\{\left(HX+N_{k,i}\right)\left(HX+N_{k+1,i}\right)^{*}\right\} \\ &= \left\|HX\right\|^2 + E\left\{N_{k,i}N_{k+1,i}{}^{*}\right\} + 2E\left\{HXN\right\} \\ &= \left\|HX\right\|^2, \end{aligned} \tag{59}$$

and:

$$\begin{aligned} E\left\{\left\|\left(H_{k,i}X_{k,i}+N_{k,i}\right)\left(H_{k+1,i}X_{k+1,i}+N_{k+1,i}\right)^{*}\right\|^2\right\} &= E\left\{\left\|\left(HX+N_{k,i}\right)\left(HX+N_{k+1,i}\right)^{*}\right\|^2\right\} \\ &= E\left\{\left\|\left\|HX\right\|^2 + N_{k,i}N_{k+1,i}{}^{*} + 2HXN\right\|^2\right\} \\ &= \left\|HX\right\|^4 + E\left\{\left\|N_{k,i}N_{k+1,i}{}^{*}\right\|^2\right\} + 4E\left\{\left\|HXN\right\|^2\right\} \\ &= \left\|HX\right\|^4 + \sigma_n^4 + 4\frac{\sigma_n^2}{2}. \end{aligned} \tag{60}$$

Finally, we have:

$$Var\left\{\frac{1}{N_p}\sum_{i=1}^{N_P} P_{k,i}{}^{*} P_{k+1,i}\right\} = \frac{1}{N_p}\left(\sigma_n^4 + 2\sigma_n^2\right). \tag{61}$$

By writing $C = \left(I + jQ\right) + \left(n_I + jn_Q\right)$ with $\left(I + jQ\right)$ a determinist constant complex number of power 1 and $n_I + jn_Q$ a complex white noise of variance σ_n^2 and assuming $Q << I$ (that is Q/I close to zero and I close to 1) and $E\left\{n_I{}^2\right\} << 1$, then:

$$Var\left\{Arg\left\{C\right\}\right\} = \frac{\sigma_n^2}{2}. \tag{62}$$

This can be demonstrated as follows:

$$\begin{aligned} Var\left\{\tan^{-1}\left(\frac{\mathrm{Im}\left\{C\right\}}{\mathrm{Re}\left\{C\right\}}\right)\right\} \approx Var\left\{\frac{\mathrm{Im}\left\{C\right\}}{\mathrm{Re}\left\{C\right\}}\right\} &= E\left\{\frac{\left(\mathrm{Im}\left\{C\right\} - E\left\{\mathrm{Im}\left\{C\right\}\right\}\right)^2}{\left(\mathrm{Re}\left\{C\right\} - E\left\{\mathrm{Re}\left\{C\right\}\right\}\right)^2}\right\} \\ &= E\left\{\frac{\left(Q+n_Q\right)^2}{\left(I+n_I\right)^2}\right\} - E\left\{\frac{Q+n_Q}{I+n_I}\right\}^2 \\ &= \frac{E\left\{Q^2\right\} + E\left\{n_Q{}^2\right\}}{E\left\{I^2\right\} + E\left\{n_I{}^2\right\}} - E\left(\frac{Q}{I}\right)^2 \end{aligned}$$

$$Var\left\{\tan^{-1}\left(\frac{\mathrm{Im}\{C\}}{\mathrm{Re}\{C\}}\right)\right\} \approx Var\left\{\frac{\mathrm{Im}\{C\}}{\mathrm{Re}\{C\}}\right\} = \frac{E\left\{n_Q{}^2\right\}}{1+E\left\{n_I{}^2\right\}} \approx E\left\{n_Q{}^2\right\} \approx \frac{\sigma_n^2}{2} \quad (63)$$

Using this approximation, the standard deviation of the residual frequency error is given by:

$$\sigma_{df} = \frac{1}{2\pi T_{Hybrid}}\sqrt{\frac{\sigma_n^4 + 2\sigma_n^2}{2N_p}}. \quad (64)$$

Figure 90 and Figure 91 compares the simulated and theoretical values of the standard deviation of the sum of the correlations of the pilot symbols and the standard deviation of the residual frequency error that has been estimated. Those figures clearly validate the approximation obtained above.

It is possible to compute the probability *p* to have an estimated error greater than the expected precision, knowing the SNR so the value of σ_n^2:

$$\Pr\left\{\left|df - \hat{df}\right| > f\right\} = erfc\left\{\frac{f}{\sqrt{2\sigma_{df}^2}}\right\}. \quad (65)$$

If the channel estimator performs a temporal mean over 5 hybrid symbols, we obtain:

$$f_{\max} = \frac{1}{2\times 5\times T_{hybrid}}. \quad (66)$$

Table 36 gives the probability of the fine time error exceeding different thresholds for a set of SNR. Similarly, Figure 92 gives the error rate of the algorithm FFS for various SNR. It appears that the frequency estimation works correctly around the SNR at which the decoder is able to correct most of the errors (that is to say starting from SNR= -1dB for the modulation QPSK 1/2).

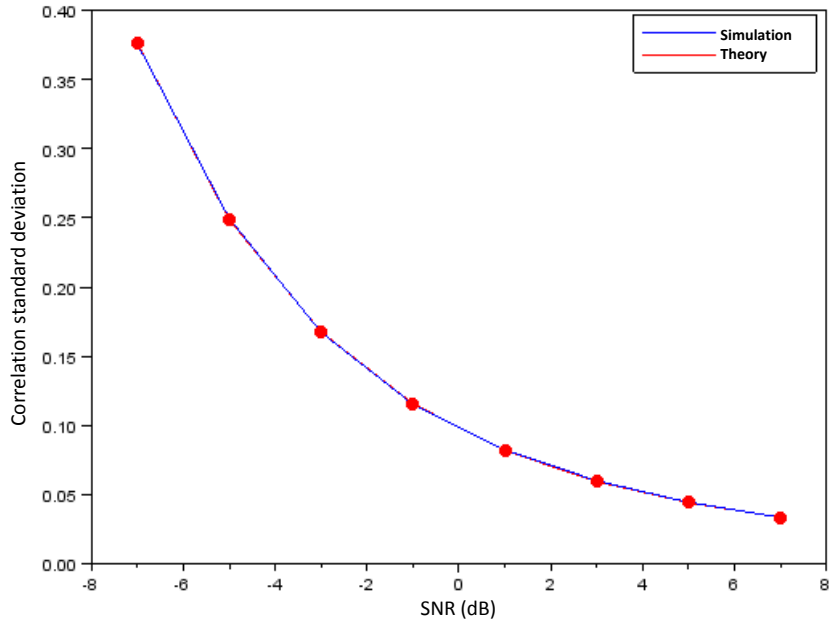

Figure 90: Standard deviation of the sum of the correlations of the pilot symbols.

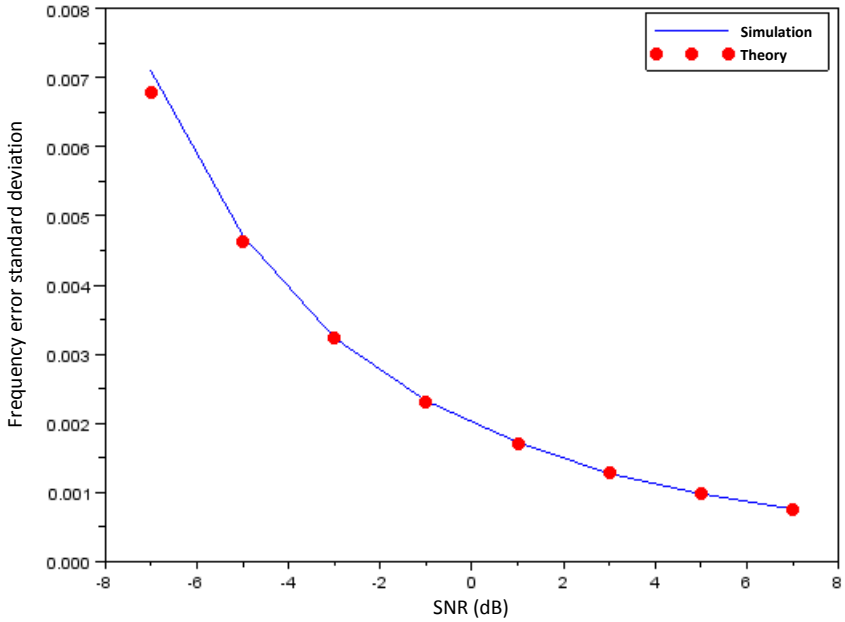

Figure 91: Standard deviation of the residual frequency error that has been estimated.

Table 36: Probability of the error FFS to be greater than various values in function of the SNR.

SNR(dB)	Pr(df>dfmax)	Pr(df>dfmax/2)	Pr(df>dfmax/4)	Pr(df>dfmax/8)
-7	0,0286988	0,274043	0,58	0,78
-5	0,0013288	0,1085272	0,42	0,69
-3	0,0000044	0,0216426	0,25	0,57
-1	1,53E-10	0,0013684	0,11	0,42
1	3,19E-18	0,0000135	0,03	0,28
3	5,04E-31	6,98E-09	0,00	0,15

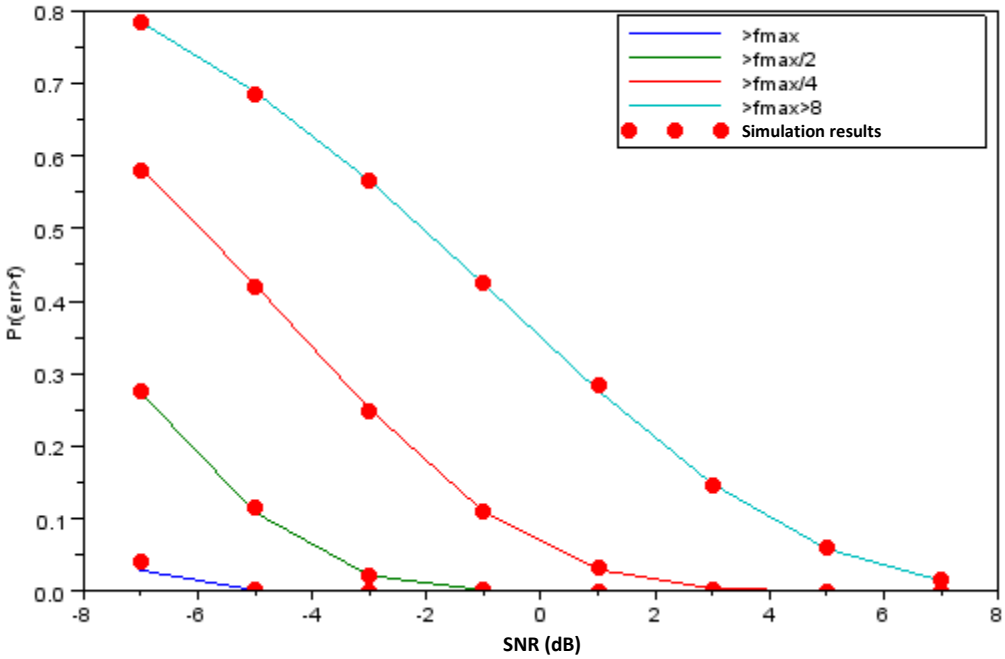

Figure 92: Error rate of the algorithm FFS for various SNR.

2.3.5.7 Conclusion

The previous sections have addressed three synchronization algorithms based on the P1 symbol that have an influence on the demodulation of the rest of the frame:

1. P1 detection + coarse estimation of time synchronization (CTS) + fractional frequency error estimation
2. Integer part of the frequency error estimation (IFS)

3. Fine time estimation of the start of the P1 symbol (FTS)

From the previous studies, it is shown that the following conditions need to be satisfied to achieve good performances:

1. P1 detection: SNR > -8dB
2. IFS : SNR > -8dB + CTS < 1200 samples
3. FTS : SNR > -20dB + frequency error < 0.5

If the P1 detection is successful, the probability to see the following two algorithms (IFS and FTS) fail is very low. Moreover, in the rare cases where IFS and/or FTS fail, either because of low SNR or bad coarse time synchronization, the threshold on the correlation peak FTS allows the detection of such failure and the LLRs can be forced to zero.

However, it is observed that for very low SNR where P1 detection works, but with a fractional frequency error slightly greater than the authorized maximum value of FFS:

$$f_{error} \geq f_{FFS\max} = \frac{1}{2T_{hybrid}\left(1+\frac{1}{GI}\right)} = \frac{1}{2\times 6\left(1+\frac{1}{8}\right)} \approx 0,074\,. \tag{67}$$

This frequency error is high enough to make the FFS fails, but it is too low to make FTS fails: it is consequently not possible to detect it using the X128 correlation peak threshold.

If SNR remains low on the frame, the LLRs calculated in function of the SNR will be quasi zero and the false information caused by FFS failure will not be considered.

However if the SNR increases during the frame, the LLRs increase (in absolute value) but will be wrong: their values will not correspond to the confidence of symbols having a frequency error too high.

Some cases have been observed on LMS ITS channel: it can happen that even for a higher SNR BER can increase if during P1 synchronization SNR is low and then increases during the frame reception. The frame is detected but with a high residual frequency error. The LLR being high because of the SNR being high on the rest of the frame, the decoder will cause packets of errors.

In order to solve this problem, several solutions can be envisaged:

- Add a more robust estimator of the residual frequency error before processing data and pilots: a possible estimator is described in Section 2.3.5.2.5.
- Reduce the confidence of the symbols given by the synchronization: a threshold on the LLRs at the input of the decoder is fixed as a function of the maximal LLR values sufficient in order to have a proper decoding on AWGN channel.
- Add a fractional error detector: if fractional error is too high, the LLRs are set to zero.

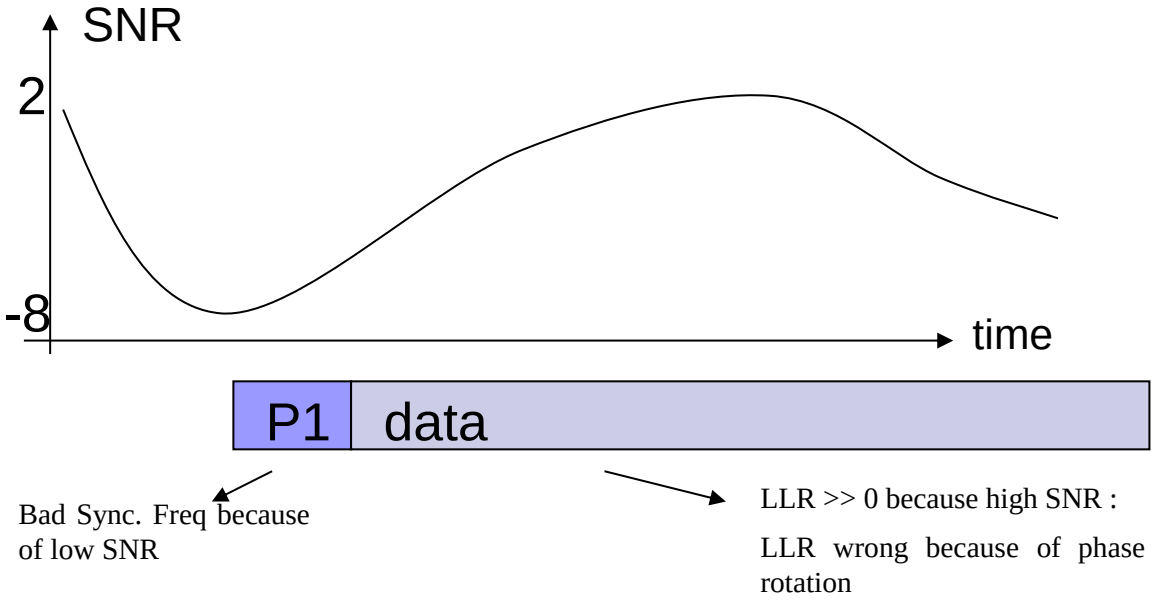

Figure 93: Illustration of the LLR issue due to SNR varying between P1 detection and data.

2.3.5.7.1.1 LLRs saturation

The saturation of the LLRs is useful in the case where synchronization can lead to an actual P1 detection but to a residual frequency error too high compared to the temporal filter used for channel estimation.

If frequency error is too high, the demodulated data will be wrong but the LLRs can be high if the SNR increases during time.

It is possible to limit the confidence of the decoder for the demodulated data without penalizing the rest of the link. The principle is to define a maximal value for the LLRs. This value is defined in function of the used modulation and the SNR for an AWGN channel for which there is no error.

For example, for a QPSK 1/3 the BER is nearly zero when SNR is greater than -1dB on AWGN channel, and for a QPSK 1/2 for SNR greater than 1dB. The LLRs distributions are depicted on Figure 94. The LLRs will be limited to 6 for the QPSK 1/3 and to 8 for the QPSK 1/2.

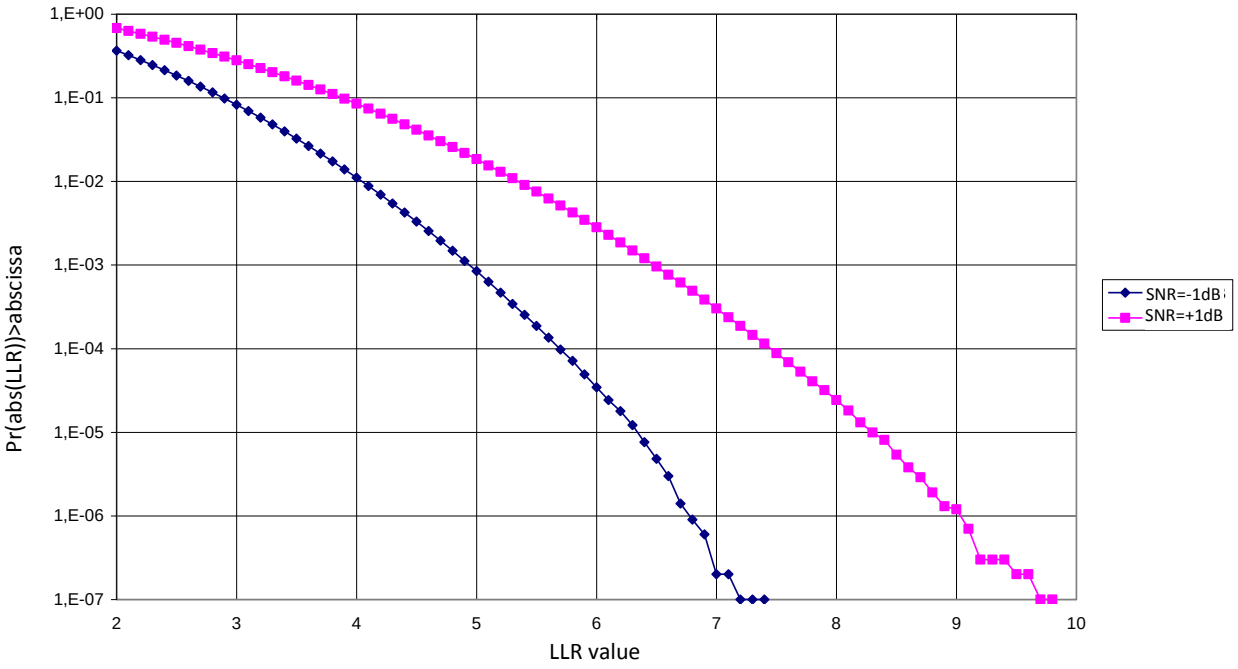

Figure 94: Statistics on maximal absolute value of LLRs for a QPSK at SNR = -1dB and 1dB.

2.3.5.8 Overall performances evaluation

This section evaluates by means of simulations the impact of the synchronization algorithms on the overall performance of the SC-OFDM receiver.

2.3.5.8.1 Simulator description

2.3.5.8.1.1 Functional block diagram

The simulator that has been used implements the SC-OFDM signal generation, the propagation channel emulation and the signal reception. The functional block diagram of the transmitter and the receiver is depicted respectively on Figure 95 and Figure 96.

Figure 95: SC-OFDM transmitter.

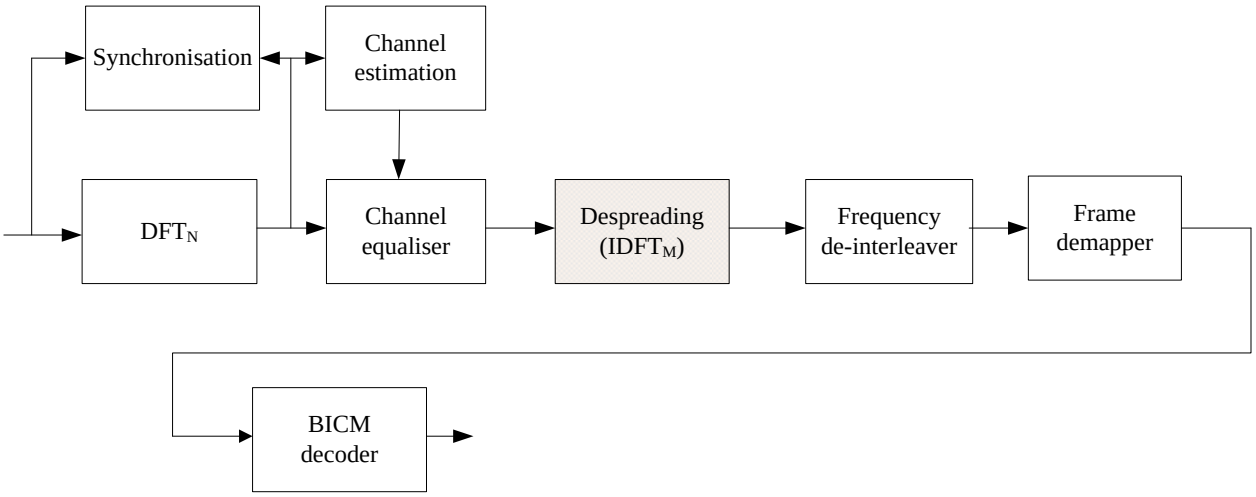

Figure 96: SC-OFDM receiver.

2.3.5.8.1.2 Synchronization blocks

All the synchronization algorithms presented in the previous sections have been implemented in the simulator. The architecture of the P1 synchronization block is shown on Figure 97.

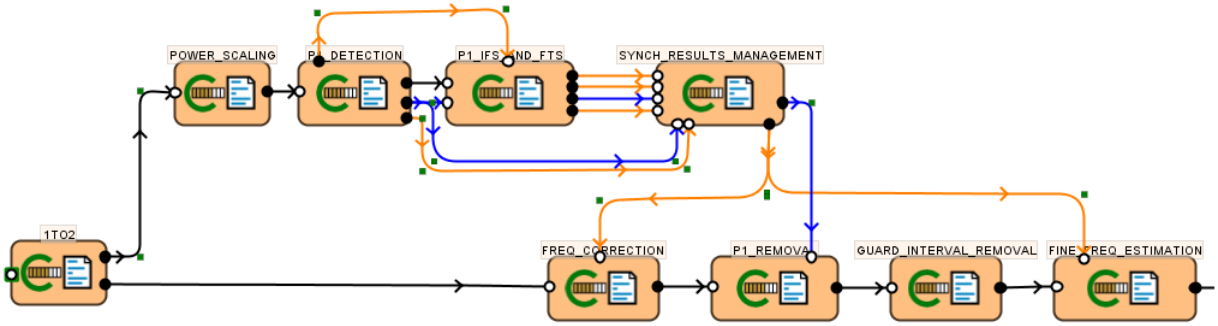

Figure 97: Synchronization blocs before OFDM demodulation.

The receiver can be configured in order to operate according to the following modes:

- PCE :Perfect channel estimation and perfect synchronization
- RCE PS: Real channel estimation, perfect synchronization. In this case the receiver uses a channel estimation algorithm
- RCE RS: Real channel estimation, real synchronization. In addition of channel estimation, the synchronization blocks are activated

2.3.5.8.1.3 Channel estimation

The channel estimation is performed using the hybrid symbols. Their repartition for SC-OFDM is recalled on Figure 98.

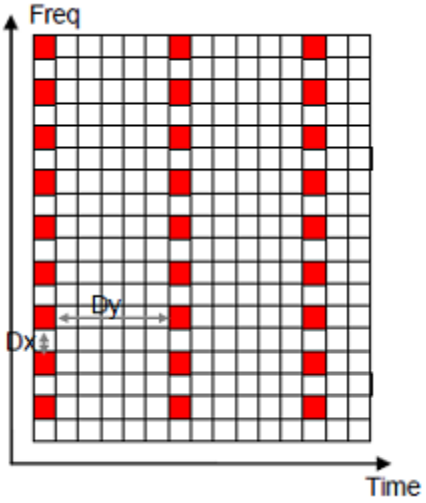

Figure 98: SC-OFDM hybrid symbols.

The channel estimation algorithm implements the following steps:

- Step1 : filtering in the frequency domain
  - The channel is observed at pilots' sub-carrier level (1 sub-carrier over 2) for each hybrid symbol.
  - A frequency filter in applied on these pilot sub-carriers. It is constructed based on the guard interval method:
    - This method consists in defining a filter bank that has a cut off frequency in inverse proportion to the guard interval.
    - The filter is selected bases on the length of the guard interval. It is usually chosen to be large enough so as to contain a certain amount of channel correlation.
  - Linear interpolation in the frequency domain over all the subcarriers of the data based on the filtered estimated values.
- Step 2: filtering in the time domain
  - The number of coefficients of the filter is chosen as a function of the maximum residual Doppler frequency accepted by the system:
    - TF0: order zero corresponds to no filtering
    - TF1: order 1 is a filtering over 3 consecutive symbols
    - TF2: order 2 is a filtering over 5 consecutive symbols
    - TF3: order 3 is a filtering over 7 consecutive symbols
  - The user decides which time domain filter to use depending on the external Doppler and the precision of the synchronization algorithms.
  - The filter is applied for each subcarrier of the hybrid symbols

- A linear interpolation is applied on all the subcarriers of the data inserted between two consecutive hybrid symbols.

2.3.5.8.2 Simulation results

Simulations have been carried out using 5 different propagation channel models:

1. AWGN channel,
2. TU6 channel with a mobile speed of 60 km/h,
3. A Rice channel with *K*=5 and a mobile speed of 60 km/h,
4. LMS open channel,
5. LMS ITS channel.

The simulations have been performed for the following receiver models:

- PCE : Perfect channel estimation and perfect synchronization
- RCE PS : Real channel estimation, perfect synchronization
- RCE RS :Real channel estimation, real synchronization

For real channel estimation, several temporal filters are used: TF0 to TF3.

2.3.5.8.2.1 AWGN channel

Figure 99 depicts the BER performance obtained through the simulation of 1000 P1 symbol and a time interleaving of 0.19 seconds.

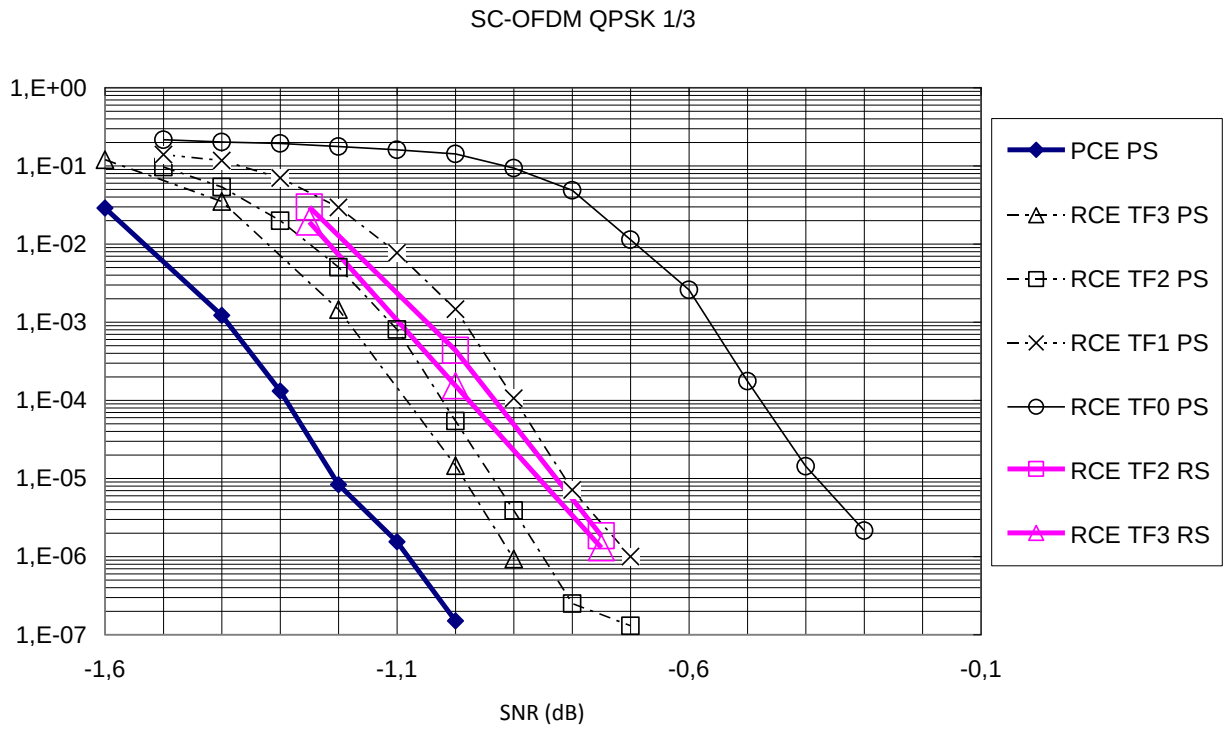

Figure 99: BER for an AWGN channel for a QPSK 1/3.

Compared to the receiver with perfect channel estimation and synchronization:

- The total loss due to synchronization and channel estimation is less than 0.5dB
- The loss due to synchronization is about 0.1dB

Figure 100 shows the performances obtained with real channel estimation and real synchronization for 2 interleaving duration: 7.45s and 0.28s.

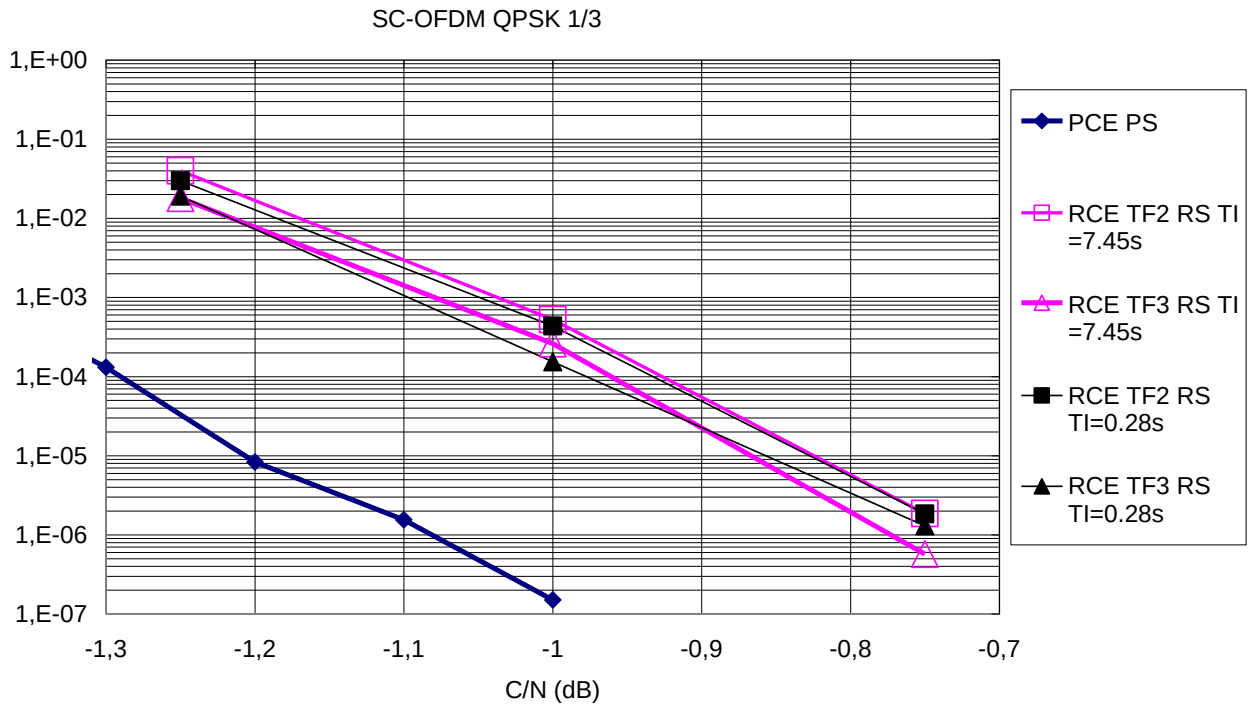

Figure 100: BER for an AWGN channel for a QPSK 1/3 with various interleaving time.

The interleaving depth has no effect on the performances. This is not surprising as the channel is constant over time and the synchronization algorithms always work at these SNR values (as shown in the previous chapters). Figure 101 shows the performances for a QPSK ½. It can be seen there is an incidence on the synchronization.

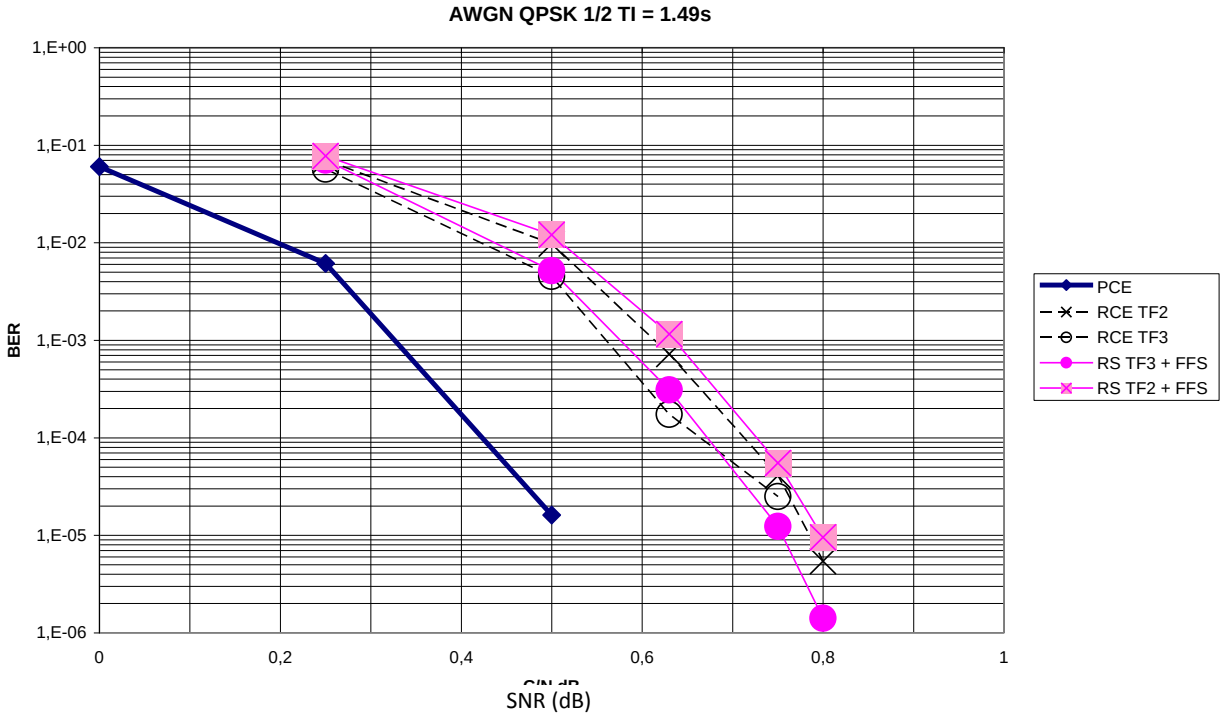

Figure 101: for an AWGN channel for a QPSK ½.

2.3.5.8.2.2 TU6 channel at 60km/h with SNR-based P1 detection threshold

The simulations have been performed with the following parameters:

- QPSK ½ modulation
- Interleaving time Ti of 0.28s or 1.49s
- The P1 detection threshold is computed using the method depending of SNR and the values:
  - Kn = 5
  - Ks = 55

Figure 102 and Figure 103 displays the BER performance respectively for a time interleaving of 0.28 and 1.49s. From these two figures it can be noticed that:

- The loss due to the synchronization process is low (at most 0.1dB), as expected at these SNR values.
- The loss increases if the size of the time domain filter for channel estimation increases. For example 0.3dB for TF3 composed of 3×2+1=7 hybrid symbols, instead of 2×2+1=5 hybrid symbol for TF2.
- The performances are better (0.25dB) when the interleaving time increases from 0.28 to 1.49 sec, all the curves are translated according to this value.

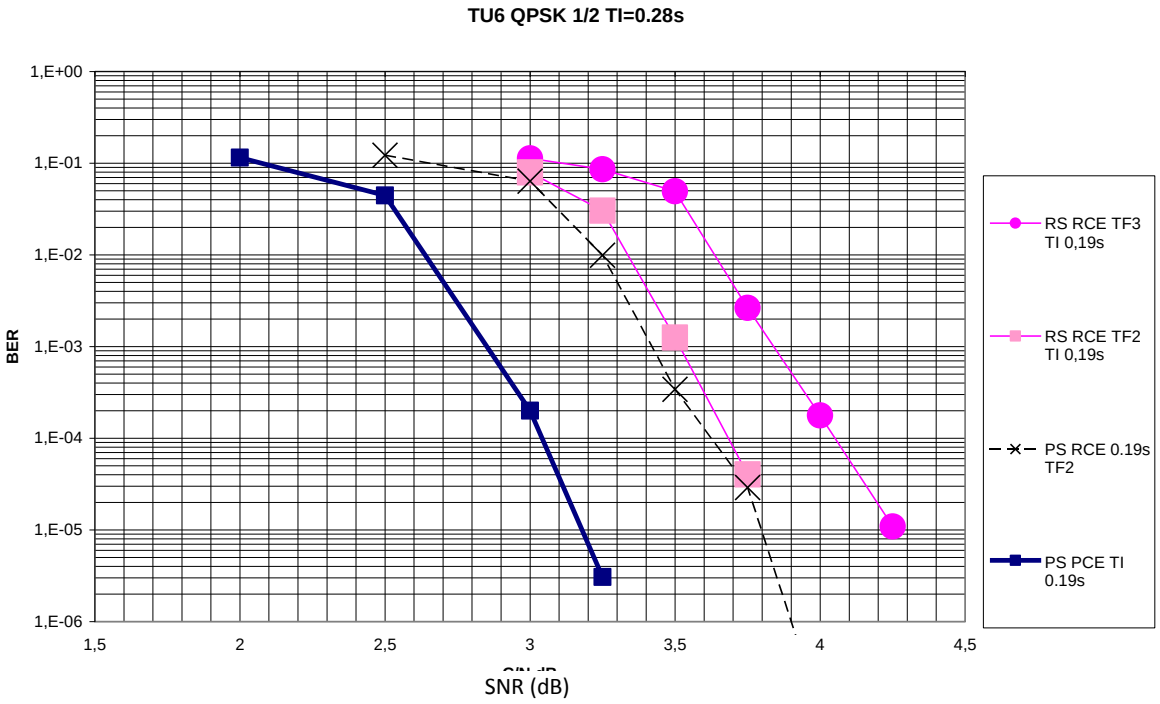

Figure 102: BER on TU6 channel with QPSK 1/2 and Ti=0.28s.

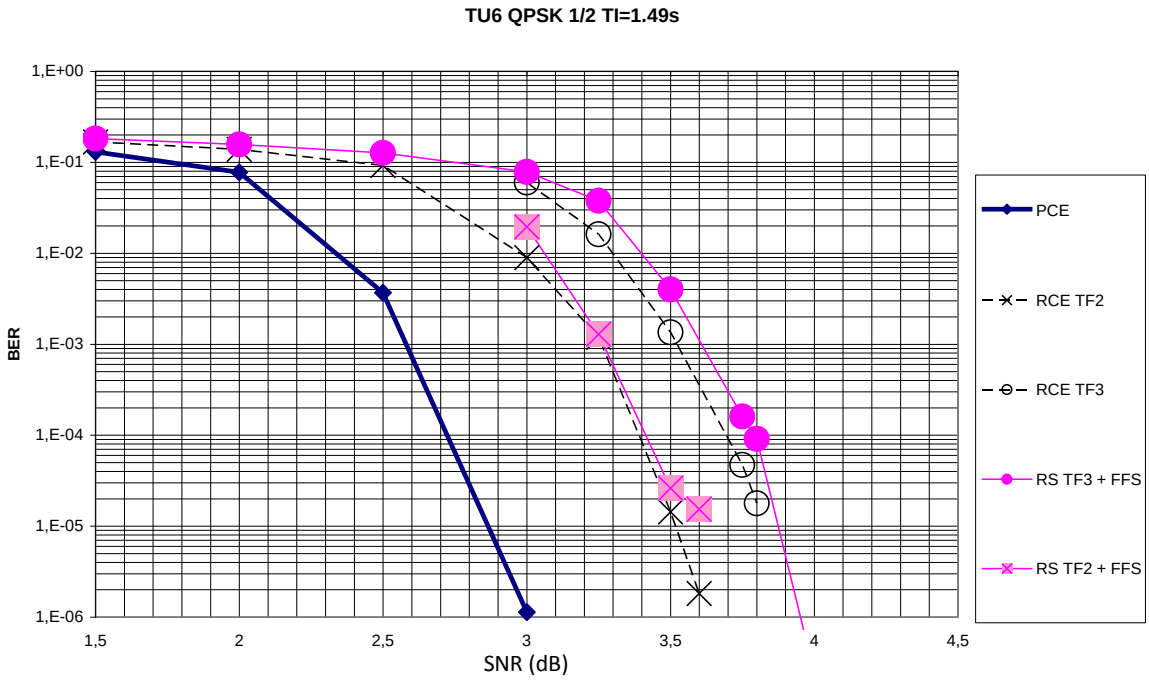

Figure 103: BER on TU6 channel with QPSK 1/2 and Ti=1.49s.

2.3.5.8.2.3 TU6 channel at 60km/h with fixed P1 detection threshold

The previous results were obtained using a threshold computation mechanism depending on the SNR. This section considers the fixed threshold computation. In this case, the single parameter *K* has been chosen in order to go from 25 to 55 with a step of 3 (25, 28 …. 55), and a value of 110 has been tested as well.

The values 25, 55 and 110 give good results on the LMS and RICE channels. With TU6 the same results are expected but with an interleaving time of 0.19s it is not the case. Depending on the chosen value of K the performance of the P1 detection algorithm varies:

- If K=25 to 36, some false alarms imply that the following P1 will not be detected and the BER is degraded
- If K= 39 or 42 no error is encountered and the performances are optimal
- If K=45 to 55 or 110 some non-detection occur and the BER is degraded

Figure 104 depicts the performance figures obtained in the case of a fixed threshold. It appears that the use of the fixed threshold computation method can provide good results if the coefficients are chosen appropriately.

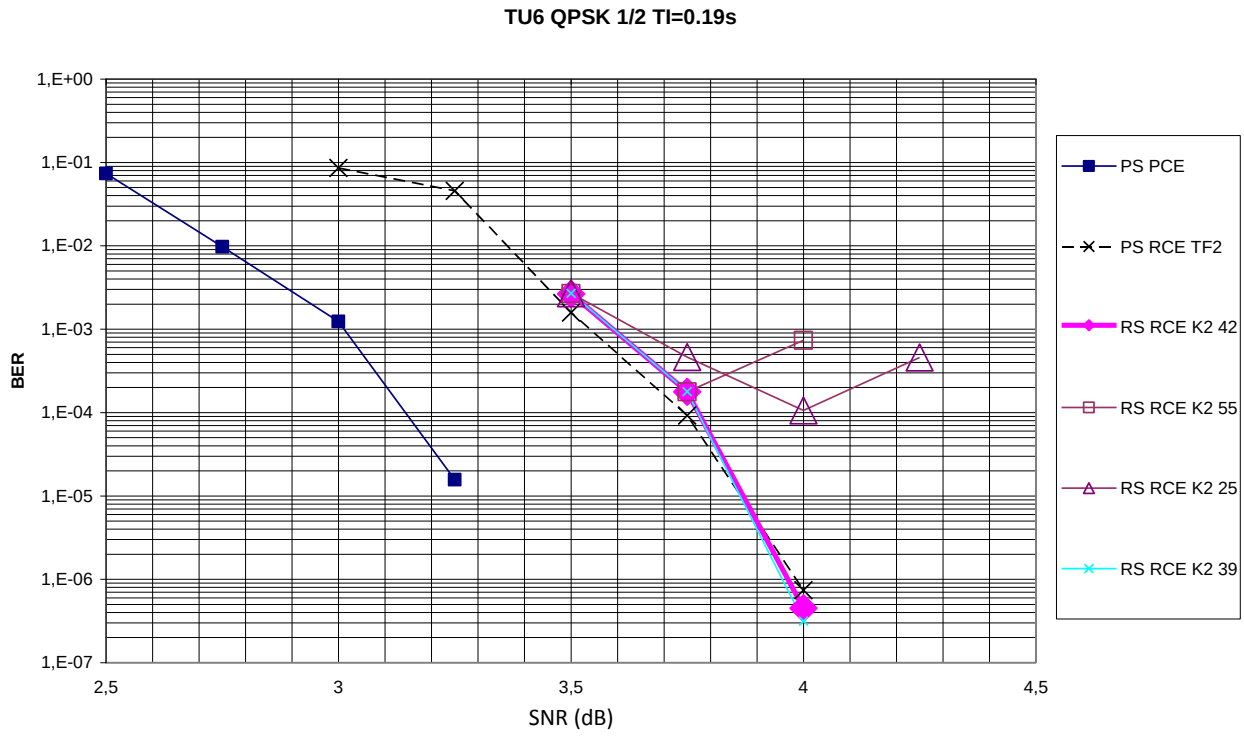

Figure 104: Performances on TU6 channel QPSK 1/2 TI=0.19s fixed P1 detection threshold, various parameter settings.

2.3.5.8.2.4 LMS open channel

The simulations have been performed with the following parameters:

- QPSK ½ modulation
- Interleaving time Ti of 0.28s or 1.49s
- Speed of 60 km/h

As shown on Figure 105 and Figure 106, the results are similar to those obtained with the AWGN channel: there is nearly no loss due to the synchronization mechanisms, and the interleaving time has nearly no effect on the performances (0.1dB).

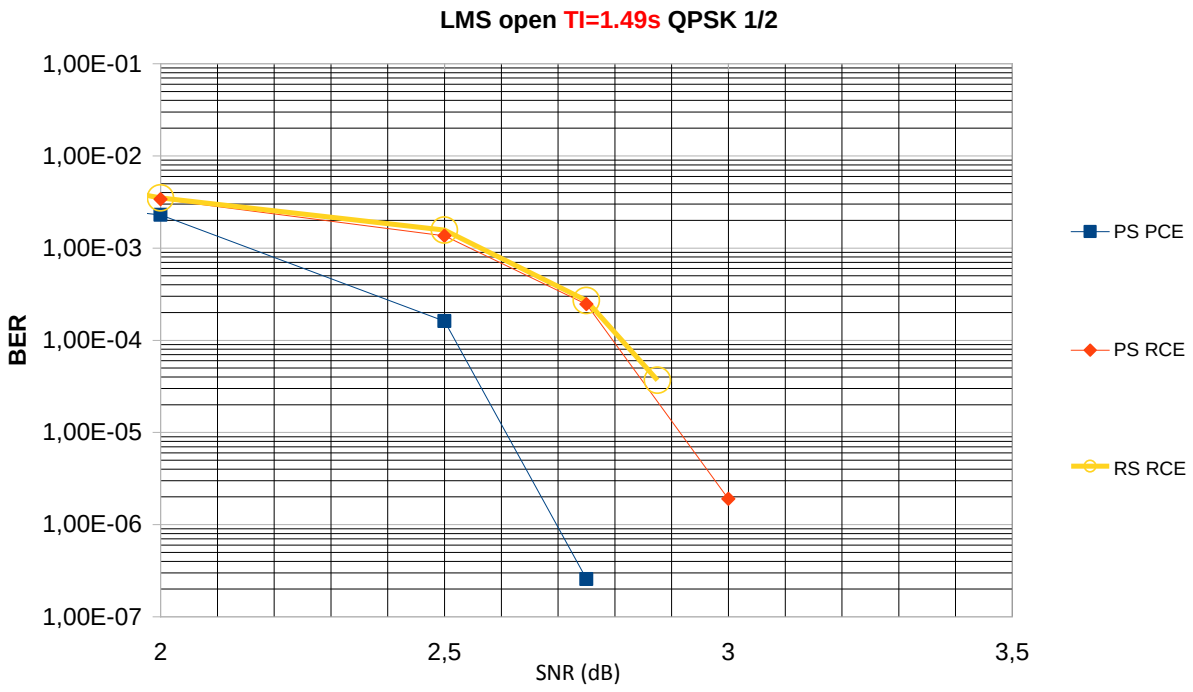

Figure 105: BER on LMS open channel with QPSK 1/2 and TI=1.49s.

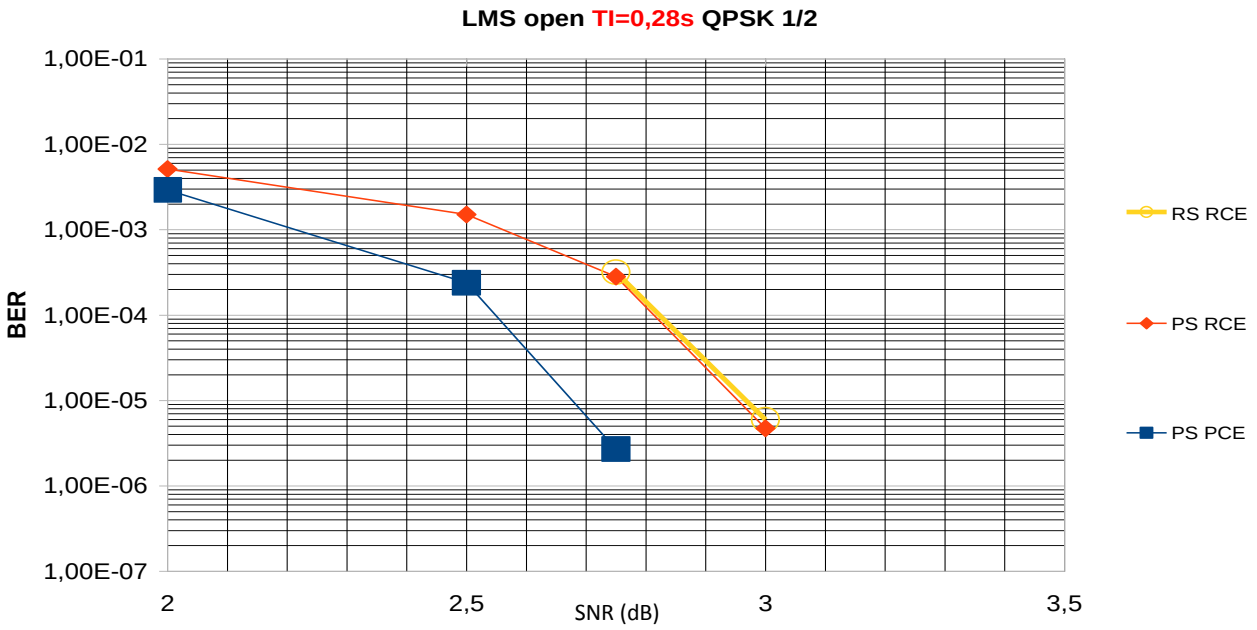

Figure 106: BER on LMS open channel with QPSK 1/2 and TI=0.28 s.

2.3.5.8.2.5 RICE channel with K=5 at 60 km/h

The AWGN, LMS open and TU6 channels do not contain deep fading. The attenuations that are encountered do not decrease the SNR to the values at which the synchronization algorithms fails. Consequently no performance losses have been observed on these channels when the P1 detection threshold is chosen correctly.

However for the RICE channel with *K*=5 and the LMS ITS channel at 60km/h, deep attenuations are observed. Those fading make the SNR drop below the admissible SNR required by the synchronization algorithms and in some cases some P1 symbols may not be detected.

If a P1 symbol is not detected, the LLRs are set to zero, and if the time interleaving is too short losses will be observed. The performances will also decrease when too many P1 are not detected.

Figure 107 below shows that the losses can reach 1.5dB with a QPSK 1/3 and an interleaving time of 1.49 seconds.

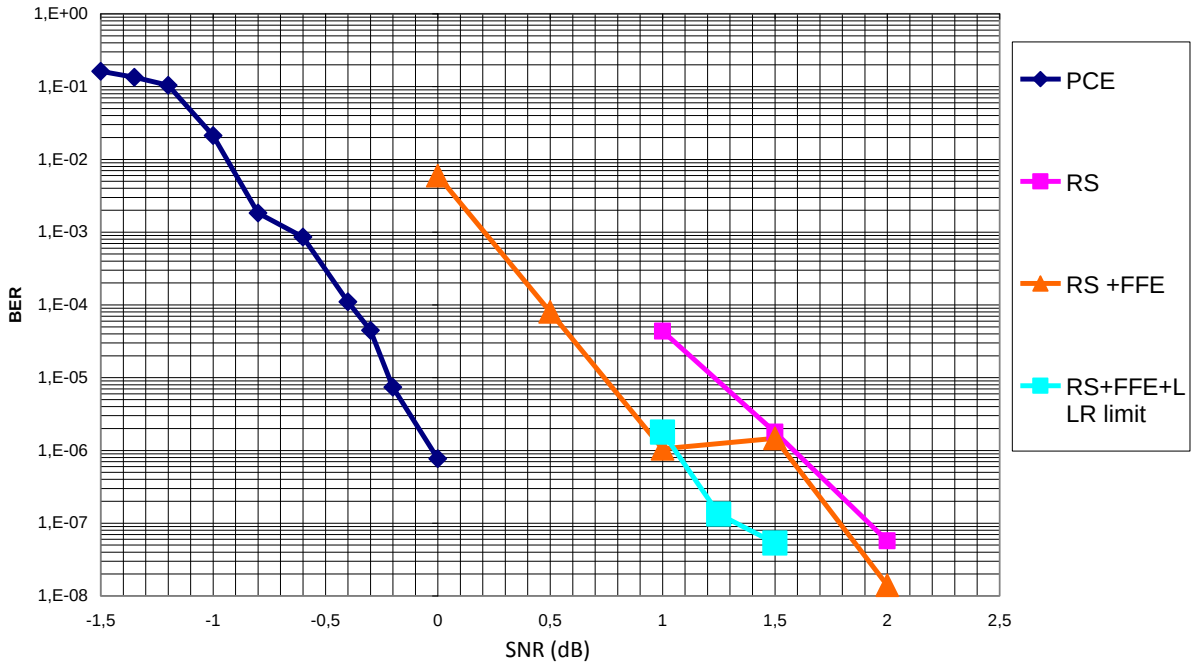

Figure 107: BER on RICE channel with K=5 for a QPSL 1/3 and 3 methods of synchronization.

Figure 107 shows the results for 3 synchronization methods:

- Blue curve: the reference curve with perfect synchronization and channel estimation.
- Magenta curve: the standard P1 detection using an adaptable threshold (Kn = 5 and Ks = 55). The loss is about 1.5dB.
- Orange curve: the fine frequency correction is activated; it allows improving the BER for low SNRs.
- Light blue curve: the fine frequency correction is activated and the LLRs limitation as well. It improves the BER for high SNRs.

The simulations are made with 10^9 bits of data corresponding to 10.000 P1 and 191.132 code words, representing 271 packets of 1.49 seconds.

The errors occur in packets when there are too many non-detected P1 symbol over 1.49 seconds (about 40 P1). In this case, the decoder is not able to correct the missing data.

For 10^9 simulated bits with a BER= 10^{-5} with synchronization, only 1, 2 or 3 packets of errors are observed: it is too small to obtain a good statistics and performance curves are to be taken carefully.

The phenomenon described in Section 2.3.5.7 is observed for the FFE only: in certain cases, even at high SNRs the BER curve increases due to detected P1 with a high residual error frequency. In these simulations, the LLRs are not set to zero and the decoder cannot correct the errors on data.

2.3.5.8.2.6 LMS ITS channel at 60 km/h

Like for the RICE channel, the LMS ITS channel shows strong fading that may cause non detections of P1 symbols. For example a fading of 1second will impact about 40 P1 symbols. The modulation is QPSK 1/3

and interleaving time is 1.49 second. For each point 10^9 bits were transmitted. Curves shown on Figure 108 are obtained using a P1 detection threshold depending on SNR (method 1) with:

- Kn = 5 and Ks = 55
- Kn = 15 and Ks = 55

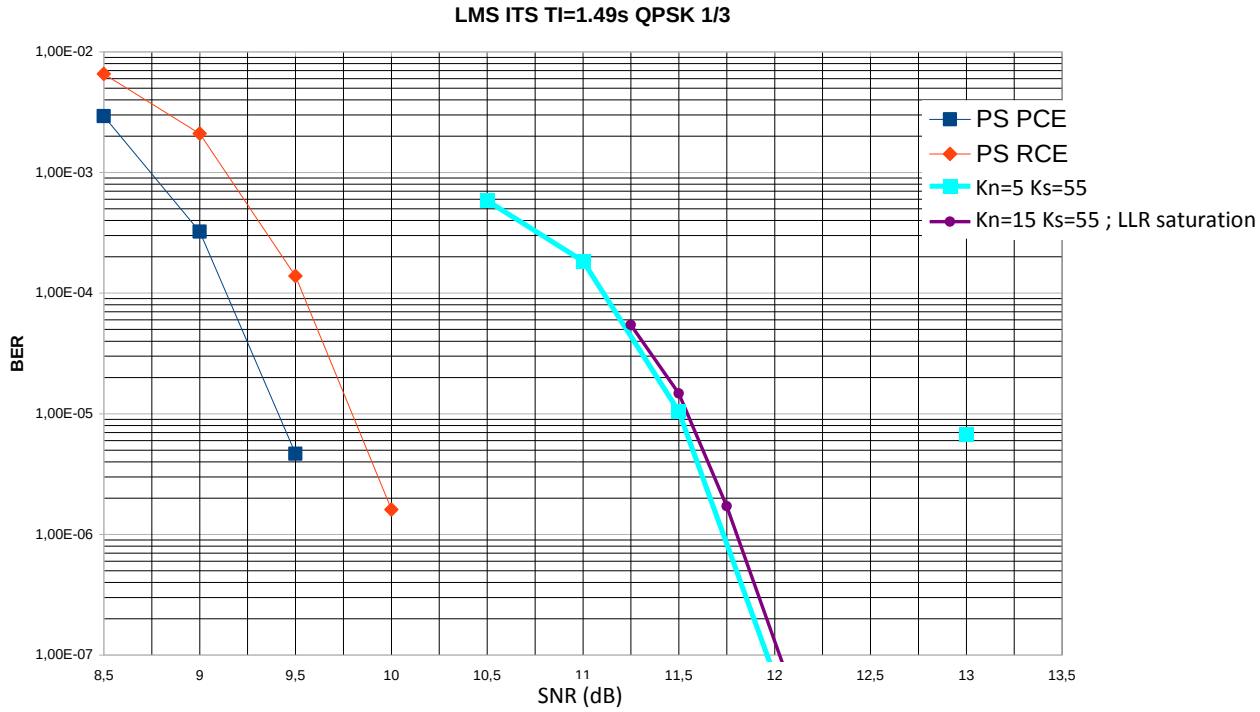

Figure 108: BER on LMS ITS channel.

The curves represent:

- In blue, the reference curve with perfect channel estimation and perfect synchronization
- In red, real channel estimation and perfect synchronization
- In light blue, basic synchronization
- In purple, synchronization with LLRs saturation activated

For the basic synchronization (RS RCE), there is an error appearing at SNR=13dB whereas it was error free at SNR= 12.5dB. This is due to a P1 detected during a fading for which the frequency estimation was wrong, as described if chapter 2.3.5.7. By activating the LLRs limitation, this phenomenon disappears.

2.3.5.8.3 Conclusion

As presented in the first sections, the synchronization algorithms are quite robust for SNR values higher than -3dB. For the propagation channels for which no deep fading are observed, the synchronization algorithms do not degrade the BER, as the synchronization algorithms work correctly at the considered SNR values. For AWGN, TU6 and LMS OPEN cases, the degradation brought by synchronization compared to the perfect synchronization case (with real channel estimation) is about 0.1dB.

However over the RICE channel with K=5 and the LMS ITS channel both showing deep fading, several consecutive P1 symbols may not be detected causing packet errors. In the presented simulations the

interleaving time was chosen to be short (less than 1.5 seconds) and in this condition, the wrong P1 detections cause BER degradations. The losses for these channels spread from 1 to 2 dB. Taking into account that the DVB-NGH traffic is made of bursts (by opposition to continuous transmission in DVB-SH), these amount of losses appear quite reasonable in comparison to erasure channels.

3 COGNITIVE RADIO

'White Space' is a label indicating a part of the spectrum, which is available for a radio communication application (service, system) at a given time in a given geographical area on a non-interfering basis with regard to other services with a higher priority.

Cognitive radio system (CRS) is defined as a radio system employing technology that allows the system to obtain knowledge of its operational and geographical environment, established policies and its internal state and to dynamically and autonomously adjust its operational parameters and protocols according to its obtained knowledge in order to achieve predefined objectives and to learn from the results obtained.

White space devices or CRS use sensing and/or geo-database [and/or beacon] in order to use White Space spectrum.

The foreseeing applications of CRS are many. One possibility is allow users the ease of installation and configuration of at home devices. The use of white spaces may enable access to high quality video services as well as sharing/navigation of content stored locally within the home or office. Another important category of device may be as an access point or base station, providing a gateway to the Internet.

Three techniques have been proposed to assist the white space devices in finding unoccupied channels.

With spectrum sensing, devices try to detect the presence of protected services in each of the potentially available channels. Spectrum sensing essentially involves conducting a measurement within a candidate channel, to determine whether any protected service is present. When a channel is determined to be vacant, sensing is typically applied to adjacent channels to determine what constraints there might be on transmission power, if any. Some channels may be excluded, because the occupying service is not amenable to protection by sensing.

In the Geo-location approach, cognitive devices measure their location and make use of a "geo-location" database to determine which channels they can use at their current location. They are unable to transmit until they have successfully determined from the database which channels, if any, are available in their location. In this case parameters such as location accuracy and frequency of database enquiry are important.

Finally the Beacons method uses signals which can be used to indicate that particular channels are in use by protected services. The use of beacons can ease the performance requirements on devices that use spectrum sensing, by increasing the likelihood of detection at higher threshold values. The interference protection provided to licensed users comes at a cost in spectrum capacity as well as the cost of purchasing and operating the beacons.

3.1 Requirements

3.1.1 Estimation of whites spaces

White spaces are available for a radiocommunication application (service, system) at a given time in a given geographical area with regard to other services with a higher priority on a national basis. On the second part of the project it is aimed to perform an estimation of white spaces. As we will see further in detail in next chapters a geolocalization database allows the receiver to detect wheter to transmit or not. One main objective of this project is to construct one or several geolocalization databases. This will allow us to analyse further in detail de actual spectrum. The database may have information related to position, threshold to transmit etc...

3.1.2 Emission Protection

Many ways to protect signal are available but the most important thing to determine in all of them is the electric field.

The electric field strength available may not be a fixed value. The maximum allowable interfering field strength and received power are calculated according to some complex equations. The estimation of the amount of spectrum available as white space depends on several factors, as the White Space Device (WSD) characteristics, the topology of the area, the national rules governing the use of channels adjacent to those used by DTT, and many others. As some of these factors still have to be defined by national or international regulators, a possible approach to estimate the amount of white space is to make several assumptions whenever needed.

Estimation of the amount of spectrum potentially available for WSD depends on rather a geolocation database and/or sensing approach is adopted.

3.2 Description of Technologies

The main ideas under each of the following techniques are presented. In any case much further studies must be carried on, on let´s say real life or real world to have a more realistic approach.

3.2.1 Sensing

This approach is based on listening for the signals from primary and other licensed services in the band before transmitting. The reliability of the spectrum sensing technique is defined by the detection threshold set in the cognitive radio device. The detection threshold of electric field strength available for transmitting is then the key point. This method allows for dynamics protection against interference. The device must be sensing in a continuously way while in other methods may not be necessary.

Key parameters for spectrum sensing include:

- The sensing threshold
- Periodicity of re-sensing on channels that have been detected as vacant
- Sampling duration

The sensing techniques used so far are LBT and DAA.

Sensing methods can be in general divided to two categories: energy detection and feature detection. The energy detection is to detect the signal power in the channel under study. The detector can be either wide band matching the channel bandwidth or narrow band with a possibility to slide it across the channel. Advantage of an energy detector is that it is independent of the radio system to be detected and as such future proof and capable of adapting to any new system introduced into the band. Disadvantage is low sensitivity due to the noise floor and possibility to false alarms. An energy detector alone is not a feasible solution, but can perhaps be used as one element in the detection process.

Feature detector is trying to use certain known characteristics of the signal that is to be detected. This may be some specific pilot carrier signal, preamble, continual or scattered pilots in OFDM signal, certain periodicity (GI) or sequence in the signal or in it’s spectrum. Using these features will result in a processing gain, which will enable detection below the noise floor in the usual sense. Drawback in the feature detector is that it is dependent on the specific features and may have difficulties to adapt to any new radio system introduced later in the band. To some extent this may be solved by designing some flexibility to the detector.

3.2.2 Geolocation

This approach is based on a database in order to determine which the conditions are for the WSD. The database must provide enough information for the device in order to start transmit. The threshold of electric field strength for transmission must be one of this information. The important or key points are that the receiver must know its location in a quite precisely and quickly way and secondly how accurate is the database. The database must be done in advanced by multiple measurement but must be also upgrade frequently with new subscribers.

They different method but one is the Ask-Before-Talk frequency scheme (WSD connects to database) the device can conveniently register their locations in the database. The question of how frequently the database should be updated, and how often WSD should query it is of great interest to study.

3.2.3 Beacon

Beacons method uses signals to indicate that particular channels are in use by protected services. The use of beacons can ease the performance requirements on devices that use spectrum sensing, by increasing the likelihood of detection at higher threshold values. The interference protection provided to licensed users comes at a cost in spectrum capacity as well as the cost of purchasing and operating the beacons. There are different Beacon setups possible.

Enable beacon: If the beacon is detected, channel can be used. With enabling beacons, a network of beacon transmitters covering an entire country or region in which WSD are allowed to operate would be required. The devices would only function when they received authorization from one of these beacons. Each device would need to be fitted with a beacon receiver, and fine-grain control over individual devices would not be possible without a back-end database.

Disable beacon: If the beacon is detected; TV channel is occupied. The concept was based on enhancing detection of wireless microphones through the operation of low powered beacons to provide a "bubble of protection" in locations where PMSE equipment is in use.

Beacon as pilot channel: identifies locally used TV channels, i.e. local database. A single beacon operating in a locally unused TV channel where this beacon would carry a list of channels in use by all PMSE systems at that location.

Distributed geolocation database:

A transmitter network is used to distribute the information given in a database to regional transmitting 'databases'.

3.2.4 Combined

The combination of different techniques like sensing and geo location database techniques may allow a cross checks of the information obtained by sensing techniques with a database and vice versa.

In the first case the distance from the DTT station and form the broadcasting coverage may be determined accurately and thus reduce

In the second case, sensing technique will complete the information of the users of the spectrum with the unlicensed users and thus protect the transmission.

3.3 Sensing studies

The following chapters are describing an experimental implementation of a sensing device in a mobile computer.

3.3.1 Spectrum sensor embedded to a mobile device

In order to conduct field tests using a device with realistic form factor a spectrum sensor was embedded into a Nokia N900 mobile computer with all functionalities. The choice caused some extra challenges since the N900 has not been designed for a mobile TV receiver. Spectrum sensor hardware has been designed on a separate printed circuit board (PCB) and it has been equipped with hardware which enables to receive desired frequency bands and realize all spectrum sensor functionality, see Figure 109. Figure 110 shows the two complete signal paths that have been implemented on the PCB from an antenna element to a FPGA. Two separate RF frontend chips were required: one for UHF frequencies and one for IEEE802.11a/b/g (2.4/5.8 GHz). The used RF receivers are commercial RFIC and they are controlled by the FPGA. The analogue baseband data is digitized for the FPGA using two dual 10 bit AD converters operating at maximum rate of 80 MHz, depending on the system under detection. Feature detector algorithms for spectrum sensing have been implemented on the FPGA.

Figure 109. The spectrum sensor detector board inside N900 mobile phone.

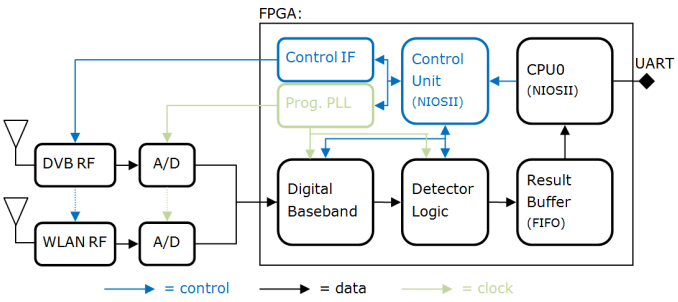

Figure 110. Blocks on the detector board.

Communication between sensor board and the mobile device is done using a universal asynchronous receiver/transmitter (UART). The data rate between the sensor board and mobile device is 1 Mbit/s.

The spectrum sensor board is located inside the display slider case of the device. A custom plastic riser, see Figure 111 was required between the display and the bottom of the case to allow sufficient space for the board. Sensor board is located just behind of the display and on top of the slider mechanic. The slider mechanic is made of metal, as is the background of the display element. To ensure sufficient antenna efficiency both antennas had to be placed to the fin of the plastic riser that is outside the metal frame. It should however be noted that this is only due to the fact that the device has not been designed for spectrum sensor use.

Antenna design, especially at UHF band, is the utmost challenge in a spectrum sensor design. Best efficiency can be achieved with external antennas but for consumer devices embedded antennas have become de facto solutions. Relative bandwidths of the both antennas, UHF and WLAN, are reasonably high. Size and the location of the antennas inside the mobile device limit their efficiency and matching as well as the surrounding mechanics. Sizes of the antennas has been tried to keep as small as possible without losing performance too much. Antenna miniaturization in a mobile device scale is more problematic for an UHF antenna due to its longer electrical (and physical) length compared to a WLAN antenna.

Figure 111. Spectrum sensor prototype implementation on N900 mobile phone.

3.3.2 System requirements related to spectrum sensing

Two very different kinds of target systems were addressed: DVB-T as an example of rather static TV primary system and 802.11a/g as an example of system having very dynamic traffic characteristics. Goal was to implement sensing strategy to measure both temporal and spectral characteristics of target systems. Another aspect was to measure spatial channel utilization in the field. We ended up in this phase to traditional channel numbering instead of generalized notation for cognitive radios in order to simplify control.

TV primary sensing requirement by FCC is -114 dBm sensitivity level averaged over a 6 MHz channel. This corresponds to -112.7 dBm averaged over a 8 MHz DVB-T channel. In order to measure UHF channel utilization, selected strategy is to make single detection per channel at each studied location. This requires quite low false alarm rate e.g. 1% and high probability of detection e.g. 99%. Excluding antenna losses, the sensor prototype presented in this work could reach these requirements with a sensing time of approximately 115 ms. However, for the longest detection time, i.e. 460ms, the headroom for antenna losses is only about 5dB.

In order to understand practical limitations of the platform and analyze filed test properly the prototype and its core entities were characterized both separately and as a complete system.

3.3.3 Antenna

Two antennas were implemented inside the presented mobile spectrum sensing device. For UHF frequencies a commercial antenna based on planar technology has been used. Dimensions of the antenna are 45 mm x 5

mm and it has been designed to work at frequency range from 470 to 750 MHz (DVB-H EU). Antenna for 802.11a/b/g has been realized as a wideband structure which covers frequency range from 2 to 6 GHz. It has been implemented directly to the same PCB than the spectrum sensor. It requires slightly more area than the UHF antenna (32 mm x 8 mm).

Both antennas were measured with and without the device mechanics to understand differences compared to conventional stand-alone antenna testing, and to evaluate actual performance in the field. Measurement results for the UHF antenna are presented in Figure 112 (left) and wideband antenna in Figure 112 (right). Deterioration of the efficiency of the UHF antenna due to mechanics is significant (6-8 dB) at low frequencies. The wideband antenna behaves better and its efficiency deterioration due to mechanics is only 1-2 dB over the whole band. The efficiencies of the antennas are -18-(-7)/-3/-6-(-4) dBs at UHF/2.4/5 GHz bands, respectively, depending on the specific channel. The results clearly indicate the issue of antenna performance at UHF band in small devices.

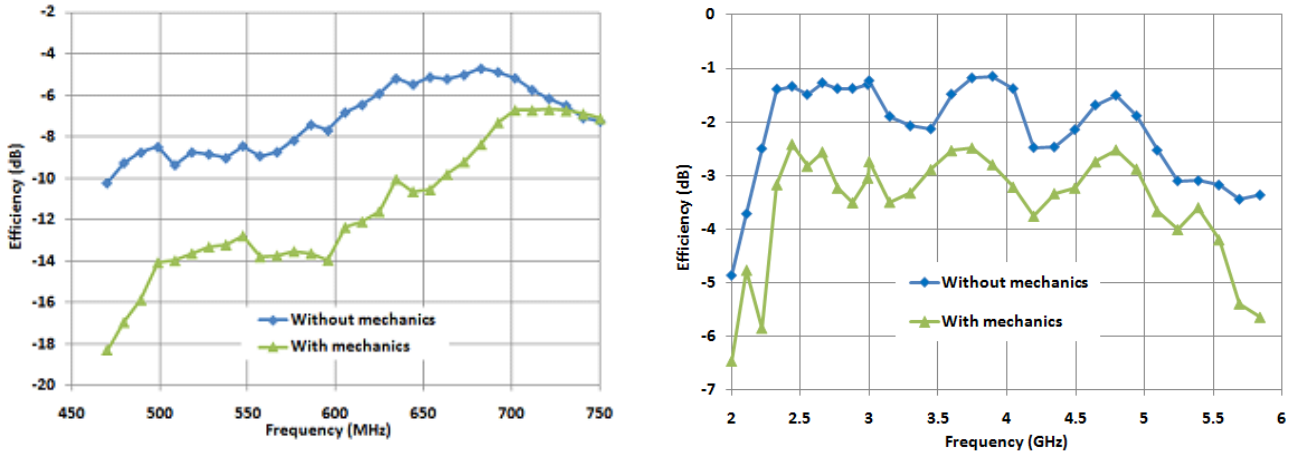

Figure 112. Efficiency of the UHF antenna (left) and for comparison the WLAN-antenna (right).

3.3.4 RF-parts

The used RF receivers are commercial RFIC and they are based on a direct-conversion architecture. Baseband filters are adjustable and they support several bandwidths used in different standards. Block diagrams of the receivers are presented in Figure 113. Typical noise figure (NF) of all receivers without front-end filter is around 4 dB depending on the band. Typical insertion-losses of front-end filter are 1.8 dB at UHF/2.4 GHz bands and 1.4 dB at 5 GHz band.

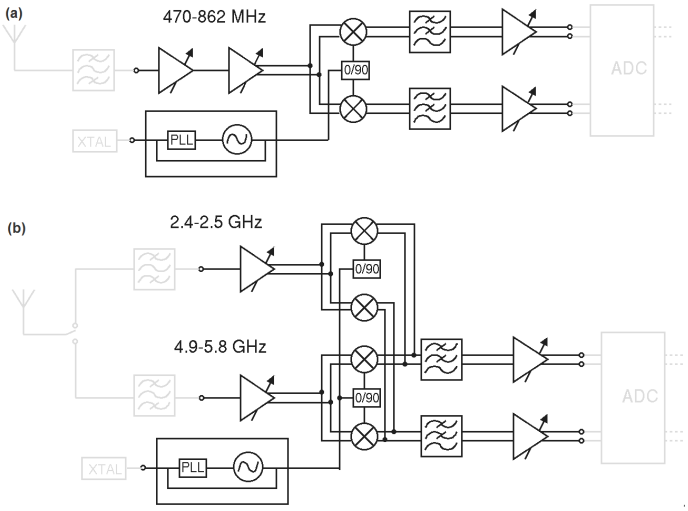

Figure 113. Block diagram of the UHF (a) and 802.11 a/b/g (b) receiver.

3.3.5 Detector

Detector core on the FPGA is developed from the FFT-based cyclostationary feature. The structure of the detector is shown in Figure 114. The fixed-size-FFT implementation utilizes decimation after autocorrelation to control the detection time. Test for the presence of cyclostationary at given cyclic frequency (α) is performed from the FFT of the decimated autocorrelation signal.

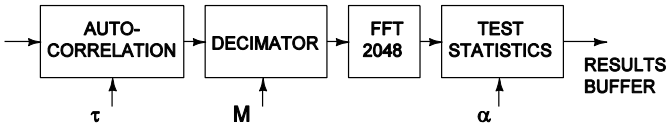

Figure 114. Structure of the implemented cyclostationary feature detector.

In this implementation, the range of selectable decimation ratios is extended up to M=2048 to support longer detection times. Similarly, the maximum autocorrelation delay (τmax) is increased to 8192. The modifications were required to enable detection of very long OFDM symbols used in DVB-T signals. The detector implementation utilizes 16k logic elements, 406k memory bits and 84 9-bit multiplier elements. The figures are 10.2%, 13.7% and 14.6% of all available resources on the FPGA, accordingly.

Detector sensitivity was measured for a WLAN signal at 2.4 GHz ISM band and for a DVB-T signal at the UHF band. Parameters related to modulation, signal bandwidth and transmit frequency of both systems are summarized in Table 37. During the measurements, the antennas were bypassed and the signal generator was connected directly to the RF receiver inputs, therefore the results exclude any antenna effects. The RF receivers operate at maximum gain. Detection times for WLAN and DVB-T were set to 0.8 ms and 460ms, accordingly. False alarm rate is 5%.

Table 37. Specifications of the primary signals used in detector performance measurements.

	WLAN	**DVB-T**
Modulation:	OFDM	OFDM
FFT-size (N_{FFT})	64	8192
Length of cyclic prefix (N_{CP})	16	1024
No. of non-zero subcarriers	52	6817
Subcarrier modulation	16-QAM	16-QAM
Transmit frequency	2437 MHz	670 MHz
Bandwidth	20 MHz	8 MHz

The measured sensitivities are presented in Figure 115 (left) for DVB-T and in Figure 115 (right) for WLAN signal. DVB-T detection reaches 95% probability of detection when the received power is about -117 dBm, while for the WLAN detection received power of -102 dBm is required. Both figures are below the thermal noise floor. Figure 115also show ideal simulation results for the same signals. The differences between simulated and measured probability of detections almost entirely match and are accounted by the non-zero noise figures of the RF receivers. The primary reason that DVB-T detection outperforms WLAN detection by such a large margin is the longer detection time that can be utilized in DVB-T detection. WLAN detection time is limited on the other hand by implementation, where larger FFT would be required to keep the cyclic frequency under the Nyquist frequency for larger decimation ratios, and on the other hand by duration of WLAN signal bursts which is already on the same scale with the detection time.

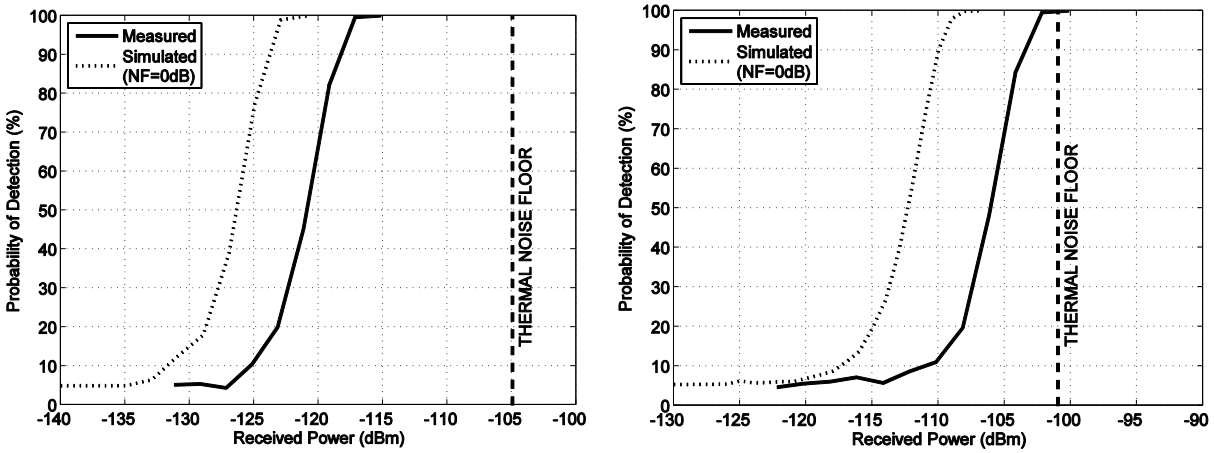

Figure 115. Measured DVB-T (left) and WLAN (right) probability of detection compared to simulated performance. Simulation utilizes ideal receiver (NF=0dB).

3.3.6 Platform Performance

Overall performance for the spectrum sensor hardware has been determined in the laboratory measurements. A 5 dB NF for UHF receiver path was measured at 660 MHz and it is only 1 dB more than NF of the pure UHF receiver. For dual-band 802.11a/b/g receiver, 5 dB and 6.5 dB NF at 2.427 and 5.130 GHz were measured, respectively. IIP3 of –10 dBm, -1 dBm and -1 dBm were measured for UHF, 2.4 and 5 GHz bands, respectively.

When combined with antenna results the overall sensitivity of the signal detection for DVB-T signals at UHF band will be from –100 to –108 dBm depending on the channel of interest. This is significantly higher than FCC requirements but shows feasible values for small devices if the integration time of the detection is kept reasonable. IIP3 of the UHF receiver with antenna corresponds 8 - (-3) dBm compared to 0 dB antenna in the field tests, At some channels platform noise caused by processors and other noisy components in the device will further deteriorate the performance. However, those could be mostly avoided with proper design when UHF band requirements will be taken into account initially in the design of the device and its mechanics. For WLAN OFDM signal detection, the sensitivities using parameters given earlier in this paper will be –101 and –98 dBm (2.4 /5 GHz) including the antenna.

3.3.7 Measurements

Two sets of field tests were carried out in capital area in Finland using the device described above. First measurement set was done mostly outdoors in urban Ruoholahti area in Helsinki. Two sensors were used, both using internal antennas. The measurement set consists of spectral samples from 37 different locations, shown in Figure 116. One spectral sample includes detection time, GPS location, band, channel, received signal strength in dBm and DVB-T detection statistics from UHF channels 34 to 60 (578 – 784 MHz). Detection time was set to 460 ms and detection statistics positive detection threshold to produce constant false alarm rate of 1%. Measured signal strengths are shown in Figure 117. Corresponding estimated probabilities of DVB-T detections on different channels are shown in Figure 118. There is DVB-H repeater in the area, detected on channel 35. Espoo TV transmitter station is transmitting on channels 32, 35, 44, 46, and 53.

Table 38. DVB-T transmitter parameters.

DVB-T transmitters	Espoo	Tallinn
Latitude:	60.1778	59.4713

Lognitude:	24.6403	24.8875
Mast heigth:	313 m	272 m
Transmission power:	47 dBm	42 dBm
Occupied channels	32, 35, 44, 46, 53	45, 59, 64

TV transmissions on measurement range are detected with high probability. Channel 59 is occupied by Tallinn TV transmitter on average 78 km away. Open source Splat! radio propagation calculation tool, using Longley-Rice Irregular Terrain Model and NASA SRTM-3 Version 2 Elevation Models, was used for field strength estimation. Used transmitter parameters are shown in Table 38. , receiver was assumed to be 3m above sea surface. Estimated field strength, shown in Figure 119. in Ruoholahti area is 20-60 dBµV/m. Field strength has large variation within 1 km radius in urban area. With measured prototype antenna efficiency of -7.5 dB, it corresponds -123 – (-83) dBm signal input power at the receiver. Taking measured detector sensitivity into account we end up 0.6 to 1 detection probability of Tallinn TV transmitter in Ruoholahti, Helsinki. Tallinn transmission on channel 45, adjacent to much stronger Espoo TV transmitter on channel 44 and 46, is masked and it cannot be detected. One must remember that transmissions from Tallinn are out of the reach for typical TV reception setups in Helsinki households.

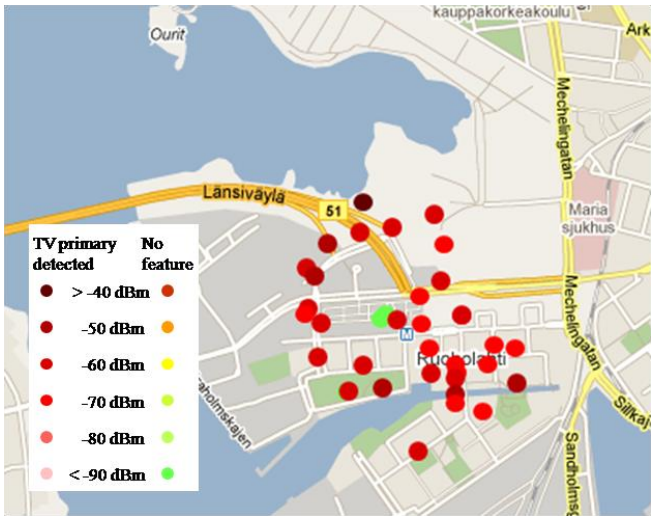

Figure 116. Measurements results on UHF channel 44 (658 MHz) in Ruoholahti, Helsinki.

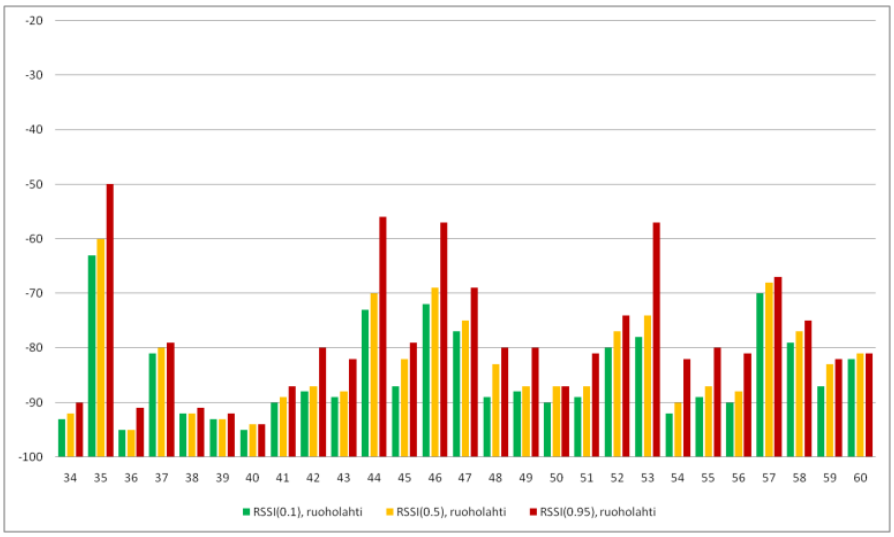

Figure 117. Received signal strength (RSSI[dBm]) upper limit for 10%, 50% and 95% of measured samples in Ruoholahti.

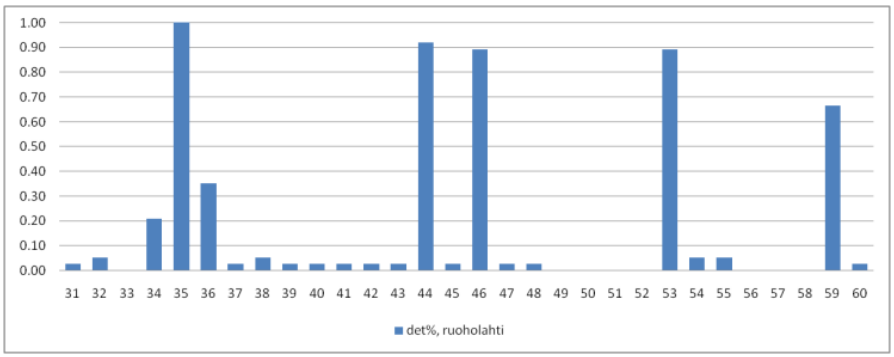

Figure 118. Measured probability of DVB-T detection, n = 37 per UHF channel, average distance to Espoo transmitter 15 km and 78 km to Tallinn transmitter.

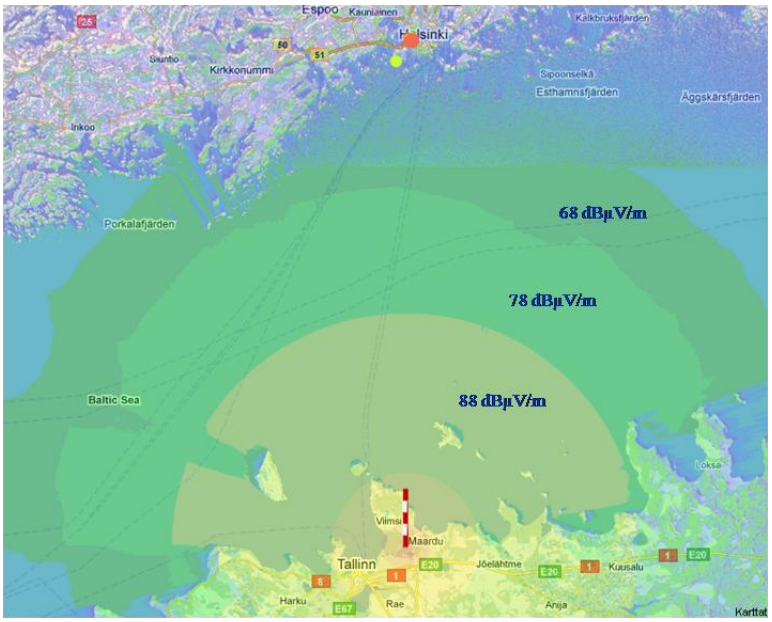

Figure 119. Simulated field strengths on UHF channel 59 (778 MHz) from Tallinn TV tower, distance to Helsinki 77 km.

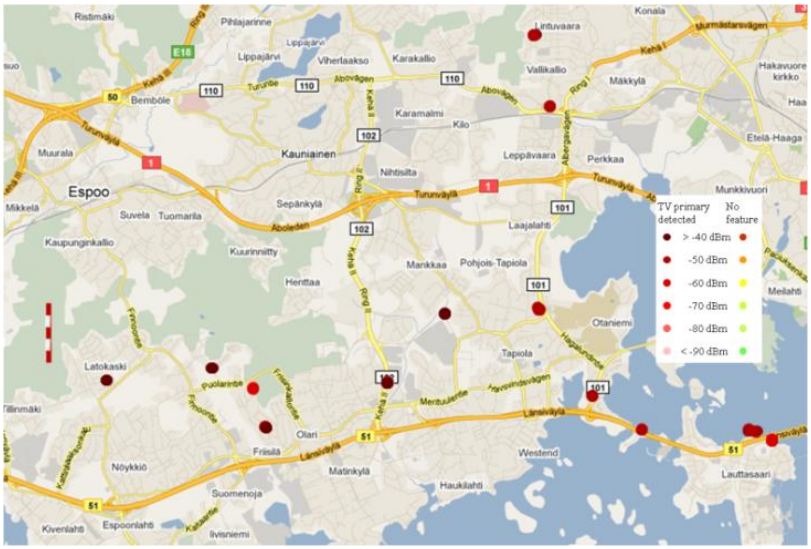

Figure 120. Results on UHF channel 44 (658 MHz) in Espoo, average distance to Espoo TV tower is 8 km.

Second set was measured outdoors in suburban Espoo and target was to evaluate performance of the spectrum sensor in the vicinity of strong TV transmitter. Measurements were done using two sensors one with internal antenna and another with external reference dipole. Measurement locations and results for occupied channel 44 (658 MHz) are shown in Figure 120. Measured signal power on occupied channels was from -65 dBm up to -32 dBm, when using external reference dipole, as shown in Figure 121. The RSSI[dBm] limits tell how many percent of measurement samples have smaller RSSI value than presented. Basically this presents values of observed cumulative distribution function with 10%, 50% and 95% probabilities. TV signal strength is from 10 to 30 dB more than in the Helsinki measurement set. Main difference between results measured using internal and external antennas is that antenna efficiency of internal antenna is on average 7.5 dB lower than external reference dipole. Results using internal antenna are shown in Figure 122. Difference in antenna efficiency means additional noise figure of 7.5 dB, which decreases sensitivity and increases linearity of receiver. In addition there is also device induced noise in internal antenna measurements.

Figure 123 shows the detection results over all channels with external and internal antennas. The antenna performance difference is very clear. Overall it can be seen that a high number of false detections happen due to the IM-products. There is also clear tradeoff between sensitivity and linearity. This is evident with the lower false alarm rate of the internal (lower gain, less signal power) antenna.

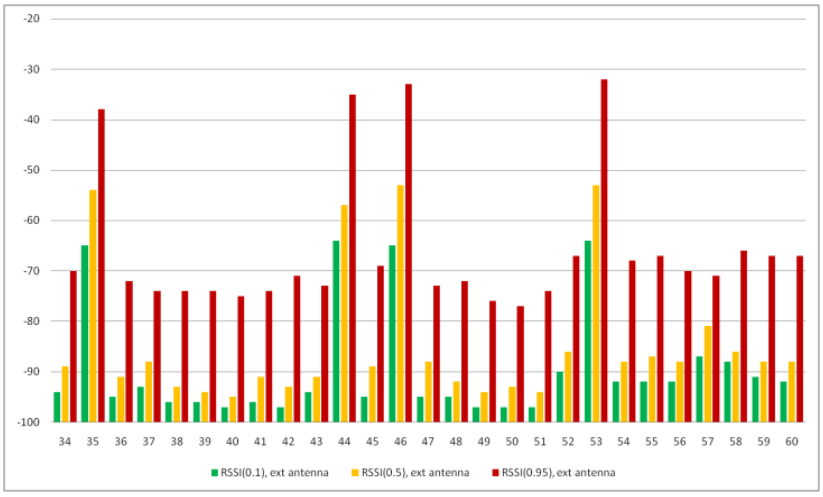

Figure 121. Received signal strength (RSSI[dBm]) with external antenna, upper limit for 10%, 50% and 95% of measured samples in Espoo.

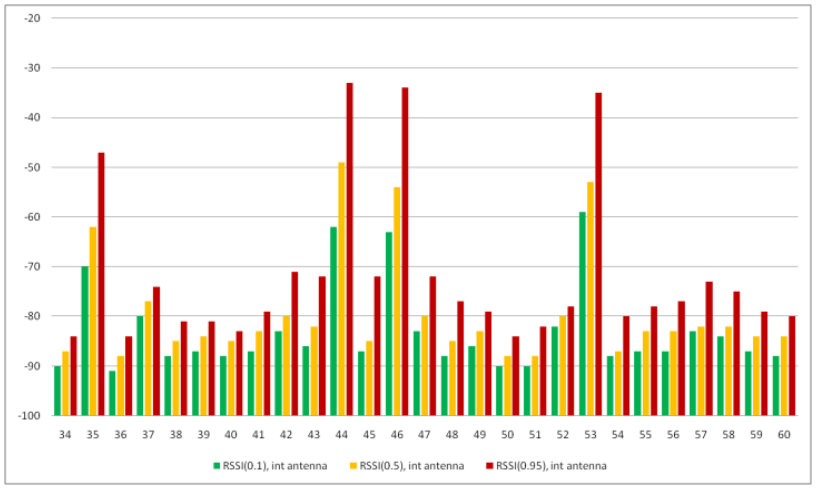

Figure 122. Received signal strength (RSSI[dBm]) with internal antenna, upper limit for 10%, 50% and 95% of measured samples in Espoo.

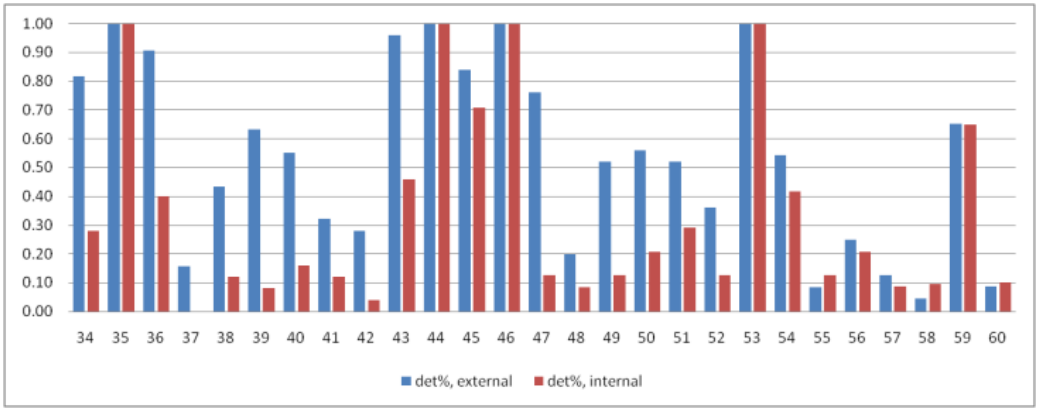

Figure 123. Measured probability of DVB detection, number of detections is 26 per channel, average distance to Espoo transmitter 9km and 78 km to Tallinn transmitter.

3.3.8 Conclusions

A practical spectrum sensor has been implemented in a mobile device. Key performance tradeoffs have been shown in the laboratory tests and functionality proven in the field with TV-signals. The key challenge is antenna integration and the strictest sensing requirements cannot be met using a single device and especially single shot decisions. However by collecting more samples, position information and combining the results from several devices better results could be expected.

Single device single snapshot detection is too unreliable due antenna gain minima, interference, and fading to protect primary users. Just tightening of sensitivity requirement does not help, because IM-products cause desensitization, masking, and false alarms, thus reducing available capacity for secondary users. Methods like geo location databases have to be used for reliable operation. Collaborative sensing averages antenna gain and radio propagation problem. However presented trade-offs between sensitivity in sensor linearity requirement and sensitivity has to be taken into account in algorithm development.

3.4 Spectrum Occupancy and Hidden Node Margins for Cognitive Radio Applications in the UHF Band

The feasibility of the idea of "cognitive radio" [53] for the UHF band is strongly dependent on the border conditions of the UHF band occupancy. Also, and not in a less relevant position, the potential propagation channel and attenuation of the signal radiated from cognitive devices are also key parameters to be analyzed before a sensible discussion on the feasibility of the technology is raised. This work aims at providing field measurement data that could serve as a reference for the technical discussions around the possible use of White Spaces in the UHF band. This work does not aim at providing an "a priori" opinion on the use of this spectrum management approach.

In principle, Cognitive Radio proposes that user devices perform a dynamic adaptation of their physical layer to the radio environment on a secondary use of the spectrum basis. The Cognitive Devices (CD) would use information gathering techniques to make intelligent choices for their radio resources: choosing the operating frequency, maximum ERP, modulation parameters etc. These techniques are based on Spectrum Sensing and on geolocation databases that will provide each device a reference of the use of the spectrum in the location where the device is operating. With this technology, unlicensed services could temporally use the white spaces of a certain broadcast service area.

Spectrum Sensing techniques are based on signal detection by different signal processing methods. In any of the techniques a problem called Hidden Node Margin (HNM) is a major issue. The HNM represents the difference of the channel usage estimation by the CD and the actual spectrum picture at the receiving antenna of the primary service (in our case Digital TV). Due to this HNM an occupied channel would be identified as free (White Space) by a CD and a potential interference to the primary (to be protected) service would occur.

Previous work on this topic can be found in [54][55][56][57][58]. A theoretical study from the BBC [59] has proposed a reference value of 40 dB for outdoor HNM (10 m to 1.5 m margin) and an additional 20 dB attenuation for the indoor case. Other studies have obtained values that range from 16.6 dB to 33 dB on channel 22.. Additional work has based the results on the field strength simulated values provided by different algorithms, including results with 3D ray tracing and conventional UHF empirical and semi empirical methods (ITU-R P.1546). In this case, the values range from 4 to 46 dB.

This work tries to provide consistent values from a carefully planned measurement campaign.

This work is organized as follows. Section 2 contains a description of the methodology and scenarios. Section 3 contains a discussion on the channel occupancy decision threshold. Section 4 presents a sample of the results that are expected at the end of the project and a discussion based on the first results. Finally, Section 5 contains the conclusions at this stage of the work.

3.4.1 Methodology and Scenarios

The first step of this survey was to elaborate an environment classification that would allow extrapolation of the measurement results and conclusions to a number of real cases as wide as possible.

Table 39 shows the features of the different scenarios that have been considered for the measurement campaign. The same table contains the first three measurement locations of the trial that have been used as the reference data for this work. A higher number of locations have been already planned for a next phase of the research work.

Outdoor roof and indoor measurements were carried out in the three environments. Indoor measurements were performed in each floor of the building under tests, using a dipole antenna at 1.5 m. above the ground level.

At each location, the man-made-noise was evaluated in two frequencies, 408MHz (radioastronomy frequency) and 520MHz (free frequency) to determinate the channel occupancy decision threshold. After obtaining the reference noise value, 1MHz 100 power measures were taken starting from 470MHz up to 870MHz. A second measurement round was carried out at a selected list of channels using a 100KHz resolution bandwidth in order to obtain more accurate data at frequencies where potential doubts of occupancy could appear.

Table 39: Environment Description

	Urban	Suburban	Rural
Characteristics	Buildings with more than 3 floors Heavy traffic	Low-rice buildings and duplex Little traffic	Isolated houses. Usually surrounded by vegetation or in open areas
Place	Bilbao 43º15’40.46’’N 2º56’54.80’’O	Lezama 43º16’25.15’’N 2º49’46.59’’O	Maruri 43º23’02.78’’N 2º52’19.50’’O

The measurement system consisted of an ESPI test receiver (Rhode and Schwarz) connected to a PC and a set of antennas. A calibrated dipole was used for 1MHz measurements (ETS-LINDGREN 3121-D). A logperiodic antenna was used for taking measurements with a 100 kHz resolution. The system was controlled from a PC where data files were also recorded for further analysis. The Test Receiver was configured with a pre-amplifier for higher sensitivity.

Figure 124: Measurement System. Examples of suburban and urban environments

3.4.2 Decision Threshold

The choice of threshold is an important decision. Its value sets up the condition for channel occupancy decision. If the power measured is above the threshold, the device would decide that the channel is being used. In the same way, if the power is lower than the threshold, the device will decide that the channel is empty.

The election of this parameter has been a difficult choice. Low values lead to noise values higher than the threshold and may mislead the device. On the opposite case, if the threshold is too high, when a signal is extremely low, the device can decide that the channel is empty when it's not, and create interferences.

Based on other researches all the measurements were analyzed with a threshold 3 and 4dB above the power measures. A usual value for this threshold in the literature is 5 dB [56]. It was found that the Radio Noise in rural and suburban environments is below the receiver internal noise (-105 dBm/1MHz, -115 dBm/100kHz). In the case of urban spots, the Radio Noise was 3 dB higher than the equipment threshold.

3.4.3 Measurements

The power values measured along the frequency band from 470MHz to 870MHz were compared with the decision threshold. The results obtained are shown in Table 40, for band occupancy calculation. The figures represent the percentage of occupied channels as detected at each location.

Table 40: Spectrum Occupancy

	Rural	Suburban	Urban
Site	Mean percentage	Mean percentage	Mean percentage
Register	%20.00	%20.00	%20.00
Roof	%27.00	%32.25	%28.25
4rd floor			%21.50
3rd floor			%26.75
2nd floor	%18.00	%17.50	%25.00
1st floor	%20.00	%20.00	%25.00
Street		%22.25	
Basement		%3.00	%7.50

The spectral occupancy decision is higher at the roof of each building than the register. These channels present at the roof but not detected at lower locations are signals coming from transmitters outside the service area of the potential interfered transmitters. In any of the cases the spectral occupancy never exceeded the %32 of the band. If a higher threshold is assumed, 4dB above the measurements, the results are very similar and the percentage is reduced by %1.

The hidden node margin has been calculated as the difference of the signal power measured at the roof and all the floors. To show some results (Table 41) we have chosen the channel 22.

Table 41: Hidden node margin

	Rural	Suburban	Urban
Site	HNM(dB)	HNM(dB)	HNM(dB)
4rd floor			17.53
3rd floor			8.21
2nd floor	17.14	16.30	8.85
1st floor	23.50	15.76	12.35
Street		17.91	
Basement		28.86	38.34

The results obtained agree with the references available in the literature. Some theoretical estimations mention values close to 60 dB if indoor reception is considered [59] and in [54] HNM values were obtained

in real measurements for different scenarios providing a 28.5 dB difference for outdoor measurements in a 90% of the locations. The values range from 18 dB for rural cases to 37 dB for dense urban spots. Considering that the trials of this work are indoor, an average building penetration losses need to be added to our values. In that case, the value obtained in the trial ranges from 8 dB to 38 dB (rural and dense urban cases respectively).

3.4.4 Conclusion

The present work investigated the spectral occupancy of the UHF band allocated for TV broadcasting trough real measurements performed in urban, sub urban and rural scenarios at roof, middle floor and basement. Results have shown that a top occupancy of 32% of the bandwidth is achieved in the roof and that the hidden node margin obtained range from 8 to 38 dB on channel 22 depending on the environment and lead to the conclusion that cognitive communications to be performed in the UHF TV band need the joint use of geolocation databases and spectrum sensing technique to avoid harmful interference to the primaries services of the broadcasters.

3.5 Mobile digital terrestrial television network measurements for studying measurement-based geolocation database update algorithms

It is problematic to determine how a well a given network works. It is essential to have knowledge on the geographical coverage of the network and where the coverage holes lie. There are several methods to solve this problem with the network coverage, but each of them has its drawbacks.

Two most straightforward methods are predictions and measurements. In predictions you use a model to calculate the signal quality in a given point by using the information about the environment and the transmitters. However, the predictions have proven not to be very accurate. With measurements it is problematic to know how many measurements are needed to get a signal level map accurate enough for your needs. And as the measurements are costly to do, there will always be a tradeoff between cost and accuracy.

Interpolation is a method where we calculate the coverage at locations where measurements have not been made by using the data from the places where the measurements have been made. The focus of the measurements conducted in this report is to study different algorithms and methods for interpolation and to find the optimal places to do the measurements.

Thus, our aim is to study how we can do a minimal amount of costly measurements and achieve as accurate signal level map as possible. The main objective for the use of these algorithms is in the geolocation database update algorithms that are to be used in cognitive networks. Cognitive networks are networks that can utilize the available spectrum more intelligently than the current networks. The spectrum has been auctioned to primary users, but is not fully utilized. The free frequencies in the spectrum could be used by the secondary users in cognitive networks. An accurate coverage map needs to be built so that the cognitive devices can have knowledge on what frequencies and power levels they can use in a given geographical location. This information will be given to the device by the geolocation database where it will be calculated with the database update algorithms.

The measurements in Turku DVB-H test network have been performed using two different measurement devices: handheld and bike mounted. First we analyze how well the measured signal strengths correspond to the predicted ones. Then we move on to do further study with the database algorithms and try to find the optimal places where to do the measurements. The first measurements were conducted by measuring unplanned routes around the Turku test network area. We evaluated three different measurement-based geolocation database update algorithms with these measurements and chose the most accurate of them for closer study. In the latter measurements we use more sophisticated methods to pick the measurement points

so that they would give optimal results with the database update algorithms, in particular with the chosen Kriging algorithms.

3.5.1 Turku Test Network

Turku Test Network has two transmitters working in the single-frequency network (SFN; both transmitters in use) mode on channel 38 (610 MHz). The network covers a relatively large geographical area and covers diverse environments including urban, suburban and rural locations. The area and transmitter locations are illustrated in Figure 125.

The Vanha Studio transmitter is located in an urban area in the city center of Turku. The antenna is mounted on a rooftop of an apartment building, which is approximately 40 meters high.

The Pääskyvuori transmitter is mounted on a TV tower in the suburban area and has antenna height of 92 meters. Both antennas use horizontal polarization. The Effective radiated powers (ERP) are 1000 watts for the Vanha Studio transmitter and 250 watts for Pääskyvuori transmitter.

The Test Network is used and maintained by a group of private companies and educational institutes to research and study different Digital Terrestrial Television (DTT) broadcast standards. The test network uses DVB-H standard with the following parameters:

FFT mode: 8k
Guard Interval: 1/8
Bandwidth: 8 MHz
Modulation: QPSK
Code Rate: 2/3

Figure 125: Turku Test Network map.

3.5.1.1 Signal level prediction maps for Turku Test Network

The signal level prediction maps are created by the Finnish national broadcasting company Digita with their proprietary propagation models and are used as a reference comparison values for the conducted field measurements. The prediction maps cover an area of 37,75km*37,75km with a resolution of 55m*55m per pixel. The prediction maps are available for all the possible scenarios in Turku test network: SFN,

Pääskyvuori and Vanha Studio. Figure 126 illustrates the signal level map for the SFN network. The colours indicate the received signal strength (RSSI) in dBm and the x/y-axes the pixel in the map.

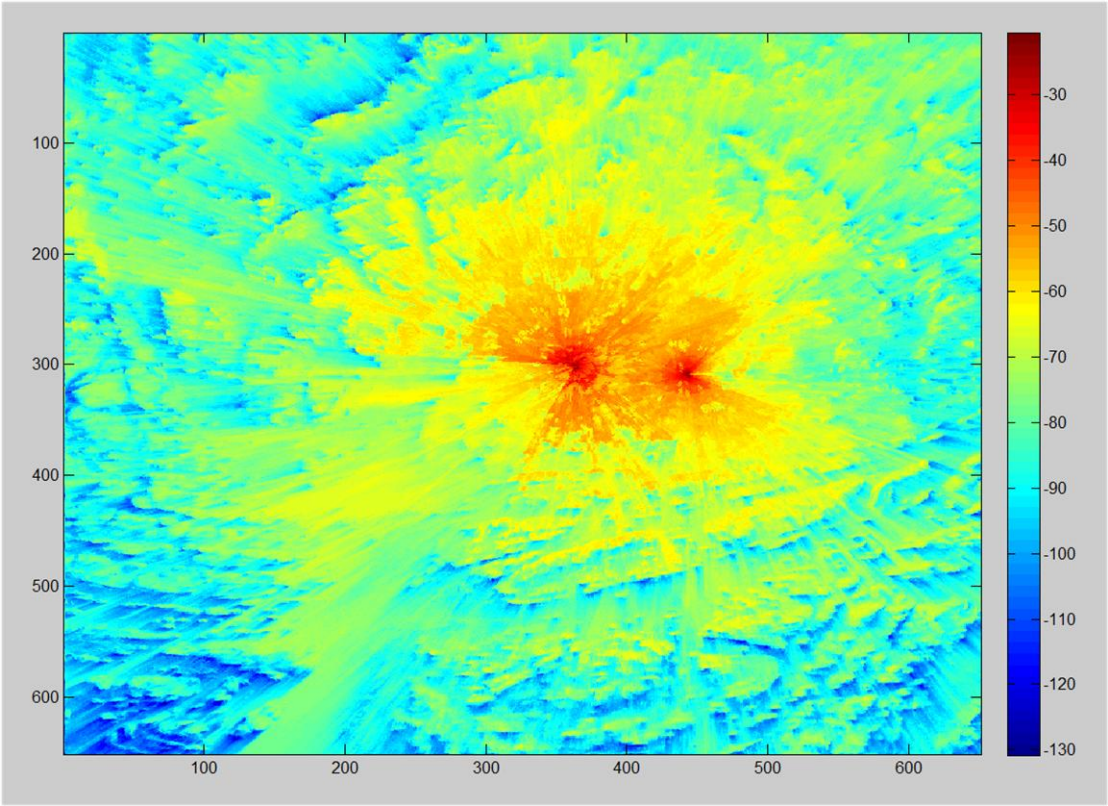

Figure 126: SFN signal level prediction map.

3.5.2 Turku Test Network signal strength Measurements

The test measurements were performed with two different setups: mobile phone measurement device and bike mounted R&S TSM-DVB. Both setups give the results in the same format: location and time information from the GPS and a measured RSSI (Received Signal Strength Indicator) value from the test network on 610 MHz. All of the measurements have been conducted at a height of 1.5m above ground level. The antenna gains have been excluded from the results.

The measurements can be performed in three different scenarios with our two transmitters: SFN or with just Pääskyvuori or Vanha Studio transmitter turned on. Both setups and their respective measurements are presented in this chapter. The bike setup proved to be more accurate than the mobile phone measurement device, so we chose the bike setup to be used for the further study of the geolocation database update algorithms.

3.5.2.1 Nokia N900 mobile measurement device

Spectrum sensor hardware is implemented on a separate printed circuit board (PCB) which is integrated inside the display slider case of the N900 phone, as illustrated in Figure 127. Detector core on the FPGA is developed from the FFT-based cyclostationary feature detector. The device has an internal antenna, but the measurements were performed with an external consumer grade monopole DTT-antenna because the device-induced noise was too high when using the internal antenna.

The properties of the device are presented in more detail in ENGINES task force report TR5.1. Mainly we use only the GPS information and the received signal strength, but also the detection information is stored in to the SQL database running in the mobile device and can be used for further study.

Figure 127: Nokia N900 with the sensing PCB.

3.5.2.2 Conducted measurements with N900

The N900 measurements were conducted in three different scenarios. In the first scenario we used both transmitters in SFN and in the latter two we used Pääskyvuori and Vanha Studio transmitters separately.

3.5.2.2.1 SFN

The SFN measurements were conducted in urban area in the center of the city, suburban areas in eastern Turku and in the city of Kaarina. The measurement routes and transmitters locations are shown in Figure 128.

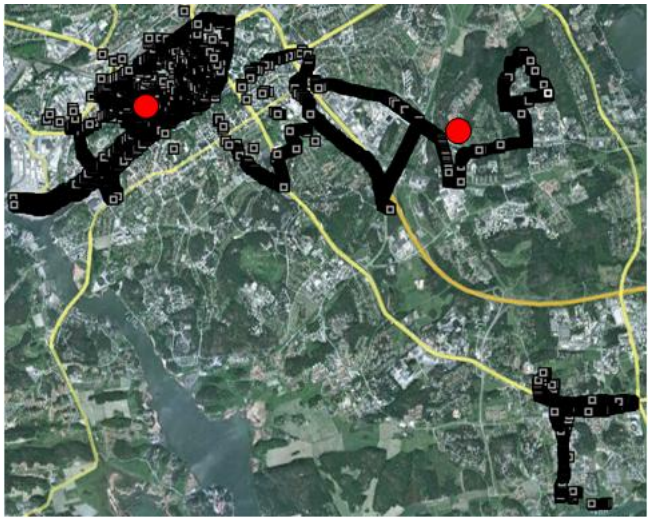

Figure 128: SFN measurement points with N900. The transmitters are marked with red dots.

The average standard deviation was 2.90dB within a 55x55m pixel. Figure 129 represents the difference in RSSI between the measurements and our mathematically produced prediction map. The majority of the samples are in the area between -25 dB to +5 dB - this means that the tendency is that the measured RSSI values are considerably lower than those given by the prediction.

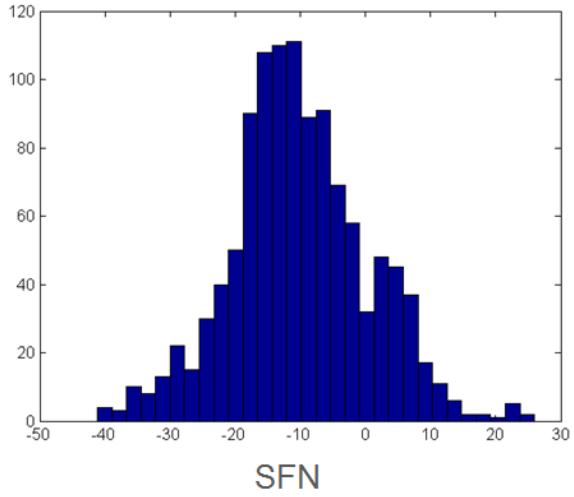

Figure 129: Histogram on difference in RSSI between the measurements and the prediction in SFN with N900.

3.5.2.2.2 Pääskyvuori

Pääskyvuori bike measurements were conducted in an urban area in the city center and suburban areas north and south the center. The transmitter is marked with red dot in Figure 130.

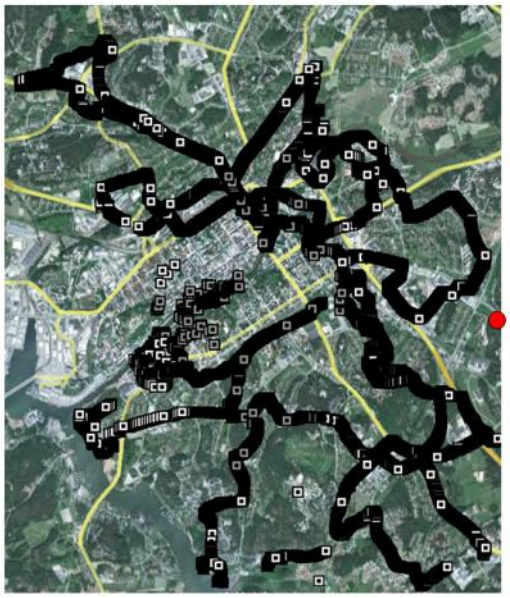

Figure 130: Pääskyvuori measurement points with N900.

The average standard deviation was 2.69dB within a 55x55m pixel. Figure 131 illustrates the difference in RSSI between the measurements and the prediction map. Most of the samples are in the area between -10 to +10 dB and the highest peaks are close to 0 dB. Thus, Pääskyvuori measurements give results that are more congruent with the prediction map than the results from the SFN case. However, the distribution is still quite different from the prediction.

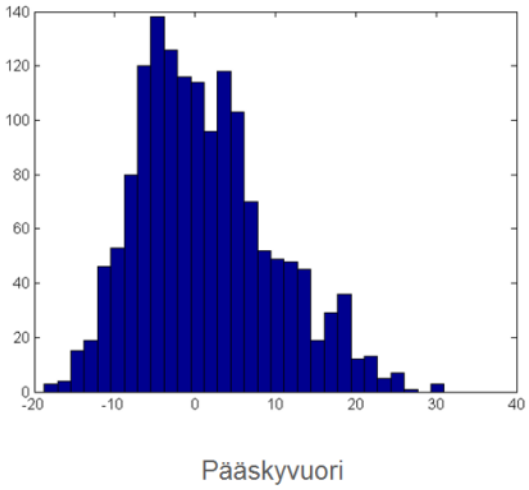

Figure 131: Histogram on difference in RSSI between the measurements and the prediction with Pääskyvuori transmitter and N900.

3.5.2.2.3 Vanha Studio

Vanha Studio measurements were conducted in an urban area in the city center and suburban areas south of the center. The transmitter is marked with red dot in Figure 132.

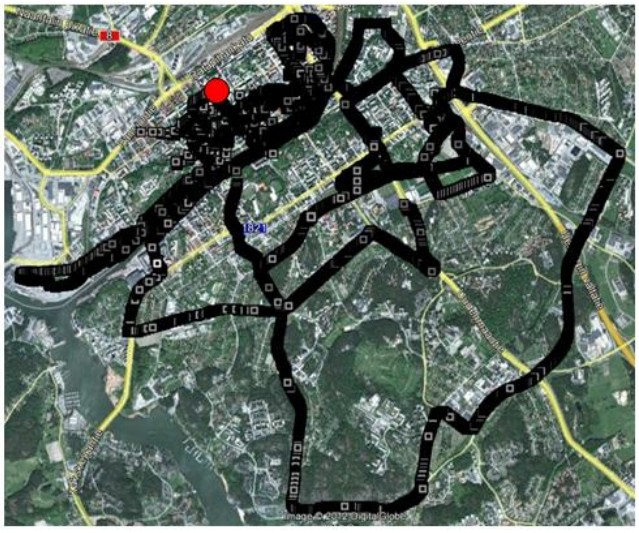

Figure 132: Vanha Studio measurement points with N900.

The average standard deviation was 6.31dB within a 55x55m pixel, which is noticeably higher than in other cases. Figure 133 represents the difference in RSSI between the measurements and the prediction map. Most of the samples are in the area between -20 to 0 dB and the highest peaks are close to -10 dB. Thus, this indicates that the Digita prediction for Vanha Studio is not as accurate as the prediction for Pääskyvuori transmitter. This could also explain similar results in the SFN measurements.

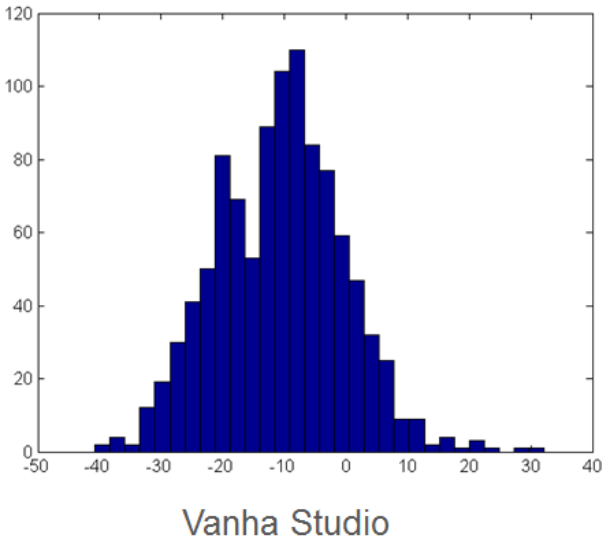

Figure 133: Histogram on difference in RSSI between the measurements and the prediction with Vanha Studio transmitter and N900.

3.5.2.3 R&S TSM-DVB bike measurements

The bike measurements were conducted with R&S TSM-DVB DVB-T/H Diversity Test Receiver illustrated in Figure 134. The device operates on a 12V battery and weighs only 1,4 kilograms, so it is low-power consuming and mobile and thus well-suited for mobile DVB-T/H coverage measurements.

Figure 134: R&S TSM-DVB DVB-T/H Diversity Test Receiver.

The input sensitivity is from -92dBm to -20 dBm and the level accuracy ±2 dB when operating on temperatures from +15 °C to +50, and ±3 dB on temperatures of 0 °C to +15 °C. We used a horizontal isotropic dipole antenna in these measurements.

The location information is provided by a Garmin GPS receiver, which can operate with its own battery or an external 12V battery. It has its own antenna to receive the GPS satellite signals.

The R&S TSM-DVB is controlled with a notebook with Windows XP and a specific LabView-based application for the measurements. The measurement results from TSM-DVB are saved to a notebook with the time and location information from the GPS device. The setup is illustrated in the block diagram presented in Figure 135.

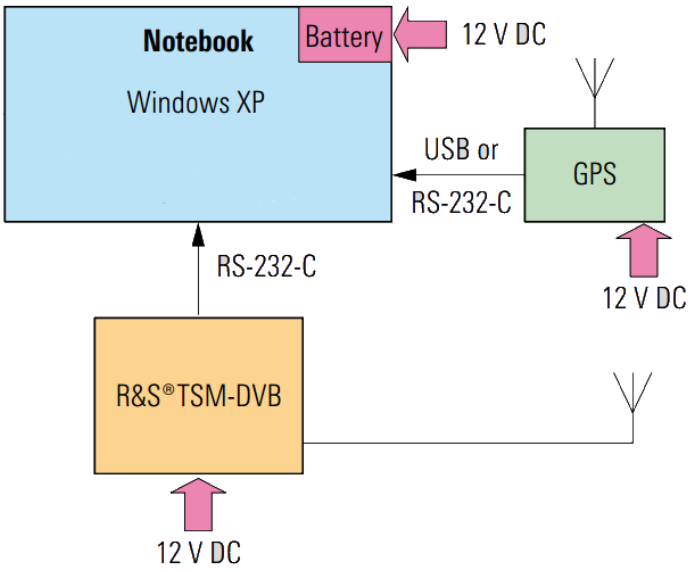

Figure 135: Bike measurement equipment setup.

The equipment is then installed into a cart which can be attached to a bike. Thus, we have a practical measurement system for mobile coverage measurements which can also produce more accurate results than the feature detector integrated into a small mobile phone. The bike with the measurement equipment attached is shown in Figure 136.

Figure 136: The measurement bike and equipment on field.

3.5.2.3.1 Conducted measurements with R&S TSM-DVB

The measurements in the test network were conducted in two different scenarios. In the first scenario we were using both transmitters in SFN and in the second scenario only the Pääskyvuori transmitter.

3.5.2.3.2 SFN

The SFN measurements were conducted in the center of the city, close to the Vanha Studio transmitter (marked with a red dot in Figure 137). Pääskyvuori transmitter is just outside the map, in the middle of the right-hand side.

Figure 137: SFN measurement points with R&S TSM-DVB.

The average standard deviation was 3.73 dB within a 55x55m pixel. Figure 138 represents the difference in RSSI between the measurements and the prediction map. The Figure shows that the majority of the samples are in the area between -20 to 0 dB. This means that the tendency is that the measured RSSI values are considerably lower than those given by the prediction, as was the case with N900 SFN measurements.

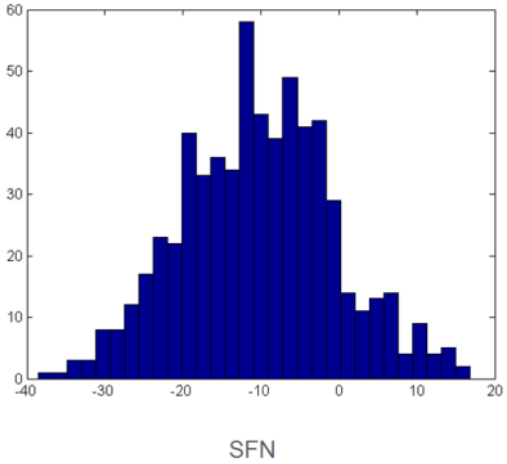

Figure 138: Histogram on difference in RSSI between the measurements and the prediction in SFN with R&S TSM-DVB.

3.5.2.3.3 Pääskyvuori

Pääskyvuori bike measurements were conducted in a geographical area of around 10x15km, reaching from Hirvensalo to Turku Airport and to the city of Kaarina. The transmitter is marked with a red dot in Figure 139.

Figure 139: Pääskyvuori measurement points with R&S TSM-DVB.

The average standard deviation was 2.62 dB within a 55x55m pixel. Figure 140 represents the difference in RSSI between the measurements and the prediction map. Most of the samples are in the area between +10 to -20 dB and the highest peak is close to 0 dB. Thus, Pääskyvuori measurements give results that are more congruent with the prediction map than the SFN case, but the distribution is still quite different between the prediction and the measurements.

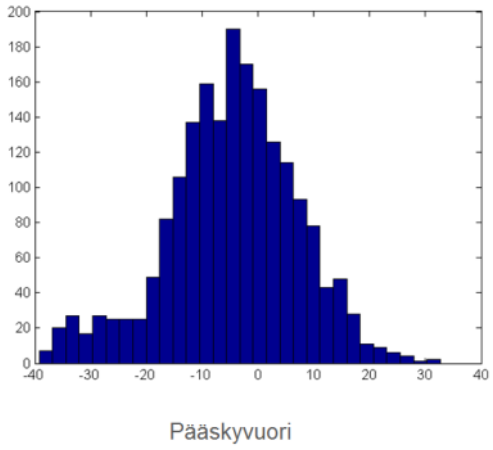

Figure 140: Histogram on difference in RSSI between the measurements and the prediction with Pääskyvuori transmitter and R&S TSM-DVB.

3.5.3 Geolocation database update algorithms

3.5.3.1 Comparison of the initially chosen algorithms

In this chapter we introduce the measurement results in to the database. In the first stage the database simply averages the samples from the same geographical location, that is, the most recent value is the average of the sensed samples and introduces them into the original prediction map, as illustrated Figure 141 a. These values are further processed by different database update algorithms which utilize the spatial correlation in DTT signal power. Three algorithms are examined here:

- *Two-dimensional median filter*. If there is more than a single WSD user within the geographical area defined by the window size, the filter selects the median value of the sensed sample and sets this value in the center pixel.
- *Adaptive Wiener filtering* utilizes the local characteristics of an image in the filtering process.
- *Ordinary Kriging* is a method regularly used in geostatistics. It uses interpolation to estimate the value of a variable in an unobserved location from observations at known locations. Given a known variogram, a value in a point of a region can be estimated using data in the local neighborhood.

The original prediction map corrected with the sensing samples and the resulting maps from different database update algorithms are presented in Figure 141.

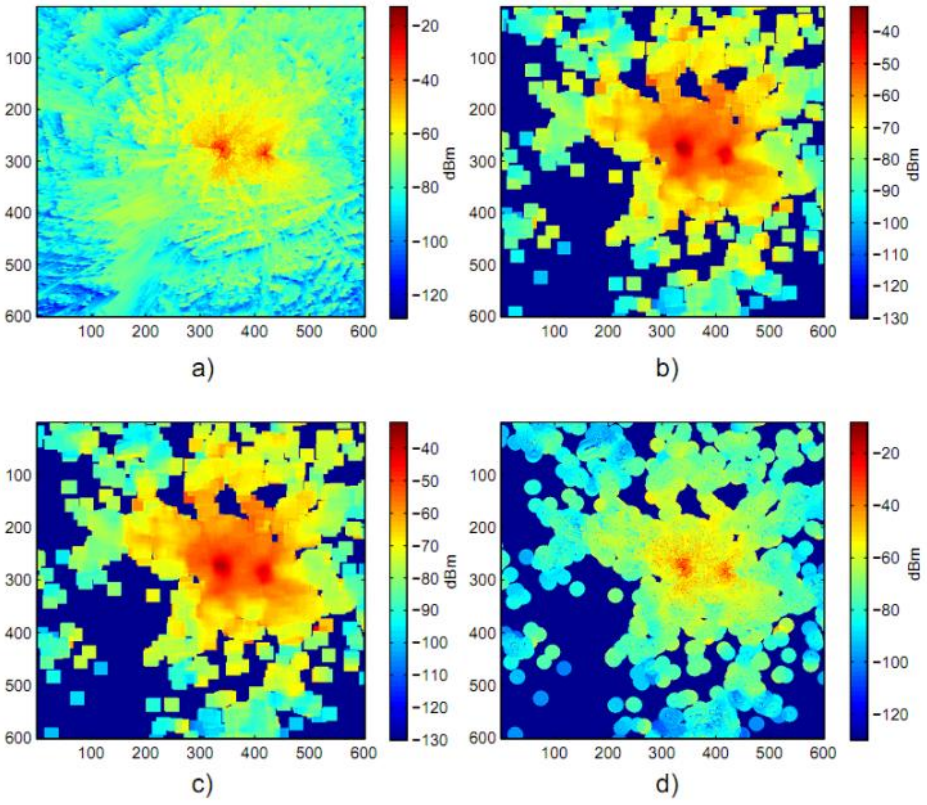

Figure 141: State of the radio environment after 1000 sensing samples. a) is the original propagation prediction map corrected with sensing samples (reference), b)) Median filter, c) adaptive Wiener filter and d) Ordinary Kriging.

As can be seen from Figure 141, two-dimensional median filter and adaptive Wiener filter have a notable smoothing effect when compared with the Ordinary Kriging, which is an exact interpolator and preserves the original samples. Thus, the mean square error between the reference map and the algorithms is noticeably lower in Ordinary Kriging than the other algorithms.

The conclusion drawn from our database algorithm study is that the Ordinary Kriging can efficiently exploit the spatial correlation of the propagating radio waves when predicting the field in unmeasured locations, while the other compared algorithms provide less accurate results. However, further analysis and measurements are still needed in order to determine how exactly the prediction model and measurements should be combined and what would be the best locations for the measurements. Thus, we chose the most suitable database update algorithm, Ordinary Kriging, for the algorithm to perform more in-depth analysis in. The measurements for the deeper analysis will be conducted with the R&S TSM-DVB, which gives us more accurate results than the mobile phone measurement device.

3.5.3.2 Ordinary Kriging with triangular grid

To perform further analysis of the geolocation database update algorithms, we defined an area of 4x4 km and chose the measurement points with a triangular grid, as shown in Figure 142 and Figure 143. By filling the plane regularly with equilateral triangles we can perform measurements from 200 points that have approximately the same distance to each other. The points have been fitted to the road map, so the identic distance between each of the points is not completely true in our case, but the distances between the spots are on similar level most of the time. measurement points are illustrated in Figure 143 and the used Vanha Studio transmitter is in the top-left corner of the map.

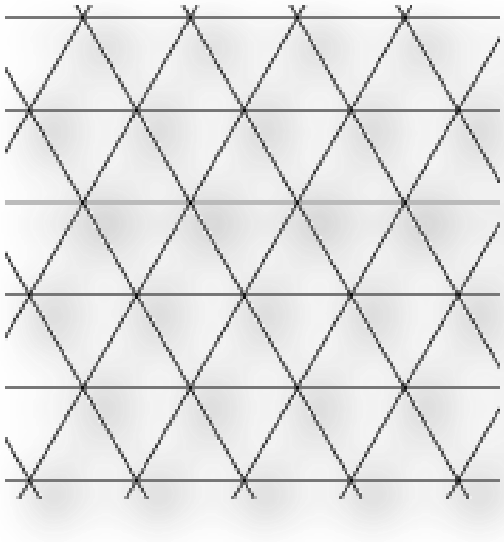

Figure 142: Triangular grid

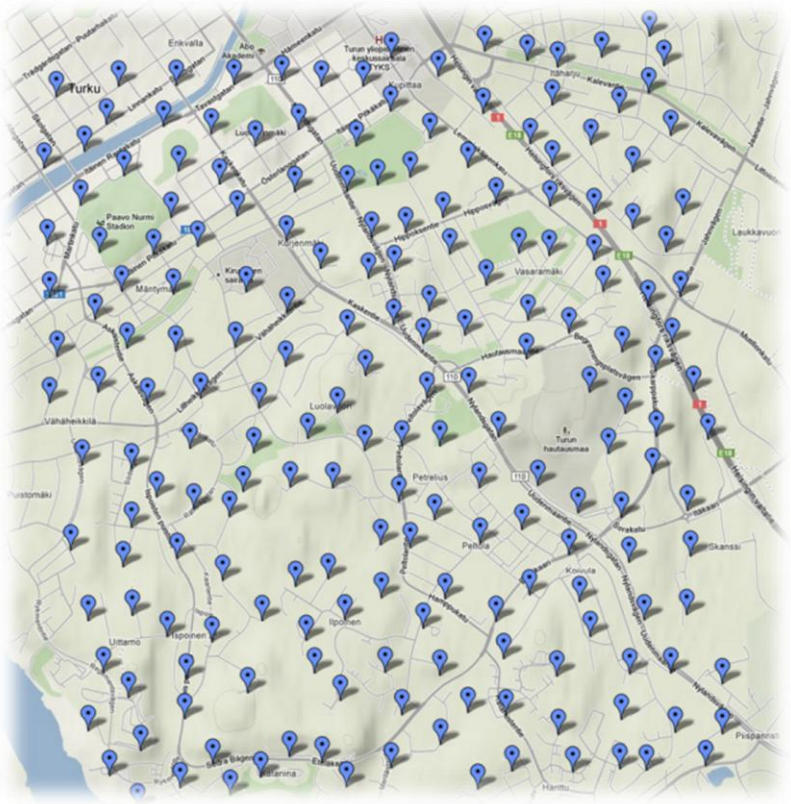

Figure 143: Triangular grid measurement points.

Because we are performing the measurements in a smaller area than previously, the ERP of the Vanha Studio transmitter is now down from 1kW to 200W so we can have larger variation between the measured field strengths inside our area than with the higher transmitter power that was used in previous measurements.

Figure 144 shows a signal level map created from the performed triangular grid measurements by using Ordinary Kriging algorithm, which was the most efficient algorithm in our comparison in the previous section. Red and yellow color correspond to strong signal level, green and blue to weaker but still usable signal level and magenta indicates weak signal. The effect of hills and terrain can be clearly from the blue and magenta areas which have weaker signal levels.

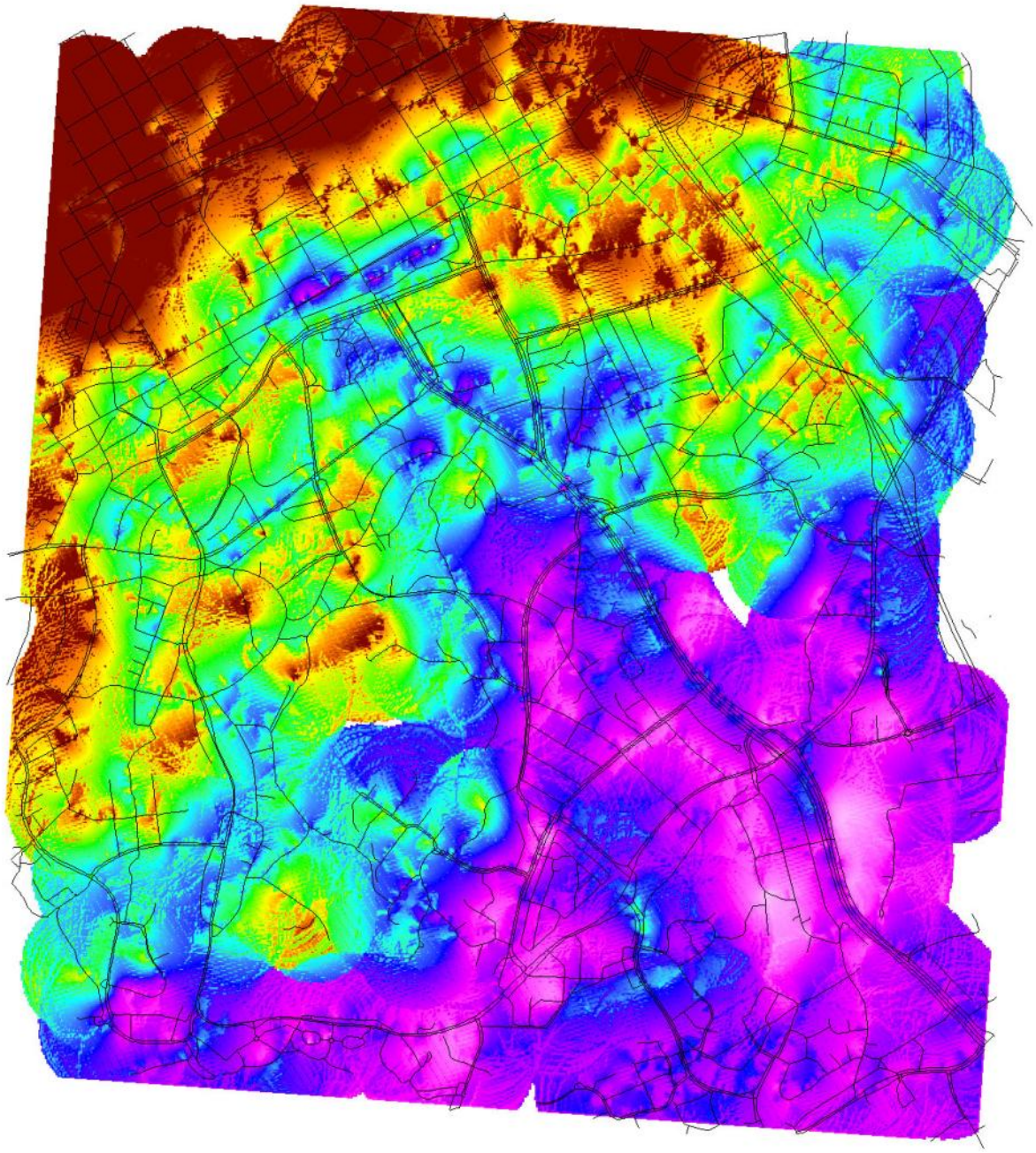

Figure 144: Signal level map formed with Ordinary Kriging from the triangular grid measurements.

In the next phase we will use the same area, but the measurement locations will be chosen with spatial simulated annealing method to search for the optimal points to for the measurements. Spatial simulated annealing uses the correlation model obtained from the triangular grid measurements to create a variogram which can then be used in the search for the optimal measurement points. By using the optimal measurement points and Ordinary Kriging we should achieve more accurate signal level map than with only triangular grid.

3.5.4 Conclusions & future research

The presented measurements have been a starting point for studying database update algorithms for cognitive radio systems. However, while studying these algorithms the knowledge on how and where the measurements should be performed has increased. Therefore, algorithms are being developed to find out the best possible measurement locations for the database update algorithms. This allows more systematic and organized measurements in the future.

The main focus of the study will be on Ordinary and Universal Kriging algorithms. Universal Kriging is a variant of Ordinary Kriging which adds a local trend to it. The local trend is a continuous and slowly varying trend surface on top of which the variation to be interpolated is superimposed. The assumption of a 'constant' mean in Ordinary Kriging is replaced by a prior trend model that is incorporated in the predictions. Thus, we should be able to create even more accurate signal level maps with Universal Kriging.

The measurements will also be used for generating a hybrid propagation model for Turku Test Network. The model is currently being constructed by Aalto University in Finland and it consists of a land use map with ten classes and a terrain height map.

4 SUMMARY

This document presents the studies on novel access technologies such as hybrid access technologies and cognitive radio. First, an overview on broadcasting systems incorporating satellite transmission was given. In the following the topics and the most important outcomes are summarized.

The link budget requirements for the DVB-NGH satellite component in OFDM mode for the 1.7 MHz band. The calculation of link budgets requires C/N performance evaluation for all the supported physical modes war presented. In the process of the DVB-NGH standardization, such inputs are generally derived to be published in the Implementation Guidelines. As this process has not yet started in the DVB-NGH standard, not all the required figures were available. The figures provided in this document have been thus derived from DVB-SH inputs as many aspects regarding the satellite component are similar.

The SC-OFDM for the implementation of the satellite transmissions in the DVB-NGH Hybrid Profile. It was shown that the SC-OFDM modulation is intrinsically robust to the Power Amplifier non-linear degradations with the ability to operate with a reduced OBO in comparison to OFDM and a total degradation improved by 1.6 dB. It is thus possible to improve the power efficiency of the PA while improving the coverage. It must be pointed out that this result still holds when considering the PAPR reduction solutions for OFDM such as the Tone Reservation approach used in DVB-T2. This kind of solution actually performs well for large IBOs but not for the small IBOs (a few dBs) commonly used in satellite transmissions. In a third wing, the section showed that the SC-OFDM behaves similarly to OFDM when it comes to compensate for the degradation due to the channel and mobility, either in SISO or MIMO.

The Convolutional interleaving scheme selected for the Long TI Feature of DVB-NGH. It was shown that the best performance is achieved by single FEC with a uniform CI profile. The performance of single FEC with the CI uniform-late profile is reduced about 2 dB compared to the CI uniform profile. CI with TI length of 10s achieves gains between 6-8 dBs.

The robustness of L1 signaling schemes provisioned in the DVB-NGH standard for the satellite segment. In a first study, it was shown that the mechanisms devised in the Terrestrial profile to improve L1 signaling robustness satisfy the requirements of the Satellite path. However, with some configuration of Additional Parity (AP2), L1-dyn repetition is needed. In addition, with AP3 configuration, the robustness of L1 signaling is enough to get better performance than data. Globally, it appears that the mechanisms assumed for the Terrestrial profile (4k, AP/IR and Fabrice decoding) when used in conjunction with L1-dyn repetition meet the requirements of the Satellite path. In a second study, it was shown that the Additional Parity mechanism is getting more efficient when associated with spreading. Nevertheless, despite of hard receiving conditions in satellite mobile environment, it has been seen that reduced spreading could be introduced

providing more robust modulation (BPSK), very low coding rate (~1/6) and reduced size code (LDPC 4K), as it is approved now in the NGH standard. The selected scheme is well suited for the scenario with a 600ms spreading duration between satellite frames. Nevertheless, for satellite transmission, only satellite NGH frames are emitted (Stand-alone mode) with 250 ms spreading duration that might be a weak point. Fortunately, NGH standard implements another mechanism, Incremental redundancy (not studied here) enabling using another previous frame to carry other bit redundancy.

Time and frequency synchronization algorithms in the context of satellite transmissions with application to the SC-OFDM waveform. This part of the report described a set of algorithms designed for improving the performance of time and frequency synchronization over the satellite channel. Most of these algorithms rely on the DVB-T2/NGH P1 symbol that also serves to detect DVB-T2/NGH transmission. The whole range of synchronization needs is covered starting with the coarse time synchronization (CTS), the estimation of the fractional frequency offset (Fractional Frequency error Synchronization - FFS), the estimation of the integer frequency offset (Integer Frequency Synchronization - IFS) and Fine Time synchronization (FTS). It was shown that the P1 detection is very robust (for SNR down to -8dB). If the P1 detection is successful, the probability to see IFS and FTS fail is very low. Moreover, in the rare cases where IFS and/or FTS fail, either because of low SNR or bad coarse time synchronization, the computation of an appropriate threshold on the correlation peaks allows the detection of such failure. Interestingly, it was shown that with the LMS ITS channel, it may happen that if the SNR increases over the frame, LLRs values and thus the detected bits might be erroneous even for high SNRs due to an a high residual frequency error during P1 synchronization. Solutions to overcome this issue were proposed.

The overall performances of an SC-OFDM system have been evaluated when applying the proposed algorithms. It was shown that synchronization algorithms are quite robust for SNR values higher than -3dB. For the propagation channels for which no deep fading are observed, the synchronization algorithms do not degrade the BER, as the synchronization algorithms work correctly at the considered SNR values. For AWGN, TU6 and LMS OPEN cases, the degradation brought by synchronization compared to the perfect synchronization case (with real channel estimation) is about 0.1dB. However over the RICE channel with K=5 and the LMS ITS channel both showing deep fading, several consecutive P1 symbols may not be detected causing packet errors. In the presented simulations the interleaving time was chosen to be short (less than 1.5 seconds) and in this condition, the wrong P1 detections cause BER degradations. The losses for these channels spread from 1 to 2 dB. Taking into account that the DVB-NGH traffic is made of bursts (by opposition to continuous transmission in DVB-SH), these amount of losses appear quite reasonable in comparison to erasure channels.

Further, the studies performed within ENGINES project on *cognitive radio* were presented. First the cognitive radio concept was briefly described. Further an experimental implementation of a sensing device in a mobile computer was presented accompanied with sensing measurement results.

Field measurement data that could serve as a reference for the technical discussions around the possible use of White Spaces in the UHF band was provided. Results have shown that a top occupancy of 32% of the bandwidth is achieved in the roof and that the hidden node margin obtained range from 8 to 38 dB on channel 22 depending on the environment and lead to the conclusion that cognitive communications to be performed in the UHF TV band need the joint use of geolocation databases and spectrum sensing technique to avoid harmful interference to the primaries services of the broadcasters. Also, field measurements used for studying geolocation database update algorithms were presented.

5 REFERENCES

[1] ETSI EN 300 421 V1.1.2, "*Digital video broadcasting; Framing structure, channel coding and modulation for 11/12 GHz satellite services (DVB-S2)*", August 1997.

[2] ETSI EN 302 307, V1.2.1, "*Digital video broadcasting; Second generation framing structure, channel coding and modulation systems for Broadcasting, Interactive Services, News Gathering and other broadband satellite applications (DVB-S2)*", April 2009.

[3] ETSI EN 302 583: "*Digital Video Broadcasting (DVB); Framing Structure, channel coding and modulation for Satellite Services to Handheld devices (SH) below 3 GHz*", January 2008.

[4] A. Axel and S. Stina, "*Implementation of writing references*", in Proc. Dummy, Turku, 2011.

[5] Dov Wulich, "*Definition of Efficient PAPR in OFDM*", in IEEE Communications Letters, nol. 9, no. 9, September 2005.

[6] D. Wulich, N. Dinur, and A. Gilinowiecki, "*Level clipped high order OFDM*," IEEE Trans. Commun., vol. 48, pp. 928-930, June 2000.

[7] C. Ciochină, "*Conception d'une couche physique pour la liaison montante dans des systèmes de radiocommunications mobiles cellulaires*," PhD Thesis, July 2009.

[8] S. Kaiser, "*OFDM Code-Division Multiplexing in Fading Channels*," IEEE Trans. Commun., vol. 50, no. 8, pp. 1266-1273, August 2002.

[9] A.M. Mourad, "*on the system level performance of MC-CDMA systems in the downlink*," PhD Thesis, January 2006.

[10] J. Tellado, "*Peak to Average Power Reduction for Multicarrier Modulation*," Ph.D. thesis, Stanford University, 2000.

[11] C. Ciochina, F. Buda and H. Sari, "An Analysis of OFDM Peak Power Reduction Techniques for WiMAX Systems," *IEEE International Conference on Communications, ICC'06*, Istanbul, Turkey, June 2006.

[12] Wireless World Research Forum, *Technologies for the Wireless Future*, vol. 2, John Wiley & Sons, Ltd, 2006.

[13] ETSI EN 302 755 V1.1.1, "Digital Video Broadcasting (DVB); Frame structure channel coding and modulation for a second generation digital terrestrial television broadcasting system (DVB-T2)," September 2009.

[14] M. D. McKinley, K. A. Remley, M. Myslinski, J. S. Kenney, D. Schreurs, B. Nauwelaers, "EVM Calculation for Broadband Modulated Signals," 64th ARFTG Conf. Dig., Orlando, FL, pp. 45-52, Dec. 2004.

[15] ETSI EN 302 307 v1.2.1: "Digital Video Broadcasting (DVB); Second generation framing structure, channel coding and modulation systems for Broadcasting, Interactive Services, News Gathering and other broadband satellite applications," August 2009.

[16] C. Rapp, "Effects of the HPA-nonlinearity on a 4-DPSK/OFDM signal for a digital sound broadcasting system," European Conference on Sattelite Communications ECSC'91, Liège, Belgium, Oct. 1991.

[17] F. Pérez-Fontán, et al., "Statistical Modelling of the LMS Channel," IEEE Trans. on Vehicular Technology, vol.50, no. 6, pp. 1549-1567, 2001.

[18] ETSI TS 102 584 v1.2.1, "Guidelines for the Implementation for Satellite Services to Handheld devices (SH) below 3GHz," 2011.

[19] ETSI EN 302 755 v1.3.1, "Digital Video Broadcasting (DVB); Frame Structure Channel Coding and Modulation for a Second Generation Digital Terrestrial Television Broadcasting System (DVB-T2)," Oct. 2011.

[20] ETSI TS 102 831 v1.2.1q, "Digital Video Broadcasting (DVB); Implementation guidelines for a second generation digital terrestrial television broadcasting system (DVB-T2)," February 2012.

[21] 3GPP TS 36.211 V10.4.0: "3rd Generation Partnership Project; Technical Specification Group Radio Access Network; Evolved Universal Terrestrial Radio Access (E-UTRA); Physical Channels and Modulation (Release 10)," December 2011.

[22] D. C. Chu, "Polyphase Codes With Good Periodic Correlation Properties", IEEE Trans. on Information Theory, vol. 18, no. 4, pp. 531-532, July 1972.

[23] J. Tellado, "Peak to Average Power Reduction for Multicarrier Modulation," Ph.D. thesis, Stanford University, 2000.
[24] C. Ciochină, "Physical layer design for the uplink of mobile cellular radiocommunication systems," PhD Thesis n° 2009PA112300, Université de Paris-Sud, Faculté des Sciences d'Orsay (Essonne), France, 2009.
[25] C. Rapp, "Effects of the HPA-nonlinearity on a 4-DPSK/OFDM signal for a digital sound broadcasting system," European Conference on Sattelite Communications ECSC'91, Liège, Belgium, Oct. 1991.
[26] C. Ciochina, F. Buda and H. Sari, "An Analysis of OFDM Peak Power Reduction Techniques for WiMAX Systems," IEEE International Conference on Communications, ICC'06, Istanbul, Turkey, June 2006.
[27] D. Wulich, N. Dinur, and A. Gilinowiecki, "Level Clipped High Order OFDM," IEEE Trans. on Communications, vol. 48, no. 6, pp. 928-930, June 2000.
[28] M. D. McKinley, K. A. Remley, M. Myslinski, J. S. Kenney, D. Schreurs, B. Nauwelaers, "EVM Calculation for Broadband Modulated Signals," 64th ARFTG Conf. Dig., Orlando, FL, pp. 45-52, Dec. 2004.
[29] ETSI EN 302 307, V1.2.1, "Digital video broadcasting; Second generation framing structure, channel coding and modulation systems for Broadcasting, Interactive Services, News Gathering and other broadband satellite applications (DVB-S2)", August 2009
[30] DVB TM-NGH183, "Land Mobile Satellite Propagation channel model," May 2010.
[31] DVB TM-NGH063r5, "DVB-NGH Channel Models," November 2010.
[32] P. Moss, T. Yeen Poon, and J. Boyer, "A Simple Model of the UHF Cross-Polar Terrestrial Channel for DVB-NGH," BBC White Paper WHP205, Sept. 2011.
[33] F. Pérez-Fontán, et al., "Statistical Modeling of the LMS Channel," IEEE Trans. on Vehicular Technology, vol.50, no. 6, pp. 1549-1567, 2001.
[34] ETSI TS 102 584 v1.2.1, "Guidelines for the Implementation for Satellite Services to Handheld devices (SH) below 3GHz," 2011.
[35] ETSI EN 302 583: "Digital Video Broadcasting (DVB); Framing Structure, channel coding and modulation for Satellite Services to Handheld devices (SH) below 3 GHz", January 2008.
[36] G. Faria, J. A. Henriksson, E. Stare, and P. Talmola, "DVB-H: Digital Broadcast Services to Handheld Devices," Proc. of the IEEE, vol. 94, no. 1, pp. 194-209, 2006.
[37] TM-NGH 1319, "L1 signalling robustness in the SAT path", Hognsil Jeong.
[38] TM-NGH 1158, "Simulation Results of L1 signalling LMS channel", Hognsil Jeong.
[39] TM-NGH 1159, "PF72 4k codes for L1 signalling", Hognsil Jeong.
[40] TM-NGH 105, "Proposal for improving the performance of l1 signalling in mobile channels", Samsung, Nokia, 23-24 March 2010.
[41] G. Faria, J. A. Henriksson, E. Stare, and P. Talmola, ``DVB-H: Digital Broadcast Services to Handheld Devices," *Proc. of the IEEE*, vol. 94, no. 1, pp. 194-209, 2006.
[42] ETSI TS 102 772 v1.1.1, "Multi-Protocol Encapsulation – inter-burst Forward Error Correction (MPE-iFEC)," 2010.
[43] D. Castelain, "*SC-OFDM for the satellite component - New results*", DVB/NGH, Jeju meeting, October 2010.
[44] F. Pérez-Fontán, M. Vázquez-Castro, C.E. Cabado, J. Pita García, E. Kubista, "Statistical Modelling of the LMS channel", IEEE Transactions on Vehicular Technology, Vol. 50, No.6, Nov. 2001, pp. 1549-1567.
[45] F. Pérez-Fontán, M. Vázquez-Castro, S. Buonomo, J.P. Poiares-Baptista, B. Arbesser-Rastburg, "S-Band LMS propagation channel behaviour for different environments, degrees of shadowing and elevation angles", IEEE Transactions on Broadcasting, Vol. 44, No.1, March 1998.
[46] R. Prieto-Cerdeira, F. Perez-Fontan, P. Burzigotti , A. Bolea-Alamanac, I. Sanchez-Lago, "Versatile two-state land mobile satellite channel model with first application to DVB-SH analysis", Int. J. Satell. Commun. Network., vol. 28, no. 5-6, pp. 291-315, 2010.
[47] TM-NGH 473, MIMO_LMS executable software, ESA.
[48] TM-NGH 472, Reference Document for Executable "MIMO_LMS.exe" of the Dual Polarization MIMO LMS Channel Model, ESA.

[49] K. Liolis, J. Gomez-Vilardebo, E. Casini, A. Perez-Neira, "Statistical modeling of dual-polarized MIMO land mobile satellite channels", IEEE Transactions on Communications, Vol. 58, No.11, Nov. 2010, pp. 3077-3083.
[50] Y.R. Zheng, C. Xiao, "Improved Models for the Generation of Multiple Uncorrelated Rayleigh Fading Waveforms", IEEE Com. letters, Vol. 6, N. 6, Juin 2002
[51] ETSI draft TR 102 831, DVB Bluebook A133, "Implementation Guidelines for a Second Generation Digital Terrestrial Television Broadcasting System (DVB-T2)," June 2010.
[52] SE43 Technical and operational requirements for the possible operation of cognitive radio systems in the 'white spaces' of the frequency band 470-790 MHz
[53] J. Mitola III and G.Q. Maguire, Jr. Article Title: Cognitive Radio: Making Software Radios More Personal. IEEE Personal Communications,vol.6 , no.4, pp.13-18. August 1999.
[54] B.S. Randhawa, Z. Wang, I. Parker. Report Title: Analysis of hidden node margins for cognitive radio devices potentially using DTT and PMS spectrum. January 2009.
[55] S. Contreras, G. Villardi, R. Funada, H. Harada. Report Title: An investigation into the spectrum occupancy in Japan in the context of TV White Space Systems. 6th International ICST Conference on Cognitive Radio Oriented Wireless Networks and Communications, 1 June - 3 June 2011 - Osaka, Japan.
[56] R.I.C.Chiang, G.B.Rowe, K.W.Sowerby: A queantitative Analysis of Spectral Occupancy Measurements for Cognitive Radio. IEEE Research, 1550-2252 pp.3016-3020, 2007.
[57] M. López-Benítez, A. Umbert and F. Casadevall. Report Title: Evaluation of Spectrum Occupancy in Spain for Cognitive Radio Applications, Dept. Signal Theory and Comn.,UPC, Barcelona, Spain.IEEE 2009.
[58] M.Barbiroli, C.Carciofi, A.Guidotti, D.Guiducci: Evaluation and analysis of the hidden node margin for cognitive radio system operation in a real scenario. Proceeding of the 5th European Conference on Antennas and Propagation.
[59] M. Waddell.: Compatibility Challenges for Broadcast Networks and White Space Devices. BBC Research White Paper, WHP 182, January 2010.